National Conference on Biological Imaging: II. Clinical Aspect: Papers Presented at the Conference (1984)

Pages
207

Size
8.5 x 10

ISBN
0309324688

National Academy of Sciences

NATIONAL CONFERENCE ON BIOLOGICAL IMAGING

II. CLINICAL ASPECT

PAPERS PRESENTED AT THE CONFERENCE

October 16-18, 1983

National Academy of Sciences

Washington, D.C.

National Academy Press

Washington, D.C. 1984

PREFACE

CECIL H. GREEN
Texas Instruments
Dallas, Texas

A. D. SUTTLE, JR.
Marine Biomedical Institute
University of Texas Medical Branch at Galveston

In late 1977, the concept of spin resonance--particularly its potential therapeutic application in oncology--was brought to our attention. Traditional academic opinion convinced us that it had no practical application, but the idea stimulated our interest in the physical sciences and engineering advances related to diagnosis and therapy.

Accordingly, we began to review the literature and read of advances in the general subject of medical imaging. We were especially impressed with positron emission tomography (PET) and magnetic resonance imaging (MRI). They appeared to complement computer-assisted tomography, single-photon tomography, ultrasound, and such procedures as heavy-ion imaging that we considered rather esoteric. Both of us were impressed by the enormous advances that had been made in computation both in hardware and software and in the application of efficient high-speed computers for the reduction of data, whether in computer-assisted tomography, in ultrasonics, or in the evaluation of seismic and other geophysical data. We were certain that the efficient and imaginative use of computers would benefit any modern field of technology.

We noted a common thread: several elements seemed to be associated with all these developing techniques. First, of course, was the effective use of computer science. The excellent computer hardware and innovative software made it possible to generate diagnostic imaging data quickly and accurately. Moreover, such computer techniques were capable of enhancing images, accentuating contrast, and improving resolution. All this could be done with a minimum of invasive exposure and without repetitive studies. We were also impressed with the advances in electronics, especially those related to solid-state physics. The development of solid-state circuits resulted in instrumental techniques that would have been impossible with vacuum tubes. Solid-state circuitry also

permitted reliability of production and ease of quality control. We noted the widespread application of cryogenics and superconductivity, not only in the development of magnets for MRI, but also in connection with the requirement of a small accelerator to produce isotopes for PET. In short, the advances in physical science and engineering had provided tools that would benefit the investigative scientist, the clinician, and, most important, the patient.

Further discussion with our friends skilled in the physical sciences and the healing arts convinced us of the likely rewards of a meeting in which vital information could be exchanged among scientists, engineers, and clinicians. The resulting conference, which was held at the Scripps Clinic and Research Foundation in La Jolla, California, in November 1980, assessed many of the newer modalities, compared them with traditional imaging techniques, and evaluated their limitations and advantages. The consensus was that MRI and PET were the most promising of the concepts. However, it was recognized that other imaging techniques were emerging.

Over the next 3 years, we continued to follow developments and were particularly gratified to observe the gigantic strides being made in MRI with the production of superb images and techniques for chemical analysis of tissue. We also noted substantial improvements in the resolution of PET and the advancement of other imaging procedures. The success of MRI and the general developments in the field convinced us that a second conference on the subject would be justified. We planned a stronger clinical content aimed at a clinical updating of accomplishments not only in MRI, but also in PET and other imaging modalities. We also elected to invite a number of outstanding young scientists who we felt would be the imaging leaders of the future.

Although the second conference, held at the National Academy of Sciences in Washington, D.C., in October 1983, stressed MRI, it also reviewed PET and other imaging modalities. Several papers were presented on the application of computer science to biological imaging and on the role of magnets, particularly superconducting magnets.

No two individuals could possibly acquaint themselves with all the outstanding authorities in these diverse and rapidly developing fields. We were fortunate to have willing friends who joined us as sponsors of the conference and gave liberally of their time and their knowledge. To our fellow sponsors, we express our deep and sincere thanks. We are most grateful to the presidents of the National Academy of Sciences, The National Academy of Engineering, and the Institute of Medicine for graciously joining us in sponsoring this second conference and for the use of the facilities of the National Academy of Sciences.

The authorities who presented information were the heart of the conference, and we are most appreciative of and deeply indebted to each of them. We are particularly obliged to two of the speakers, Thomas F. Budinger and Paul C. Lauterbur, who developed, for separate publication, an excellent summary of material presented at this conference and of other relevant information on nuclear magnetic resonance (Science 226:288-298, 1984). Finally, we thank the many interested people who thoughtfully and critically participated in the meeting and in the discussions that followed the presentations of formal papers.

As these fields advance in the future, we hope that it will be possible to arrange a third conference to review additional important developments, which we are sure will be forthcoming.

CONTENTS

CROSS STRANDS LINKING PHYSICS AND MEDICINE

ROBERT HOFSTADTER
Department of Physics
Stanford University

Physics and medicine have had a close relationship since about 1000 A.D., when the first developments of these disciplines started to take shape. In modern times, the medical sciences have seized on new developments in physics, no matter how sophisticated, and applied them almost immediately to the care of patients. Some of the examples discussed below will illustrate how this has come about.

One can easily demonstrate the association of physics and medicine by assembling a table in which the various branches of physics can be correlated with branches of medicine. This correspondence is shown in Table 1. It is remarkable that the correlation is so complete. Even relativity physics finds application in medicine. This will be discussed later. Table 2 exhibits the specific topics that will be presented here and the names of scientists associated with the work.

In preparing this article, I was struck with wonder and delight by the amount of detailed new information and procedures arising from medicine and biology in the last few decades. There is no way to convey the excitement I experienced in learning about these subjects, but I hope that readers may be influenced to the extent that they may experience delight similar to mine.

The first topic concerns the subject of light and optics. In medicine, the early microscopists were captivated by their greatly enlarged view of a formerly invisible world. For example, Malpighi showed that capillaries carry blood and transfer it from arteries to veins, and this completed Harvey's theory of the circulation of the blood. The compound microscope was created in the seventeenth century by unknown inventors in the Netherlands and was applied to medical research in the same century by the early microscopists. The development of physics and medicine advanced in parallel, and the light microscope constitutes a good example of this association.

TABLE 1

Correlations between Physics and Medicine

Physics	Medicine
Statics (mechanics)	Orthopedics
Dynamics (mechanics)	Heart motion
Elasticity and strength of materials	Orthopedics
Fluid statics	Blood pressure
Fluid dynamics	Blood flow in vascular system
Surface tension	Capillary action
Sound and acoustics	Stethoscope, ultrasound, acoustic microscope
Electricity	All life processes, ion transfer at membranes
Magnetism	Nuclear-magnetic-resonance imaging
Light and optics	Light microscope, laser therapy, fiber optics
Heat and thermodynamics	Heat balance
Kinetic theory and statistical mechanics	Brownian motion, osmosis, diffusion of gases
Atomic physics and spectroscopy	"Chemical shift" in NMR imaging, lasers in medicine
Molecular physics	Genetics, antibodies, protein structure, electron microscope
Ultraviolet and infrared energy	Skin treatment and imaging
X rays	Radiology, CT imaging
Quantum mechanics	Electron diffraction microscope
Relativity	Synchrotron radiation imaging
Crystallography	Structure of proteins
Solid-state physics and semiconductors	Computers in medicine, scintigraphy
Nuclear physics	Radioisotope labeling, nuclear medicine, radiation therapy
Radioactivity	Positron emission tomography (PET)
Elementary particle physics	Pion therapy
Accelerators, cyclotrons, etc.	Tumor therapy, Hodgkin's disease
Astronomy and astrophysics	Discovery of helium, treatment of asthma (obsolete)

TABLE 2

Topics Selected from Table 1 and Presented in Discussion

Physics	Medicine and Biology	Scientists
Light and optics	Light microscope	S. I. Alhazen (1000 A.D.), R. Bacon (1267 A.D.), T. Moufet, A. V. Leeuwenhoek (1700 A.D.), M. Malpighi
Ultrasound	Ultrasonography, echocardiography	B. Carroll, C. F. Quate
Quantum mechanics-wave mechanics	Electron microscope	M. Planck, L. De Broglie, C. J. Davisson, L. H. Germer, G. P. Thomson, H. Busch, M. Knoll, E. Ruska
	Bacteriophage T4	D. J. De Rosier, A. Klug
	Tobacco mosaic virus	R. Williams
	Purple membrane of Halobacterium halobium, connexon-light driven hydrogen ion pump in photosynthesis, gap junctions	P. N. T. Unwin, R. Henderson, G. Zampighi
Crystallography	Antibody structure, protein structure	R. Kornberg, D. R. Davies
Nuclear physics	Nuclear medicine	H. Anger, I. R. McDougall
	Positron emission tomography (PET)	M. M. Ter-Pogossian, M. E. Phelps, D. E. Kuhl, T. F. Budinger, N. A. Lassen, G. L. Brownell, etc.
Elementary particle physics	Radiation therapy, Hodgkin's disease	H. Kaplan, C. W. Miller, S. Rosenberg
X rays	Imatron	W. Roentgen, D. Boyd, R. Rand
Magnetism	Magnetic-resonance imaging	F. Bloch, E. Purcell, P. C. Lauterbur, L. Kaufman
Relativity (and elementary particle physics)	Synchrotron-radiation imaging	A. Einstein, E. B. Hughes, E. Rubenstein, R. Hofstadter, C. A. Mistretta

The applications of the light microscope in biology and medicine are so numerous that it is inappropriate to list them here. One need think only of the ability to see cell structure and the composition of the interior of the cell's nucleus.

Light waves supply us with the means to illuminate and delineate the details of many small objects, such as cells. In recent years, sound waves have also been used to view objects, both large and small. When applied to study of the human body by echo-detecting techniques, ultrasonography has proved to be very valuable. When applied to very small objects, ultrasound can be used to study details in a manner quite different from the optical approach, and the degree of contrast will have different qualities in the two techniques. Because very small wavelengths can be used, the ultrasound technique allows one to build a microscope. This has been done by Quate and his colleagues, who have been able to study cells, surfaces, integrated-circuit chips, and many other small objects. Figure 1, supplied by Quate,[7] shows acoustic micrographs of two normal cells colliding in a culture. After collison, each cell rebounds and moves away. This behavior is different for abnormal cells. These examples of acoustic images indicate that the acoustic microscope has new potential for examining microscopic structure.

The electron microscope is a good example of an application of very sophisticated ideas in physics. In the 1920s, German scientists, such as Busch and Braun, were attempting to make better oscilloscopes, and they needed to obtain as high an electron-beam intensity as possible. They attempted to collect the largest possible fraction of electrons coming out of the hot filament--the source of the electrons. They used a uniform magnetic field for concentrating and focusing the outgoing beam, as shown in Figure 2. The electron trajectories were helices surrounding the direction of the magnetic field, which was provided by a large surrounding solenoid. They later found that they could use small, efficient solenoids with nonuniform magnetic fields to accomplish the same goal. After a great deal of groundbreaking research in electron trajectory studies, they began to appreciate the idea of making images. Such scientists as Ruska and Knoll found that they could make a microscope by using their new knowledge, and, encouraged by the de Broglie discovery that particles had wave-like properties, they set as their goal the improvement of imaging qualities that could surpass the light microscope in the resolution of detail. Figure 3 is a schematic diagram of the illumination system and the imaging system in a transmission electron microscope. This represents the practical outcome of the early research to improve oscilloscope design. In the figure, the object plane is shown above the second solenoid (objective lens). In the most recent electron microscopes, the object table can be rotated so that transmission

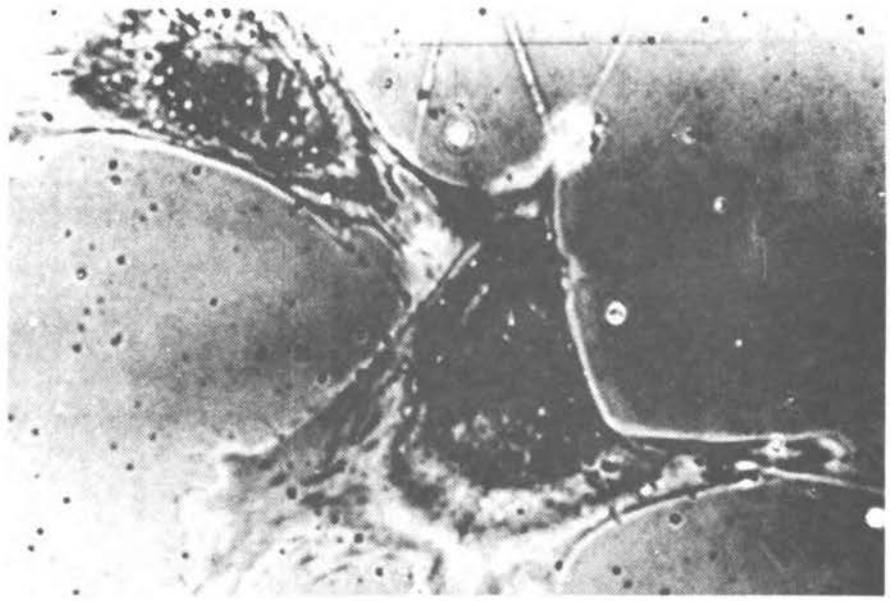

(a)

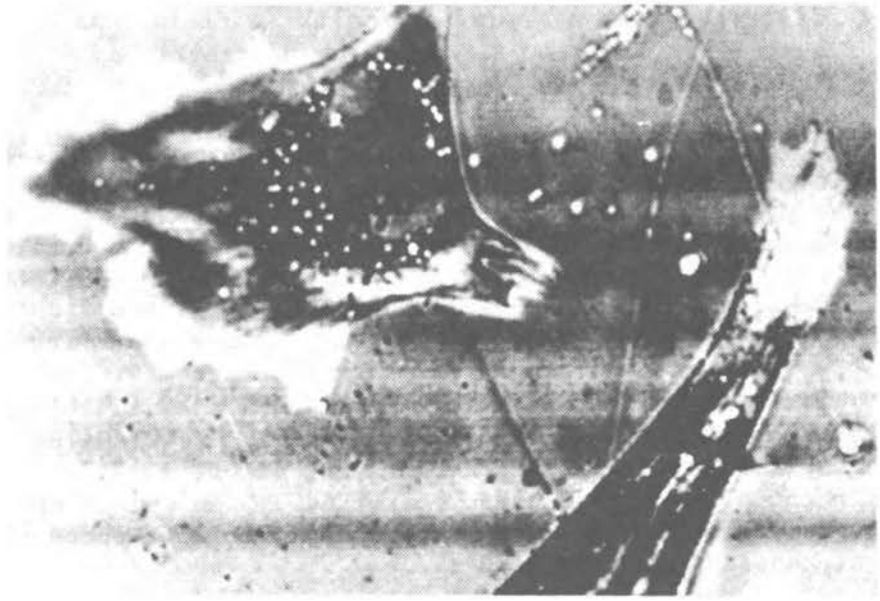

(b)

FIGURE 1 Acoustic microscope images of two colliding cells in culture. For normal cells, collisions resemble scattering in physics. Images show "scattering." Abnormal cells do not behave in same way. Reprinted with permission from Quate.[7]

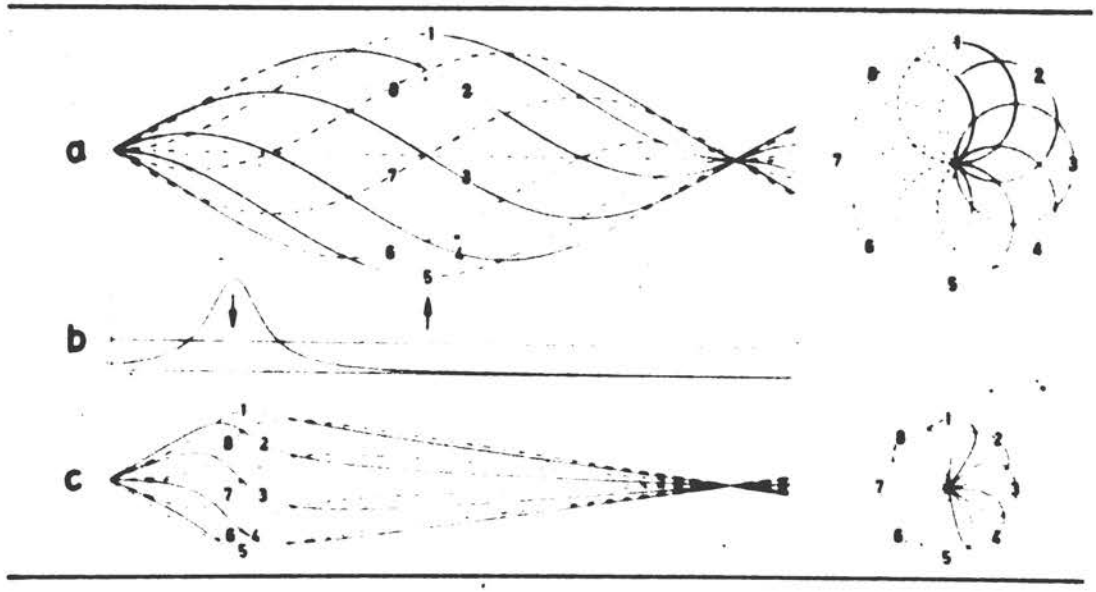

FIGURE 2 Electron paths: a, uniform magnetic field, and c, nonuniform magnetic field. b, two magnetic profiles. Reprinted with permission from Ruska.[8]

images can be obtained with different directions of electron passage through the object. The purpose of such tilting is to get a three-dimensional image, rather than a simple two-dimensional one.

With the electron microscope, one could see for the first time very small creatures, such as the T4 bacteriophage. An electron microscopic image of this phage[14] is shown in Figure 4. At present, this image might be called a low-resolution image; and much more detail can be obtained than is shown here. Nevertheless, in such an image, details as small as 35 Å may be observed. In the light microscope, the resolution is limited by the wavelength of the light used, and good resolution is considered to correspond to 2,500 or several thousand angstroms.

The T4 phage is an example of a virus that can multiply rapidly by thrusting its DNA into a bacterium wherein it reproduces itself at the expense of a destroyed bacterium. Therefore, it would be most interesting to know more about how the injection process takes place. It is clear that help in this direction would be furnished by being able to "see" more detail in the phage. De Rosier and Klug[2] developed a method to reveal the desired detail. They used

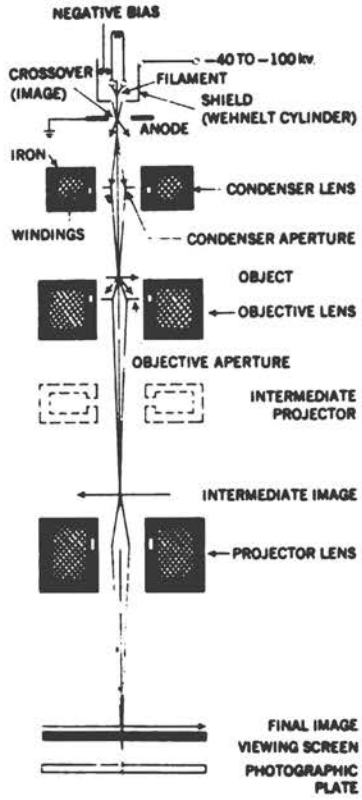

FIGURE 3 Schematic diagram of transmission electron microscope.

an electron microscope to obtain a micrograph by transmission at a particular angle of tilting of the objective stage. The electron-beam intensity is then recorded and an optical-diffraction pattern of the recorded image is made. The optical densities in this image are then measured and digitized. More than one such projection can be made. This method[2] is summarized in Figure 5. Each projection can supply the information needed to obtain Fourier transforms in two dimensions. The three-dimensional representation of the image can then be obtained by Fourier synthesis of the different projections. In this way, the phage "tail" has been studied, with the results given in Figure 6. To show the detail achieved, De Rosier and Klug made a model that appears in the figure. The length of the model represents only one-third of the actual length of the virus. The long dimension of the tail is roughly 900 Å, and the width is about 250 Å. The core diameter is about 30 Å. Helical symmetry is clear in this most interesting structure. In the interior of the model, one can see the core. The outer layers form a sheath; when the sheath contracts, the DNA is expelled through the core and can be inserted into a bacterium. This remarkable configuration of proteins is characteristic of many of the small objects studied with this sophisticated technique that makes use of the electron microscope.

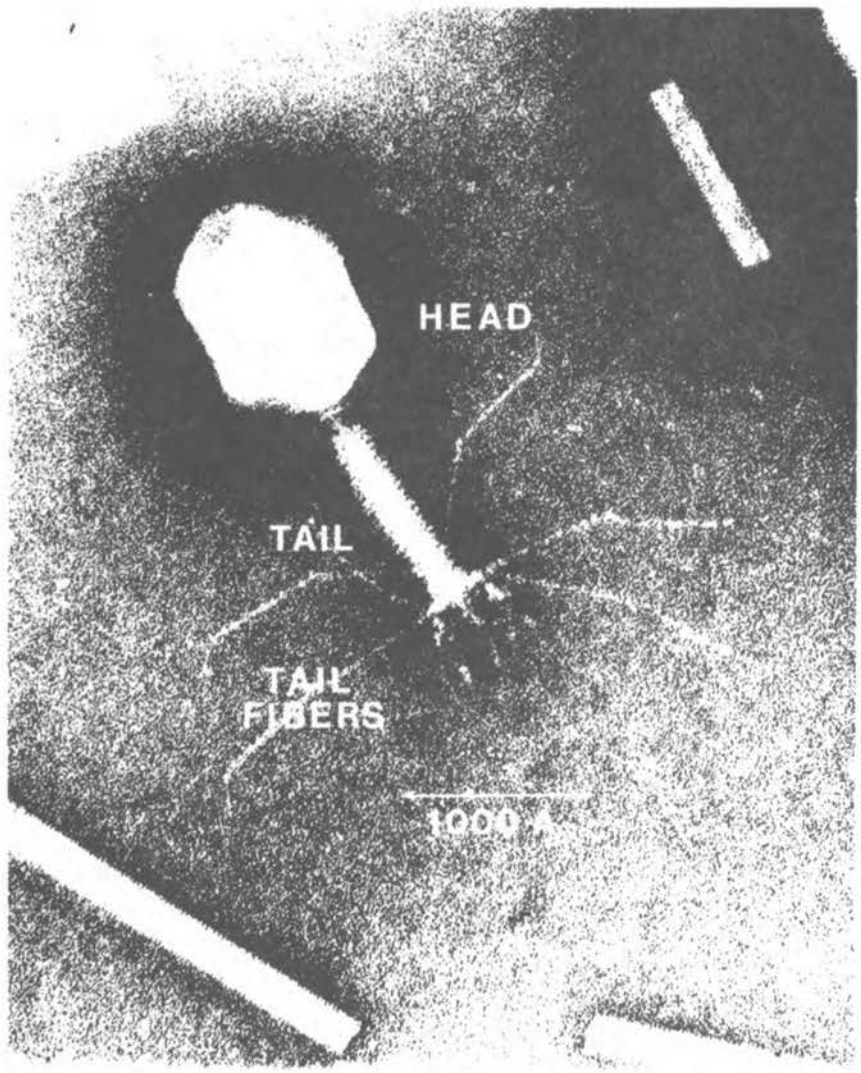

FIGURE 4 Electron microscope image of T4 bacteriophage. Reprinted with permission from Williams and Fisher.

Another example of the detail that can be observed is the tobacco mosaic virus. Figure 7 illustrates a model of part of the structure, showing protein subunits and an RNA strand that runs through the surrounding units.[6] Still another example was provided by Henderson and Unwin,[3] who have studied bacteriorhodopsin in the purple membrane. The purple membrane is part of the cell membrane of a salt-loving bacterium called Halobacterium halobium. A model of this protein structure is shown at the left in Figure 8. Bacteriorhodopsin, a membrane protein synthesized by the bacterium, provides an example of a proton pump that may be driven

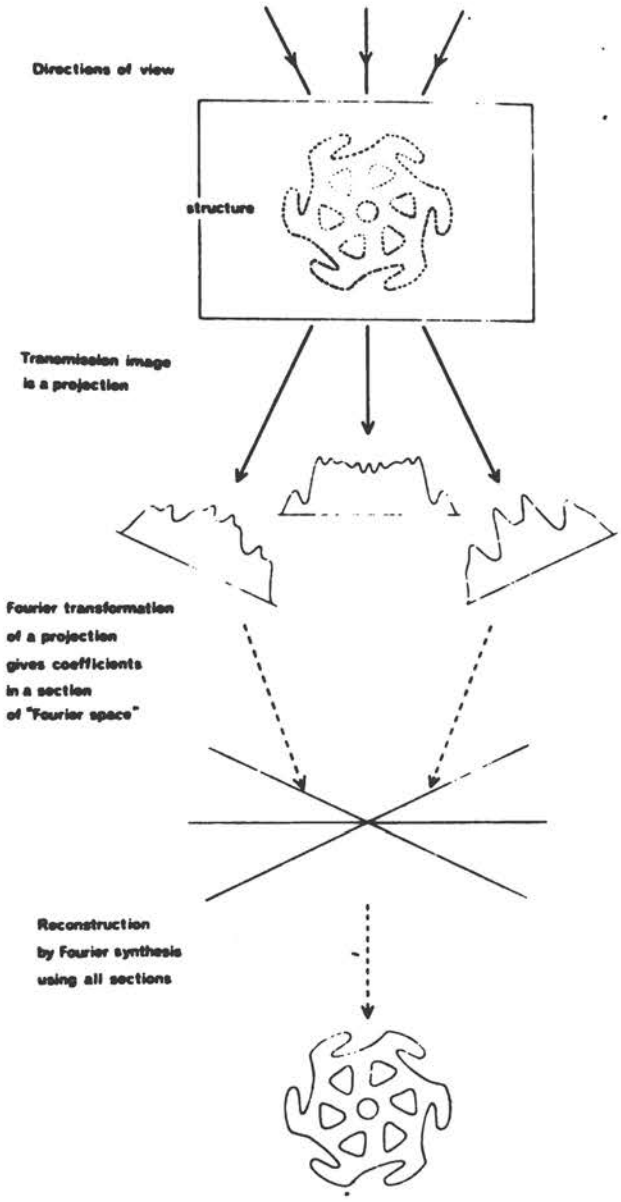

FIGURE 5 Schematic presentation of method used by De Rosier and Klug in reconstructing protein structure from images obtained with electron transmission microscope. Reprinted with permission from De Rosier and Klug.[2]

by light or by chemical processes. The model shows that bacteriorhodopsin is constructed of seven parallel α-helical parts, as shown in Figure 8. Exactly how the pump is stimulated is now being studied. Figure 9 shows another structural unit called a

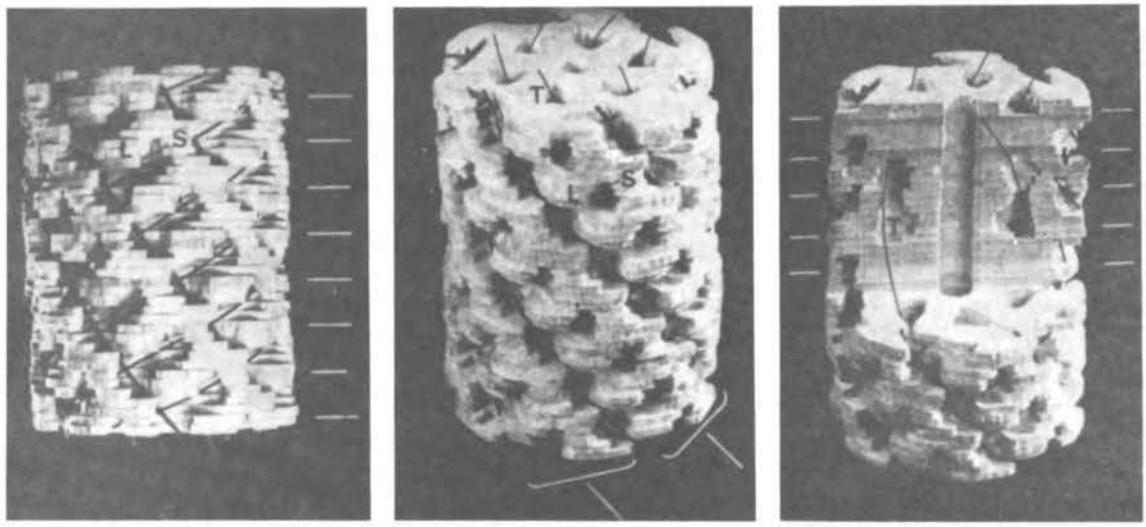

FIGURE 6 Model of tail of phage T4. (a), side view. (b), forward tilting of model. (c), similar to (b) with front half removed, thus exposing core. Reprinted with permission from De Rosier and Klug.[2]

connexon,[12] an example of a so-called gap junction between communicating cells. Transfer of material between cells, through connexons in the membranes, is carried out in the manner shown in the figure. In this model of connexon structure, a rotation of the subunits by about 5^{o} in twist will close the structure and prevent transmission of small molecules and ions. Transmission is allowed by the opposite twist.

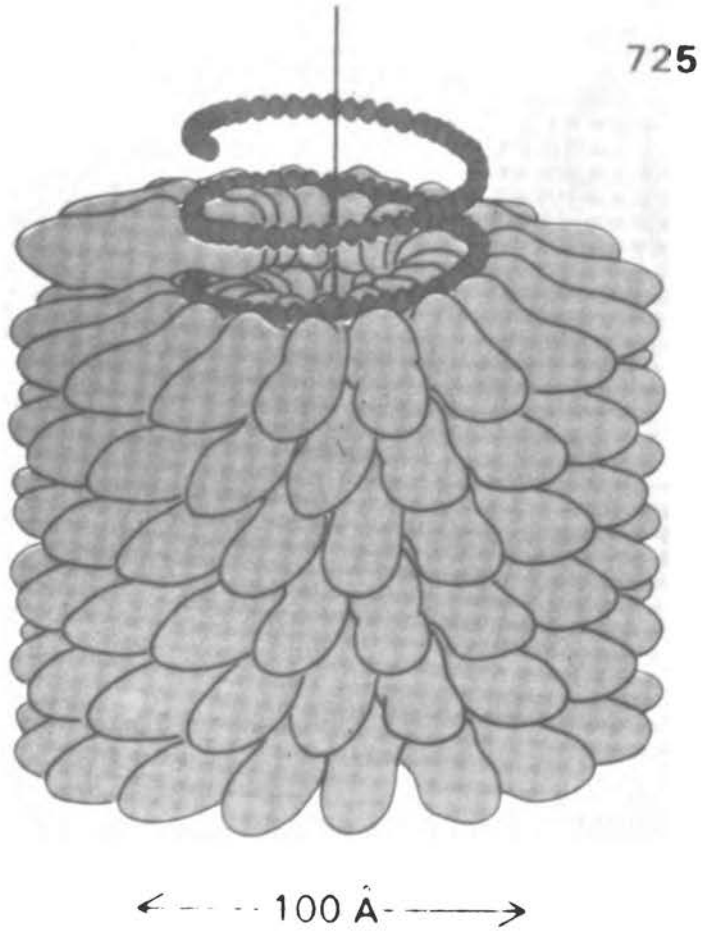

FIGURE 7 Model of small part of extended structure in tobacco mosaic virus. Helical protein subunits surround strand of RNA. Reprinted with permission from Klug and Caspar.[6]

The next item concerns antibodies and crystallography. To a physicist, it might seem strange at first to juxtapose these two subjects, inasmuch as crystals are rigid and inflexible and have little to do with life processes, which require motion and flexibility. However, antibodies may be just large molecules that function according to a program laid out by life processes. Figure 10 shows a drawing of an intact antibody (DobIgG molecule), due to Davies and colleagues,[9] with antigen-active regions at the ends of the two arms. These side arms are called F_{ab} units, and the central arm is called the F_c unit. Uzgiris and Kornberg[13] at Stanford have recently developed a new approach in which he investigates the process of crystallizing antibodies and presumably other proteins in the form of two-dimensional crystals. The

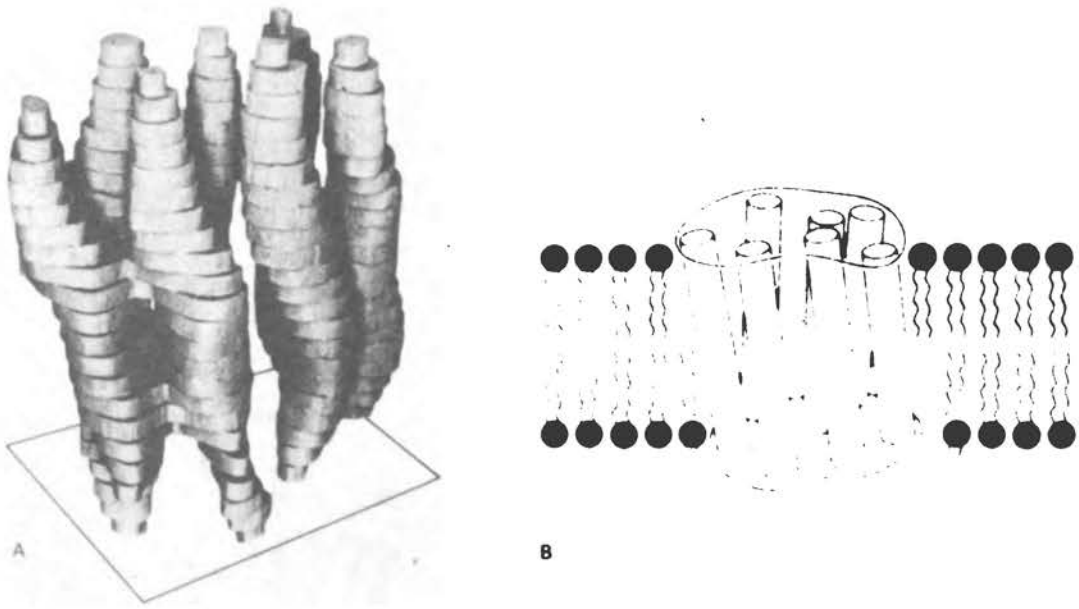

FIGURE 8 Left, model of bacteriorhodopsin protein structure. B, schematic diagram of α-helical structures shown in A as they might appear in lipid bilayer of purple membrane of bacterium. See text for further disussion. Reprinted with permission from Henderson and Unwin[3] (A) and Stryer[10] (B).

possibility of preparing such arrays could increase the power of the electron-diffraction imaging process, because many identical units can be studied in the same image at the same time and noise will average out while the individual unit images are built up coherently. This also means that much less damage will be done by the electrons to any individual antibody unit, in that the beam will be spread out over the whole assembly. As an example, Kornberg has worked on an antigen-antibody complex of N-dinitrophenyl phosphatidylethanolamine (DNP-PE), with a monoclonal anti-DNPIgG antibody of the γ1 subclass.

The two-dimensional technique used by Kornberg involves a process, originally developed by Langmuir and Blodgett, in which a monolayer of lipid material is formed in a monomolecular film. Some of the detailed procedures needed in this process are shown in Figure 11. The film is transferred to a solution in which the desired antibody is adsorbed onto the monolayer. The crystallization process results after a suitable period in the desired two-dimensional crystal. The two-dimensional array is easier to study than some of the three-dimensional structures we have described

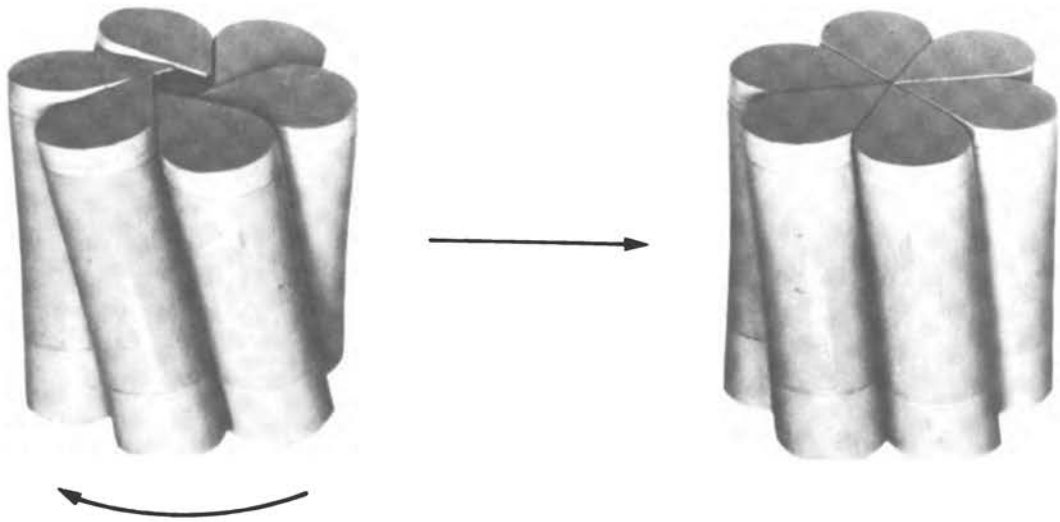

FIGURE 9 Models of closing and opening phases in transfer process of connexon. Reprinted with permission from Unwin and Zampighi.[12]

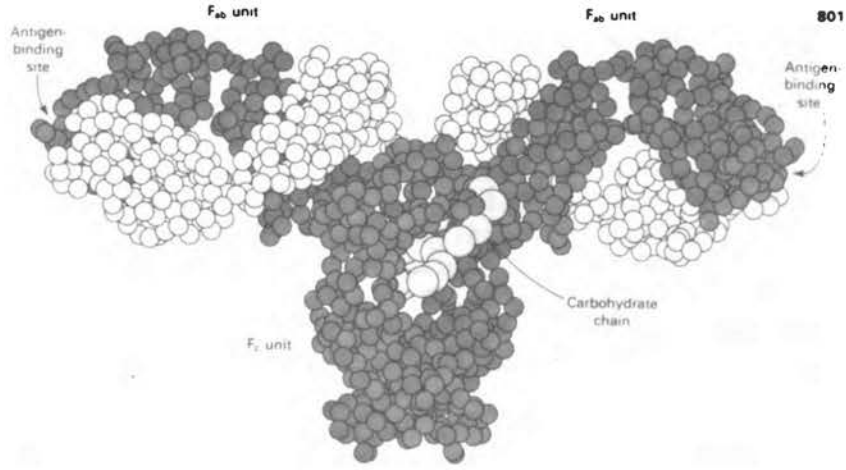

FIGURE 10 Model of intact human antibody (DobIgG). Reprinted with permission from Silverton et al.[9] See text for discussion.

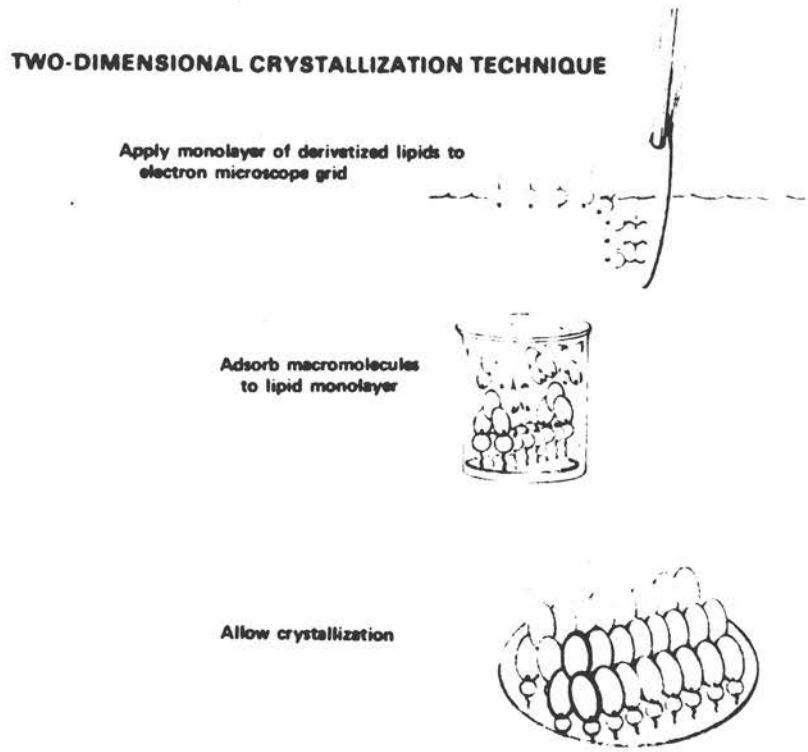

FIGURE 11 Technique used by Kornberg in producing two-dimensional crystals. Lipid, dinitrophenyl phosphatidylethanolamine (DNP-PE), and monoclonal anti-DNPIgG antibody were used in this work, as described in text. Reprinted with permission from Uzgiris and Kornberg.[13]

earlier. Figure 12 shows an electron micrograph of the two-dimensional crystal; the regularity of the image is impressive. Next, as in the method developed by Klug, an optical-diffraction pattern is formed by sending laser light through the regular micrograph image. This results in a series of spots, such as is shown in Figure 13. This beautiful pattern may be analyzed by a well-known Fourier method, and the image of the individual antibody structure may be synthesized. The electron-density profile results from such a synthesis, and Figure 14 shows what it looks like. Figure 15 shows the same profile with the contour lines "fuzzed." The regularity of the image is striking, and the hexagonal symmetry is evident.

The correspondence between the electron-density profile and the antibody structure was demonstrated by Kornberg. The F_c fragment is shown in Figure 16, and the joining of the other two fragments in

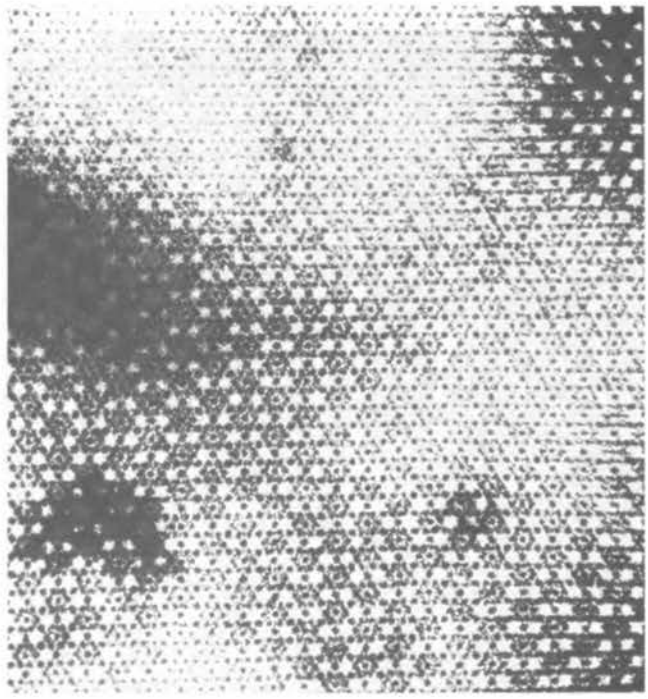

FIGURE 12 Electron micrograph of two-dimensional crystalline array of material described in caption of Figure 11.

Figures 17 and 18. The fit is beautiful and precise. The early ideas about the structure of this antibody are consistent with the new findings, and more detail should now become available. Having established the usefulness of this new approach, one could begin to investigate other protein structures. To study other systems, it should be possible to prepare samples by the technique indicated in Figure 19, and perhaps it will even be possible to produce new protein structures in this way.

The next topic, nuclear medicine, is concerned with diagnosis of disease in internal organs noninvasively with gamma rays. This technique is not new and owes a great deal to the pioneering work of Anger, who used NaI(Tl) as the basic detector for studying gamma rays and their energies. The NaI(Tl) scintillation detector was discovered by me in 1948. McDougall, at Stanford University Hospital, is responsible for the following four figures, which are based on the Anger camera technique. Figure 20 shows the type of facility used to make the nuclear medicine images. It allows tomographic studies to be made by rotation of the detector camera around the patient. Figure 21 shows two images made under different contrast conditions of the bony skeleton of a patient who was given the radioelement ^{99}Tc, in the form of a phosphate, as the source of the gamma rays. The image shown can be compared with images from

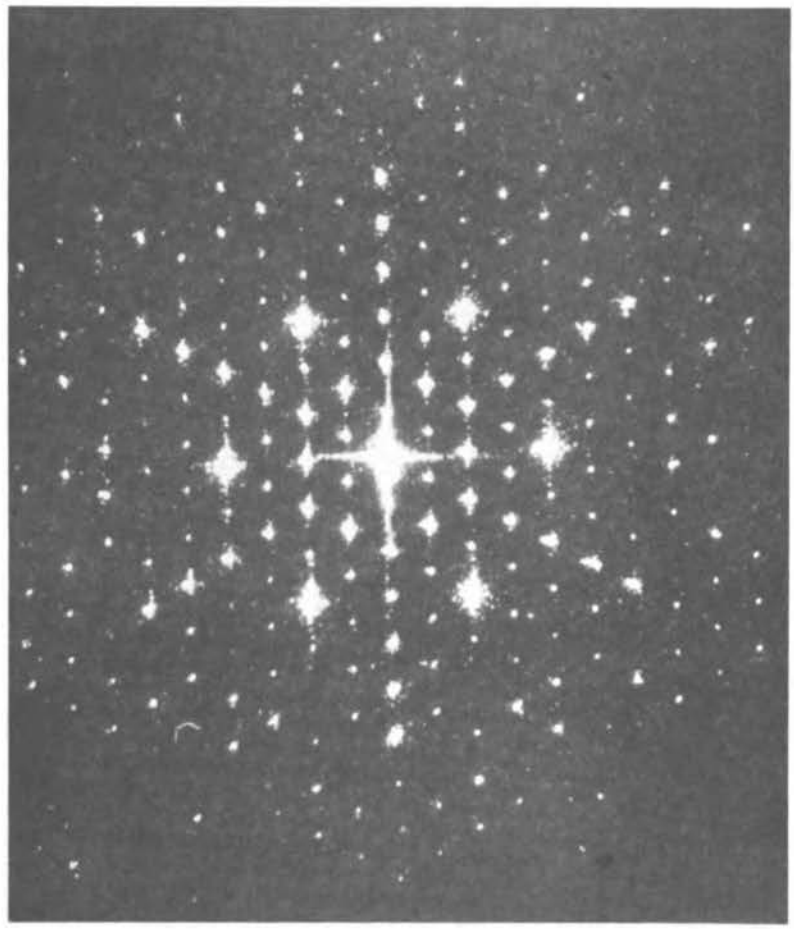

FIGURE 13 Optical diffraction pattern corresponding to electron micrograph of Figure 12.

normal subjects, and thus the onset of a disease can be detected and the course of a disease followed. The second example is related to liver studies. Figure 22 shows four images taken at 15-min intervals after administration of technetium aminodiacetic acid to a normal person. The top image on the left is the first image, and the order runs clockwise. Bile is being sent into the gall bladder and then into the gut in a normal fashion. Acute cholecystitis is the condition shown in Figure 23; a gallstone blocks the duct between the liver and the gall bladder. The second figure is dramatically different from the first, which represents normal functioning.

Another aspect of nuclear physics also uses gamma rays--this time from the annihilation of positrons into two equal-energy gamma rays emitted almost precisely at an angle of 180° with respect to

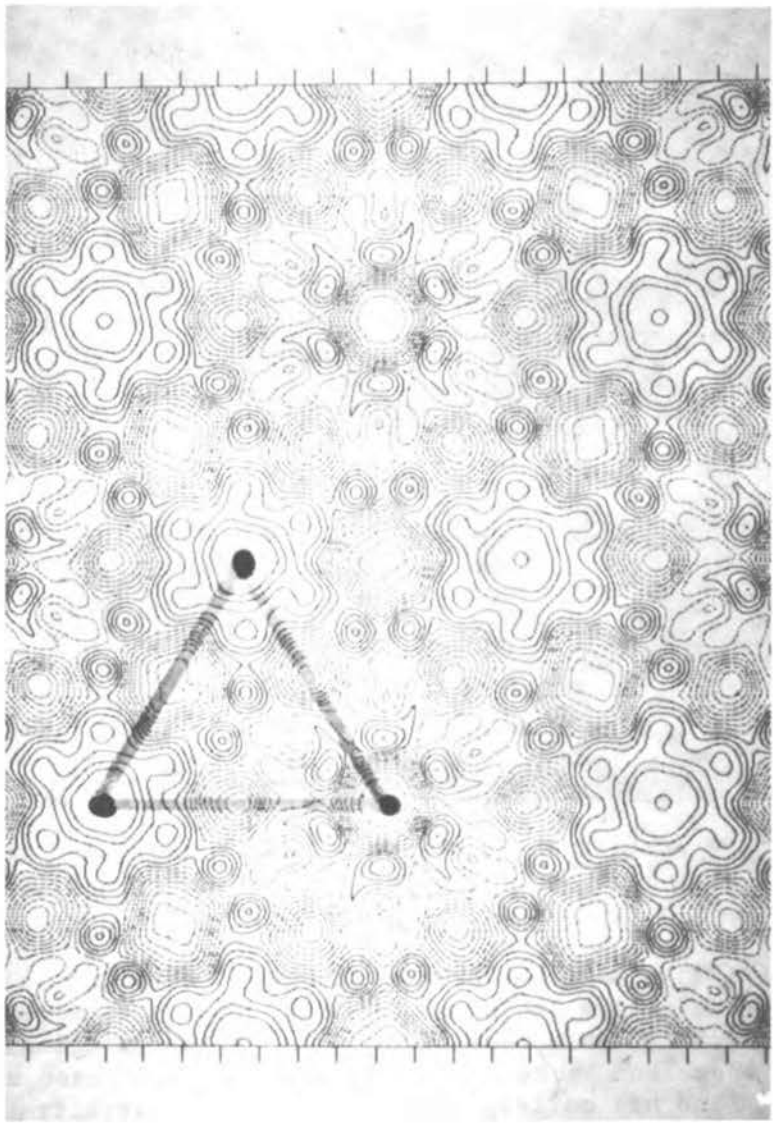

FIGURE 14 Electron density profile obtained from Fourier synthesis of pattern in Figure 13.

each other. Positrons emitted by the radioelement are stopped within less than a millimeter of their points of origin in the organ to be investigated. Practically instantaneously, the two gamma rays are emitted near the stopping position. This technique was invented by Brownell many years ago, and there has been a resurgence of interest in it. It has many new applications to noninvasive studies of the brain and other organs. The technique is called positron emission

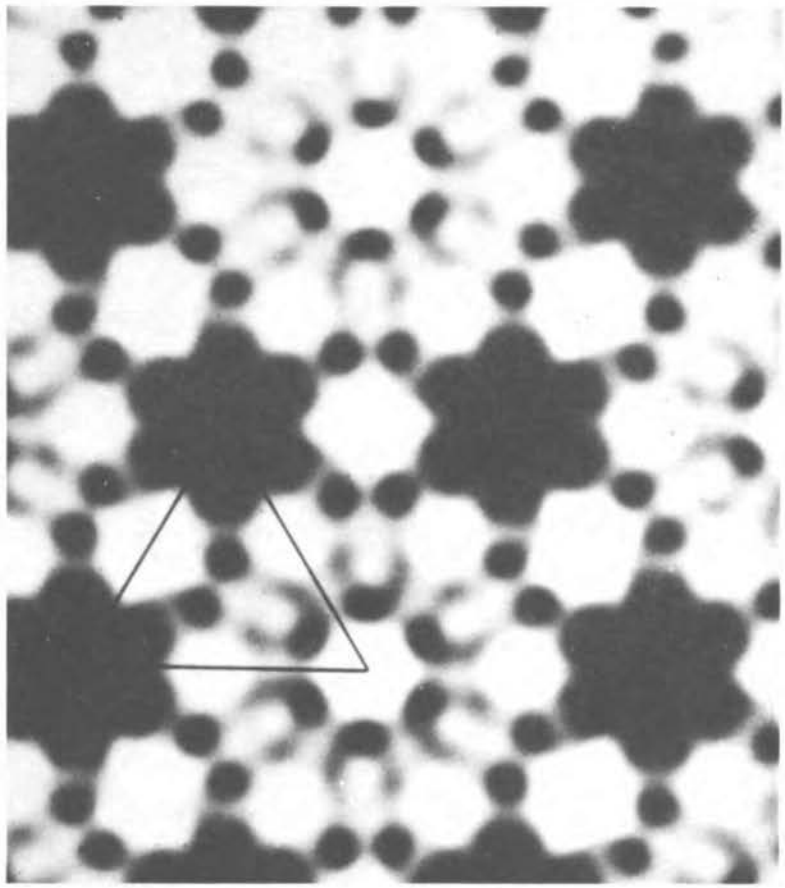

FIGURE 15 Same profile as in Figure 14, but with fuzzed contour lines; hexagonal symmetry is now easy to see.

tomography (PET), and it has been exploited by many groups, including investigators listed in Table 2. Even the time-of-flight coincidence technique has been used to detect the two gamma rays to distinguish them from background. This approach has been used by Ter-Pogossian and his colleagues at Washington University in St. Louis[11] and indeed represents a refined and sophisticated technique taken from nuclear physics. The PET method uses one or more rings of detectors in modular form to detect the gamma rays. With the algorithm associated with 180^{o} emission, the image can be reconstructed. The general idea of the technique can be represented by the schematic diagram of Figure 24.

With the PET procedure, brain scans can be carried out with a resolution of less than a centimeter, perhaps as little as 5 mm. Figure 25 shows a tomographic scan of a young man who was asked to concentrate on a Sherlock Holmes story. It shows that he is

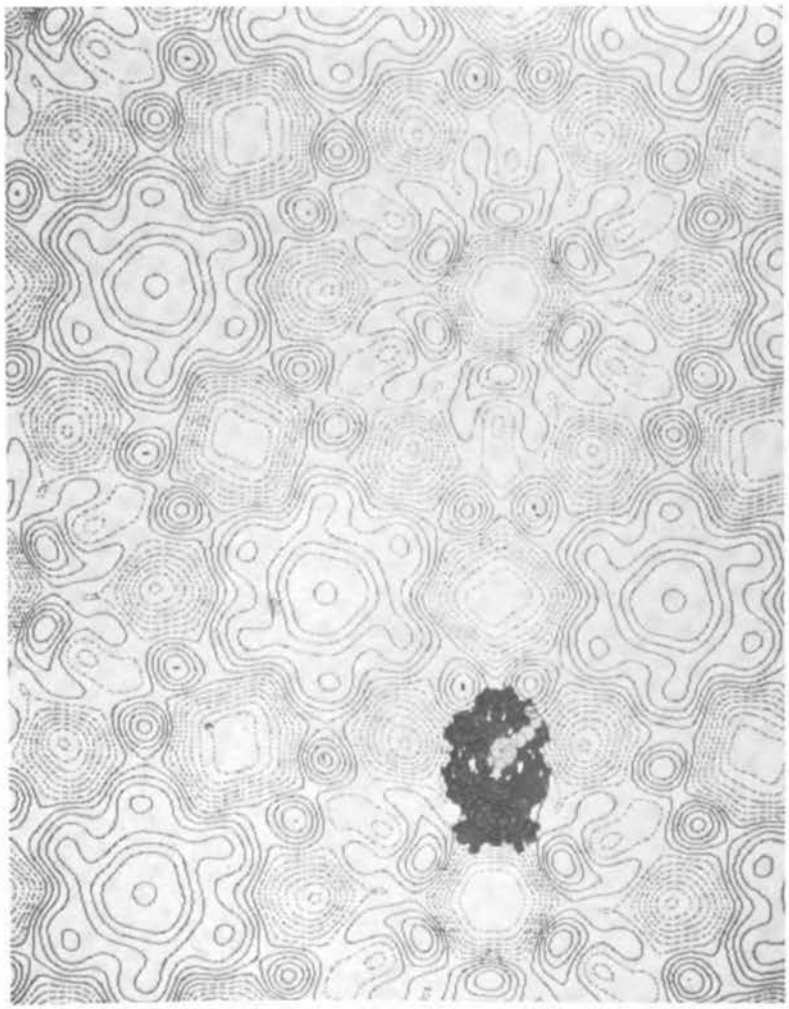

FIGURE 16 F_c fragment discussed in text and obtained by Fourier synthesis; corresponds to model of Silverton et al.[9] Figure courtesy of R. Kornberg.

listening: in the image at the left, his brain is using a considerable amount of glucose in the auditory cortex. The glucose has been attached to a compound containing the radioactive positron source ^{18}F1. Observation of a correlation between thought conditions and metabolism in the brain is new and remarkable and is an example of the connections that have been demonstrated between physical and mental efforts and specific regions in the brain. This effect was first discovered by Lassen in Copenhagen, who used a variant of the tomographic method--single-photon tomography, instead of the two-gamma method used in the PET technique.

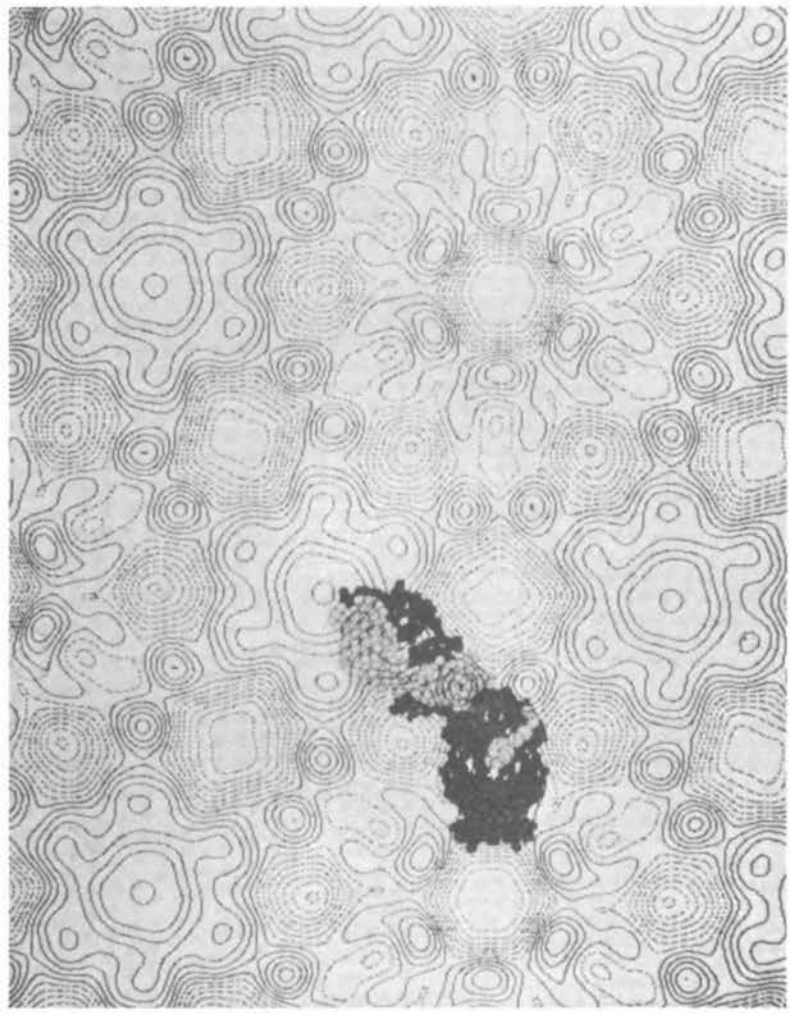

FIGURE 17 Joining-on of one F_{ab} fragment. Figure courtesy of R. Kornberg.

Lassen found that when a patient moved his hand a particular part of his brain would "light up," and when he moved another part of his body another part of his brain lit up. From such observations, we can see the possibility of localizing, by a noninvasive and in vivo method, activities in the brain almost immediately after an action, whether physical or mental. These results suggest new kinds of studies in mental retardation, schizophrenia, epilepsy, stroke, and other disorders of the brain.

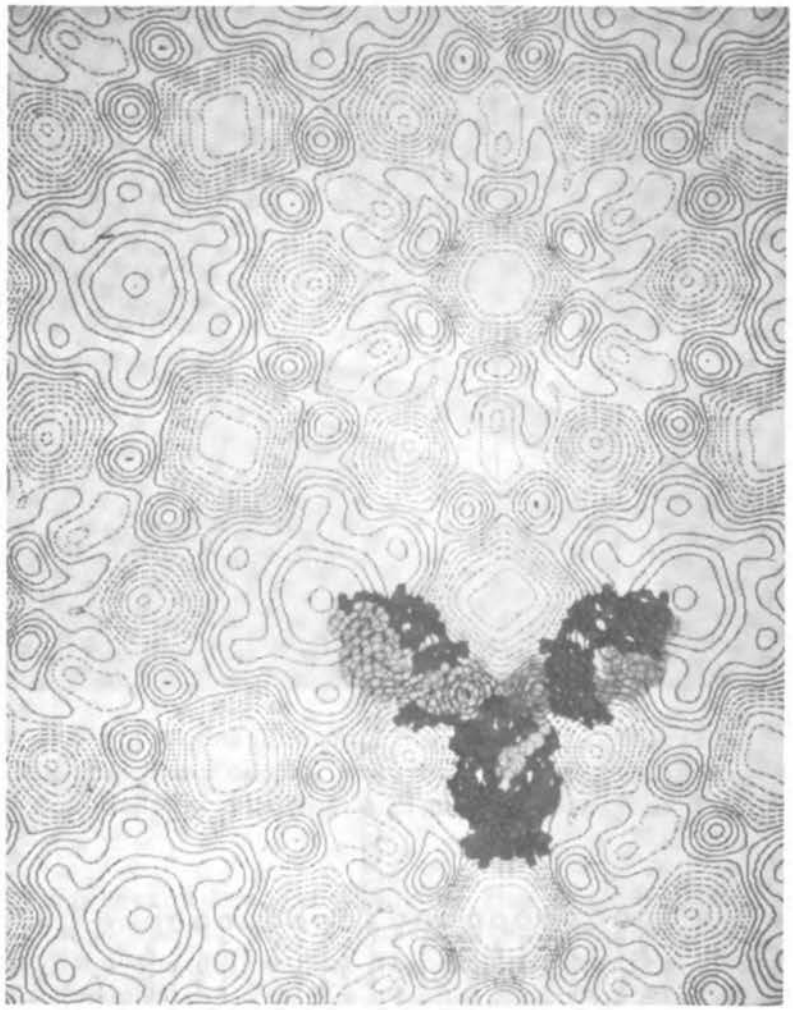

FIGURE 18 Joining-on of other F_{ab} fragment, completing model shown in Figure 10. Figure courtesy of R. Kornberg.

Not every relationship between physics and medicine is confined to imaging, although we have concentrated on such matters up to this point. Physics has contributed in many ways to therapy. In the late forties and early fifties, linear electron accelerators were built in England and the United States by such pioneers as Harvie, Fry, and Hansen for use in nuclear and high-energy physics and for possible use in medical therapy. The motivation in medicine was the clear recognition that radiation in the multimegavolt range could be successful in treating cancer. Miller in England and Kaplan in the United States first made the application to medicine.

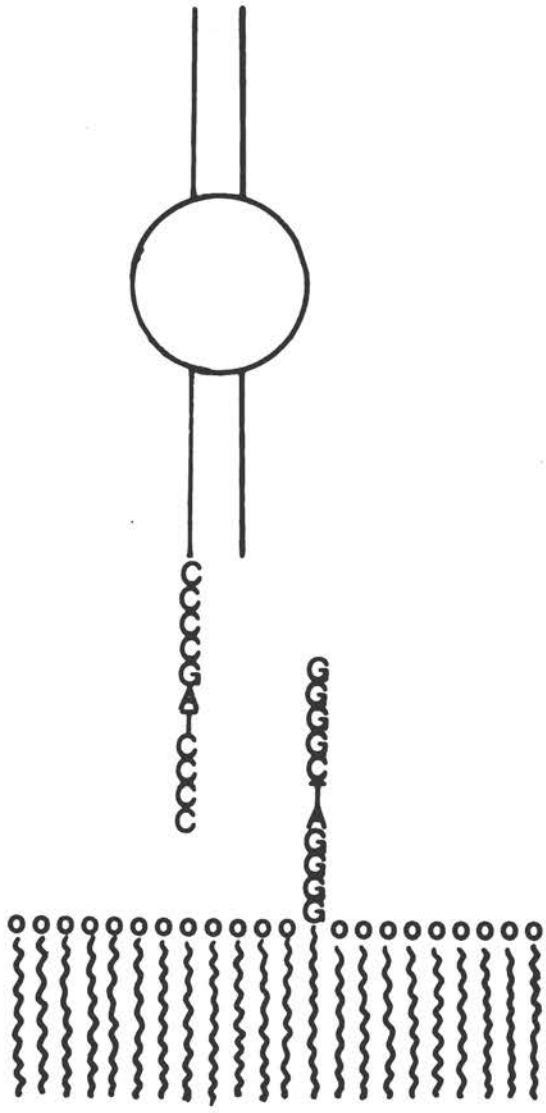

FIGURE 19 Possible extension of two-dimensional crystallization technique.

As an example of a successful approach, we cite Kaplan's work on the treatment of Hodgkin's disease. Ginzton, Kaplan, and Mallory developed a linear accelerator in 1955 at Stanford for medical use, and this machine has been used very successfully over the intervening years. Figure 26 is a photograph of Kaplan (on the left) with this accelerator, taken while it was under construction about 28 years ago. Figure 27 demonstrates the dramatic improvement in

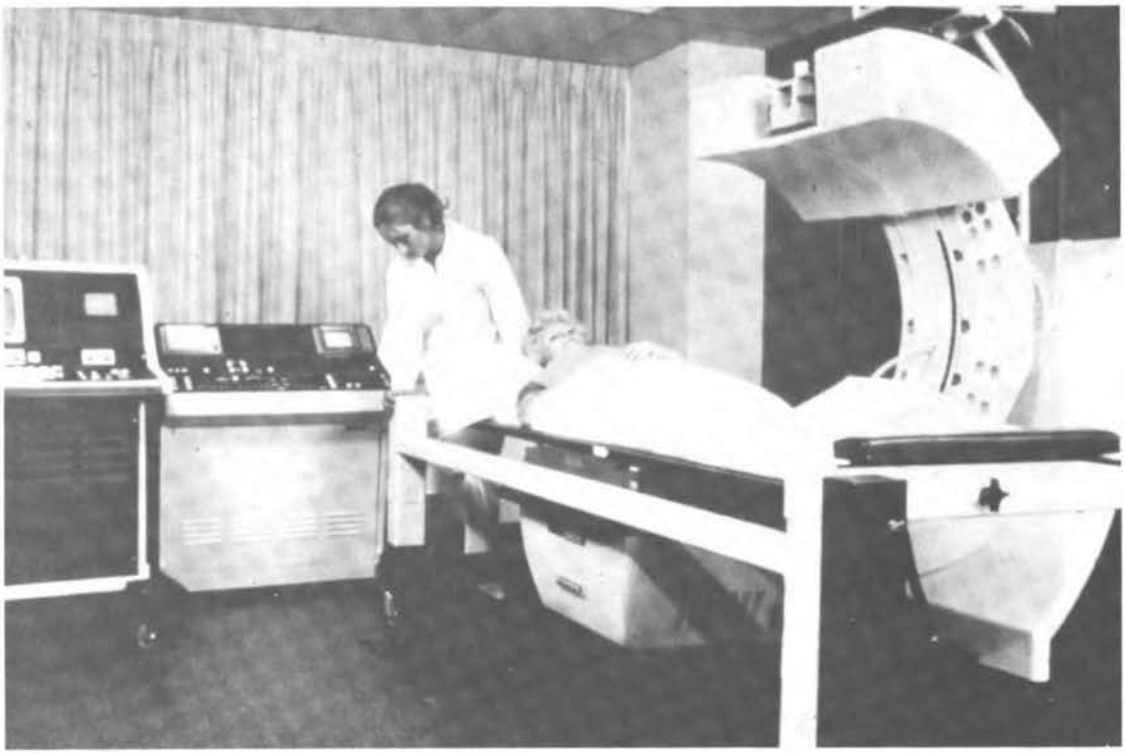

FIGURE 20 Stanford nuclear-medicine diagnostic facility contains Omega gamma camera made by Technicare and allows tomographic studies. Figure courtesy of R. McDougall.

the survival fraction brought about by the use of the accelerator, which, as stated above, is a sophisticated device arising from the original need to do nuclear and high-energy physics. In this case, the active therapeutic agent is a combination of x rays and gamma rays, which are produced by bremsstrahlung--electromagnetic radiation of various wavelengths that accompanies the stopping of a high-energy electron in matter.

The next application describes dynamic x-ray imaging with a new device. This device is being introduced into the medical profession for studies of the heart while in motion, for blood flow through the chambers of the heart, and for other applications that require x-ray images of internal organs in motion. The device is called an Imatron and involves the technique of computed tomography (CT) using x rays. Very large intensities are needed to freeze motion, and conventional x-ray tubes do not have sufficient target yields. To avoid the overheating in a single x-ray target, many targets are used. The full intensity of the electron beam can then be applied to each target. At the same time, if all the targets are arranged

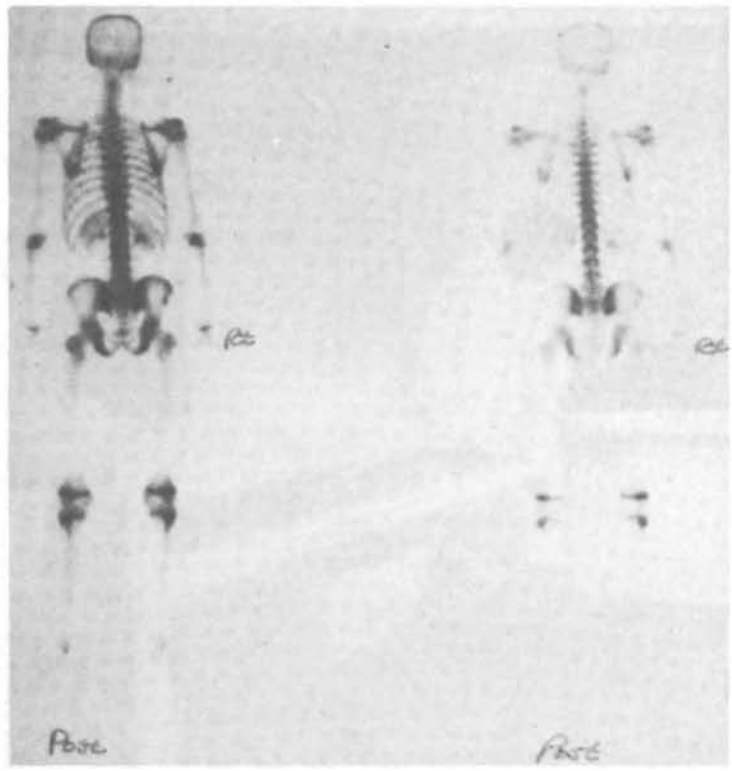

FIGURE 21 Images of skeleton of patient taken by Omega camera after administration of ^{99}Tc. Two images taken with different contrast. Figure courtesy of R. McDougall.

in an arc of a circle, one can immediately use the full power of CT. For the electron beam to be able to strike the multiple targets, a beam-deflection system is used; and the extremely small inertia of the beam makes rapid transversal of all the targets possible. To get the highest intensity in the electron beam, focusing on the targets is carried out, and this is very important if there is to be enough x-ray yield to "stop" motion. Figures 28 and 29 show the practical configurations that have proved useful. Images of the heart in motion are shown in Figure 30. The successive images were taken in 50-ms exposures, 8 ms apart. The case illustrated represents dysfunction of the intraventricular septum. The figures related to the Imatron were provided by D. Boyd and R. Rand, who are developers of this interesting facility.

Because a large part of this conference concerns magnetic resonance imaging (MRI), it is not my intent to discuss this method. However, I cannot resist showing a superb example of an image taken by Kaufman at the University of California, San Francisco. Figure 31 represents a section through a human head.

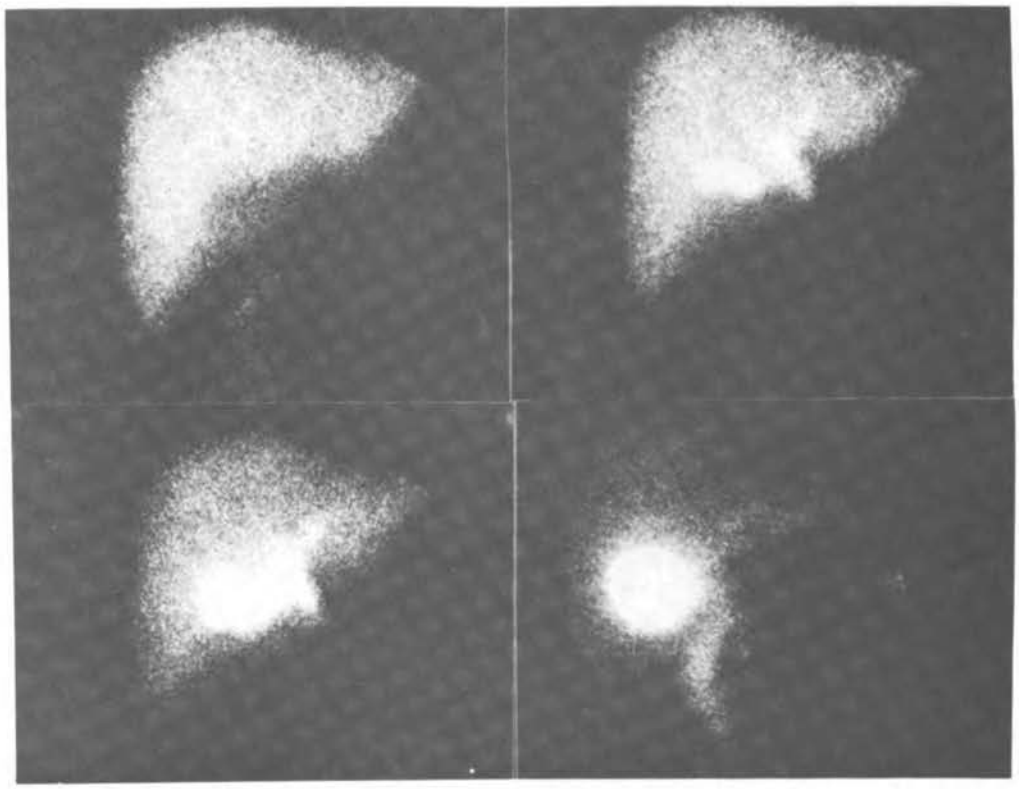

FIGURE 22 Liver studies using succession of four images taken at 15-min intervals after administration of ^{99}Tc-aminodiacetic acid. Patient shows normal functioning. Images are in the order top left, top right, bottom left, and bottom right; first one is at upper left. Figure courtesy of R. McDougall.

The detail exhibited in the figure is breathtaking and is a result of the famous discovery of nuclear induction by Bloch and Purcell--a process originally aimed at finding the magnetic moments of atomic nuclei. The importance of MRI can hardly be overstated, and the remarkable thing about it is that it is completely noninvasive and nonionizing.

The last association I will speak of between physics and medicine concerns what may appear to be the most unlikely application of Einstein's relativity physics. This application involves our own research into the imaging of the human coronary arteries. It is well known that the methods of such imaging that are now used developed out of the necessity of finding approaches in which the motion of the arteries, lying on the surface of a beating heart, could be imaged in sufficient detail to allow assessment of the amount of blockage, caused by plaque, in those arteries. Such

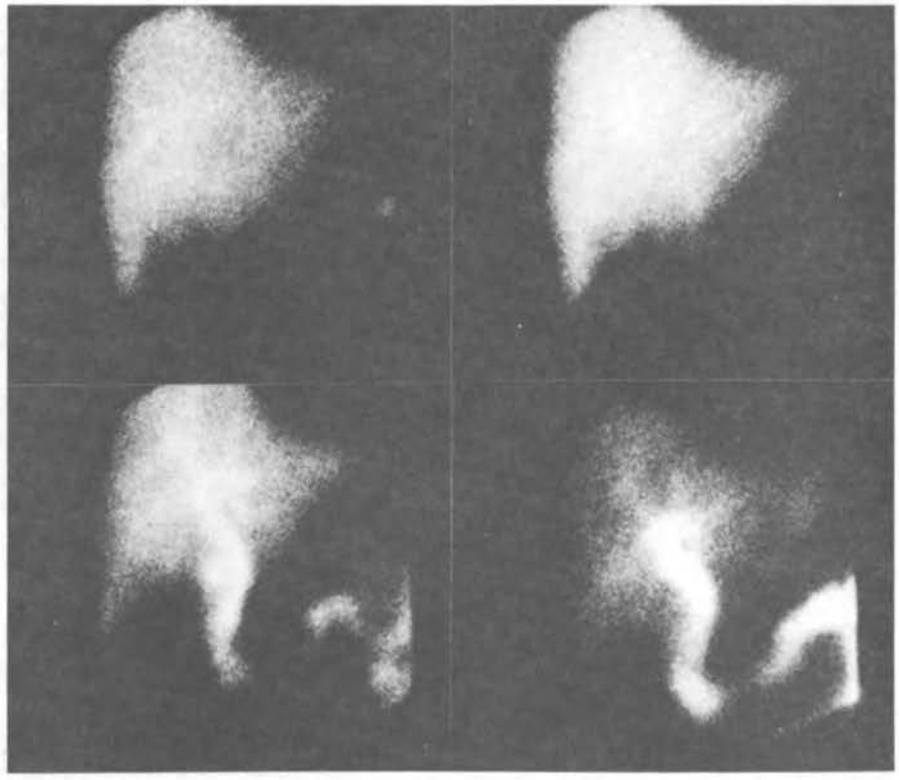

FIGURE 23 Similar to Figure 22, but patient has gallstone blockage. See text for further discussion. Figure courtesy of R. McDougall.

necessity has dictated the placement of catheters in major coronary vessels and injection under external pressure of dyes opaque to the x rays that are used in radiologic diagnosis. Moreover, the x-ray sources that need to be used represent the state of the art in intensity and filtration. All together, the medical procedure is arduous, involves hospitalization, is uncomfortable, and bears a risk that is not negligible. I will not go into details, but one may imagine that a noninvasive solution to coronary artery visualization would be of great benefit to those who suffer from coronary occlusion or conditions leading to coronary heart disease.

For this reason, Hughes, Rubenstein, and I initiated some studies several years ago into a new method of using synchrotron radiation that is Bragg-diffracted so as to become virtually monoenergetic. By using a sharply delimited x-ray beam that is confined to a thin strip and is nearly monoenergetic, we can tune the energy to the K-edge of iodine (33.16 keV), which is the absorbing element in the dye used in the standard imaging processes. Then, by a method first described by Jacobson[5] in

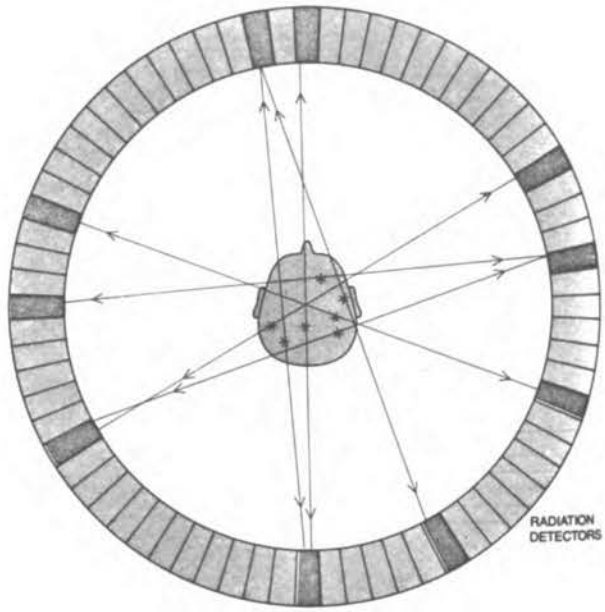

FIGURE 24 Schematic presentation of ring of detectors for two gamma rays of positron annihilation in PET technique. Two gamma rays are emitted back to back and in coincidence with each other. Many such coincident events can gradually be synthesized to form image. Reprinted with permission from Ter-Pogossian et al.[11]

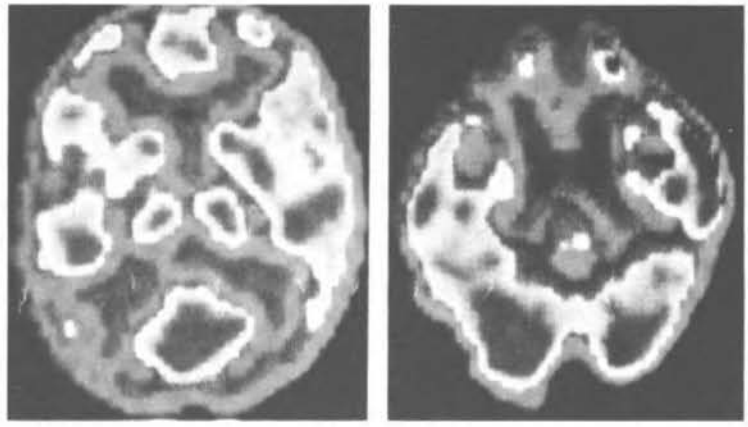

FIGURE 25 Tomographic scans by PET method of brain of young man who was asked to concentrate on Sherlock Holmes story. See text for further discussion. Scans were produced by John Mazziotta and colleagues of UCLA. Reprinted with permission from U.S. Medicine.[1]

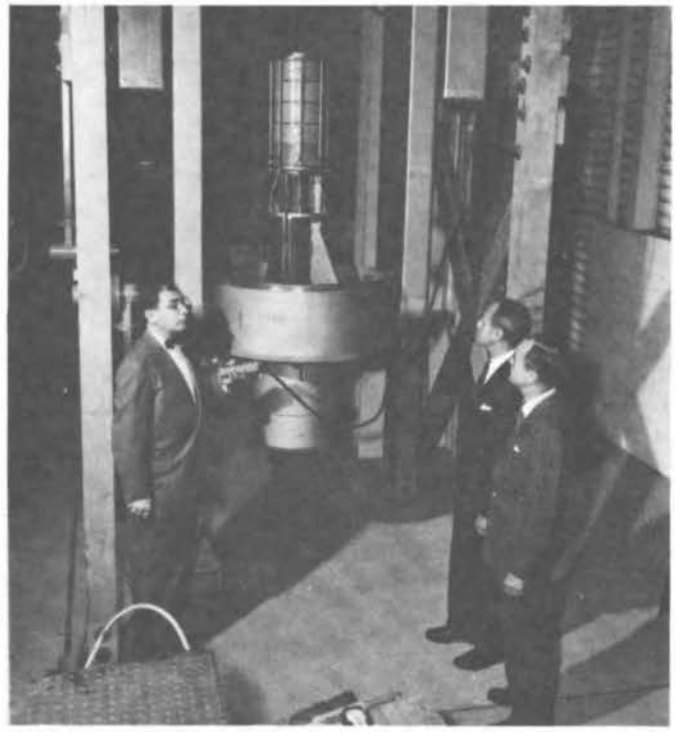

FIGURE 26 Photograph of H. S. Kaplan, left, with linear electron accelerator produced for successful treatment of Hodgkin's disease.

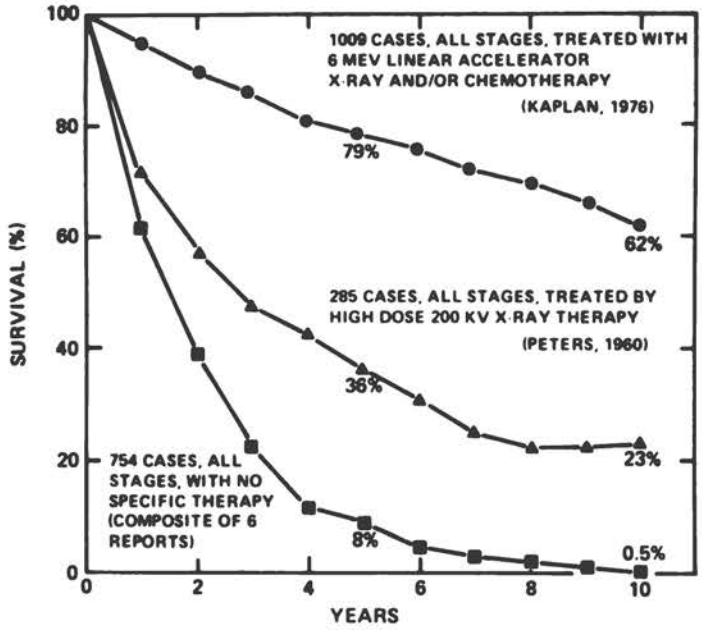

FIGURE 27 Survival rates in Hodgkin's disease in patients treated with Kaplan electron linear accelerator technique and other treatment modes. Figure courtesy of H. S. Kaplan.

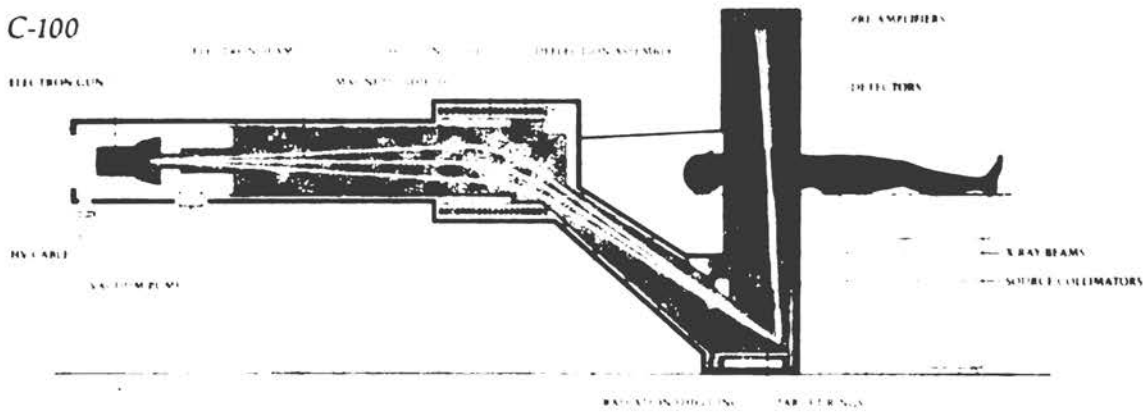

FIGURE 28 Side view of new commercial CT device, Imatron. Figure courtesy of R. Rand.

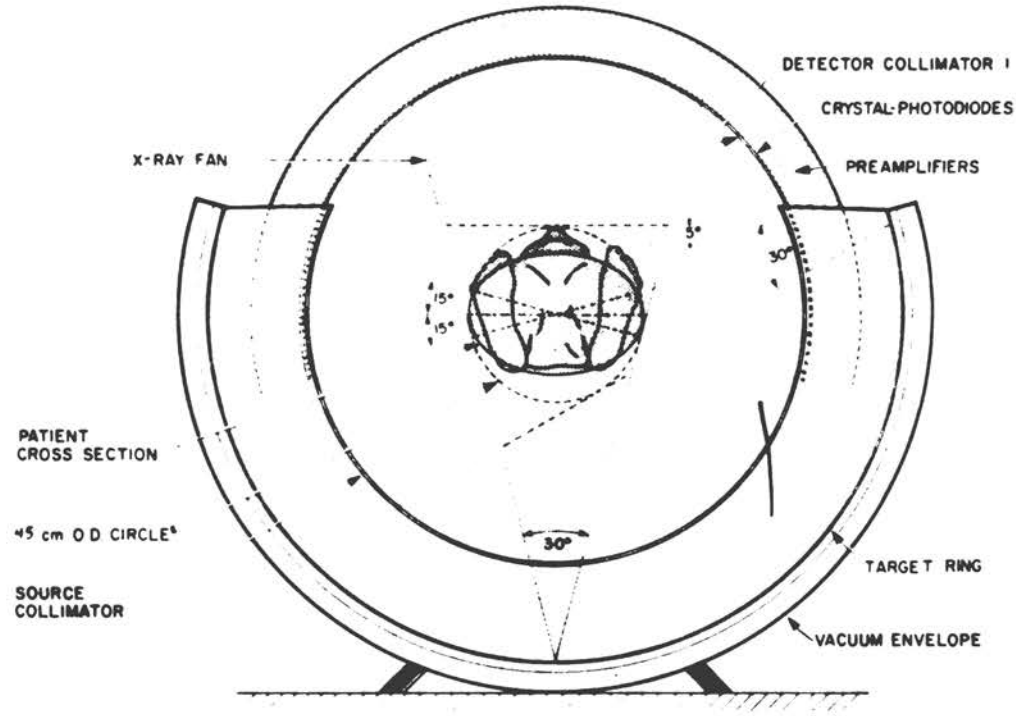

FIGURE 29 Fan of x rays issuing from single struck target in Imatron. Figure courtesy of R. Rand.

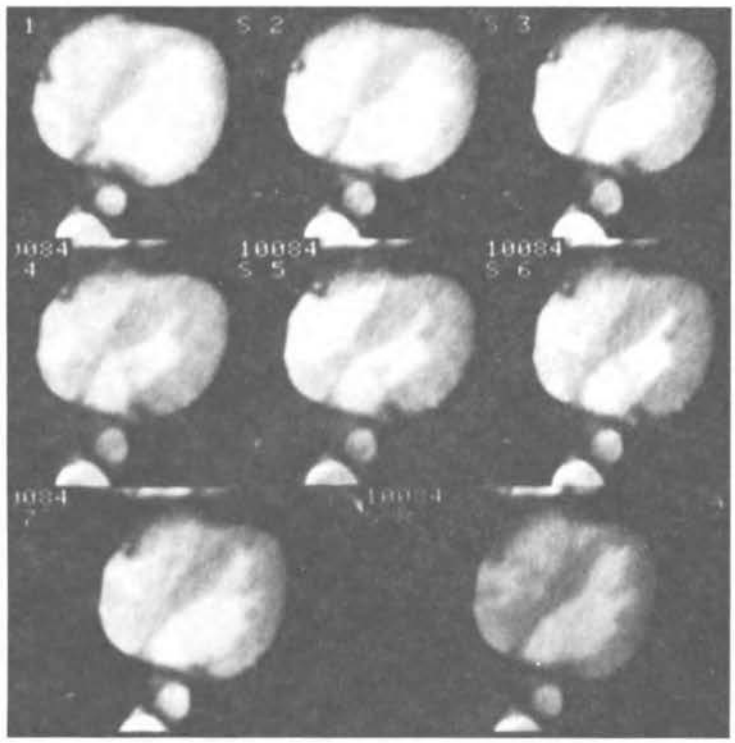

FIGURE 30 Successive images of beating heart with dysfunction of intraventricular septum. Figure courtesy of R. Rand.

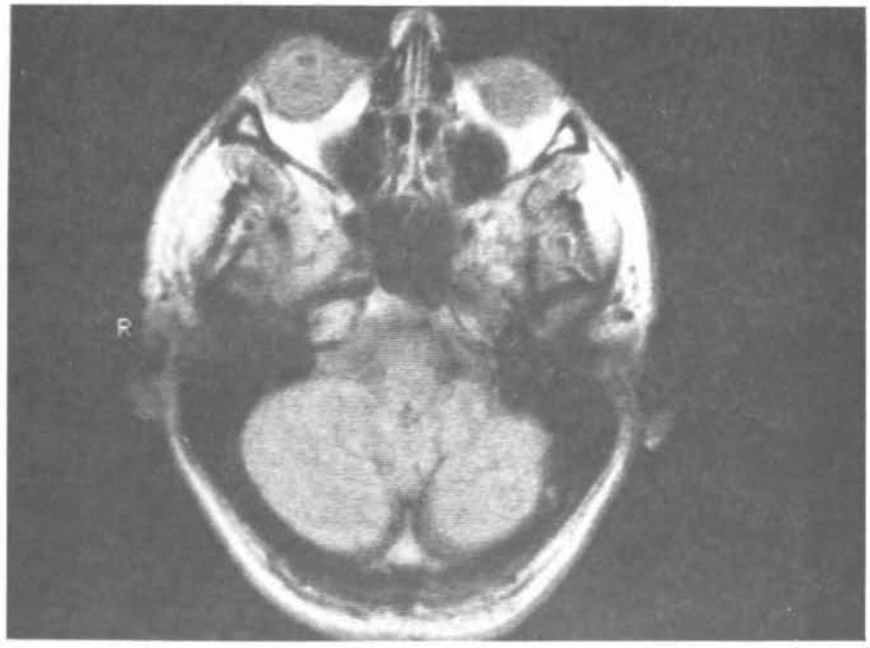

FIGURE 31 Clear and detailed MRI image of section through human head. Figure courtesy of L. Kaufman.

1953, a subtraction of two transmitted intensities--one slightly above and one slightly below the K-edge--removes all artifacts from the recorded image and exhibits only the vessels filled with iodine solution. Artifacts, in this case, include bone and tissue, which appear in all unsubtracted images and which usually make examination of blocked arteries difficult, if not impossible. Figure 32 shows how the vertical jump in absorption coefficient at the K-edge makes a large difference in the actual absorption of 33-keV radiation, whereas bone and tissue--containing only carbon, nitrogen, hydrogen,

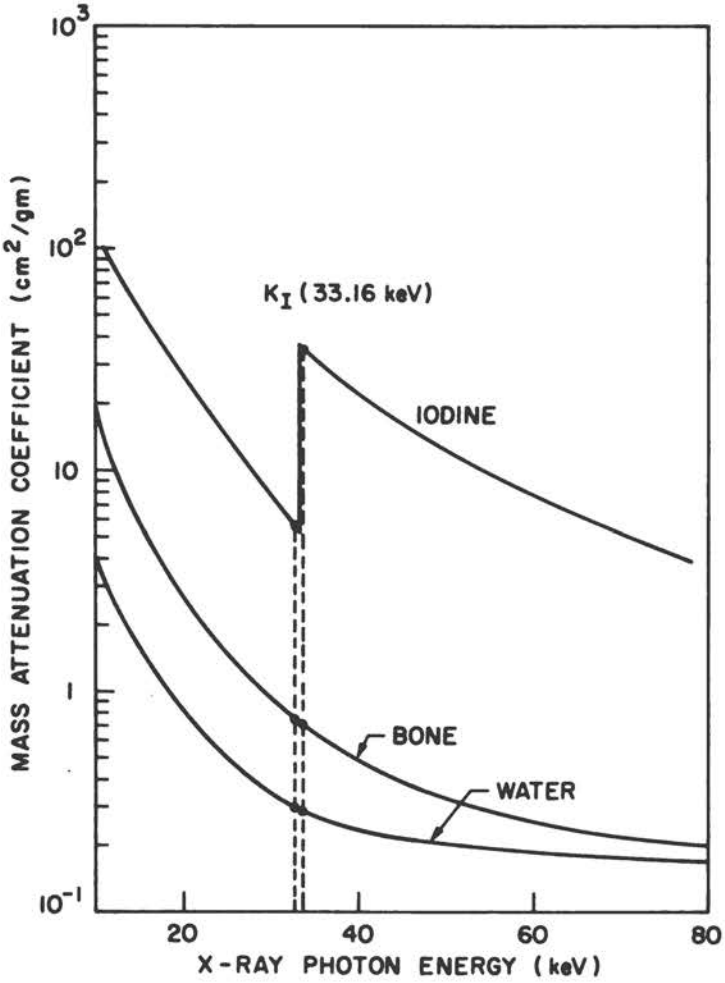

FIGURE 32 Behavior of absorption cross section for x rays in neighborhood of K-absorption edge of iodine. Also included are corresponding behaviors of bone and water (latter represents tissue). In digital subtraction technique, iodine jump will show presence of iodine, but bone and tissue absorption will cancel out. Reprinted with permission from Hughes et al.[4]

and oxygen--disappear in the subtracted image of transmitted intensity. Digital subtraction with computer techniques allows almost instantaneous recording of the desired image.

The use of Bragg diffraction to make monoenergetic x rays produces a great loss in intensity, because of the narrow energy interval extracted from a continuous x-ray beam. It is therefore necessary to use the greatest possible source strength, and x-ray tubes whose targets are struck by electrons simply do not have adequate yields. One must find a new source of x rays not subject to the conventional limitations. Here is where the theory of relativity gives us the necessary geometric beam profile and the required beam intensity to make the K-edge method possible. The Lorentz transformation, such an intimate part of Einstein's theory, causes the continuous x-ray beam radiated by electrons traveling in a horizontal circular path to be confined to a thin vertical strip whose width depends on the angular arc that determines the extent of the tangential x radiation viewed by the Bragg monochromator. The beam so produced is illustrated in Figure 33, and an experimental layout permitting examination of phantoms and excised pig and calf hearts, obtained in butcher shops, is shown in Figure 34.

With such a facility, developed at the Stanford Synchrotron Radiation Laboratory, a storage ring, customarily used for high-energy physics, is used as the source of the synchrotron radiation. Figure 35 shows results obtained with an excised pig heart whose coronary arteries have been filled with a Renografin solution,[4] the dye used in standard practice for arteriography and angiography. Many problems arise in applying the method to examination of human patients. One concerns the reduction in contrast when the arteries are viewed in the same straight lines as the already filled heart chambers. Another, already solved by our approach, is the instantaneous "freezing" of the image of the moving coronary arteries. With a very short interval between the two images formed at the two slightly different energies, such as a few milliseconds, the subtracted image eliminates defocusing and the image should be sharp, although possibly distorted a small amount from top to bottom. Although some problems are anticipated, they can be studied by in vivo methods with laboratory animals. A small number of experiments have been carried out at Stanford University, with encouraging results. One result, obtained with a dog, is shown in Figure 36. This figure shows a single coronary artery whose image has been made clearer by edge-enhancement techniques. Other encouraging results have been obtained. Much remains to be done, but the result shown in Figure 36 is promising, for much of the technique now used is made difficult by the lack of an x-ray beam wide enough to picture the entire heart region in the dog. A new beam in preparation will be wide enough to view the entire human heart. In about a year and a half, it is hoped, human studies can

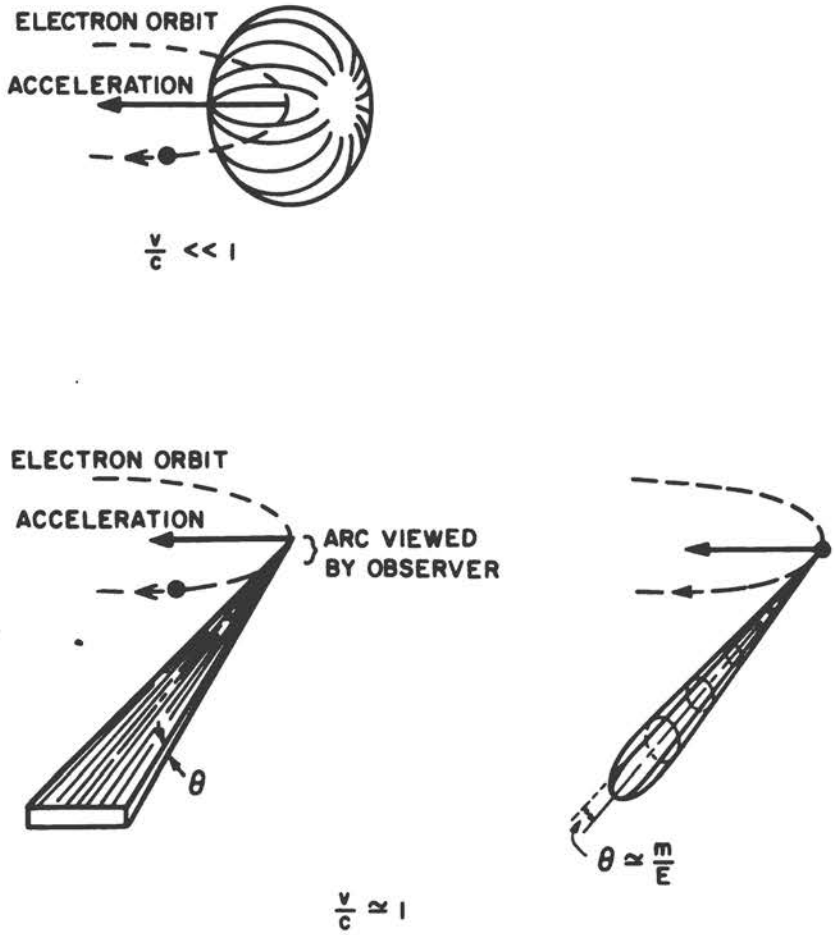

FIGURE 33 Pattern of radiation emitted by electrons traveling in curved arcs. Top, speed of electrons is low, compared with speed of light. Bottom, speed is virtually speed of light. Radiation pattern's height is markedly reduced in lower part of figure, because of Lorentz transformation, intimate part of Einstein's theory of relativity. Storage ring can keep electrons in such curved paths when electromagnetic energy is supplied to electron beam in microwave cavities, to compensate for energy radiated in form of synchrotron radiation. Such radiation includes visible light, ultraviolet light, and x rays in continuum. Bragg diffraction by crystal monochromator extracts nearly monoenergetic band from this wide continuum. Energy of band may be varied by changing angle of incidence of beam on monochromator and represents method used in proposed new technique of coronary angiography described in text. Figure courtesy of H. Winick.

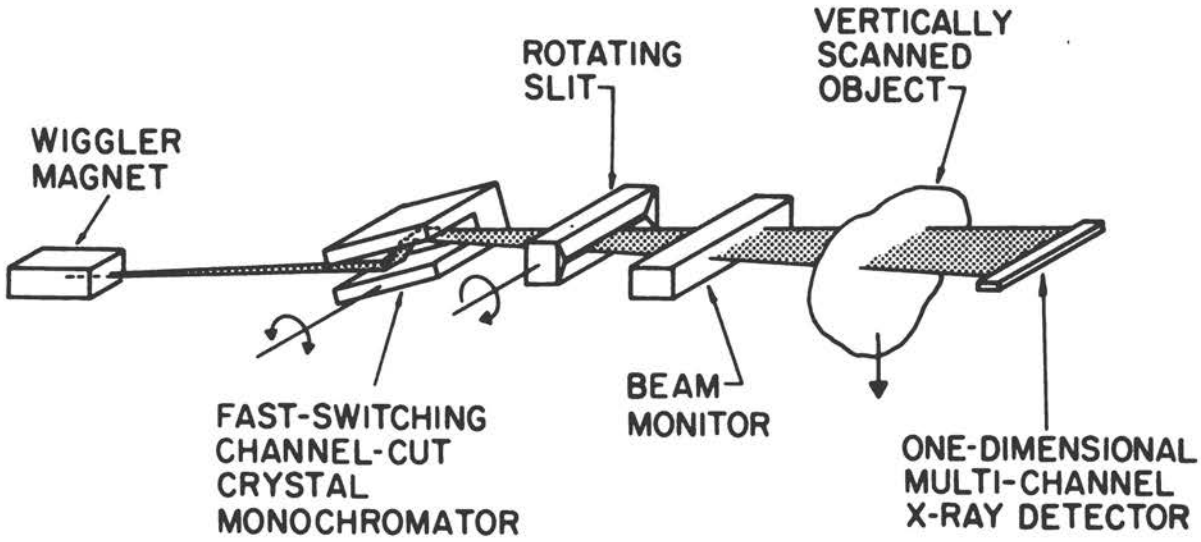

FIGURE 34 Schematic diagram of x-ray beam used in experiments on phantoms and excised pig and calf hearts. Storage ring providing beam is at Stanford Synchrotron Radiation Laboratory. Reprinted with permission from Hughes et al.[4]

be started. Arterial catheterization will not be required, because a satisfactory image, with a good signal-to-noise ratio, may be expected from the very large intensity provided by the storage ring's synchrotron radiation and the further enhancement of the intensity by the "wiggler,"[15] placed in a straight section of the storage ring.

The application of synchrotron radiation to the important technique of coronary angiography thus appears to be a most unexpected and dramatic application of sophisticated methods of high-energy physics to medical practice. It is sincerely hoped that the experiments that will be carried out in the near future will be successful enough to provide early warning of potential coronary problems in humans.

(a)

(b)

FIGURE 35 Digitally subtracted images of arterial system in excised pig heart for projection angles of (a) 30° and (b) 75° relative to A-P (0°) projection. Iodine concentration, 20 mg/ml. Reprinted with permission from Hughes et al.[4]

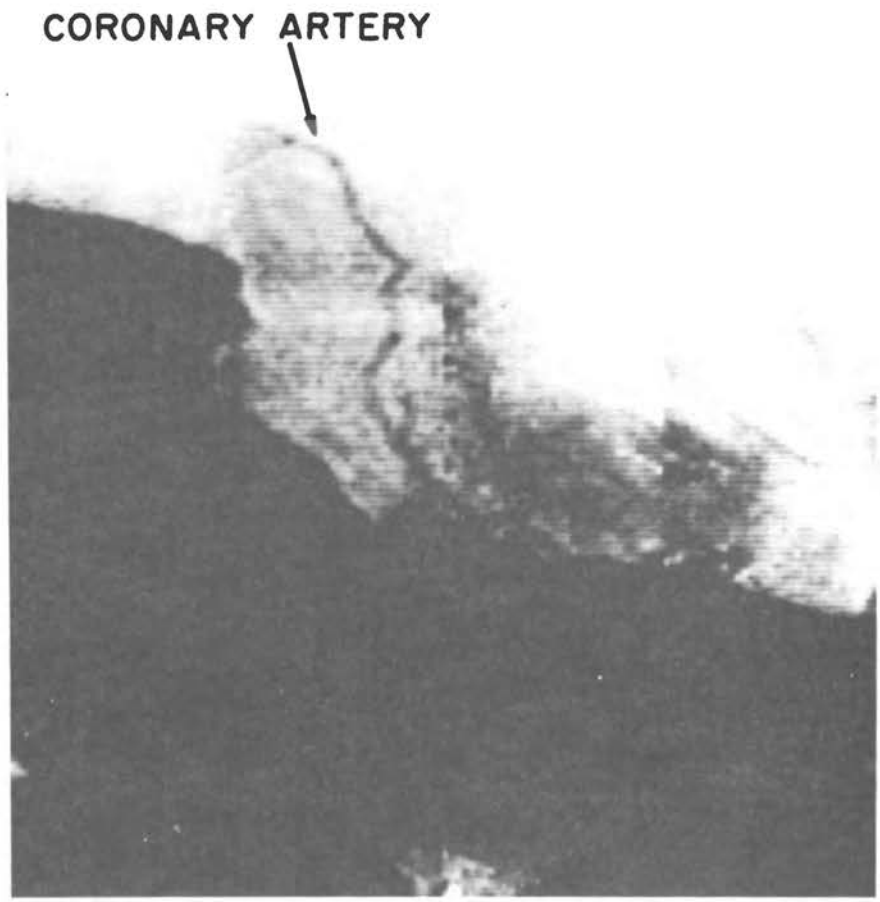

FIGURE 36 Image of single coronary artery observed in in vivo examination of dog, edge-enhanced to show outline more clearly. See text for further discussion. Reprinted with permission from Hughes et al.[4]

ACKNOWLEDGMENTS

I wish to thank Drs. Donald Kennedy and Andrew D. Suttle, Jr., for their invitation to present this paper at the National Conference on Biological Imaging. I would also like to thank Dr. Cecil H. Green for his encouragement during the preparation of the work reported here. I am especially grateful to Drs. D. Boyd, B. A. Carroll, E. L. Ginzton, H. S. Kaplan, L. Kaufman, R. G. Kornberg, I. R. McDougall, C. F. Quate, R. Rand, E. Rubenstein, and P. N. T. Unwin for their generous contributions in material and time toward the preparation of this paper. However, they are not responsible for any defects that may appear in this presentation of their work. Finally, I wish to thank Drs. E. B. Hughes, H. Winick, and H. D. Zeman for providing several figures for the text and N. B. Bettini for help in preparing the manuscript.

REFERENCES

1. Brain scanning forges new frontiers. U.S. Med. 19(13):1, 1983.

2. De Rosier, D. J., and A. Klug. Reconstruction of three dimensional structures from electron micrographs. Nature 217:130-134, 1968.

3. Henderson, R., and P. N. T. Unwin. Three-dimensional model of purple membrane obtained by electron microscopy. Nature 257:28-32, 1975.

4. Hughes, E. B., H. D. Zeman, L. E. Campbell, R. Hofstadter, U. Meyer-Berkhout, J. N. Otis, J. Rolfe, J. P. Stone, S. Wilson, E. Rubenstein, D. C. Harrison, R. S. Kernoff, A. C. Thompson, and G. S. Brown. The application of synchrotron radiation to non-invasive angiography. Nucl. Instrum. Meth. 208:665-675, 1983.

5. Jacobson, B. Dichromatic absorption radiography; dichromography. Acta Radiologica 39:437-452, 1953.

6. Klug, A., and D. L. Caspar. The structure of small viruses. Adv. Virus Res. 7:225-325, 1960.

7. Quate, C. F. Microwaves and imaging. Stanford Eng. Fall/Winter:22, 1981-1982.

8. Ruska, E. The Early Development of Electron Lenses and Electron Microscopy. Stuttgart: S. Hirzel Verlag, 1980. 140 pp.

9. Silverton, E. W., M. A. Navia, and D. R. Davies. Three-dimensional structure of an intact human immunoglobulin. Proc. Natl. Acad. Sci. USA 74:5140-5144, 1977.

10. Stryer, L. Biochemistry. 2nd ed. San Francisco: W. H. Freeman, 1981. 949 pp.

11. Ter-Pogossian, M. M., M. E. Raichle, and B. E. Sobel. Positron-emission tomography. Sci. Amer. 243(4):170-181, 1980.

12. Unwin, P. N., and G. Zampighi. Structure of the junction between communicating cells. Nature 283:545-549, 1980.

13. Uzgiris, E. E., and R. D. Kornberg. Two-dimensional crystallization technique for imaging macromolecules, with application to antigen-antibody-complement complexes. Nature 301:125-129, 1981.

14. Williams, R. C., and H. W. Fisher. An Electron Micrographic Atlas of Viruses. Springfield, Ill.: Charles C Thomas, 1974. 128 pp.

15. Winick, H., and J. E. Spencer. Wiggler magnets at SSRL: Present experience and future plans. Nucl. Instrum. Meth. 172:45-53, 1980.

TECHNICAL DEVELOPMENT OF NUCLEAR MAGNETIC RESONANCE IMAGING

REX RICHARDS
Merton College
Oxford University

Nuclear magnetic resonance (NMR) spectra contain a rich mine of information. When it has been quarried, that mine has proved of immense value in an extraordinary range of studies. The information in nuclear resonance spectra reveals subtle differences between human tissues and changes in some of the chemical reactions going on in various organs.

The information in nuclear resonance spectra is contained in five independently measurable characteristics and in their dependence on the strength of applied magnetic fields and on changes in physical charcteristics, such as temperature.

Nuclear resonance is induced when a sample placed in a uniform magnetic field, B_0, is irradiated with weak electromagnetic radiation of angular frequency $\omega_0 = \gamma B_0$, where γ is the magnetogyric ratio of the nucleus concerned, and $\omega_0 = 2\pi\nu_0$, where ν_0 Hz is the frequency of the applied radiofrequency radiation.

The strongest resonances (with the largest γ) come from hydrogen nuclei--proton resonances, apart from tritium, which need not concern us here. Proton resonances are about 15 times stronger than phosphorus resonances, and carbon-13 resonances are even weaker than phosphorus resonances (carbon-12 has no nuclear magnetic moment).

The intensity of resonance depends on the number of nuclei per unit volume of sample and in a known way on other factors, so it can be used as an absolute measure of the concentration of nuclei in a sample.

Each resonance is normally associated with two relaxation times, T_1 and T_2, which can be measured separately. T_1 is the characteristic time for the exchange of energy between the nuclear spins and the thermal motion of the matter containing them. This

so-called spin-lattice relaxation is induced by components of the random molecular motion, which lie near ω_0 and near $2\omega_0$. When the molecular motion is very slow, as in solids, there may be few components near ω_0 or $2\omega_0$ and T_1 may be long. In viscous fluids, where molecular motion is strong near ω_0 and $2\omega_0$, T_1 is short; but in mobile fluids, where molecular motion is fast, the components near ω_0 and $2\omega_0$ become weak, and T_1 may once more be long. The value of T_1 can vary from minutes (or even hours in some solids) to less than 1 ms in a viscous liquid and to a few seconds in a mobile fluid like water. T_1 varies a good deal for proton resonances in biologic tissue and is important in medical imaging.

The spin-spin relaxation time, T_2, is a measure of the rate at which the nuclear spins can exchange energy among themselves. It is affected by frequency components of molecular motion near zero, as well as by those near ω_0 and near $2\omega_0$. It is therefore short in rigid materials, where molecular motion is slow, and usually long in mobile fluids, when it approaches the value of T_1. Because of its dependence on molecular motion, it varies much in the proton resonances of soft biologic tissue, so it is another important characteristic in imaging. It turns out that the nuclear resonance line width is inversely proportional to T_2, so resonances are generally broad in solids (short T_2) and narrow in liquids (often long T_2).

In an NMR experiment, the field of B_0 experienced by the nuclei is not precisely equal to the field, B_{LM}, of the laboratory magnet, because of the diamagnetism of all matter that arises from weak electric currents induced by the applied magnetic field in the electron clouds of the molecules of the sample. These induced currents usually flow in such a way as to weaken the field, so B_0 is likely to be less than B_{LM}. Because this effect is induced by the applied magnetic field, it is proportional to it, and we can write $B_0 = B_{LM}(1 - \sigma_i)$, where σ_i is the effect of the electron clouds of the molecules in shielding the nucleus, i, from field B_{LM}. For proton resonances, σ_i usually lies in the range 0-10 ppm; for phosphorus resonances, it is in the range 0-200 ppm. It is also sensitive to the chemical environment of the nucleus in the molecule. These variations of σ are thus called chemical shifts; they give us important chemical information and are the basis of imaging studies that seek to observe chemical reactions in different parts of the body.

The other independently measurable parameter is the so-called spin-spin coupling constant. This characterizes a weak magnetic interaction between nuclei in the same molecule that is transmitted through the electrons of the chemical bonds. It constitutes structural information of great importance in high-resolution NMR; but it is not resolved in hydrogen resonances under the conditions of medical imaging, so I shall not refer to it further here.

IMAGING

An image of the body can be obtained by measuring its proton density as a function of position; for this purpose, we take advantage of the direct relationship between proton density and nuclear-resonance intensity. The problem is in distinguishing between resonances that arise from different points. We use the relationship between the frequency, ω_0, of the resonance and the magnetic-field strength, B_0 (for the moment, we neglect the tiny difference between B_0 and B_{LM}): $\omega_0 = \gamma B_0$. If we could make B_0 inhomogeneous, so that every point in space experienced a different magnetic-field strength, then every point would be characterized by a particular value of ω; the <u>intensity</u> of the resonance as a function of frequency, ω, would then tell us how the density of protons varied in space. Unfortunately, it is not practical to do this, but the same result can be obtained by successive application of magnetic-field gradients to a uniform magnetic field, B_0.

The principle can readily be understood by reference to a simple cylindrical sample. Suppose that we have some way of selecting a narrow slice of this sample and wish to know how the proton density varies across the slice. Let us imagine that the slice is in the xy plane and that it is divided along the x axis into 16 segments, as shown in Figure 1. If we now place the sample in a uniform field,

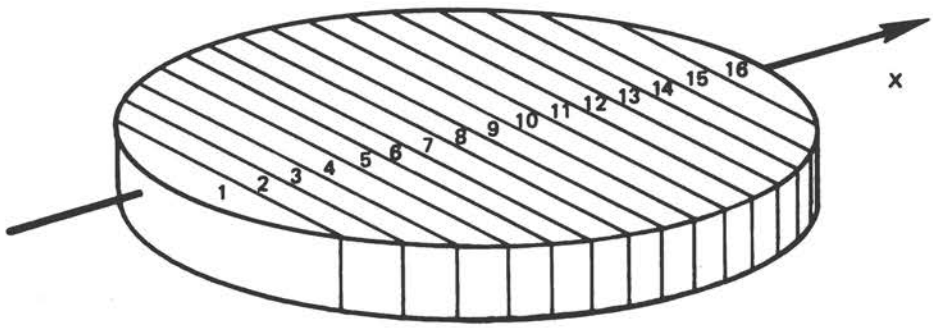

FIGURE 1 Field gradient along X axis separates series of elements that give resonances at different frequencies, depending on their positions along X axis.

B_0, along the z axis and apply a linear field gradient along the x axis so that the value of B_0 is smaller for segment 1 than for segment 16, we can write

$$B_x = B_0 + xG_x,$$

where B_x is the field experienced by the xth segment and G_x is the linear field gradient along the x direction. A nuclear-resonance signal would then be obtained over a range of frequencies such that

$$\omega_x = \gamma B_x = \gamma(B_0 + xG_x) = \nu_x/2\pi \ .$$

The intensity of the resonance at $_x$ would be proportional to the number of protons in segment x, and the whole spectrum would have an intensity distribution with frequency that measured a <u>projection</u> of the proton density of the sample along the x axis, as in Figure 2; or, if there were two cylinders, the projection would be as in Figure 3. The projections in Figure 2 would not define an image of the object. But if other field gradients were applied at different angles in the xy plane, a set of projections would be obtained from which an image of the original object could be reconstructed (Figure 3).

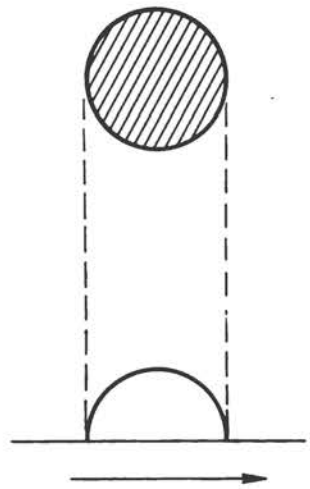

FIGURE 2 Projection of proton density along one axis.

In general, to define an image of an object with m^2 elements of area in a thin section (pixels), as in an m x m square, m projections are required at different angles between 0^o and 180^o. This procedure, known as projection reconstruction, is similar in principle to the methods used for x-ray tomography, and the computer algorithms are much the same.

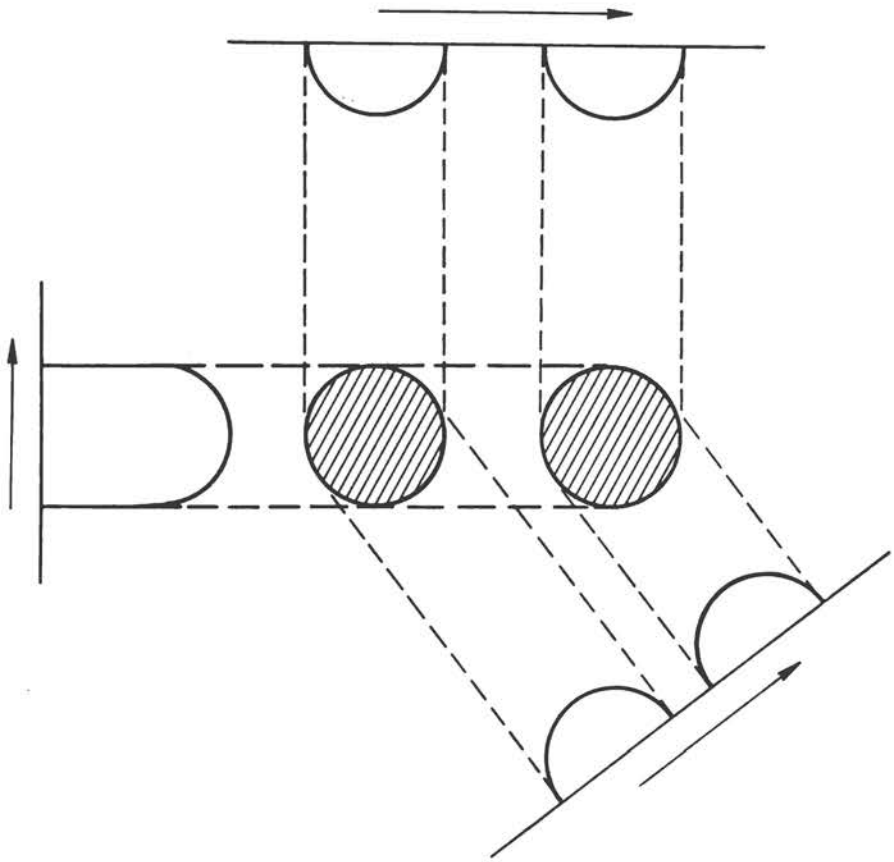

FIGURE 3 Projections of proton density along three axes.

There is a great variety of procedures for interpreting NMR responses, but they all involve the use of field gradients.[1,3,4] They vary from relatively simple sensitive-point or sensitive-line techniques in which only a single small element or line of elements is observed at a time and the image is built up by successive measurements on different points or lines to echo-planar imaging or three-dimensional Fourier-transform methods in which responses are collected from the whole sample simultaneously.

In considering methods of imaging, we are concerned with resolution, time of measurement, and contrast.

RESOLUTION AND SIGNAL-TO-NOISE RATIO

The detail in an image must depend on resolution, i.e., on the size of the smallest element of sample that can be measured. NMR is an inherently weak effect, so signal-to-noise (S/N) ratio constitutes a serious problem. The smaller the element of sample we wish to resolve, the smaller the source of signal; but noise is being collected from the whole sample all the time, so resolution must be limited by the S/N ratio.

Brunner and Ernst[1] analyzed the S/N ratio for various techniques. Clearly, the techniques that collect signals from a whole sample simultaneously should be better than the simpler ones, which have to scan points or lines successively through the sample. However, the more sophisticated techniques impose severe engineering problems, and it may well be that some compromise between the simpler and the theoretically most efficient methods may turn out to be the most satisfactory.

The S/N ratio is very sensitive to the applied field strength and so to the NMR frequency; for a nonconducting sample, it increases roughly as $\omega_o^{7/4}$. It seems, therefore, that one should make measurements at the highest practical magnetic-field strengths, and this is to a large extent limited by cost. There are, however, important engineering limitations on the highest frequency at which one can operate a large radiofrequency coil; and, because of the electric conductivity of biologic tissue, the penetration depth of radiofrequency radiation decreases as the frequency increases. It appears that at frequencies below about 10 MHz no very important image distortions or artifacts arise from these conductive losses; if higher frequencies are desired, image-correction routines may be required. However, a further effect, arising from the noise emanating from the conducting tissues of the body, is likely to limit the improvement of the S/N ratio as the frequency rises. It is difficult to estimate the result of all these conflicting effects, and the optimal field strength is controversial.

The S/N ratio can always be improved by a factor of $t^{1/2}$ by accumulating signal for longer times, t, but of course for patient care there must be a limit on the time of measurement. Furthermore, because of motion in the body, it would obviously be desirable to limit the time of measurement so as to obtain nearly "instantaneous" pictures. This can be achieved only by using methods in which signal is collected from a large part of the sample simultaneously, and outstanding among these is Mansfield's echo-planar imaging. This method offers the prospect of yielding high-quality moving pictures of the body.

CONTRAST

Relaxation times T_1 and T_2 are often different, and their values vary widely from one type of tissue to another.[3,4] Means must therefore be provided for the physician to call up images that depend on T_1 and on T_2. For example, a computer could be asked to present images in which proton densities were shown only for protons with particular ranges of T_1 and of T_2, images showing the variation in T_1 or T_2, or combinations of them. By adjusting these ranges, contrast can be altered and improved, just as a histologist uses different stains to highlight different features of a preparation. In clinical practice, contrast in soft tissue, even in areas enclosed by bone, is one of the great strengths of NMR imaging; we ought therefore to consider contrast-to-noise ratios, rather than simply signal-to-noise ratios. This introduces a further complication into the choice of optimal field strength, because T_1 and T_2 themselves vary with B_0.

CHEMICAL IMAGING

The early measurements at Oxford in 1974 of phosphorus-31 resonances in rabbit and frog leg muscle made it clear that a tremendous amount of information on some chemical reactions is accessible through these studies. This work has been pioneered and exploited, particularly in G. K. Radda's laboratory at Oxford, and extensive investigations on patients have already been made. The techniques have been well summarized by Gadian.[2]

Most of the useful work so far has been done by the primitive sensitive-point technique. But there is no reason in principle why the more efficient imaging methods should not be so arranged as to preserve the chemical-shift information while providing density images. Such procedures have already been described, and some preliminary results on tissue have been published. This adds an exciting dimension to imaging techniques, and time will show whether it is possible to achieve the necessary S/N ratios in reasonable times. Perhaps the ideal would be an instrument that could collect all the resonance information from a patient in a few minutes and store it in computer backup memory, so that the physician could select from it at leisure the information required. But it might prove more reliable and economical to use a separate instrument for chemical-shift studies of particular organs.

MAGNETS

A large magnet is required to produce the B_0 field over the volume of the patient. The field homogeneity and stability should

be about 10 ppm or better; some ways of interpreting the NMR responses to give an image are more sensitive to field homogeneity than others.

The magnetic field may be produced by air-cored coils, electromagnets or permanent magnets with ferromagnetic cores, and superconducting solenoids.

Air-cored magnets are relatively inexpensive, relatively light, and easy to install, and they give excellent access to the patient. They require accurately controlled power supplies and fluid cooling to remove the power required (many kilowatts). They are not practical for fields above about 0.2-0.3 T.

Electromagnets and permanent magnets require much less power (in fact, none for permanent magnets) and are therefore very reliable and troublefree, and they permit good patient access. Their weight is likely to present a serious limitation, however.

Superconducting magnets are almost essential for fields above about 0.3 T. Some 60 such magnets are already in use and have proved very reliable. The addition of refrigerators will make servicing of the cooling reservoirs necessary only very infrequently. Much higher fields of the required homogeneity and stability can be produced with superconducting magnets, which are commercially available for up to 2 T, but existing magnets are in the form of solenoids, so patient access is not quite so convenient as for air-cored coils.

Air-cored magnets and superconducting magnets generate large stray fields around themselves, especially when operating at high field strengths. This can create problems in a hospital environment, because the stray fields can affect cardiac pacemakers. It is essential to keep all mobile ferromagnetic objects well away from the magnets. A stray field can be reduced by guiding the return flux through some sort of ferromagnetic armature or by shielding the magnet with steel plate; measures of this kind are, however, bound to bring with them the danger of distorting the field homogeneity inside the magnet.

REFERENCES

1. Brunner, P., and R. R. Ernst. Sensitivity and performance time in NMR imaging. J. Magn. Reson. 33:83-106, 1979.

2. Gadian, D. G. Nuclear Magnetic Resonance and Its Applications to Living Systems. New York: Oxford Univ. Press, 1982. 197 pp.

3. Kaufman, L., L. E. Crooks, and A. R. Margulis, Eds. Nuclear Magnetic Resonance Imaging in Medicine. New York: Igaku-Shoin, 1981. 242 pp.

4. Manfield, P., and P. G. Morris. NMR Imaging in Biomedicine. Advances in Magnetic Resonance, Suppl. 2. New York: Academic Press, 1982. 354 pp.

REAL-TIME ECHO-PLANAR IMAGING OF CHILDREN

PETER MANSFIELD
Department of Physics
University of Nottingham

INTRODUCTION

Since the principles of nuclear magnetic resonance (NMR) imaging of discrete structures were first introduced in 1973,[5] a number of practical imaging techniques have emerged which directly or indirectly utilize these principles.[3,6-8] It was clear from the early work and subsequent development that complete two- or three-dimensional images could be obtained from a single special projection of the object in magnetic-field gradients, provided that the object were represented by a point array. Since this approach is a one-shot procedure, the time to obtain such an image can be extremely short. Naturally, in medical imaging, the subject is not a discrete spin-density array and there is unfortunately no special projection axis for inhomogeneous, continuously distributed spin distributions. Nevertheless, I proposed a way around the problem in 1976.[3] The method, now known as echo-planar imaging (EPI), involves the superposition of an effective lattice on a selectively excited slice[2] through the subject. By exploiting the special properties of spin echoes,[1] the signals from the spin distribution within the slice are made to behave as though they originated from a real discrete lattice. In this case, a special projection axis exists which allows all points in the lattice to be simultaneously and unambiguously resolved in a single experiment lasting around 35 ms. This time is extremely short, compared with the imaging times of all other NMR imaging techniques, which are typically between 2 and 8 min.

There are a number of reasons why it is important to be able to image fast. The first reason of primary importance is involuntary motion in the body. Different parts of the body are moving on different time scales. These can be divided roughly into three regimes. Breathing occurs on a 20-s or perhaps 30-s time scale. Peristaltic motions in the abdomen occur on a slightly faster time

scale of around 3 s. The fastest time scale is that of the motion of the heart itself, which, depending on the person and the state of health, can vary quite considerably. In children, the heart rate is about twice as fast as in an adult. The time scale is therefore of the order of several hundred milliseconds.

If pictures are not obtained quickly, the resolution of an image will be impaired because of motion which produces local blurring. Images which are produced by methods which take times longer than those characterizing the object motion will involve some sacrifice of spatial resolution. Object motion, therefore, calls into question claims for high resolution.

Another important aspect is the general motion of the patient. It is difficult to keep very sick patients still, unless general anesthetics are used. This procedure is held to be undesirable, especially in children.

A second reason for imaging quickly is patient comfort and the avoidance of protracted procedures in the restrictive magnet environment.

A third reason for fast imaging is the question of patient throughput. This is especially important in Great Britain, where we have less money and resources and require to use our machines as efficiently as possible.

In the next section the real-time EPI method is briefly described. Later, the EPI technique is illustrated with some recent results obtained on children.

ECHO-PLANAR IMAGING METHOD AND APPARATUS

The imaging machine is currently based on an Oxford Instruments resistive magnet which produces a magnetic field of 1,000 gauss (0.1 T). The uniformity is about 5-10 ppm over the active volume, which is our case for imaging of children is a slice about 1 cm thick and 20 cm in diameter. Magnetic-field gradient coils designed and built in our laboratory provide the linear magnetic-field gradients necessary to define the x, y, and z coordinates. The receiver and transmitter coils are of standard saddle-geometry design.

The high-speed EPI method, as previously stated, is rooted in the principles of NMR imaging of discrete structures.[5] In order to make this clear, let us consider a two-dimensional object made up of spin magnetization discretely distributed at points on a regular square lattice. Such an object might be a set of well-spaced thin glass tubes containing water. If viewed along the principal axes,

the spin projections show enfilade views which obscure the detail within the array. However, if the array is rotated slightly, oblique views between the rows reveal all the tubes through their contents by a single special projection axis. Naturally, for this to work properly, the lattice spaces need to be large enough not to cause overlap of any tube. In this example, magnetic-field gradients, tube sizes, and spacing can all be chosen to satisfy the criterion that all tubes will be unambiguously resolved. Since in medical imaging the subjects do not come conveniently diced into a discrete array, it is necessary to modify the imaging process in such a way that the subject appears mathematically to consist of a discrete array. This is achieved by making the signal response from a selected slice of magnetization periodic in time by exploiting the properties of spin echoes. Thus, in EPI, it is the time-response function which is forced to be periodic. In a real discrete structure it is, of course, the lattice itself which is periodic.

The periodic nature of the signal response is achieved by regular reversal of the G_y gradient (for example). This causes the spin magnetization from the selected slice to dephase and rephase into a series of spin echoes. By sampling the whole spin echo train and performing a Fourier transform, the spin projection profile in G_y becomes a discrete stick spectrum. This corresponds to the enfilade view of the spin distribution within the selected slice. Slight rotation of the object gives an oblique view between the sticks which reveals the full spatial spin distribution of the effective lattice within the slice. This slight rotation is achieved in practice by application of a weak gradient G_x during the signal sampling procedure. Thus, the two-dimensional effective array is obtained in what amounts to a single-shot experiment, which takes from 10 to 100 ms.

Experimental verification of the EPI method has progressed steadily, beginning with crude static images and progressing to dynamic imaging in real time. The method is now capable of resolving the great vessels and chambers of the heart in an ungated mode. This work has been achieved with proton resonances at 4.0 MHz. The image array size is 32^2 pixels, with an in-plane resolution of 6 mm and slice thickness of 8 mm. The object field is 19.2 cm and probe access 22 cm, thus limiting our preliminary clinical work to patients up to about 14 months old.

It seems that, with the advent of EPI, the problems of object motion implicit in all low-speed imaging methods can now be overcome. The imaging speed is great enough to allow motion pictures in arbitrary planes to be constructed from a four-dimensional data set, i.e., three spatial dimensions plus time. With the use of high-field superconductive magnets, there is every chance of improving the image quality to well above that currently achievable on our apparatus.

IMAGING DETAILS AND PROCEDURES

The images presented in this paper are linearly interpolated to 256 arrays for photographic recording. The magnetic-field gradients used are $G_x = 0.13\ mT \cdot m^{-1}$, $G_y = 4.0\ mT \cdot m^{-1}$, and $G_z = 3.48\ mT \cdot m^{-1}$. The maximal switching rates for the x, y, and z gradients are, respectively, 16 $T \cdot m^{-1} \cdot s^{-1}$, 256 $T \cdot m^{-1} \cdot s^{-1}$, and 109 $T \cdot m^{-1} \cdot s^{-1}$. The estimated maximal duration over which these rates apply is about 20 μs. The selective radiofrequency (RF) pulse power has a peak of 8 W delivered to the probe, with an average power of 2 W over a 3.5-ms period.

Preliminary experiments were conducted with pigs. The gradient switching did not cause any problem with the cardiac cycle, as indicated on the ECG monitor. Volunteers' limbs were placed in the coil, and no sensation was detected. Finally, heads were imaged, again with no sensation or adverse effect. The gradient parameters were within the bounds recommended by the National Radiological Protection Board in its guidelines for clinical NMR imaging.[9,12] The magnetic-field strength was 0.94 T (940 G), which corresponds to an RF frequency of 4.0 MHz for protons.

For the EPI studies with young children, the procedure was to take 32 contiguous slices with 6-mm displacement, starting at the shoulders and moving down to midabdomen. At each level, 16 images were taken at different phases of the cardiac cycle. In the free-run procedure, the experimental repetition period was adjusted to be slightly greater than the heart period, τ_C, as measured on the ECG monitor. The precise condition is that the experimental period, τ_E equals $\tau_C(1 + 1/n)$, where n is the number of frames required to span the cardiac cycle uniformly. This procedure does not require triggering from the ECG; however, it does require that the ECG trace be recorded together with an indication of the position of each snapshot image. For this method to work well, the cardiac cycle must be steady over the experimental time. For 16 frames and τ_C of 0.5 s, this time is around 8 s.

An alternative procedure is a prospective gating mode in which all the images are triggered following a variable stepped dealy with respect to the R wave. The delay, τ_E, between successive snapshot images is the same as in the ungated mode. Prospective gating gives precise positioning of each image at equal incremental phases of the cardiac cycle, provided that the heart rate is constant. The delay time between successive snapshot images is constant for a constant τ_C. However, if τ_C varies, it means that the spin system has different times in which to relax between successive shots and therefore does not settle down to an equilibrium magnetization, especially when long spin-lattice relaxation time (T_1) components

are present in the signal. In our studies of the heart, this particular effect does not appear to present a problem, since the signal from the myocardium relaxes more or less fully in the time τ_C.

The total imaging procedure produces 512 images in around 4.5 min. These constitute a four-dimensional data set. Movie sequences or still images can be constructed from the data later for cross-sectional or sagittal views of the patient.

CLINICAL RESULTS IN CHILDREN

The intrathoracic content in a number of very young patients has been examined by EPI.[10,11] The imaging parameters used in these scans were as described above. In each case, 512 images were obtained. No sedatives or anesthetics were used in these studies.

The left side of the patient corresponds to the left and the posterior aspect corresponds to the bottom of all transections. All images show the general outline of the thorax, lung fields, and mediastinum. In addition, the arms are seen either at the top or to the sides of these images.

Figure 1 shows snapshot transections through the midthorax of a 3-month-old girl with a normal heart. She was examined to evaluate resolution of bronchiolitis and bronchopneumonia. No residual lung lesion was found. The central pulmonary arteries are seen clearly. At certain phases of the cardiac cycle, the right ventricular outflow tract, the aorta, and the superior vena cava (top left and right) are seen as black. The important bifurcation of the main pulmonary artery into its left and right branches is clearly demonstrated (bottom).

The right ventricular outflow tract and the right ventricle were identified, and the pattern of blood flow within them noted. When blood flows rapidly through the imaging plane, its signal is reduced in intensity, so vessels carrying moving blood appear dark. During right ventricular systole, blood in the right atrium is at standstill and so gives a high signal that appears white on the image. The left ventricle is separated from the right ventricle by the ventricular septum. Sequential cephalad transections show the rotation of the septum as a feature of the rotation of the bulboventricular loop during development. Movie loops of the heart from transections, or indeed any appropriate plane, show the distinctive difference between the pattern of contraction of the left and the right ventricle. Closure of atrioventricular valves (tricuspid and mitral) was seen to be fully competent. The left atrium and the pulmonary venous connection from the lungs were visible.

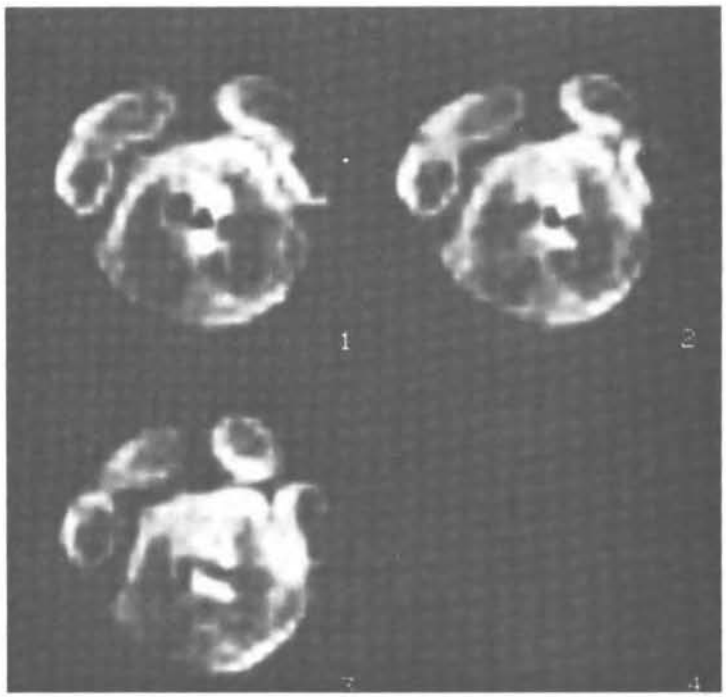

FIGURE 1 Snapshop EPI transections through the midthorax of a 3-month-old girl with a normal heart. Top left, three dark zones within heart mass from left to right correspond to right ventricular outflow tract, ascending aorta, and superior vena cava. Top right, about 6 mm cephalad. Bottom, transection passing through bifurcation of main artery. Reprinted with permission from Rzedzian et al.[10]

Pulsatile flow in both systemic and pulmonary circulation was easily seen by EPI. Figure 2 shows sagittal views in three planes at systole. Full movie loops of all planes are available. The aorta showed a remarkable flow pattern. When the aortic valve closed, flow ceased almost immediately in the posterior end of the aortic arch at the site of the former ductus. This point in the aorta appears to be a watershed. Flow continued to advance toward the abdominal aorta and up toward the great arteries leading to the neck, head, and arms.

Figure 3 shows some snapshot transections through the midthorax of a 14-month-old boy with a truncus arteriosus. Normal systemic venous and pulmonary venous connections to the heart were observed. The top left is a view near the apex. The view at the top right is in the same plane as that at the top left, but later in systole, and

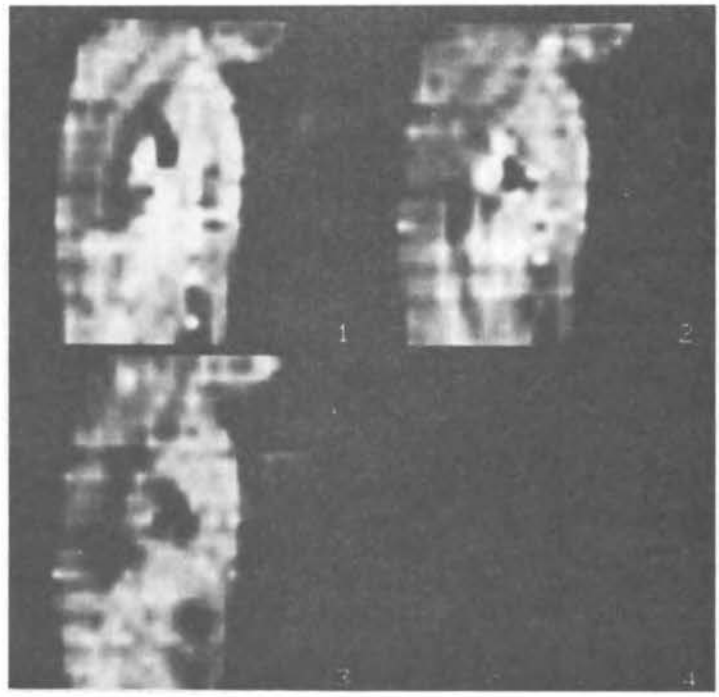

FIGURE 2 Three constructed sagittal planes of patient in Figure 1 at systole. Left of each image is posterior aspect. Top left, plane passing through ascending and descending aorta. Top right, plane to left, passing through ventricles and aorta. Bottom, plane further left, showing parts of left and right ventricles. Reprinted with permission from Rzedzian et al.[11]

shows the enlarged left ventricle. The view at the bottom left shows the left and right ventricles in systole (dark), with a clear septum, not previously demonstrated. Also seen are the left and right atria in atrial diastole; these show as bright zones corresponding to blood close to standstill. The view at the bottom right shows the papillary muscle within the left ventricle.

The top view in Figure 4 is a constructed sagittal image through the heart of the same patient as in Figure 3 and shows the truncal valve as a faint horizontal line, below which is the right ventricle in the anterior aspect and enlarged left ventricle situated posteriorly with septum and septal defect visible. The bottom view in Figure 4 is a cross-section through midheart in systole and shows an enlarged left ventricle and a contracted left atrium.

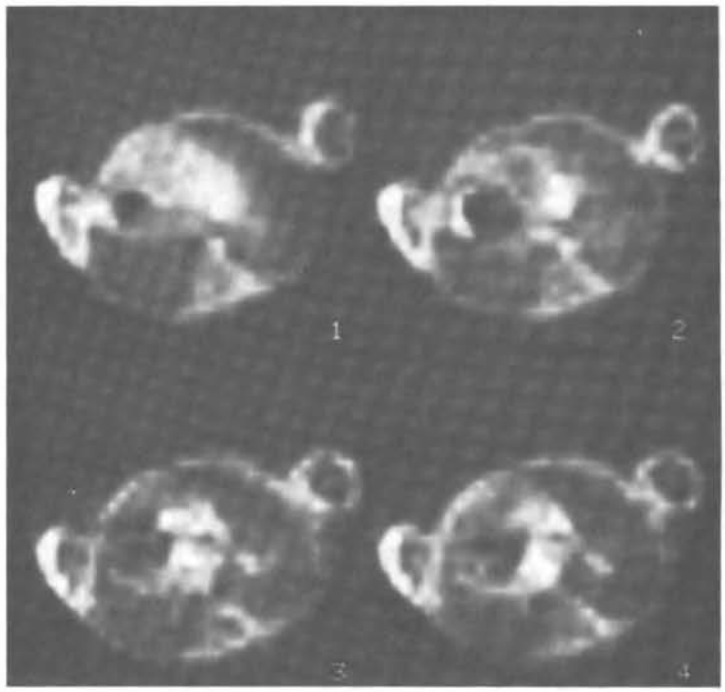

FIGURE 3 Snapshot EPI transections through midthorax of 14-month-old boy with truncus arteriosus. Left of each image corresponds to patient's left side, with posterior aspect to bottom. Top left, image near apex of heart. Top right, later in cycle. Bottom left, image showing left and right ventricles (dark) and aorta (bright). Bottom right, image showing papillary muscle within left ventricle. Reprinted with permission from Rzedzian et al.[10]

Figure 5 shows transectional imates from an oxygen-dependent 7-month-old infant with partial lobar emphysema in pulmonary dysplasia. The images through the midthorax revealed widespread dysplastic lesions (top left and right), and possible resection of the affected areas of the lung was abandoned. Clearly visible is a large lesion attached to the posterior wall of the right lung base. Contiguous cephalad transections trace this lesion throughout most of the right lung. The pulmonary arteries show pulsatile blood flow and appear dark with flow at the bottom left and bright at standstill at the bottom right.

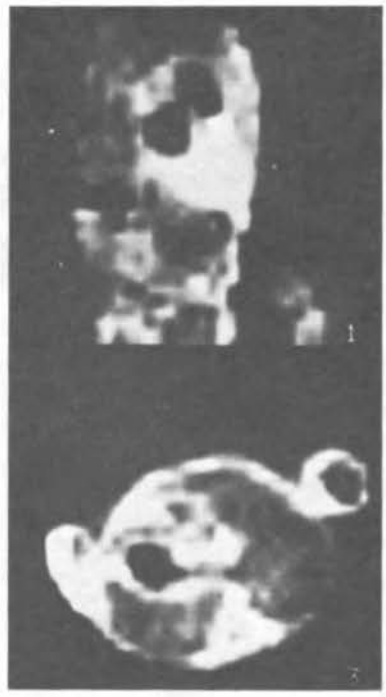

FIGURE 4 Further views of patient in Figure 3. Top, constructed sagittal view of patient at systole. Patient's back is at left. Dark zones in midthorax are heart chambers. Bottom, transection through left ventricle and atrium. Reprinted with permission from Rzedzian et al.[11]

CONCLUSIONS

Although echo-planar imaging is still at an early stage of development, we have demonstrated its clinical usefulness in a real-time mode. Considerations of involuntary motions and patient movement lead to the conclusion that, in many parts of the anatomy, claims for submillimeter resolution using slow ungated imaging methods taking many minutes simply cannot be physically justified. Despite the apparent high quality of some of these images, the question remains as to how much of the detail is attributable to motional artifact considering that much of the body is moving typically by more than 1.0 mm in the resting state. For true image resolution, the imaging time must be much shorter than the time characterizing the object motion. In many circumstances, especially in the thorax, this time is well below 1 s. EPI single-frame cine-images have an exposure time of 35 ms, and the present equipment can run at up to 10 frames per second. However, in the present work on children, the frame rate was around 2 frames per second.

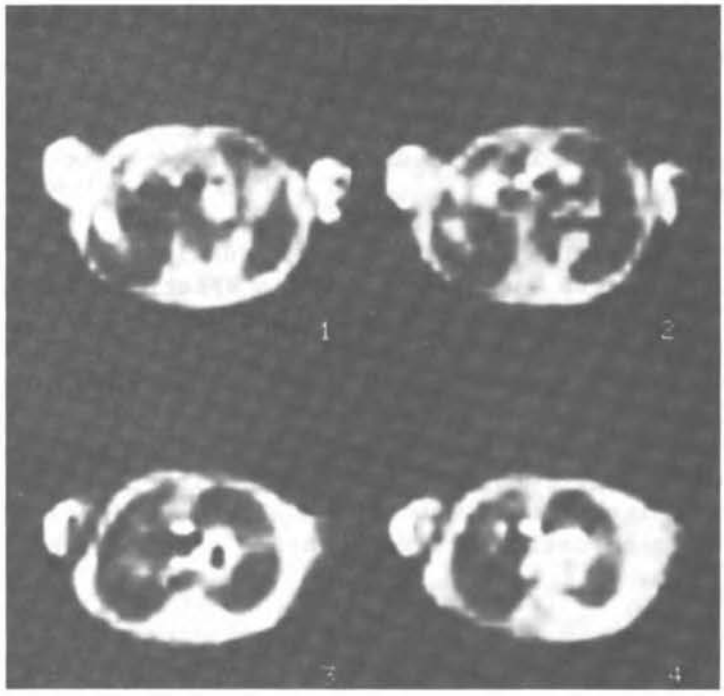

FIGURE 5 Snapshot EPI transection through thorax of 7-month-old child with pulmonary dysplasia. Top left, view showing widespread dysplastic regions in both lungs. Top right, later in cardiac cycle. Note large cystic lesion attached to posterior wall of right lung. Bottom left, view close to top of heart in systole. Bottom right, later in diastole. Note bright zones corresponding to pulmonary arteries at standstill. Reprinted with permission from Rzedzian *et al*.[11]

The images are relatively coarse, comprising 32 x 32 pixels with an in-plane resolution of 6 mm. The selected slice thickness is 8 mm. Despite their relative crudeness, the snapshot images yield a surprisingly large amount of clinically useful information. This has been valuable in assessing a child with a congenital heart abnormality and a baby with bronchopulmonary dysplasia.

The object field of our equipment is currently limited to a diameter of 22 cm, which restricts our studies to very young children. But plans are under way to expand the probe size to take adults. It is also planned to increase the array size.

All images reported are proton resonances recorded at 4.0 MHz. The single-shot signal-to-noise ratio obtained is typically 10:1. With much higher static fields produced by superconductive magnets, we expect significant improvements in both signal-to-noise ratio and true resolution of the images.

The details observed in the heart with EPI rely on the fact that blood moving rapidly through the imaging plane contributes less signal than blood at standstill. These results suggest that, with little modification, we could measure blood flow quantitatively--and in real time.

In addition to improving proton image quality, high-field superconductive magnets will allow in vivo spectroscopy and imaging to be performed on other spin species, such as ^{31}P, ^{13}C, and ^{23}Na. Theoretical proposals[4] have already suggested that spatial mapping of the chemical shift with modifications of the echo-planar technique is possible. The new methods combine spin imaging with spectroscopy, so that high-resolution spectra can be obtained at all pixels in an array. Being related to the echo-planar technique, these new approaches are potentially fast and could be of value in certain circumstances in time-course studies of tissue metabolism.

ACKNOWLEDGMENTS

The work described here was an interdisciplinary effort. The physics team comprised Drs. B. Chapman and M. Doyle and Messrs. D. Guilfoyle, M. Cawley, R. Coxon, and M. Walker. The medical team comprised Prof. R. E. Coupland, Department of Human Morphology, and Drs. P. Small and A. Chrispin of the Departments of Radiology of the Queens' Medical Centre and City Hospital, respectively. Clinical colleagues also included Drs. J. Hiller, P. R. H. Barbor, G. K. Morris, and N. Rutter, who allowed their patients to be investigated. This work was supported by major grants from the Department of Health and Social Security and the Medical Research Council in Britain.

REFERENCES

1. Garroway, A. N., P. K. Grannell, and P. Mansfield. Image formation in NMR by a selective irradiative process. J. Phys. C. 7:L457-L462, 1974.

2. Hahn, E. L. Spin echoes. Phys. Rev. 80:580-594, 1950.

3. Mansfield, P. Multi-planar image formation using NMR spin echoes. J. Phys. C. 10:L55-L58, 1977.

4. Mansfield, P. Spatial mapping of the chemical shift in NMR. J. Phys. D. 16:L235-L238, 1983.

5. Mansfield, P., and P. K. Grannell. NMR "diffraction" in solids? J. Phys. C. 6:L422-L426, 1973.

6. Mansfield, P., and A. A. Maudsley. Planar spin imaging by NMR. J. Magn. Reson. 27:101-119, 1977.

7. Mansfield, P., and P. G. Morris. NMR Imaging in Biomedicine. New York: Academic Press, 1982. 354 pp.

8. Mansfield, P., and I. L. Pykett. Biological and medical imaging by NMR. J. Magn. Reson. 29:355-373, 1978.

9. National Radiological Protection Board, ad hoc Advisory Group on Nuclear Magnetic Resonance Clinical Imaging. Revised guidance on acceptable limits of exposure during nuclear magnetic resonance clinical imaging. Br. J. Radiol. 56:974-977, 1983.

10. Rzedzian, R., B. Chapman, P. Mansfield, R. E. Coupland, M. Doyle, A. Chrispin, D. Guilfoyle, and P. Small. Real-time nuclear magnetic resonance clinical imaging in paediatrics. Lancet 2:1281-1282, 1983.

11. Rzedzian, R., M. Doyle, P. Mansfield, B. Chapman, D. Guilfoyle, R. E. Coupland, P. Small, and A. Chrispin. Echo planar imaging in paediatrics: Real time nuclear magnetic resonance. Ann. Radiol. 27:182-186, 1984.

12. Safety of nuclear magnetic resonance imaging. Lancet 2:103, 1980.

THE CLINICAL ART OF NUCLEAR MAGNETIC RESONANCE: REVIEW OF THE STATE OF THE CLINICAL ART

ALEXANDER R. MARGULIS
Department of Radiology
University of California, San Francisco

Nuclear magnetic resonance (NMR) imaging, although new, has already scored so many successes in diagnostic medicine that it has been enthusiastically introduced into all major medical centers in the United States and is expected to spread with the same rapidity in many countries of western Europe and Japan. What makes NMR imaging so attractive is that it combines the advantages of the other imaging modalities without sharing their disadvantages.[11] Like computed tomography (CT) it offers superb tomography with excellent spatial resolution. Like ultrasonography it offers a great deal of tissue information and is nonionizing. Like the medical application of radionuclides it offers the possibility of following metabolic processes and giving information about physiology. NMR imaging does all this without any known biologic ill effects and with a resolving power considerably greater than that of x-ray CT. It achieves this by having an acceptable spatial resolution of 0.8 mm at its best, which is comparable with the spatial resolution of much of today's x-ray CT equipment. The contrast resolution of NMR imaging, however, exceeds 500% in soft tissue.[5]

The greatest advantages of NMR imaging are related to the fact that the signal obtained and translated into an image is a synthesis of many more parameters than is the signal of any other imaging modality. Although images obtained with x-ray tomography depend entirely on tissue attenuation of the x-ray beam, NMR imaging provides data about hydrogen density and, through its T_1 and T_2 relaxation parameters, about the chemical and physical environment of the hydrogen protons. In addition, because it takes a finite period to register the signal from protons in the imaged plane, information is obtained about motion if the protons are moving through the plane of imaging. This provides valuable data about the patency of blood vessels, as well as permitting studies of blood flow.

In addition to these four parameters (hydrogen density, T_1, T_2, and proton motion) that provide data on which the image is based, NMR images also reflect the contribution obtained through a multiplicity of techniques. Saturation recovery, spin echo, inversion recovery, and their variations offer so many options that it is possible to tailor the technique to the problem to be studied. The various techniques do not provide the same information about disease processes. The spin-echo technique offers information about processes related to changes in both T_2 and T_1. Inversion recovery techniques usually provide more information about processes in which T_1 is critical. Furthermore, the pulse interval (TR) or spin-echo delay (TE) can be varied to obtain different types of information from the same area of the body. And it is possible to vary the number of sequences, the number of averages from which images are derived, the slice thickness, the interval between slices, the plane of imaging, the size of pixel, ECG gating, respiratory gating, and so on.

Thus, a huge amount of data must be carefully evaluated and judiciously limited so that it does not overwhelm the examiner. It is fair to state that NMR imaging is extremely promising for most areas of the body. It cannot be stated that NMR imaging is not useful for some organs; but it can be said that some organs or diseases cannot yet be studied with NMR imaging because the appropriate technique has not been designed.

Harmless paramagnetic contrast media are being developed. When they are attached to such metabolites as glucose and amino acids and followed through various parts of the body, it is hoped that normal and abnormal metabolic pathways will be unraveled. Tests like an NMR evaluation of gallbladder function will undoubtedly be developed.

It is already obvious that NMR imaging is the superior modality for examination of the brain in most conditions,[3,15] except when calcification is the most important finding; sufficient other information is usually obtained to compensate for the lack of data on calcification. NMR imaging is also the examination of choice in most conditions involving the spinal cord, as well as cancellous bone;[1,13] in the examination of the male and female pelvis;[7] and in diseases of the urinary bladder, prostate, seminal vesicles, uterus, ovary, and vagina. It allows differentiation of smooth muscle from striated muscle. Used with respiratory and ECG gating, it has greatly improved the study of the heart, mediastinum, and large vessels.[4,6] This type of gating also provides considerably better images of the liver,[9,12] spleen, and pancreas.[11] It appears that in these anatomic sites, too, NMR imaging, particularly with gating, will be the procedure of choice. The adrenal glands can be seen well; there is promise of identifying hypertrophy and even separating the cortex from the medulla with NMR imaging.[10,14]

The kidneys have also been studied to excellent advantage, and NMR imaging is very promising here, also.[8,10]

NMR imaging has some disadvantages. In the peritoneal cavity, the small bowel cannot be examined well, because of a great deal of motion in multiple directions. (The stomach, duodenum, rectum, and transverse colon, however, are seen well and will be investigated by this method.) Another disadvantage is that the patient has to be in the imager for a relatively long time. This and the depth of the instrument, which produces claustrophobia in 3-5% of patients, prevent this modality from being the one of choice for the examination of patients who need constant supervision or have multiple life-supporting systems.

NMR imaging is to be avoided in patients with cardiac pacemakers or in whom the bony cortex needs to be studied because of suspected fractures or destructive processes.[11]

Cryogenic magnets also present problems of security, inasmuch as loose metallic fragments can fly into the machine, injuring patients and damaging the equipment.

NMR imaging is progressing at an unprecedented speed, and, as more centers acquire the equipment and become involved in clinical research, it is being applied in more and more ways. The use of nuclei other than hydrogen protons and the combining of imaging with spectroscopy and paramagnetic contrast media[2] will further broaden the uses of this most exciting modality.

REFERENCES

1. Brady, T. J., M. C. Gebhardt, I. L. Pykett, F. S. Buonanno, J. H. Newhouse, C. T. Burt, R. J. Smith, H. J. Mankin, J. P. Kistler, M. R. Goldman, W. S. Hinshaw, and J. M. Pohost. NMR imaging of forearms in healthy volunteers and patients with giant-cell tumor of bone. Radiology 144:549-552, 1982.

2. Brasch, R. C. Work in progress: Methods of contrast enhancement for NMR imaging and potential applications. A subject review. Radiology 147:781-788, 1983.

3. Crooks, L. E., C. M. Mills, P. L. Davis, M. Brant-Zawadzki, J. Hoenninger, M. Arakawa, J. Watts, and L. Kaufman. Visualization of cerebral and vascular abnormalities by NMR imaging: The effects of imaging parameters on contrast. Radiology 144:843-852, 1982.

4. Gamsu, G., W. R. Webb, P. Sheldon, L. Kaufman, L. E. Crooks, F. A. Birnberg, P. Goodman, W. A. Hinchcliffe, and M. Hedgcock. Nuclear magnetic resonance imaging of the thorax. Radiology 147:473-480, 1983.

5. Herfkens, R., P. L. Davis, L. Crooks, L. Kaufman, D. Price, T. Miller, A. R. Margulis, J. Watts, J. Hoenninger, M. Arakawa, and R. McRee. Nuclear magnetic resonance imaging of the abnormal live rat and correlations with tissue characteristics. Radiology 141:211-218, 1981.

6. Higgins, C. B., P. Lanzer, R. Herfkens, E. Botvinick, and M. Lipton. Cardiovascular system, pp. 159-184. In A. R. Margulis, C. B. Higgins, L. Kaufman, and L. E. Crooks, Eds. Clinical Magnetic Resonance Imaging. San Francisco: Radiology Research and Education Foundation, 1983.

7. Hricak, H. Pelvis, pp. 229-250. In A. R. Margulis, C. B. Higgins, L. Kaufman, and L. E. Crooks, Eds. Clinical Magnetic Resonance Imaging. San Francisco: Radiology Research and Education Foundation, 1983.

8. Hricak, H., L. Crooks, P. Sheldon, and L. Kaufman. Nuclear magnetic resonance imaging of the kidney. Radiology 146:425-432, 1983.

9. Hricak, H., R. A. Filly, A. R. Margulis, K. L. Moon, L. E. Crooks, and L. Kaufman. Work in progress: Nuclear magnetic resonance imaging of the gallbladder. Radiology 147:481-484, 1983.

10. Hricak, H., and K. L. Moon. Adrenal glands and kidneys, pp. 209-228. In A. R. Margulis, C. B. Higgins, L. Kaufman, and L. E. Crooks, Eds. Clinical Magnetic Resonance Imaging. San Francisco: Radiology Research and Education Foundation, 1983.

11. Margulis, A. R., C. B. Higgins, L. Kaufman, and L. E. Crooks, Eds. Clinical Magnetic Resonance Imaging. San Francisco: Radiology Research and Education Foundation, 1983. 328 pp.

12. Margulis, A. R., A. A. Moss, L. E. Crooks, and L. Kaufman. Nuclear magnetic resonance in the diagnosis of tumors of the liver. Semin. Roentgenol. 17(2):123-126, 1983.

13. Moon, K. L., H. K. Genant, C. A. Helms, N. I. Chafetz, L. E. Crooks, and L. Kaufman. Musculoskeletal applications of nuclear magnetic resonance. Radiology 147:161-171, 1983.

14. Moon, K. L., H. Hricak, L. E. Crooks, C. A. Gooding, A. A. Moss, B. L. Engelstad, and L. Kaufman. Nuclear magnetic resonance imaging of the adrenal gland: A preliminary report. Radiology 147:155-160, 1983.

15. Young, I. R., M. Burl, G. J. Clarke, A. S. Hall, T. Pasmore, A. G. Collins, D. T. Smith, J. S. Orr, G. M. Bydder, F. H. Doyle, K. H. Greenspan, and R. E. Steiner. Magnetic resonance properties of hydrogen: Imaging of the posterior fossa. Am. J. Neuroradiol. 2:487-493, 1981.

DIAGNOSTIC SPECIFICITY OF NUCLEAR MAGNETIC RESONANCE

THOMAS J. BRADY
Department of Radiology and Medical Service
Massachusetts General Hospital

BRUCE R. ROSEN
Department of Radiology
Massachusetts General Hospital

Proton (^1H) nuclear magnetic resonance (NMR) imaging is rapidly emerging as a useful clinical diagnostic tool. Initial clinical studies in our laboratory and others have demonstrated that ^1H NMR imaging has excellent sensitivity in detecting a wide variety of lesions.[6,7,10,12,13,18,22-24,34] This sensitivity is due in part to the abundance of information in the NMR signal. Unlike x-ray computed tomography, which relies on one characteristic (x-ray attenuation), NMR has an image intensity related to many factors, including proton density, relaxation times (T_1 and T_2), flow, and diffusion.[26] In addition, the expression of these parameters depends on the radiofrequency pulse sequence and spatial encoding techniques used for data acquisition.

Initially, it was hoped that measurements of T_1 and T_2 would provide specific in vivo characterization of disease states. Experience has not supported this hypothesis. Except for some situations, such as hemorrhage,[33] lesions are likely to be associated with prolongation of T_1 and T_2. These prolonged relaxation times allow clear separation of lesions from normal structures, but not necessarily of lesions from one another.[3,16] ^1H NMR imaging is still a nonspecific indicator of histopathologic states. This low diagnostic specificity may be resolved as investigators develop more experience with NMR techniques and image interpretation, but it may require additional diagnostic strategies, such as the use of paramagnetic NMR contrast agents and in vivo NMR spectroscopy.

The use of contrast agents by radiologists in diagnostic imaging is widespread. In general, these agents directly affect the resulting image via the well-understood increase in x-ray attenuation. Unlike traditional radiologic contrast agents, paramagnetic substances affect image contrast indirectly via local interactions with tissue protons.[14,35] The key to this interaction is the local

presence of large magnetic moments characteristic of unpaired electrons. Substances with one or more unpaired electrons can dramatically enhance relaxation rates of water protons--a single unpaired electron has some 700 times the effect of an unpaired proton--and result in altered image contrast. Paramagnetic substances include transition metals (e.g., Mn^{2+}), rare earth elements (e.g., Gd^{3+}), stable free radicals (e.g., nitroxide group), and molecular oxygen.

The effect of these agents on relaxation time depends on many factors, including the concentration, magnetic moment, and electron spin-relaxation processes (τ_s) of the paramagnetic species; the distance of the proton from the paramagnetic center; the proton exchange rate (τ_m); and the correlation time of the complex (τ_c). For example, paramagnetic ions complexed to large macromolecules with a tumbling rate near the Larmor frequency will provide enhanced proton relaxation compared to the same concentration of the ionic form or complexed to small molecules. This effect is modulated by the magnetic field strength of the imaging system. In addition, for any large complex to be effective, mobile water protons must have access to the paramagnetic center and exchange rapidly. These and other factors will influence the strategies used in developing NMR contrast agents.

Although the NMR literature on paramagnetic substances is large and dates back nearly four decades, only recently have they been applied in diagnostic medicine. Using a canine model of myocardial infarction, Lauterbur *et al.* measured the T_1 of normal and infarcted regions after intravenous injection of $MnCl_2$ (100 mmol/kg).[21] T_1 values for the normal myocardium were significantly lower than those for infarcted regions. The decrease in T_1 in normal myocardium correlated well with the tissue concentration of Mn^{2+}. Using a 90-min left circumflex coronary (LCX) artery occlusion model, Brady *et al.* studied the effects of Mn^{2+} with the steady-state free-precession NMR imaging technique.[4] In this study on excised hearts, images from control animals failed to demonstrate a change in signal intensity between normal and infarcted myocardium. In dogs given $MnCl_2$ (50 mmol/kg), the normally perfused myocardium demonstrated an increased signal consistent with enhanced proton relaxation. The nonenhanced LCX distribution corresponded to infarcted regions on stained pathologic sections (Figure 1). Both studies are consistent with published radionuclei-imaging data that showed a distribution of radioactive manganese-54 proportional to myocardial blood flow.[11]

The use of paramagnetic substances in the ionic form is not appropriate for clinical studies, because of their associated toxicity. To decrease toxicity and to obtain selective tissue localization, it is necessary to attach these substances to specific

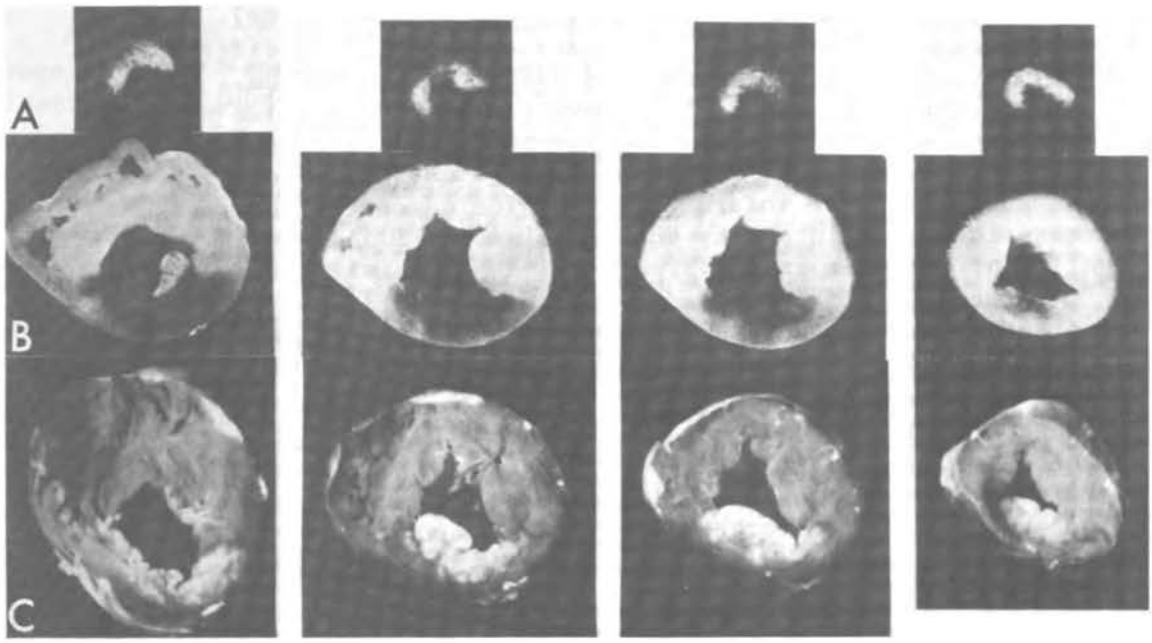

FIGURE 1 Serial thallium-201 images (A), NMR tomograms (B), and stained myocardial sections (C) at corresponding levels from dog that received ionic Mn^{2+} (at 50 mmol/kg). NMR images depict normally perfused myocardium as region of bright signal consistent with increase in proton relaxation due to paramagnetic effect on Mn^{2+}. Posterior (LCX) distribution appears dark and corresponds to regions of perfusion deficits on thallium-201 images and regions of infarcted myocardium on stained sections. Reprinted with permission from Brady et al.[4]

carrier groups, including tissue-specific liposomes, microspheres, and monoclonal antibodies. Recent work has demonstrated the feasibility of attaching paramagnetic ions to various chelates, including EDTA, to act as renal and gastrointestinal contrast agents.[31] The use of iron salts as safe, effective gastrointestinal contrast agents has been suggested, and preliminary studies in animals and man appear promising.[37] Other investigators have shown the feasibility of using a nitroxide stable, free radical in several clinical situations to provide contrast.[8] Additional strategies, analogous to those used in radionuclide imaging, can be applied with NMR contrast agents to assess the functional status of tissue.

We are investigating the use of paramagnetic ions chelated to monoclonal antibodies to provide diagnostic specificity. The Fab portion of the monoclonal antibody, antimyosin, which specifically localizes in infarcted myocardium, was labeled with Mn^{2+} in modifications of standard techniques.[20] We used a canine occlusion-reflow model and otained NMR images from the excised infarcted hearts with the spin-echo pulse sequence (TR, 200 ms; TE, 30 ms). Images from nonmanganese infarcted hearts failed to show any difference in signal intensity between normal and infarcted myocardium. (Images of these hearts acquired with an inversion-recovery pulse sequence demonstrated a decrease in signal intensity in the infarcted myocardium consistent with increased T_1.) In dogs that received the Fab Mn^{2+} complex, the infarcted myocardium demonstrated a marked increase in signal intensity on the spin-echo 200/30 image and a significant decrease in measured T_1.[5,19] In animals given ionic Mn^{2+}, infarcted myocardium had increased T_1 (not significantly different from that in infarcted controls); that suggested that the changes observed with the antibody-manganese complex were not due to free Mn^{2+}. These preliminary data show that a selective decrease in tissue T_1 can be obtained with tissue-specific monoclonal antibodies and suggest that similar strategies can be used with tumor-specific antibodies for characterizing malignant disease in vivo. Although these preliminary studies are encouraging, additional work is required to characterize these agents and evaluate them in a variety of clinical situations.

Another method of improving diagnostic specificity of NMR involves the acquisition of in vivo spectra or chemical shift data from other sensitive NMR nuclei, including ^{13}C, ^{19}F, ^{23}Na, and ^{31}P. These nuclei, like ^{1}H, have been extensively studied with NMR spectroscopy of biological samples and isolated organs.[15,32] The resonance or chemical shift position (recorded in parts per million) in the resulting spectra reflect the chemical environments experienced by similar nuclei at different molecular sites. For example, a typical ^{31}P spectrum has five or six chemically shifted resonant peaks, each reflecting particular cellular phosphorus metabolites. These spectra can be used to evaluate tissue high-energy phosphate compounds and cellular pH. Thus, the addition of chemical shift information provides another dimension that may be particularly useful in the characterization of disease.

Unlike standard ^{1}H NMR imaging, the acquisition of chemical shift information requires the use of highly homogeneous magnetic fields for adequate spectral resolution. Investigators have been successful in obtaining in vivo NMR spectral data from animals and man. Acquisition of these data usually requires specifically designed magnet systems (topical magnetic resonance, TMR) and/or surface coil data collection methods.[1] Both TMR techniques (by profiling coils) and surface coil techniques (by regional excitation

of nuclei) generate NMR signals from focal volumes inside the subject. Important metabolic data have been obtained in animals[25] and man[30] with these techniques. Because these are nonimaging techniques, uncertainty in the exact spatial localization of the NMR signal could result in volume averaging of data from a lesion and normal tissue.

A solution to this problem would involve the simultaneous acquisition of spatial and spectral data. In several approaches, imaging techniques are combined with chemical shift spectroscopy measurements.[2,9] These techniques allow extraction of spectral data from all points in the image matrix or the display of images corresponding to specific chemically shifted peaks. In vivo chemical shift images displaying various ^{31}P compounds were recently obtained in a cat.[17] For ^{31}P, the imaging time is long (some 2-4 hours) and the spatial resolution is poor (about 1 cm), but technical improvements may make this approach useful for differentiating ischemic from infarcted tissue.

Because of its excellent NMR sensitivity and widespread use in clinical NMR imaging, we have chosen to obtain chemical shift image data from the hydrogen nucleus. We used an experimental superconducting imaging magnet (Technicare Corporation, Solon, Ohio) with a field strength of 1.44 tesla, corresponding to a proton resonance frequency of 61.4 MHz. A three-dimensional Fourier transform approach was used, with two dimensions encoding spatial information and the third providing chemical shift resolution.[27] Three-dimensional Fourier transformation of the raw data yields a data matrix in which regional ^{1}H spectra corresponding to known anatomic locations can be extracted (Figures 2 and 3).

We have recently evaluated this approach in animal models of fatty-liver disease. Previous data have demonstrated that standard ^{1}H NMR imaging techniques with T_1 and T_2 measurements were unable to differentiate normal livers from those with acute fatty infiltration.[36] Using proton chemical shift imaging, we acquired data in control rats and rats with ethionine-induced fatty-liver disease. ^{1}H spectra from livers in the treated group demonstrated two dominant peaks corresponding to water and aliphatic protons. The aliphatic peak intensities correlated well with measured triglyceride concentrations.[29] In control animals, the ^{1}H liver spectra had only one strong peak, corresponding to water protons. In this disease model, we obtained regional chemical shift information that reflected the specific pathologic process.

With chemical shift imaging, one can measure relaxation times of individual chemical moieties that may be diagnostically useful. In addition, standard spectroscopic techniques, such as solvent suppression, can be implemented. With solvent suppression, a tailored pulse

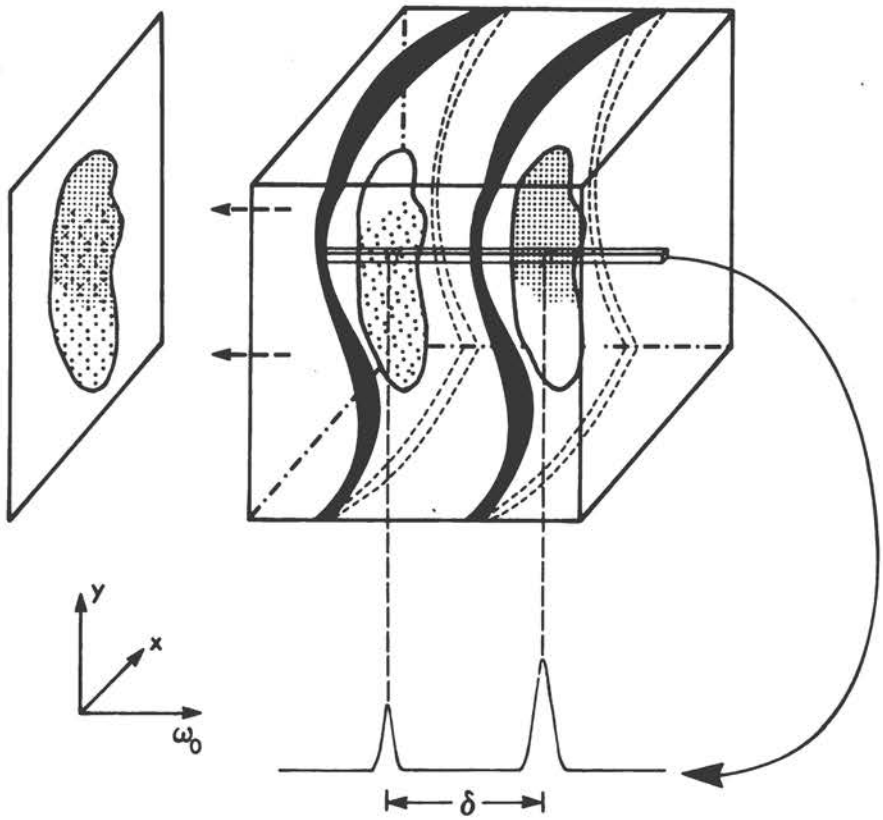

FIGURE 2 Depiction of three-dimensional data array obtained after Fourier transformation of raw data in chemical shift experiment. Spatial coordinate axes are denoted x and y; ω_0 defines chemical shift axis. Each chemical shift-resolved image is distributed about curved surface, owing to magnetic-field heterogeneity. More usual, nonchemical shift-resolved image is obtained by integrating data along ω_0 axis. NMR spectrum may be retrieved from any x,y coordinate. "Edge profiles" are obtained by displaying data contained in selected ω_0-x or ω_0-y planes. Reprinted with permission from Pykett and Rosen.[27]

train is used to saturate the dominant peak (e.g., water), allowing metabolites at lower concentrations to become "visible" with signal averaging. We have been able to implement this technique in our laboratory and have acquired images of 40 mM lactate phantoms in approximately 50 min of imaging time.[28] This approach may have

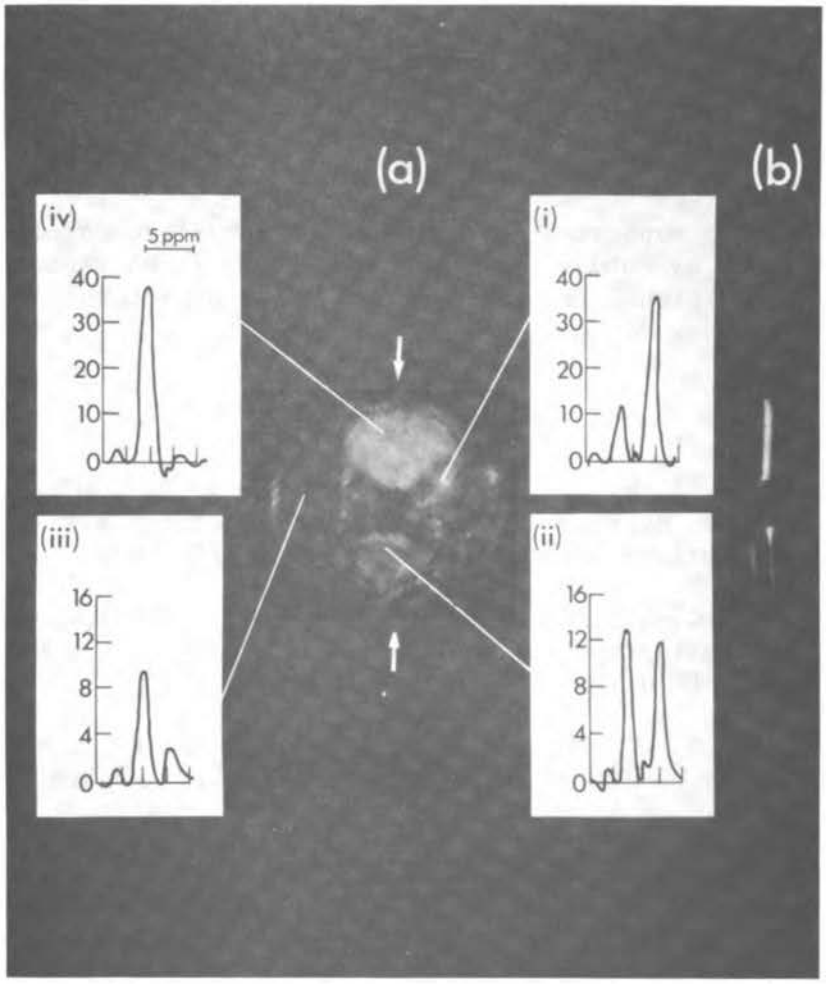

FIGURE 3 NMR data acquired from coronal section through head of normal cat. Integrated image shows usual anatomic features, and NMR spectra from selected regions (i-iv) show clearly resolved peaks corresponding largely to water and to lipid resonances (a). Edge profile (b) taken through midline of head (arrow) clearly shows both lipid and water resonances in tongue, but only water line is visible in brain. Reprinted with permission from Pykett and Rosen.[27]

enormous importance in the evaluation of ischemic conditions; however, technical factors must be resolved before this method can be applied clinically.

In summary, it is likely that ^{1}H NMR imaging will be used extensively in clinical medicine, especially where existing modalities have limitations, although its diagnostic specificity is still low. This brief review suggests that other strategies, including chemical shift NMR imaging and selective localization of paramagnetic contrast agents, may provide the necessary specificity.

ACKNOWLEDGMENTS

This work was supported in part by the Technicare Corporation, Solon, Ohio, and by Public Health Service grant 1 K04 CA00848-02, awarded by the National Cancer Institute, U.S. Department of Health and Human Services.

REFERENCES

1. Ackerman, J. J. H., T. H. Grove, G. G. Wong, D. G. Gadian, and G. K. Radda. Mapping of metabolites in whole animals by ^{31}P NMR using surface coils. Nature 283:167-170, 1980.

2. Bendel, P., C.-M. Lai, and P. C. Lauterbur. ^{31}P spectroscopic zeugmatography of phosphorus metabolites. J. Mag. Res. 38:343-356, 1980.

3. Brady, T. J., F. S. Buonanno, I. L. Pykett, P. F. J. New, K. R. Davis, G. M. Pohost, and J. P. Kistler. Preliminary clinical results of proton (^{1}H) imaging of cranial neoplasms: In-vivo measurement of T_1 and mobile proton density. Am. J. Neuroradiol. 4:225-228, 1983.

4. Brady, T. J., M. R. Goldman, I. L. Pykett, F. S. Buonanno, J. P. Kistler, J. H. Newhouse, C. T. Burt, W. S. Hinshaw, and G. M. Pohost. Proton nuclear magnetic resonance imaging of regionally ischemic canine hearts: Effect of paramagnetic proton signal enhancement. Radiology 144:343-347, 1982.

5. Brady, T. J., B. R. Rosen, H. K. Gold, B. A. Khaw, J. T. Fallon, M. R. Goldman, B. J. terPenning, T. Yasuda, and E. Haber. Selective decrease in T_1 relaxation time of infarcted myocardium with the use of a manganese-labeled monoclonal antibody, antimyosin. Works in Progress. Abstract 10. Berkeley, Calif.: Soc. Magn. Reson. Med., 1983.

6. Brady, T. J., B. R. Rosen, I. L. Pykett, M. H. McGuire, H. J. Mankin, and D. I. Rosenthal. NMR imaging of leg tumors. Radiology 149:181-187, 1983.

7. Brant-Zawadzki, M., P. L. Davis, L. E. Crooks, C. M. Mills, D. Norman, J. H. Newton, P. Sheldon, and L. Kaufman. NMR demonstration of cerebral abnormalities: Comparison with CT. Am. J. Neuroradiol. 4:117-124, 1983.

8. Brasch, R. C., D. A. London, G. E. Wesby, T. N. Tozer, D. E. Nitechi, R. D. Williams, J. Doemeny, L. D. Tuck, and D. P. Lallemand. Work in progress: Nuclear magnetic resonance study of a paramagnetic nitroxide contrast agent for enhancement of renal structures in experimental animals. Radiology 147:773-780, 1983.

9. Brown, T. R., B. M. Kincaid, and K. Ugurbil. NMR chemical shift imaging in three dimensions. Proc. Natl. Acad. Sci. USA 79:3523-3526, 1982.

10. Bydder, G. M., R. E. Steiner, I. R. Young, A. S. Hall, D. J. Thomas, J. Marshall, C. A. Pallis, and N. J. Legg. Clinical NMR imaging of the brain: 140 cases. Am. J. Radiol. 139:215-236, 1982.

11. Chauncey, D. M., Jr., H. R. Schelbert, S. E. Halpern, F. Delano, M. L. McKegney, W. L. Ashburn, and P. L. Hogan. Tissue distribution studies with radioactive manganese: A potential agent for myocardial imaging. J. Nucl. Med. 18:933-936, 1977.

12. Cohen, A. M., S. Creviston, J. P. LiPuma, P. J. Bryan, J. R. Haaga, and R. J. Alfidi. NMR evaluation of hilar and mediastinal lymphadenopathy. Radiology 148:739-742, 1983.

13. Crooks, L. E., C. M. Mills, P. L. Davis, M. Brant-Zawadzki, J. Hoenninger, M. Arakawa, T. Watts, and L. Kaufman. Visualization of cerebral and vascular abnormalities by NMR imaging. The effects of imaging parameters on contrast. Radiology 144:843-852, 1982.

14. Dwek, R. A. Nuclear Magnetic Resonance in Biochemistry: Applications to Enzyme Systems. London: Oxford University Press, 1973.

15. Gadian, D. G. Nuclear Magnetic Resonance and Its Applications to Living Systems. New York: Oxford Univ. Press, 1982. 197 pp.

16. Herfkens, R., P. David, L. Crooks, L. Kaufman, D. Price, T. Millos, A. R. Margulis, J. Watts, J. Hoenninger, M. Arakawa, and R. McRee. Nuclear magnetic resonance imaging of the abnormal live rat and correlations with tissue characteristics. Radiology 141:211-218, 1981.

17. Hilal, S. K., A. A. Maudsley, H. E. Simon, and S. Wittekoek. In vivo NMR Imaging of Phosphorus. Presented at Annual Meeting of Radiological Society of North America, Chicago, November 1983.

18. Hricak, H., L. E. Crooks, P. Sheldon, and L. Kaufman. Nuclear magnetic resonance imaging of the kidney. Radiology 146:425-432, 1983.

19. Khaw, B. A., H. K. Gold, M. R. Goldman, J. T. Fallon, T. J. Brady, T. Yasuda, B. R. Rosen, I. L. Pykett, H. W. Strauss, and E. Haber. Tomographic NMR Imaging of Experimental Myocardial Infarction Using Paramagnetic Manganese Labeled Antimyosin Fab. Presented at American Heart Association Annual Meeting, Anaheim, Calif., November 1983.

20. Krejcarek, G. E., and K. L. Tucker. Covalent attachment of chelating groups to macromolecules. Biochem. Biophys. Res. Commun. 77:581-585, 1977.

21. Lauterbur, P. C., D. H. M. Dias, and A. M. Rudin. Augmentation of tissue water proton relaxation rates in vivo addition of paramagnetic ions, pp. 752-759. In P. L. Dutton, J. S. Leigh, and A. Scarpa, Eds. Frontiers of Biologic Energetics: Electrons to Tissues. New York: Academic Press, 1978.

22. McGinnis, B. D., T. J. Brady, P. F. J. New, F. S. Buonanno, I. L. Pykett, R. L. DeLaPaz, J. P. Kistler, and J. M. Taveras. Nuclear magnetic resonance (NMR) imaging of tumors in the posterior fossa. J. Comput. Assist. Tomogr. 7:575-585, 1983.

23. Modic, M. T., M. A. Weinstein, W. Pavlicek, D. L. Starnes, P. M. Duchesneau, F. Boumphrey, and R. J. Hardy. Nuclear magnetic resonance imaging of the spine. Radiology 148:757-762, 1983.

24. Moon, K. L., H. K. Genant, C. A. Helms, N. I. Chafetz, L. E. Crooks, and L. Kaufman. Musculoskeletal applications of nuclear magnetic resonance. Radiology 147:161-171, 1983.

25. Nunnally, R. L., and P. A. Bottomley. Assessment of pharmacological treatment of myocardial infarction by phosphorus-31 NMR with surface coils. Science 211:177-180, 1981.

26. Pykett, I. L., J. H. Newhouse, F. S. Buonanno, T. J. Brady, M. R. Goldman, J. P. Kistler, and G. M. Pohost. Principles of nuclear magnetic resonance imaging. Radiology 143:157-168, 1982.

27. Pykett, I. L., and B. R. Rosen. Work in progress: Nuclear magnetic resonance: In-vivo proton chemical shift imaging. Radiology 149:197-201, 1983.

28. Rosen, B. R., T. J. Brady, and V. J. Wedeen. Application of Selective Saturation Techniques in NMR Proton Chemical Shift Imaging. Presented at 69th Scientific Assembly and Annual Meeting of Radiological Society of North America, Chicago, November 1983.

29. Rosen, B. R., I. L. Pykett, T. J. Brady, E. Carter, and J. Wands. NMR proton chemical shift imaging of experimentally induced fatty liver disease: Enhanced sensitivity over conventional NMR imaging, pp. 306-307. Berkeley, Calif.: Soc. Magn. Res. Med., 1983.

30. Ross, B. D., G. K. Radda, D. G. Gadian, G. Rocker, M. Esiri, and J. Falconer-Smith. Examination of a case of suspected McArdle's syndrome by ^{31}P nuclear magnetic resonance. New Engl. J. Med. 304:1338-1342, 1981.

31. Runge, V. M., R. G. Stewart, J. A. Clanton, M. M. Jones, C. M. Lukehart, C. L. Partain, and A. E. James, Jr. Work in progress: Potential oral and intravenous paramagnetic NMR contrast agents. Radiology 147:789-792, 1983.

32. Shulman, R. G. Biological Applications of Magnetic Resonance. New York: Academic Press, 1979.

33. Sipponen, J. T., R. E. Sepponen, and A. Sivula. Nuclear magnetic resonance (NMR) imaging of intracerebral hemorrhage in the acute and resolving phases. J. Comput. Assist. Tomogr. 7:954-959, 1983.

34. Smith, F. W., J. R. Mallard, A. Reid, and J. M. Hutchison. Nuclear magnetic resonance tomographic imaging in liver disease. Lancet 1:963-966, 1981.

35. Solomon, I. Relaxation processes in a system of two spins. Phys. Rev. 99:559-565, 1955.

36. Stark, D. D., N. M. Bass, A. A. Moss, B. R. Bacon, J. H. McKerrow, C. E. Cann, A. Brito, and H. I. Goldberg. Nuclear magnetic resonance imaging of experimentally induced liver disease. Radiology 148:743-751, 1983.

37. Wesby, G. E., R. C. Brasch, B. L. Engelstad, A. A. Moss, L. E. Crooks, and A. C. Brito. Nuclear magnetic resonance contrast enhancement study of the gastrointestinal tract of rats and a human volunteer using nontoxic oral iron solutions. Radiology 149:175-180, 1983.

FUTURE ADVANCES IN CLINICAL NUCLEAR MAGNETIC RESONANCE IMAGING AND SPECTROSCOPY

PAUL A. BOTTOMLEY
Corporate Research and Development Center
General Electric Company

Anticipating future technologic developments in a field that changes as rapidly as nuclear magnetic resonance (NMR) imaging is not difficult: as likely as not, a prophecy is fulfilled as soon as it is made! The kinds of development of the technology that I see for the near future are in two categories: consolidation and new techniques, as summarized in Table 1. This presentation deals in detail with only a subset of the headings in each category: standardization, optimization, and chemical-shift imaging.

TABLE 1

Future Developments

Consolidation:

- Standardize NMR image intensity
- Standardize measurement of ψ
- Standardize definition of spatial resolution
- Determine normal and abnormal ranges of NMR parameters
- Determine whether ^{31}P and ^{13}C spectroscopy is clinically advantageous

New Techniques:

- Optimize system at any field strength
- Chemical-shift imaging: ^{1}H, ^{31}P, ^{13}C
- Snap-shot imaging of the heart
- NMR microscope

STANDARDIZATION

The NMR signal observed in a biological imaging experiment can reflect relaxation time (T_1, T_2, $T_1\rho$), chemical shift (δ), diffusion (D), flow (v), and nuclear density (ρ). Their roles and methods of measurement are well understood from 37 years of NMR experience in physics and chemistry. For example, T_1 may be measured by partial recovery or by inversion recovery and T_2 with a Carr-Purcell sequence. These parameters and measurement techniques should be adopted in medical NMR imaging, but problems arise from the multiparameter dependence of the NMR signal.

Thus, to measure ρ alone, relaxation-time dependence must be removed, for example, by waiting several (traditionally, five) T_1s between radiofrequency pulse applications. For body fluids, with $T_1 > 1$ s, this leads to excessive patient scan times, and the NMR signals still incorporate effects of diffusion and flow. For T_2 measurement, at least four components have been observed in muscle tissue.[12] To measure them all would substantially lengthen the data acquisition process. If we assumed a single dominant component, the value measured would depend on when we measured it[6] and also on diffusion and flow if a simple spin-echo sequence were used. Moreover, because hydrogen (^1H), T_1, T_2, D, and perhaps ρ can all be increased in diseased tissue,[9] an image whose intensity depends on all these parameters can provide better discrimination than a computed image showing T_1, T_2, or ρ distributions alone.

Because images reflecting a mixture of NMR parameters are readily obtainable and minimize data acquisition and patient scan times, perhaps the image intensity itself should be considered as a useful diagnostic medical imaging parameter. Indeed, some workers have already done so.[7] The adoption of a standard image-intensity parameter requires agreement on its normalization and conditions of measurement. Defining the ^1H signal from H_2O (liquid) at 25°C arbitrarily at, say, 1,000 units as a normalization reference is an obvious choice. The standard intensity parameter of a tissue might then be defined as the intensity of the ^1H signal from the tissue observed with a partial-recovery sequence and, for example, a 200-ms repetition period. The problem remains that the value obtained will depend on the sequence timing,[5] and means must be available to allow for different timing and sequences.

Either way, adoption of a convention regarding NMR image intensity and the measurement of parameters is urgent. This should be followed by a determination of the ranges of normal and abnormal NMR parameters over the spectrum of NMR frequencies used for imaging. Although many such measurements of relaxation times have been performed, a survey of the literature reveals little agreement on normal values (P. A. Bottomley *et al.*, unpublished manuscript); Figure 1, for example, shows the reported T_1 values for liver.

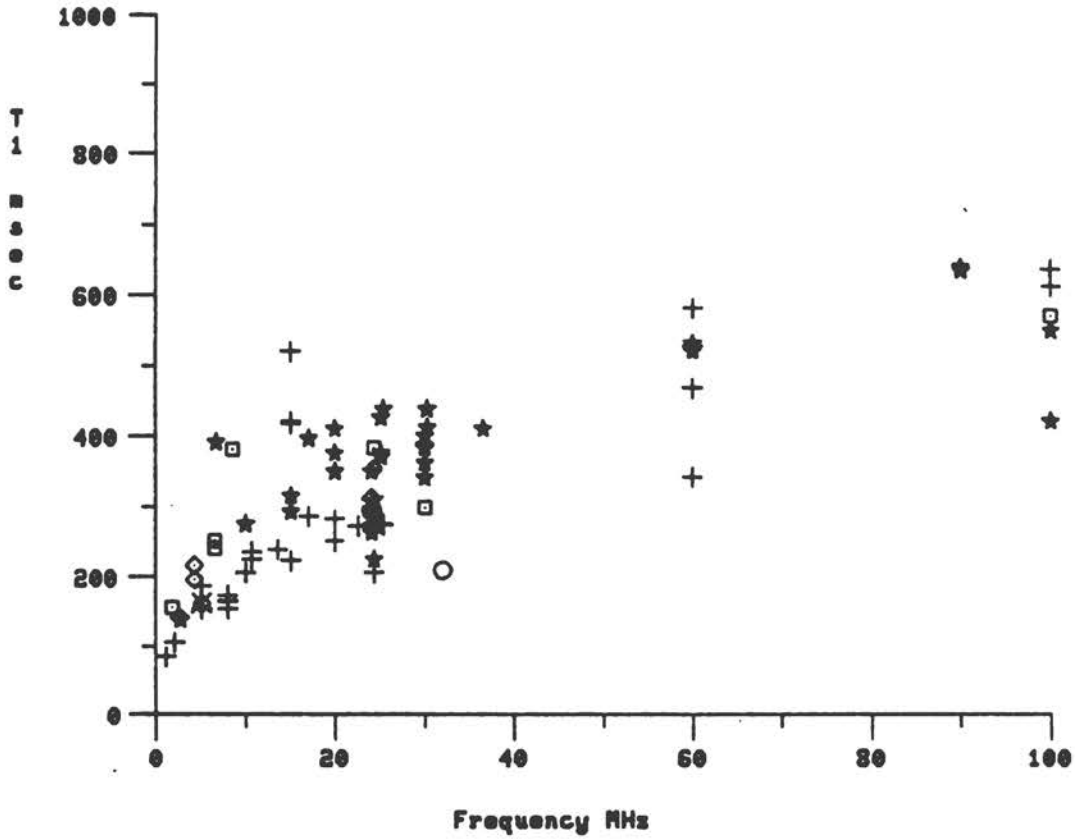

FIGURE 1 T_1 relaxation times for liver tissue vs. NMR frequency.

NEW TECHNIQUES

OPTIMIZATION OF SIGNAL-TO-NOISE RATIO

NMR imaging researchers and manufacturers continue to work on the optimization of signal-to-noise ratio, ψ. The NMR signal is proportional to the square of the NMR frequency, ν, and the noise is the sum of losses in the NMR coil and the patient, Thus, if the NMR spectrometer electronics are optimized, and dielectric losses minimized (for example, by placing a Faraday screen between coil and patient), then

$$\psi \propto \frac{\nu^2}{(\alpha a^2 \nu^{0.5} + \beta \nu^2 b^5)^{0.5}} \quad (1)$$

where a and b are the coil and sample radii, respectively, α and β are constants, and the two terms in the denominator represent contributions from coil and sample, respectively.[10]

Because patient losses cannot be reduced (except by freezing), further improvements in ψ can be achieved only by increasing the magnetic field strength ($\propto \nu$) or by reducing coil noise. The coil may be considered optimal when its noise contribution is much less than the body's contribution: the change in quality factor, Q, when the coil is unloaded, compared with that when it is loaded with the sample, is a good measure of this. For example, the Q of an unconventional 64-MHz slotted-tube resonator head coil[2] changed from 224 to 25 when it was loaded with the head, indicating that the ohmic losses in the head were about 8 times those in this coil.

Increasing the field strength is probably the most direct means of improving ψ, assuming that the electronics and coil performance remain optimized. We were recently able to obtain ^1H images of the body at 1.5 T (64 MHz), as shown in Figure 2. We measured an improvement in ψ by a factor of 11, compared with our system operating at 5.1 MHz.[1,2] This result is roughly in accord with Equation 1. At higher field strengths on NMR frequencies, the lengthening of relaxation times and the increased strength of fringing magnetic fields in the laboratory should also be considered.[8] It is likely that iron shielding will reduce the latter problem.

CLINICAL CHEMICAL-SHIFT SPECTROSCOPY

Until recently, in vivo applications of chemical-shift spectroscopy were limited to small animals by the severe demands of spectroscopy on magnet design: fields in excess of 1.0 T and homogeneity better than 1 ppm across the region of interest are required.[1] We have been able to obtain in vivo phosphorus (^{31}P), carbon (^{13}C), and ^1H chemical-shift spectra from the body by using a 1.5-T, 1-m-bore superconducting magnet.[1,2] A ^{31}P spectrum from a normal head obtained in 10 min with a 6.5-cm-diameter flat NMR "surface coil" is shown in Figure 3. Surface coils allow only the spectroscopic information from a small sensitive volume to be observed at any time.

Multiple volumes can be observed by appropriate adaptation of the imaging pulse sequence;[3,4,11] for ^{31}P and ^{13}C, however, NMR sensitivity is a severe problem. Merely changing from a surface coil to a whole-head coil is expensive in signal-to-noise ratio if

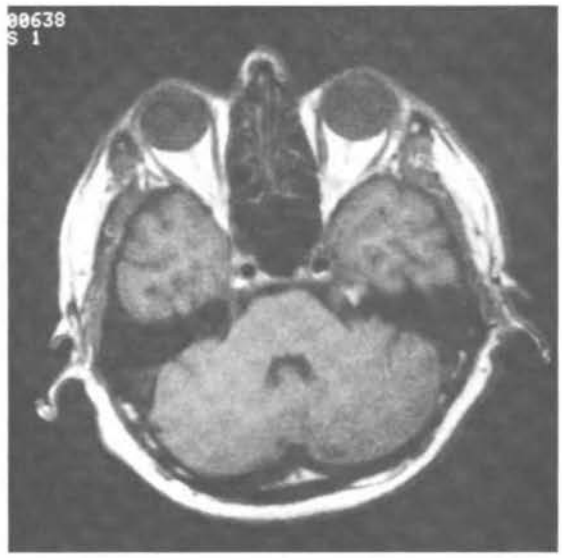

FIGURE 2 Transverse 256 x 256 pixel in 102-s image through head; recorded at 64 MHz in 102 s. Slice thickness, 4 mm. Reprinted with permission from Bottomley et al.[2]

the sensitive volume size is kept constant, because of the additional noise contributed to the head coil by the rest of the sample. Thus, we observed an approximately 6-fold reduction in signal-to-noise ratio in switching from a 6.5-cm-diameter surface coil to a 25-cm-diameter head coil for ^{31}P NMR of the same resolved volume. This is a severe blow to multiple-volume ^{31}P and ^{13}C chemical-shift imaging that uses large head and body coils: a 6-fold reduction in ψ is worth a 36-fold increase in acquisition time!

CONCLUSIONS

- The issues of standardization of NMR imaging parameters, their measurement, and the ranges of normal and abnormal values must be addressed.

- Useful head and body ^{1}H NMR images can be obtained in fields up to 1.5 T, with some improvement in signal-to-noise ratio over low field systems. Such field strengths also enable ^{31}P and ^{13}C chemical-shift information to be obtained.

- We anticipate problems with clinical three-dimensional (multiple-point) chemical-shift spectroscopic imaging where high signal-to-noise ratios, fine spatial resolution, and short patient scan times are required.

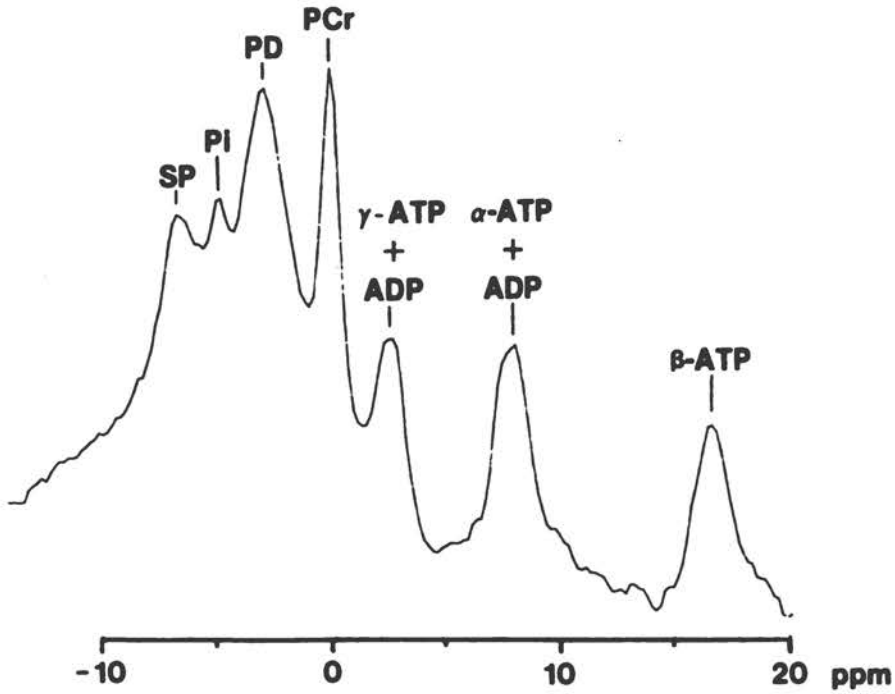

FIGURE 3 ^{31}P spectrum recorded from head with 6.5-cm-diameter surface coil. Scan time, 10 min. PCr = phosphocreatine; α -, β -, γ-ATP = α -, β -, γ-phosphates of adenosine triphosphate; PD = phosphodiesters; SP = sugar phosphate; Pi = inorganic phosphate.

REFERENCES

1. Bottomley, P. A., H. R. Hart, Jr., W. A. Edelstein, J. F. Schenck, L. S. Smith, W. M. Leue, O. M. Mueller, and R. W. Redington. Anatomy and metabolism of the normal human brain studied by magnetic resonance at 1.5 tesla. Radiology 150:441-446, 1984.

2. Bottomley, P. A., H. R. Hart, W. A. Edelstein, J. F. Schenck, L. S. Smith, W. M. Leue, O. M. Mueller, and R. W. Redington. NMR imaging/spectroscopy system to study both anatomy and metabolism. Lancet 2:273-274, 1983.

3. Bottomley, P. A., L. S. Smith, W. A. Edelstein, H. R. Hart, O. M. Mueller, W. M. Leue, R. Darrow, and R. W. Redington. Localized ^{31}P, ^{13}C, and ^{1}H NMR spectroscopy studies of the head and body at 1.5 tesla, pp. 53-54. In Scientific Program, Society of Magnetic Resonance in Medicine, 2nd Annual Meeting, San Francisco, Aug. 16-19, 1983. Berkeley, Calif.: Soc. Magn. Reson. Med., 1983.

4. Brown, T. R., B. M. Kincaid, and K. Ugurbil. NMR chemical shift imaging in three dimensions. Proc. Natl. Acad. Sci. USA 79:3523-3526, 1982.

5. Edelstein, W. A., P. A. Bottomley, H. R. Hart, and L. S. Smith. Signal, noise and contrast in nuclear magnetic resonance (NMR) imaging. J. Comput. Assist. Tomogr. 7:391-401, 1983.

6. Gore, J. C., F. H. Doyle, and J. M. Pennock. Relaxation rate enhancement observed in vivo by NMR imaging, pp. 94-106. In C. L. Partain, A. E. James, Jr., F. D. Rollo, and R. R. Price, Eds. Nuclear Magnetic Resonance (NMR) Imaging. Philadelphia: W. B. Saunders, 1983.

7. Hansen, G., L. E. Crooks, P. Davis, J. DeGroot, R. Herfkens, A. R. Margulis, C. Gooding, L. Kaufman, J. Hoenninger, M. Arakawa, R. McRee, and J. Watts. In vivo imaging of the rat anatomy with nuclear magnetic resonance. Radiology 136:695-700, 1980.

8. Hart, H. R., Jr., P. A. Bottomley, W. A. Edelstein, S. G. Karr, W. M. Leue, O. M. Mueller, R. W. Redington, J. F. Schenck, L. S. Smith, and D. Vatis. Nuclear magnetic resonance imaging: Contrast-to-noise ratio as a function of strength of magnetic field. Am. J. Roentgenol. 141:1195-1201, 1983.

9. Hazelwood, C. F., G. Cleveland, and D. Medina. Relationship between hydration and proton nuclear magnetic resonance relaxation times in tissues of tumor-bearing and non tumor-bearing mice: Implications for cancer detection. J. Natl. Canc. Inst. 52:1849-1853, 1974.

10. Hoult, D. I., and P. C. Lauterbur. The sensitivity of the zeugmatographic experiment involving human samples. J. Magn. Reson. 34:425-433, 1979.

11. Maudsley, A. A., S. K. Hilal, W. H. Perman, and H. E. Simon. Spatially resolved high resolution spectroscopy by "four-dimensional" NMR. J. Magn. Reson. 51:147-152, 1983.

12. Peemoeller, H., M. M. Pintar, and D. W. Kydon. Nuclear magnetic resonance analysis of water in natural and deuterated mouse muscle above and below freezing. Biophys. J. 29:427-435, 1980.

FUTURE DEVELOPMENTS IN PROTON NUCLEAR MAGNETIC RESONANCE IMAGING TECHNOLOGY

LAWRENCE E. CROOKS
Radiologic Imaging Laboratory
University of California, San Francisco

All instruments used to produce nuclear magnetic resonance (NMR) images have a number of common features. A strong, uniform, and stable magnetic field has to be imposed through the subject. This field has to be varied in space and time to define the location of pixels in the image. Radiofrequency energy has to be delivered to the subject to excite the nuclei. The radiofrequency signal emitted by the nuclei is detected, and its strength determines the intensities of the pixels in the image. The imaging process, data acquisition, and display are all controlled by computers.

The magnet has attracted much of the attention in discussions of NMR imaging, because of its central role in the process. The main question is what the field strength should be. Theoretical considerations predict that the NMR signal will increase as the field is increased. The theory also predicts that image signal-to-noise ratio will also increase, but more slowly. Practical factors limit the maximal value of field, i.e., the improvement that can be expected. One of these factors is the subject's absorption of the radiofrequency energy used for excitation of the nuclei and later emitted by these nuclei.[1] This absorption increases with frequency or field, inasmuch as frequency is proportional to field strength. Another factor is the design of the coil that is used to transmit and receive the radiofrequency energy.[3] Predictions based on absorption and coil limitations indicated that whole-body imaging might be difficult above frequencies of about 8-10 MHz, corresponding (for hydrogen) to magnetic fields of 0.19-0.23 tesla.[1] We published the first images obtained with a superconducting magnet at 0.35 T.[2] The contrast and resolution of these and later images indicated that the problems of higher frequencies did not prevent better performance with stronger fields. With the expectation of better performance with stronger fields, manufacturers are moving to 0.5 T and higher.

In NMR imaging, one must repeatedly measure signals from the subject to collect sufficient projections for reconstruction of the image with the desired resolution. Each signal measurement takes a short time (less than 100 ms). However, the measurement process destroys the magnetic polarization of the subject. This polarization returns with a time constant, T_1. T_1 of tissue is typically about 1 s, so this is about the time one must wait between signal measurements. The waiting time is called the repetition time, TR. If a measurement takes only 100 ms and TR is 1,000 ms, the machine is idle 90% of the time. We take advantage of this idle time to measure the signal from other, adjacent planes once every 100 ms by using selective irradiations that allow us to excite and measure a plane without disturbing its neighbors. With a TR of 1,000 ms, we obtain images of 10 planes in the time that it would otherwise take for one. For a 128-line image with four averages of the signal for each projection, the image time is 8.5 min, for an average time per slice of 51 s.[2] Thus, we have provided the option of having a TR of 2,000 ms to allow more complete recovery of polarization. With this value of TR, we image 20 slices in 17 min, and that allows complete imaging of the brain with one procedure. The long TR also produces images that are very sensitive to lesions in the brain and spine.

Cerebrospinal fluid (CSF) has a long T_1, so it requires a long TR to provide a strong signal. A long TR is useful when one wants to distinguish between CSF and the dark bone. In this case, the definition between CSF and cord is limited, but it is well defined with a short TR (500 ms), in which case CSF is dark, like bone, and contrasts well with the bright cord. With a TR of 500 ms, five slices are imaged in 4.3 min. If we have 17 min, we can select more signal averaging to get a better signal-to-noise ratio in this weaker-signal situation.

In the future, more flexibility in number of planes and spin echoes will be available. The examples cited above were for two spin echoes acquired in 60 ms. If five spin echoes are acquired, extending out to a time of 200 ms, the amount of contrast due to T_2-based signal decay will increase. It is expected that this contrast will be useful in determining the separation of edema surrounding a tumor from the tumor core. These extra echoes are not without cost: only half as many planes can be imaged at a given TR. If only one echo is needed, it can be acquired in less than 50 ms, and twice as many slices can be imaged in a given TR. For example, with a TR of 1,000 ms, 20 slices can be imaged in 8.5 min.

Additional time can also be used to increase spatial resolution. Resolution of our 128 x 128 image is 1.7 x 1.7 x 7 mm. By doubling the imaging gradients and image time, one can produce a 256 x 256 image with a resolution of 0.8 x 0.8 x 7 mm. This resolution

increase makes small lesions (such as those of multiple sclerosis) more visible, even though the signal-to-noise ratio is worse by a factor of 2.8. For 20 slices with a TR of 2,000 ms, the imaging time is 34 min.

REFERENCES

1. Bottomley, P. A., and E. R. Andrew. RF magnetic field penetration, phase shift, and power dissipation in biological tissue: Implications for NMR imaging. Phys. Med. Biol. 23:630-643, 1978.

2. Crooks, L., M. Arakawa, J. Hoenninger, J. Watts, R. McRee, L. Kaufman, P. L. Davis, A. R. Margulis, and J. DeGroot. Nuclear magnetic resonance whole-body imager operating at 3.5 Kgauss. Radiology 143:169-174, 1982.

3. Hoult, D. I., and P. C. Lauterbur. The sensitivity of the zeugmatographic experiment involving human subjects. J. Mag. Res. 34:425-433, 1979.

FACTORS AFFECTING THE DESIGN OF NUCLEAR MAGNETIC RESONANCE IMAGING SYSTEMS

G. NEIL HOLLAND
Picker International
Highland Heights, Ohio

Nuclear magnetic resonance (NMR) imaging is now entering a phase of clinical evaluation in which its strength and weaknesses as a diagnostic tool are being determined. All medical NMR imaging systems have used the proton (^1H) as the nuclear species for examination, with resonant frequencies of 1.7-64 MHz[4,5] corresponding to field strengths of 0.04-1.5 T. Initially, systems were constructed with resistive magnets for field strengths between 0.04 and 0.15 T. At 0.15 T, approximately 50-kW power dissipation is produced, and most workers regard this as a practical upper limit. Superconducting magnets have been used at field strengths of 0.15-1.5 T. The rationale for increasing field strength is the same as has driven conventional spectroscopy from 60 to 470 MHz proton resonant frequencies in little more than 15 years: improved signal-to-noise (S/N) ratio and resolution. The conventional relationship, $S/N \propto H_0^{3/2}$, does not hold true, given dielectric losses in the human body; but, even so, there is an approximately linear relationship between S/N and field strength,[3] which gives credence to the drive to higher field strengths. Field strength cannot rise indefinitely, even if improvements in magnet technology allow it to continue on an upward path. Radiofrequency (RF) phase shift and absorption in body tissue ultimately limit resonant frequency, although the estimated point at which these effects would become prohibitive[1] is far below what can be attained in practice.

Other factors come into play when one is determining the upper frequency limit of whole-body NMR imaging devices, which are associated with the efficiency of the radiofrequency coil system. Conventional coils become inefficient when the coil length is greater than $0.05\ \lambda$, where λ is the wavelength of the applied radiation.[2] Because coil size is dictated by the human body, alternative approaches that borrow heavily from microwave antenna techniques (such as the use of cavity resonators) have to be used to allow coil operation above about 40 MHz.

Some other characteristics of large superconducting magnets have to be considered. The fringe field of a 1.5-T magnet extends at least 15 m from its isocenter in three dimensions. In an unshielded environment, the operation of magnetosensitive devices, such as cathode ray tubes and photomultiplier tubes, will be impaired. High-field NMR imaging devices can be placed in entirely unshielded sites, in which case support equipment, particularly computer and display units, must be kept far from the magnet itself; or large masses of steel can be used to shield the magnet and external influences from each other. Steel shielding is not trivial, inasmuch as it requires complex analysis to determine its size and location. Depending on the permeability of the ferrous material used, upwards of 50 tons of steel may be required to shield a 2.0-T magnet. Such considerations affect the cost and complexity of site planning and construction.

A final point on magnets: It should be remembered that helium, the cryogen used in superconducting magnet systems, is a nonrenewable natural resource. It is found at low concentrations in natural gas deposits. Taking into account known sources, some estimates show that the supply of helium will be exhausted in the 1990s. The proliferation of superconducting NMR imaging systems constitutes a substantial drain on the total helium supply. Because the supply is finite, development of magnet systems to reduce the quantity of helium used will continue to take place. These developments include the use of lower-volume Dewars and of liquefiers to permit expended gas to be reused.

The use of higher field strengths also permits the acquisition of NMR signals from nuclei other than hydrogen. Biologically and clinically important nuclei include ^{31}P, ^{13}C, ^{23}Na, and ^{19}F. In a constant field, all other nuclei resonate at lower frequencies than the proton. For the nuclei listed above, the frequency has a range of approximately a factor of 4, from ^{1}H at the top to ^{13}C at the bottom. Covering this frequency range places some dictates on RF design. To facilitate easy switching between nuclei, the RF electronics should be of a broadband type capable of covering the frequency range without retuning. This is possible with the use of heterodyned receiver and transmitter circuitry. The RF coils themselves have to be changed to work with other nuclei. Regrettably, all other nuclei have lower sensitivity than the proton--a situation made worse by typically much lower biological or natural abundance. Actually imaging the distribution of other nuclei is probably not promising at whole-body sizes, because of poor signal-to-noise ratios and attendant long acquisition times. Acquiring spatial and spectroscopic information with chemical-shift imaging techniques and three-dimensional Fourier transformation therefore is unlikely to be practical. Spectroscopic information is most likely to be limited to acquisition from surface

coils, which allow much greater sensitivity (through increased filling factor). To increase information throughput (data rate), it is possible to contemplate time-shared multinuclei operation where the acquisition of signals from two surface coils resonating at different Larmor frequencies can be time-shared, or a single double-resonance coil could be used. Such techniques will further increase the complexity of the RF system.

Other elements of the NMR system are affected by the drive for the encoding of more information in the NMR signal. Techniques for spatial localization use a combination of magnetic field profiling and spectral tailoring of RF excitation. In all NMR techniques in medicine, linear field gradients are used, but the precise characteristics of the gradient waveforms are method-dependent; hence, the methods used in the NMR system affect the design of the gradient subsystem. For example, some NMR imaging techniques use relatively strong (about 5 mT/m) gradients that are quasistatic or slowly oscillating. However, most widely used two-dimensional imaging methods have less strong (1-2 mT/m) gradients applied in the form of fast-rising pulses. The characteristics of the amplifier-coil combination would be different in the two cases. The first type could use a large number of turns on the gradient coils to limit the magnitude of applied current. The second type would have coils with a small number of turns to achieve fast rise times, but require much greater current amplification. Some new techniques designed to increase the data encoding rate of the NMR imaging process use in essence a combination of the two gradient waveform types. In other words, stronger oscillating gradients applied in the form of pulses are required, and that tends to increase both the current requirement and the bandwidth of the gradient system.

Techniques for shimming the static field are determined by the NMR methods used. If only two-dimensional imaging is available, the static field is usually shimmed by a combination of passive and active means, with iron and a DC-powered shim set. Once the desired degree of homogeneity has been obtained, shimming is complete. This process is usually performed at the time of system installation. If, however, spectroscopic techniques with surface coils are to be used, a more versatile method of shimming is required, because such techniques need very high homogeneity over the surface coil sensitive volume. The ability to vary the localized shimming in a practical manner predicates a computer-controlled shim set.

Finally, the multimode operation that an NMR system is capable of implies that the computer system needs to be large and fast to handle the quantity of data that the NMR process can produce. Because NMR imaging is an inherently three-dimensional process, the computer system needs to have a large memory capacity to handle a full three-dimensional matrix.

REFERENCES

1. Bottomley, P. A., and E. R. Andrew. RF magnetic field penetration, phase shift and power dissipation in biological tissue: Implications for NMR imaging. Phys. Med. Biol. 23:630-643, 1978.

2. Hoult, D. I. Radio frequency coil technology in NMR scanning, pp. 33-39. In R. L. Witcofski, N. Karstaedt, and C. L. Partain, Eds. Nuclear Magnetic Resonance Imaging: Proceedings of an International Symposium on Magnetic Resonance Imaging, Bowman Gray School of Medicine of Wake Forest Univ., Winston-Salem, N.C., 1981. Winston-Salem, N.C.: Bowman Gray School of Medicine, 1982.

3. Hoult, D. I., and P. C. Lauterbur. The sensitivity of the zeugmatographic experiment involving human samples. J. Magn. Reson. 34:425-433, 1979.

4. Hutchinson, J. M. S., W. A. Edelstein, and G. Johnson. A whole-body NMR imaging machine. J. Phys. E. 13:947-955, 1980.

5. Society of Magnetic Resonance in Medicine. Program and Book of Abstracts, Second Annual Meeting, San Francisco, California, August 1983.

COMPUTER DEVELOPMENT AND USE IN IMAGING

RUTH M. DAVIS
The Pymatuning Group
Washington, D.C.

THE IMPORTANCE OF OBSERVATION

Throughout the centuries, observation has been essential to the practice, understanding, and advancement of the sciences and engineering. Instrumentation in turn has been essential in removing our reliance on the human eye alone for observation. Telescopes have shown us the excitement of space and of objects in space, and microscopes have allowed us to probe the microscopic--in nuclei, molecules, human tissue, and materials.

Generally, it has been instrumentation that has paced advances in observational sciences, measurement precision, and data collection and presentation. Limits on our intellectual and reasoning capabilities have, of course, been the controlling factor in advances in the analytic sciences, mathematics, and data interpretation and assimilation. But even in the latter, instrumentation has helped to overcome human limitations.

As we continue to seek scientific and engineering advances, it becomes increasingly important to vigorously apply the instruments that improve observation, to design new instruments to meet unmet needs of observation, and to promote partnerships between scientists and engineers aimed at developing observational instrumentation.

OBSERVATION AND THE COMPUTER

In the recent past--roughtly in the last 30 years--improvements in observational instrumentation have been so rapid and dramatic that the scientific and engineering world has not been able to keep up with its newly found riches. The jewel in this treasure chest has been the computer, and the setting for the jewel has been electronics and, recently, microelectronics.

The computer has come to serve as:

- The control device for observational tasks.
- The data collector.
- The data bank.
- The data handler.
- The data presenter.
- The data archiver.

Additionally, and very subtly, the computer has collapsed the time between observation and action based on observation to zero. Observation has thus become an element of a real-time process. We see this with nuclear magnetic resonance (NMR) instruments and cardiac "surgery," with space-borne imaging radar and automated weapons deployment, with ultrasonic imaging in nondestructive evaluation (NDE) coupled with immediate remote repair, and with weather imaging satellites and their automated graphic readouts for television viewing of weather data.

This broad applicability of computers in many observational scientific and engineering fields lends considerable leverage to each advance in computer capacity and performance. For example, the emphasis placed on processing of images from satellites in the early 1960s led to computational advances that were equally applicable to biological imaging. We have been benefiting from such leverage for over 20 years.

One gradual change--so subtle that it is often unnoticed--is that computers have become integral components of most modern observational instruments. It is easy to forget that the "C" in "CAT scanning" stands for "computed" (CAT = computed axial tomography). We also tend to forget that microprocessors are parts of systems for practical, noninvasive diagnostic techniques, such as positron-emission tomography (PET), medical ultrasonic imaging, and medical diagnosis using somatosensory evoked potentials.

Seeing and hearing have been and still are the primary senses in observational science and engineering. (Indeed, in this discussion we will not cover touch, taste, and smell.) Yet instrumentation improvements over the centuries, accentuated by the rapid changes of the last three decades, have extended both our visual and our acoustic observational capabilities. We have expanded from the human or visible wavelength spectrum of 0.3-0.75 μm and have simultaneously moved out of the human acoustic frequency range of

500-15 Hz to 300 MHz and above for acoustic microscopy. The opening up of the electromagnetic spectrum to observational sensors has made imagery a remarkably powerful asset in many fields of science and engineering, and computer advances of the last two decades have made image processing a most powerful instrument for observation.

SOME TECHNICAL CLARIFICATIONS

The field we refer to as automated imaging has grown up in a rather topsy-turvy manner, but fortunately is maturing nicely. By "topsy-turvy" I refer to the partial ownership of automated image processing in its early days by the mathematics, photo-interpreter, computer, and signal-processing communities. All these specialty fields advanced, applied, and tinkered with the processes of imaging.

To use a slightly revised definition:[5]

Image processing is the manipulation and analysis of a picture of an object or scene. Its major subareas include:

> . . . Digitization and compression: converting pictures to discrete, i.e., digital form: efficient coding or approximation of pictures to save storage space or channel capacity.
>
> . . . Enhancement, restoration, and reconstruction: improving degraded (low-contrast, blurred, noisy) pictures: reconstruct pictures from sets of projections.
>
> . . . Matching, description, and recognition: comparing and registering pictures to one another; segmenting pictures into parts, measuring properties of and relationships among the parts, and comparing the resulting descriptions to models that define classes of pictures.

It is useful to remind ourselves that, throughout its computer history, the primary function of image processing, has been to make it easier for people to use and interpret source imagery. The steps involved are often nonlinear, in order to match the human visual system, but when completed always leave the data as an image--i.e., a two-dimensional intensity map in the spatial domain. Such two-dimensional imagery encompasses what we refer to as the three-dimensional views of the body provided by CAT scanning and NMR imaging.

Until recently, automated image interpretation has been confined to specialized applications, generally referred to as signal processing. The functions of signal processing tend to be more varied than those of image processing. They are aimed at modifying

data for automated interpretation and often include Fourier transforms, because the interpretation need not be in the spatial domain. Signal processing is more often linear than nonlinear, inasmuch as human interpretation is not required. When a human is involved in signal processing, the data are generally presented in an abstract form, for example, in plots of power spectral density.

The general purpose of imaging has been invariant: to map, probe, measure, and characterize an object with radiation from the object either naturally or stimulated by instrumentation. In health care and medical research, a specific objective of imaging is noninvasive analyses of body parts. We are dealing with any measurable forms of energy and with the entire electromagnetic spectrum as our energy domain. I highlight the intimate association of energy or radiation with image processing, because it has been primarily through computer and electronics or microelectronics advances that the instrumentation--e.g., sensors, processors, and displays--has made the useful exploitation of nonoptical imaging and the increased resolution of exploitable imaging across the electromagnetic spectrum possible.

Acoustic, x-ray, nuclear-particle, infrared, radar, and magnetic fields are the familiar examples today of nonoptical radiation for imaging. Because its interactions with matter depend on the mechanical properties of matter, acoustic energy can provide a map or an image of an object that is not available with the use of other types of radiation. However, each of the radiative imaging processes has a contribution to make to biological and other applications, and they all exploit, as well as task, computer capacity and performance.

HIGHLIGHTS OF COMPUTER DEVELOPMENT

I propose to identify here the aspects of computer systems on which successful image and signal processing are most dependent and then to highlight the important accomplishments or current deficiencies.

The features of computer systems relevant to biological imaging appear to be:

- Real-time imaging sensors.
- Automated control of real-time imaging sensors.
- High throughput and performance of parallel-processed imagery.
- Very large on-line memory capacity.

- On-line interactive color imagery for man-in-the-loop image-processing systems.

- Very-high-speed associative and "intelligent" processing, either in conjunction with humans or totally automated; we often call such subsystems "expert systems" or "relational data base systems."

I shall attempt to treat only a few of the recent, prominent features of computer development that appear to be most relevant to achieving the best in biological imaging--specifically, computer image displays and automated image-processing architectures.

COMPUTER IMAGING AND IMAGE DISPLAYS

The phrase "one picture is worth a thousand words" is by now trite. However, I want to fall back on it one more time in highlighting the importance of computer imaging to biological imaging. Today, as throughout computer history, a principal deficiency is in input/output (I/O) systems or sensors. Communication with computers can theoretically occur via natural language, spoken or written; via pictures or images; via documents and messages; or via other sensor operating in different regions of the electromagnetic spectrum, e.g., acoustic and infrared.

Natural-language communication has been remarkably slow to develop; linear strings, symbols, or signals have severe limitations in depicting spatial entities. Hence, I have always put great emphasis on image processing or pattern recognition for communicating pictorial, spatial, or imagery information. Figuring prominently in this form of communication are the transducers that form an interface between the source imagery and the imagery displayed and processed via automated systems. This area, termed image display, constitutes the great strength of biological imaging. It also represents the portion of technology in which gains contribute the greatest leverage in application.

Digital image display, in turn, is the workhorse of automated imagery. It is distinguished from graphic display by its ability to store multiple digital images of full gray-scale range and to refresh either monochrome or color displays at real-time rates by using raster scan techniques. The applications that depend on digital displays include all those biological imaging--x-ray pictures, CAT scans, NMR images, and multiplanar images.

Although an overall goal is to automate as much of computer imaging as possible, the near term should see great concentration on the human-computer iterative image interpretation.

In the last 4 years, real-time image processing--e.g., pixel processing--has become economically feasible. The turning point was when arithmetic processor cycle times fell below the basic pixel refresh time on the image display. The next important gain occurred just recently with very large scale integration (VLSI), when not only did switching times fall below 4 picoseconds (4 ps) with complementary metal oxide on silicon (CMOS) and metal oxide on silicon (MOS) processors, but also the reduction in power consumption (e.g., heat) made possible 1.5-micrometer line-width chips with 1,000-gate density.

The problem of image-display components themselves have proved far more difficult to overcome. Cathode-ray tubes (CRTs) can handle 1,000 x 1,000-pixel color displays with useful resolution, although they are somewhat dense for human interpretation. This resolution, however, entails fundamental physical limitations. Fortunately, the low-power, solid-state flat-panel display has now become a reality with high resolution and color purity.

VLSI memories with increasing densities and decreasing costs continue to improve dramatically the volumes of refresh data that can be processed in real-time. The random access memory (RAM) chips of 64,000 bytes and especially of 256,000 bytes, coupled with the processing speeds associated with VLSI, are hastening the advent of "intelligent" color displays, so that much of the real-time image processing can be done in the display itself. An obvious example is the speedup that can occur in searching large image areas for a "small" area of interest. This processing task, handled in conjunction with a zoom system, will allow for rapid operator selection and swapping among a large stream of imagery data.[4]

A quick look at optical-scanning digitizers will complete this summary review. Optical scanners convert pictures into arrays of numbers that represent the positional distribution of optical density in the image.[3] They are integral to tomography: the transmittance of body parts to x-rays or ultrasound in various directions is converted directly to digital form for later three-dimensional recovery. They are also used routinely in hematology and cytology.

Some of the important recent advances in optical scanners have been related to satellite scanners. Mechanical scanners have long since been replaced by solid-state transducers, and multispectral scanners and vidicon cameras have made color common in image handling.

CRT scanners capable of addressing 4,000 x 4,000 nonoverlapping picture elements are well in hand. Vidicon and plumbicon cameras and orthicon tubes constitute the available set of television scanners. Generally, they are suitable for applications needing up to

1,000 x 1,000 samples, with fine tuning quadrupling that in each dimension. Television cameras are heavily used in biological imaging, in which case the relatively small scanning array and lack of geometric accuracy are not a hindrance.[3]

For greater accuracy, however, we have electro-optical scanners and solid-state scanners; the latter are finding some use in biomedical applications.

If one were to summarize the weak link in optical scanners today, it would be data base management and parallel processing software.

There is no doubt, in any case, that digital color-image displays are at the heart of advances in biological imaging.

AUTOMATED IMAGE-PROCESSING ARCHITECTURES

A dominant characteristic of image processing is the simultaneous performance of a given mathematical or logical function on each element of an extremely large set of data. In addition, image processing usually has to deal with only a small set of adjacent points, spots, or regions of the image in any one operation. The terms edge enhancement, feature extraction, blurring, etc.--all phrases associated with image processing--serve to illustrate these two distinguishing features.

The characterization of the image processing desired allows one to match it against various computer architectures to attain a best fit. Today, conventional computer architectures fall into three groups:[2]

- Pipeline computers feature the single-instruction, single-data-stream mode of operation. They are the closest progeny of the original von Neumann computer. They perform serial, continuous vector processing for image processing.

- Array processors use multiple processing elements under common synchronous control with parallel operations performed in lock-step. Image processing uses the single-instruction, multiple-data-stream mode of operation to achieve spatial parallel processing.

- Multiprocessor systems contain multiple central processing units (CPUs) or mainframes with shared memories and shared peripheral units. Image processing generally uses the interactive-multiple-instruction, multiple-data-stream mode of operation.

Most image-processing systems use array processors or pipeline processors. Some of the more complex or sophisticated image-processing systems use a hybrid pipeline-array processor architecture. It is difficult for multiprocessor architecture to achieve good algorithm partitioning or good memory and peripheral allocation among image-processing tasks.

One interesting approach to biological image processing is exemplified by what has been named the cytocomputer[6]—a special-purpose computer that uses a parallel pipeline architecture with a specially developed high-level language, C-3PL. The cytocomputer developed at the University of Michigan achieves real-time processing of gel data via stages of parallel cellular processing within a serial pipeline.

As one might expect both from the characteristics of image processing and from the examples just cited, biological image processing can most effectively and efficiently exploit the array-processor architecture, because of its "designed-in" parallel mode of operation. Two of the newer imaging systems, digital radiography and NMR, highlight the historical pattern. NMR, for example, involves three-dimensional image processing with attendant demands for very large memories and sophisticated software. One should anticipate in the very near future even greater demands for higher-speed array processors that have higher input rates and larger, higher-speed on-line memories.[1]

Looking at NMR again as a potential stellar performer in biological imaging, we note that the computational burden of NMR is equal to if not greater than that of computed tomography (CT) scanning. In particular, fast Fourier transformation (FFT) routines are essential and emphasize not only the need for parallel processing to obtain higher speed, but also the need for the higher-speed VLSI technology. Picosecond switching speeds found, for example, in Josephson junction circuitry will be welcome.

In a typical array-processor tomography scanner that uses FFTs for convolution calculations, it is useful to obtain a feeling for recent advances in high-speed imaging. A typical set of computations for a single CT cross section totals some 50 million calculations. When this is translated to 200-nanosecond add/multiply circuitry, the resulting processing time for a complete cross section is 5 seconds.[1] Even this engineering accomplishment will probably improve by a factor of 10 in the next few years.

In concluding this short visit to computer architecture, we might ask, "What are some of the pressures that biological imaging is placing on computer science and engineering?" I suggest that some of the more important pressures will arise from demands for:

- Increased image resolution, which in turn demands even greater computer power.

- Improved image quality, which depends on more complex projection schemes.

- Increased need for higher data-transfer rates, which will probably necessitate different data bus structures.

- More interactive displays and more sophisticated sensor transducers, which will lead inevitably to more control microprocessors.

Hence, the future includes more raw power and speed, more sophisticated algorithms, and certainly VLSI circuitry.

CONCLUSIONS AND OBSERVATIONS

Experience has shown that, in computerized systems with the complexities of image processing, the design and operational costs will be some 10 times greater if man is kept in-the-loop than if the system is totally automated. Hence, it probably is well worth a heavy investment in research and development to remove humans as members of an image-processing system. Benefits of such a large investment accrue directly to a particular image-processing system, however, only when the investment is shared. The associated front-end costs are normally too high for a supplier or customer of a single (i.e., unique) system.

Expert systems or knowledge-based systems (KBS), although extremely useful for dialogue between user and computer, will be too costly for implementation in image-processing systems for some 2-5 years, i.e., until the late 1980s. A rule of thumb is that "rule" in an expert system costs (and will continue to cost for 2-5 years) about $2,000. A typical high-performance biological-imaging system can be expected to have between 1,000 and 3,000 rules. Hence, a rough estimate of the cost of an expert biological-imaging system would be between $2 and $6 million--and this is just for system software, not for data update and management software.

"Intelligent" automated imaging sensors are keystone equipment components for real-time automated imaging. Although work on these components has been continuous since the late 1940s, rapid advances have occurred only in the last half-decade, with the miniaturization of electronics, reduction in price, and the supplanting of analog devices with digital devices in real-time sensors. Sophistication, flexibility, and reliability are relative newcomers to imaging sensors, and a major obstacle to their introduction and use in systems is the lack of an adequate engineering manpower pool.

Customers have more often than not had to be their own "handymen" in handmade prototypes of instruments for real-time imaging systems. I must add that this is not true, for example, in totally automated remote-space imaging. Unfortunately, until we build a better cadre of dedicated engineers with the appropriate skills, the "critical mass" necessary for wide-scale application and technology transfer will be missing.

The development of real-time biological-imaging systems should be given high priority in computer research. The singularly important advances in medical diagnostics depend on these systems--so also do many hoped-for discoveries in medical research.

Medical reserarchers, perhaps more than researchers in any other science, have found great satisfaction in team arrangements with electronic and computer specialists to achieve what today is popularly termed synergy. This is in contrast with the "arms-length" approach typical of most scientific or professional development of computer applications. Such arrangements rank with the best of entrepreneurial techniques and should be nurtured and protected. A capability to rapidly develop and apply dedicated technology is easily as important as the more antiseptic, sterile forward advance of technology.

The technologic deficiencies of biological imaging that warrant the greatest allocation of scientific and engineering resources are:

- Algorithmic and logical foundations for the real-time processing of spatial or imagery information, especially matching and recognition.

- Computer-system architectures optimized for image processing.

- Refresh memories, video rate processing, and the image-display component itself of computer image-display systems.

I conclude by pointing out the obvious: the futures of biological imaging, medical diagnosis, and many lines of medical research are inextricably linked to advances in computers, microelectronics, sensors, and software. It behooves us to understand the latter sufficiently to be able to participate in their application to the former.

REFERENCES

1. Alexander, P. Array processors in medical imaging. IEEE Computer, June 1983, pp. 17-30.

2. Hwang, K. Computer architectures for image processing. IEEE Computer, January 1983, pp. 10-12.

3. Nagy, G. Optical scanning digitizers. IEEE Computer, May 1983 pp. 13-24.

4. Reader, C., and L. Hubble. Trends in image display systems. Proc. IEEE 69:606-614, 1981.

5. Rosenfeld, A., and A. C. Kak. Introduction, pp. 1-9. In Digital Picture Processing, 2nd ed. Vol. 1. New York: Academic Press, 1982.

6. Sternberg, S. R. Biomedical image processing. IEEE Computer, January 1983, pp. 22-34.

COMMENTS ON DATA ACQUISITION IN NUCLEAR MAGNETIC RESONANCE IMAGING

DONALD B. TWIEG
Department of Radiology
University of Texas Health Science Center at Dallas

It is useful in discussing medical imaging to conceive of the imaging process as taking place in two stages (see Figure 1): in the first, information on the object to be imaged is encoded into raw data; in the second, the raw data are decoded to produce images. This view, developed by Wagner and Brown,[9] can be applied usefully to several imaging modalities. In x-ray computed tomography, for instance, the raw data produced in the encoding stage are the entire set of projections used to reconstruct an image. The decoding stage (in Wagner and Brown's terminology, the display stage) consists in this case of the reconstruction computations and image display. In any imaging modality, it is in the encoding, or acquisition, stage that fundamental limits on image quality are established.

It is also in the acquisition stage that nuclear magnetic resonance (NMR) imaging differs greatly from the other kinds of medical imaging. Much of the current interest in NMR imaging centers on its versatility--its ability to image several fundamentally different physical characteristics (e.g., proton densities and relaxation times) and its potential for revealing biochemical distinctions by chemical-shift imaging. In NMR imaging, the data-acquisition process is versatile in yet another way, which has not been recognized or used widely. NMR image encoding--via radio-frequency pulses, gradient waveforms, and sampling procedures (see Figure 1)--is subject to a degree of control unprecedented in medical imaging. This control of the acquisition process might be used to influence image quality and imaging times and thus to improve the effectiveness of clinical NMR imaging. I will discuss here how this flexibility arises and how it influences the quality of NMR images.

One can think of an image, whether a scene or a cross-sectional picture of a body, as a mixture of detailed structures (such as leaves in a forest scene) and larger, smoother features (such as a large mountain in the background). This is often helpful in

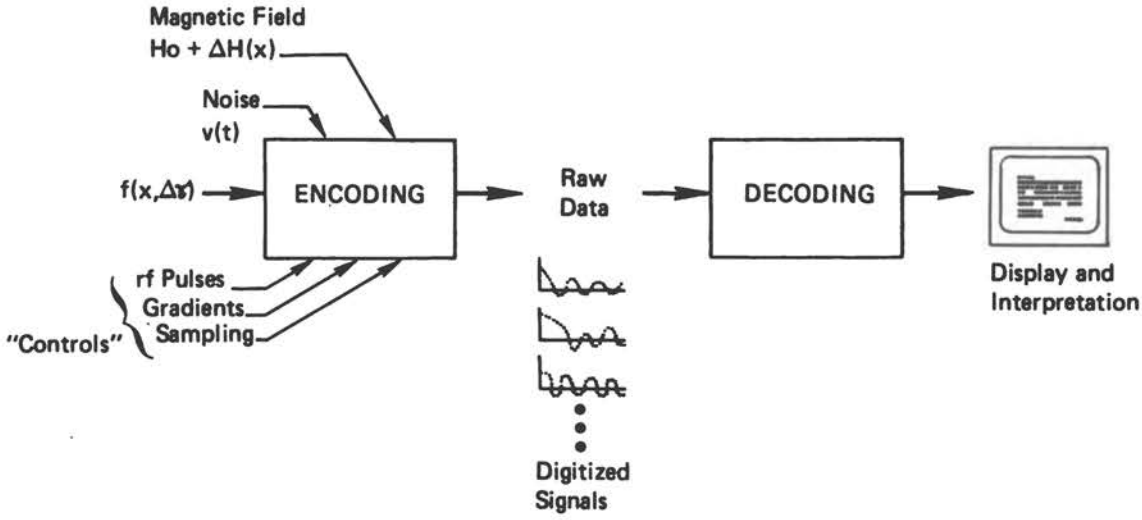

FIGURE 1 Schematic overview of NMR imaging process, indicating two stages of encoding and decoding, as example of general imaging model of Wagner and Brown.[9] Images displayed at end of process are formed from raw imaging data by decoding process. Ability of decoding process to represent original object distribution (in general, a function of position relaxation times and gyromagnetic ratio) is limited by ability of encoding operation to convert appropriate information into raw data (see text). In NMR imaging, encoding is subject to influence of instrumental factors, such as field inhomogeneity and noise and to some degree of control via radiofrequency pulses, field gradients, and sampling schedules.

characterizing imaging systems, because most systems yield images that are imperfect in a systematic way--that is, a system can be characterized by the deficiencies in the images it produces. For instance, if an imaging system cannot successfully represent very fine details in one scene, it will fail predictably in representing fine details in any scene, and it will be said to have poor spatial resolution.

Because the Fourier components make the concepts of fine and coarse details mathematically more precise, they make possible subtle and useful quantitative descriptions of imaging performance; we can describe imaging performance for many systems in terms of how

well they characteristically render the Fourier components. This sort of quantitative description (for instance, the transfer function, a mathematical description of a system's sensitivity to fine and coarse image features) has been valuable in comparing and designing optical imaging systems and various medical imaging systems.

The Fourier components can be seen as a set of sinusoidal waves in two dimensions (see Figure 2). Each component has its own number of waves per unit distance, and the troughs and crests of the waves make a distinct angle with the horizontal axis. They may be regarded as the elementary constituents of any image, the image being completely described by how much of each component it "contains." Thus, given the amounts of the components present in some otherwise unknown image, one can reconstitute the image exactly by adding the components in those amounts. (In mathematical terms, the Fourier components are basis functions for the image distributions.)

Consider a simplified picture of what happens during acquisition of two-dimensional NMR image data (see Figure 2). Suppose we have a uniform two-dimensional object (Figure 2a), with all magnetization vectors initially parallel in the horizontal plane and the main magnetic field applied along the vertical axis. (A preliminary rf pulse, or sequence of pulses, is necessary to move the vectors from their equilibrium positions aligned with the magnetic field into the horizontal plane.) If there is no gradient across the object, all vectors will precess (rotate in the horizontal plane) at the same rate under the influence of the magnetic field, and a plot of one of the components of the vectors will be a constant function of position and of time. If a linear field gradient is applied across the object, the magnetization vectors will precess more rapidly where the total field has been increased by the gradient field and will continue to precess at the same rate where the gradient is zero (at the lower left of each vector array in Figure 2). Thus, after some period, the vectors on the right will have precessed through some phase angle relative to the vectors on the left, and the vectors in between will have precessed through linearly increasing phase angles from left to right. Thus the y components of the magnetization vectors across the object at any given time during the application of the gradient can be plotted as a sinusoidal surface. Furthermore, the surface will become more "wrinkled" with time, as the magnetization vectors at one side accumulate more and more phase lead over the vectors at the other side. At some times during this undulation, the x- or y-amplitude surface of the uniform spin distribution will have become folded exactly into the form of one of the elementary Fourier components.

The raw data of NMR imaging are digitized versions of rf signals emitted by the imaged object and induced in a coil. At any given time, the signal induced in the coil corresponds to the sum of the

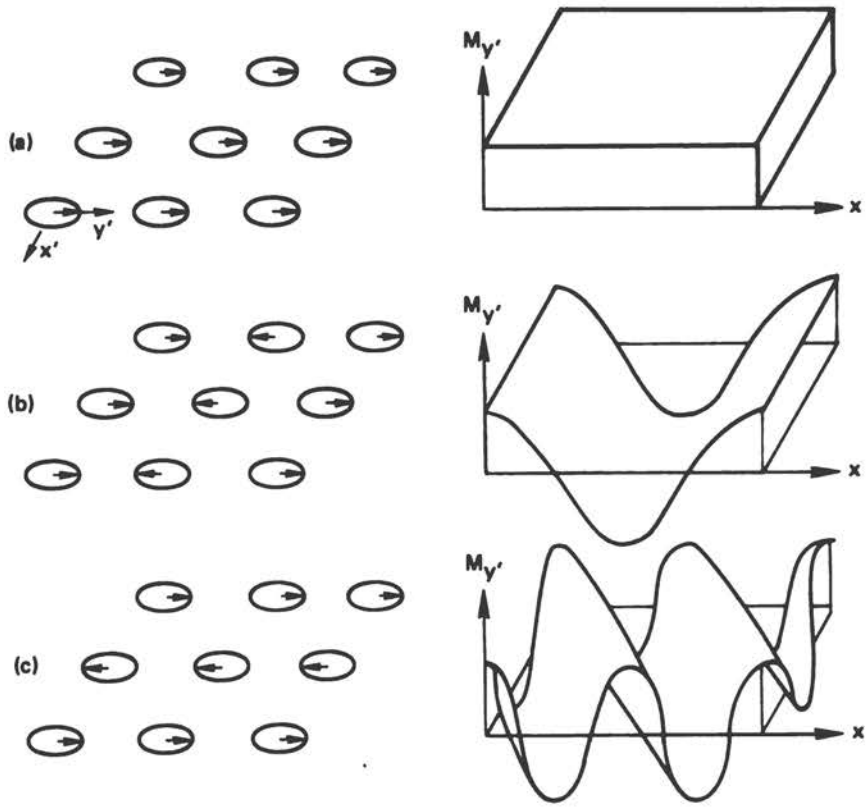

FIGURE 2 (a) Array of magnetization vectors within uniform object after excitation. Because vectors are initially in phase throughout object, spatial distribution of either of vector components is uniform. (b) After magnetic-field gradient has been applied across object (with field higher on right), vectors on right have precessed one complete cycle, and vectors at intermediate positions have precessed through intermediate phase angles. $M_{y'}$ component is now distributed as sinusoidal surface in space. (c) Spatial distribution of phases and $M_{y'}$ component at moment after application of both x and y gradients.

minute signals contributed by all the magnetization vectors in the object. (This rf signal is usually "phase-sensitive detected"--converted to an audiofrequency signal--before it is digitized.)

At some moment during the application of a gradient, the magnetization vectors in an object will have been undulated into a sinusoidal wave corresponding to a particular Fourier component.

The detected signal at that moment represents exactly the amount of that Fourier component present in the object (Figure 3). (Although it does not alter the conceptual picture, it should be noted that the signal and the Fourier components are generally complex quantities.)

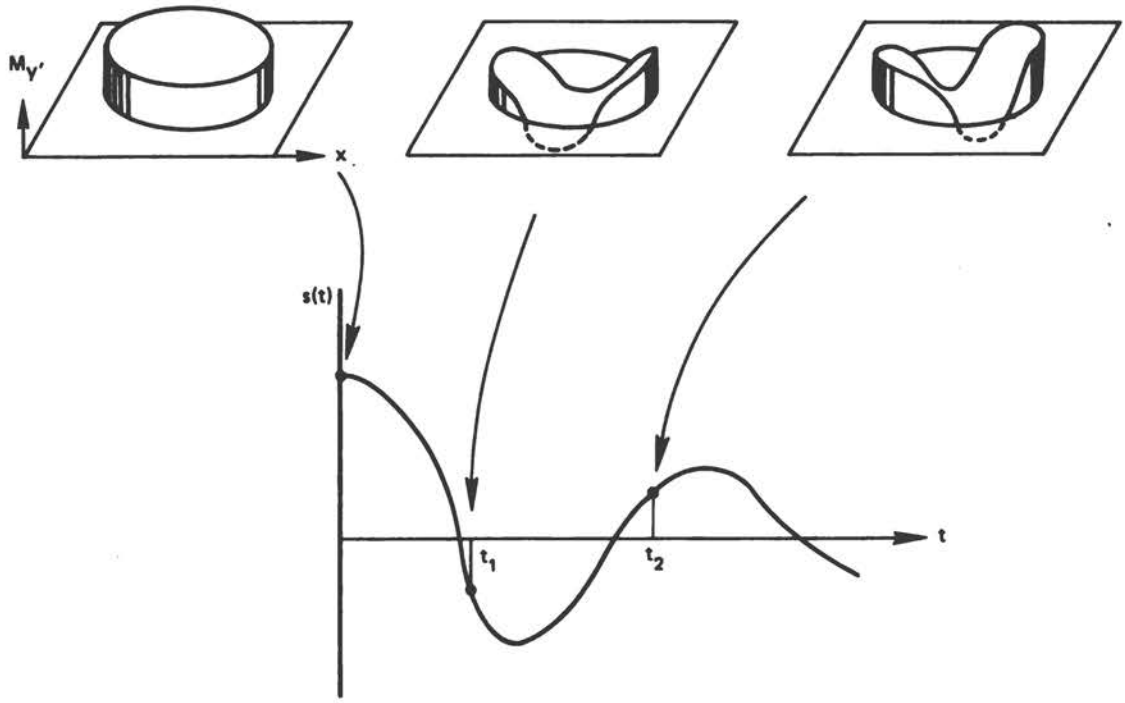

FIGURE 3 NMR signal obtained while gradient is applied to two-dimensional circular uniform object. Signal at t = 0, before gradient has undulated magnetization vectors, is sum of magnetization vectors in object, corresponding to "D.C." Fourier component of object. As time progresses, object's magnetization vector components are effectively undulated by gradient field into successively higher-frequency Fourier components, and signal represents content of these components in object. In addition to x gradient, which caused progressive undulation in x direction, y gradient was applied between t_1 and t_2, causing slight undulation in y direction seen at t_2.

This is the basic step in NMR image-data acquisition, for it is through a series of such individual measurements that we can measure all the Fourier components needed to reconstitute an image. Reconstituting a desired image consists of adding the Fourier components in the amounts suggested by the noisy measurements. In general terms, to make the measurements one undulates the distribution of

magnetization-vector components into each of the needed Fourier components in turn, by applying some combination of gradient waveforms and sampling the rf signal.

The picture we have presented (Figure 3) is appropriate for imaging an isolated plane of spins. To obtain an isolated plane for two-dimensional imaging, it is common to use a preliminary rf pulse and gradient combination to excite the spins selectively in a relatively thin slab. The same principle of undulating the spin-vector components into sinusoidally varying waves in space applies to three-dimensional NMR imaging also,[3,5] although it is more difficult to visualize the process.

In most NMR imaging methods, the raw data produced in the encoding process are easily interpreted--each datum is simply a noisy measurement of one of the Fourier components. Which component the datum represents depends on how the field gradient across the object has been changed before measurement. The degree of undulation in a given direction depends on the strength of the gradient in that direction and on the time elapsed since the excitation pulse. In fact, the degree of undulation is simply proportional to the integral of the gradient up to that time. (Most NMR imaging methods in current use operate according to this description; the relatively inefficient "sensitive-point" methods, which scan through one spatial point at a time, do not operate this way.)

It is convenient to represent each Fourier component by a location in a planar array, where its distance and direction from the origin correspond to its degree of undulation (its wave number) and the direction in which the waves are oriented, respectively (see Figure 4). At any time, the rf-signal value represents a single-sample value in this plane. The point being sampled moves from moment to moment along a continuous path, its direction determined by the direction of the gradient vector at each moment, and its speed determined by the instantaneous strength of the gradient.

Because the Fourier components needed to reconstitute an image form an array in the space of spatial frequencies and the value of spatial frequencies is often represented by the vector k, we call the sampling path determined by the particular gradient waveforms of an NMR imaging method its "k trajectory." To sample the two-dimensional array of Fourier components completely, most NMR imaging methods use a series of different k trajectories (Figure 5).

Now that we have a picture of NMR image-data acquisition in general, we can consider its versatility and how that versatility can be exploited. How are the Fourier components related to image quality and the visual interpretation of images?

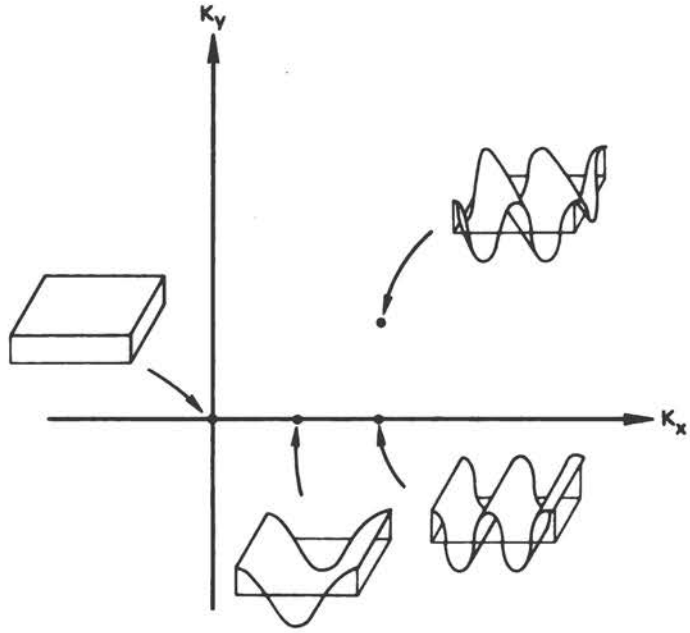

FIGURE 4 Fourier components can be positioned in array in spatial-frequency plane (k plane). Some Fourier components and their positions are shown. Radiofrequency signal represents measurement of Fourier components along continuous path driven through k plane by current direction and magnitude of applied gradient field.

Let us consider a simple example. Roughly speaking, the most important information regarding the fine details of an image is represented in the higher-frequency Fourier components, and that regarding the coarser details in the lower-frequency Fourier components. In imaging systems that are very insensitive to the higher spatial frequencies and in which noise is a factor, the higher frequencies tend to be dominated by noise; in the images produced by these systems, it is hard to distinguish low-contrast details (such as small lesions or vessels in a clinical image). Once such an image has been acquired, one can "smooth" it computationally to reduce the visually distracting high-frequency noise. Unfortunately, the high-frequency components of the details one might like to see (e.g., small, low-contrast lesions or vessels) are suppressed unavoidably with the high-frequency noise components. The real problem is that the most important Fourier components (those representing the features we were most interested in detecting) were measured with insufficient accuracy.

It should be emphasized that image processing, and in general the decoding stage of the imaging process, can correct for simple insensitivity to individual Fourier components, but cannot improve

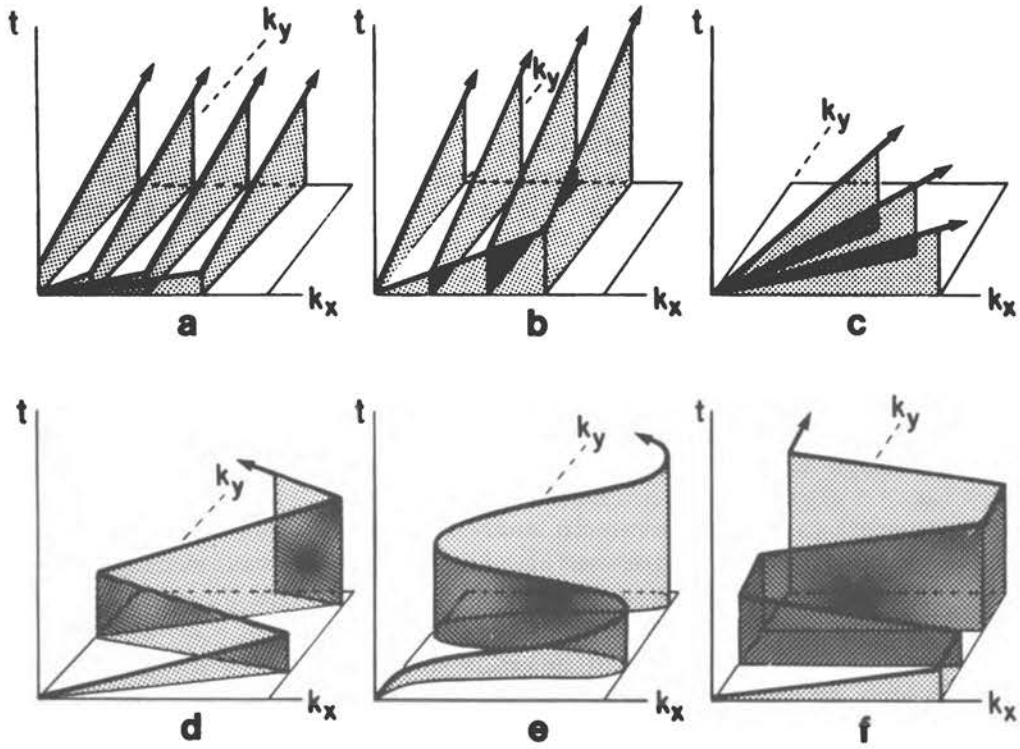

FIGURE 5 Frequency-plane sampling paths ("k trajectories") for selected NMR imaging methods: a, spin-warp method,[1] in which series of signals is observed during constant y gradient and after progressively larger x-gradient pulses. b, original Fourier method,[2] in which k_y columns are scanned after x-gradient pulses of constant amplitude, but progressively longer duration. c, projection-reconstruction method,[4] in which constant gradients are applied at various angles to scan array of Fourier components radially. d, e, f, three methods that vary gradients in time to sample all Fourier components after single excitation, greatly reducing minimal image-data acquisition period. Sawtooth trajectory of d represents echo-planar method.[6] Reprinted from Twieg.[7]

the accuracy with which they are represented in the final image. There is no magic in image reconstruction, processing, or display--information that has not been acquired in the raw data is simply not accessible for display, no matter how well the second imaging stage operates. (This is a fundamental reality enunciated by Wagner and Brown.[9] In the case of NMR imaging, this limitation is manifested in the fact that the signal-to-noise ratios for Fourier components are determined at acquisition and cannot be improved thereafter.

Part of the versatility of NMR imaging is that, within limits, we can trade off accuracy of measurement among the Fourier components at the time of acquisition. Which ones should we choose to measure more accurately in practice? The answer depends on what we hope to see in the image. If we want to detect small and faint lesions, which may exist in a cross-sectional image, we should measure the higher-frequency components especially accurately, perhaps even at the cost of accuracy in the low-frequency components. A more detailed prescription for weighting the measurements must rest on a more detailed model of how a human observer interprets an image in the context of a particular task.

In the general case, and even in such specific cases as the problem of imaging to search for small and faint lesions, rational guidelines for weighting measurement accuracy among the Fourier components are likely to be rough and largely empirical. Nevertheless, even reasonable empirical guidelines should improve image quality, inasmuch as conventional imaging methods (which use constant gradients during data acquisition) systematically measure the lower spatial frequencies more accurately than they probably need to in many cases and measure the often more interesting higher-frequency components less accurately than they should for many imaging tasks.[7,8]

Now that we know why one might want to manipulate the accuracy of Fourier-component measurement during acquisition, let us consider how it can be done. Because the raw data obtained from the NMR signal are measurements of the individual Fourier components for the image to be reconstructed and displayed, the sensitivity and accuracy with which the NMR imaging system measures the Fourier components, and hence the system's imaging-quality characteristic, are determined at the time of data acquisition.

Figure 5 is a plot of k trajectories for several two-dimensional imaging methods. The k plane is at the bottom, with the time axis vertical. The k trajectories are indicated by the lines ending in arrows, and the k values being sampled are shown below on the k plane. The three methods depicted on the top row are (a) the spin-warp method,[1,5] (b) the original Fourier method,[2,5] and (c) the projection-reconstruction method.[4,5] Each of these uses multiple

k trajectories to sample the Fourier components. The components that the k trajectory samples at larger values of t are those for which the method has less sensitivity, because of relaxation. Note that the projection-reconstruction method samples radially, and the others rectilinearly. Decoding in projection reconstruction therefore involves more than the straightforward process of performing a Fourier transform on the data--this is usually accomplished by one of the back-projection algorithms also used in x-ray computed tomography.

Many NMR imaging methods, using different gradient waveforms and sampling procedures, are possible in theory. Each has its own characteristic relative accuracy of rendition of the components, which depends on how much relaxation has occurred when each component is sampled and on how much time is devoted to signal-averaging that component.[7,8]

Relaxation influences the sensitivity of imaging methods to the individual Fourier components. During the time between the rf exciting pulse and the sampling of a Fourier component, the magnetization vectors in the object being imaged relax exponentially. Thus, components measured later in the acquisiton process are measured less sensitively than those measured earlier.

Relaxation also influences the accuracy with which Fourier components are measured. Although the magnetization vectors--and the signals they emit--decay during data acquisition, the mean noise added to the signal remains constant. The signal-to-noise ratio of the measured Fourier component therefore also depends on the time at which it is sampled.

None of the methods depicted in Figure 5 do so, but it is possible to vary sensitivity and accuracy among the Fourier components by changing the rate at which the sampling path (directly under the k trajectories in Figure 5) moves from one component to the next. When the signal is sampled appropriately, this has the effect of "signal-averaging," measuring more accurately the components that are sampled for longer periods. Thus, within broad technical constraints, one can manipulate the gradients to alter Fourier-component measurement accuracy without changing the imaging-system hardware.

The choice of k trajectories (i.e., of gradient waveforms) establishes not only relative Fourier-component accuracy, but also the minimal imaging time for the method. The three methods depicted in the lower row of Figure 5 can acquire complete images in a much shorter period than the "conventional" methods depicted in the upper row, because they scan the Fourier components during a single acquisition period.

A distinctive feature of NMR imaging is that characteristics of the imaging-system hardware responsible for data acquisition are not the only major determinants of image quality in acquisition, as are collimator and crystal geometry in x-ray and gamma-ray computed tomography. NMR imaging characteristics depend strongly on how the gradient waveforms change during data acquisition, on the timing of rf pulses, and on how the signals are sampled. In a well-designed NMR imaging system, these are controllable over a broad range by a computer, so imaging characteristics can be highly variable in a given imaging instrument.

NMR imaging has unprecedented versatility, not only because it can form images based on any of several physical characteristics, but also because data acquisition, the stage at which image-quality limits are set, is subject to an unprecedented degree of control. We have barely begun to exploit this versatility sensibly in the pursuit of improved imaging performance.

REFERENCES

1. Edelstein, W. A., J. M. S. Hutchison, G. Johnson, and T. Redpath. Spin warp NMR imaging and applications to human whole-body imaging. Phys. Med. Biol. 25:751-756, 1980.

2. Kumar, A., D. Welti, and R. R. Ernst. NMR Fourier zeugmatography. J. Magn. Reson. 18:69-83, 1975.

3. Lai, C.-M., and P. C. Lauterbur. True three-dimensional image reconstruction by nuclear magnetic resonance zeugmatography. Phys. Med. Biol. 26:851-856, 1981.

4. Lauterbur, P. C. Image formation by induced local interactions: Examples employing nuclear magnetic resonance. Nature (London) 242:190-191, 1973.

5. Mansfield, P., and P. G. Morris. NMR Imaging in Biomedicine. Chapter 4. New York: Academic Press, 1982.

6. Mansfield, P., and I. L. Pykett. Biological and medical imaging by NMR. J. Magn. Reson. 29:355-373, 1978.

7. Twieg, D. B. Generalized Fourier nuclear magnetic resonance (NMR) imaging methods. Proc. Soc. Photo. Opt. Instrum. Eng. 347:354-364, 1982.

8. Twieg, D. B. The k-trajectory formulation of the NMR imaging process with applications in analysis and synthesis of imaging methods. Med. Phys. 10:610-621, 1983.

9. Wagner, R. F., and D. G. Brown. Overview of a unified SNR analysis of medical imaging systems. IEEE Trans. Med. Imaging, MI-1(4):210-214, 1982.

DESIGN AND DEVELOPMENT OF IMAGING MAGNETS

P. A. WOLFF
Francis Bitter National Magnet Laboratory
Massachusetts Institute of Technology

INTRODUCTION

Previous papers in this conference have demonstrated that nuclear magnetic resonance (NMR) can produce high-quality images of the human body. Those images are made possible by precision NMR spectrometers containing exceedingly uniform magnetic fields. The magnets at the heart of these systems are complicated, sophisticated electric devices, but, so far in the conference, little has been said about them. The aims of this paper are to outline the principles of NMR magnet design and to give some indication of the problems that a magnet engineer faces in building a state-of-the-art system. These principles and problems will be discussed in the light of experience gained at the National Magnet Laboratory (NML) in designing and building such systems. Although NML is not yet a leader in the imaging field, it has an excellent magnet group that, through previous experience in building high-field NMR spectroscopy magnets, is well equipped to deal with the problems posed by imaging magnet design and construction.

NML's entry into the imaging field was made possible by a remarkable collaboration with IBM Instruments Inc. (III). Three IBM staff members are working with NML's magnet-technology group in what we view as an engineering research venture. III is providing generous support for the program; its goal is research into the design and construction of state-of-the-art NMR imaging systems, including magnets, spectrometers, computers, and software. The first magnet, a head scanner of 60-cm bore, is now approaching the assembly state. A second, full-body system will be built during the coming year. The goal, in both cases, is to explore the limits of the technology with respect to field homogeneity, field strength, and magnet shimming capability, rather than to develop commercial systems.

NMR MAGNET SPECIFICATIONS

NMR imaging magnets and NMR spectroscopy magnets have a number of features in common: both require exceedingly uniform fields, both use superconductor technology, and the design problems for the two are similar. Thus, it is instructive to compare their features; Table 1 gives specifications for the two types of systems. Analytic magnets have high fields (10-14 T) to spread out the NMR spectrum and extreme homogeneity (1 in 10^8) over a small volume. Typically, the region of homogeneity has a radius of 0.05-0.1 times the bore of the magnet. Imaging magnets produce lower fields (about 2 T and lower) and lower homogeneity (1 in 10^6). However, the volume of the homogeneous region must be large in both absolute and relative terms. For example, in the head-scanning system that NML and III are building, the uniform region is designed to be 12.5 cm in radius--the size of a volleyball. Its radius is 0.2 times the bore. This requirement--high homogeneity over a sizable fraction of the magnet volume--makes NMR imaging magnet design at least as demanding as that of NMR spectroscopy magnets.

TABLE 1

Comparison of NMR Spectroscopy and Imaging Magnets

- Superconducting Solenoids for Spectroscopy

Field range	6-14 T
Aperture	5-10 cm at room temperature
Uniformity	10^{-9} in 5-mm sphere
Current	40-200 A
Stored energy	50-1,000 kJ

- Imaging

Field range	0.3-2 T
Aperture	0.5-1 m
Uniformity	$1o^{-6}$ in 0.25-0.5 m

It is also interesting to compare the three technologies that have been used in the fabrication of image magnets. Table 2 lists specifications of permanent, resistive, and superconducing magnet systems. Sheer weight seems to preclude extensive use of permanent magnets. Resistive magnets are useful in the low field range (say, 0.15 T), but require inordinate power at the higher fields (1-2 T) now being considered for imaging. For example, a 1.5-T resistive, whole-body imaging magnet dissipates 5 MW. Such power is not

TABLE 2

Specifications of Whole-Body Imaging Systems

- Permanent Magnet (Electromagnet)

  0.3 T

  No magnet power (energizing or cooling)

  Shimming and gradient pulsed power 20 kV

  Small fringing field

  Weight, about 100 tons

- Water-Cooled Resistive Magnet

  0.15 T

  Power, 50 kV (200 kV for 0.3 T)

  Fringing field, 10 gauss at 3.5 m

  Weight, about 1-2 tons

- Superconducting Magnet

  2.0 T

  Refrigeration power, 10 kV

  Liquid hellium ($500-1,000/year for 1 or 2 refills)

  Fringing field, 10 gauss at 8 m

  Weight, about 1-2 tons

normally available in a hospital environment; magnet cooling would also present problems. Thus, for convenient, flexible operation over the full field range contemplated (0.1-2 T), there is no alternative to superconducting magnets. NML is committed to them, despite the inconvenience of liquid-helium cooling. The cryogenic technology has, in fact, progressed to the point where liquid-helium cooling is inexpensive and relatively simple to maintain.

Superconducting magnets are especially advantageous when operated in the persistent mode. Currents in the main coils and superconducting shim coils are initially adjusted to provide the field desired and to compensate design errors and stray fields. The resulting homogeneous field can be maintained unchanged essentially forever via persistent superconducting currents. This statement is made with some confidence, inasmuch as, in its high-field analytic NMR facility, NML observes field drifts less than 1 part in 10^8 over several months of operation in the persistent mode.

COMPENSATED COIL SYSTEMS

We now consider the problem of generating a magnetic field, uniform to 1 part in 10^6, over a volume 12.5 cm in radius. A long solenoid generates a uniform field. Unfortunately, the solenoid must be exceedingly long to achieve the homogeneity required. The difficulty is illustrated in Figure 1, which shows a finite solenoid with diverging field lines and an axial field that decreases with distance (z) from its center. For small distances,

$$B_z(z) \simeq B_z(o)\left[1 - \frac{3}{2}\left(\frac{a}{b}\right)^4\left(\frac{z}{a}\right)^2\right]. \qquad (1)$$

The parameter $\delta \equiv (z/a) \simeq 0.4$ at the edge of the homogeneity zone. Thus, one requires that $(a/b) \simeq 1/20$ to reduce the correction term in Equation 1 to 10^6. This ratio, in turn, implies a solenoid 15 m long, which is impractical.

The problem outlined above can be overcome, conveniently and economically, by using a compensated-coil system consisting of a finite solenoid plus compensating end coils, as illustrated in Figure 1. This configuration is the basis for most high-homogeneity magnets. As shown in Figure 1, the field of the compensating coils at $z = 0$ has curvature opposite that of the solenoid. Thus, by adjustment of the turn density of the end coils relative to the central solenoid, one can cancel the field curvature at $z = 0$. Second-order compensation is achieved by controlling a single parameter. In practice, the coil design of Figure 1(c) has several other adjustable features, including the correcting-coil length, spacing, and radius. A detailed analysis shows that, by making use of all these degrees of freedom, one can build a compact,

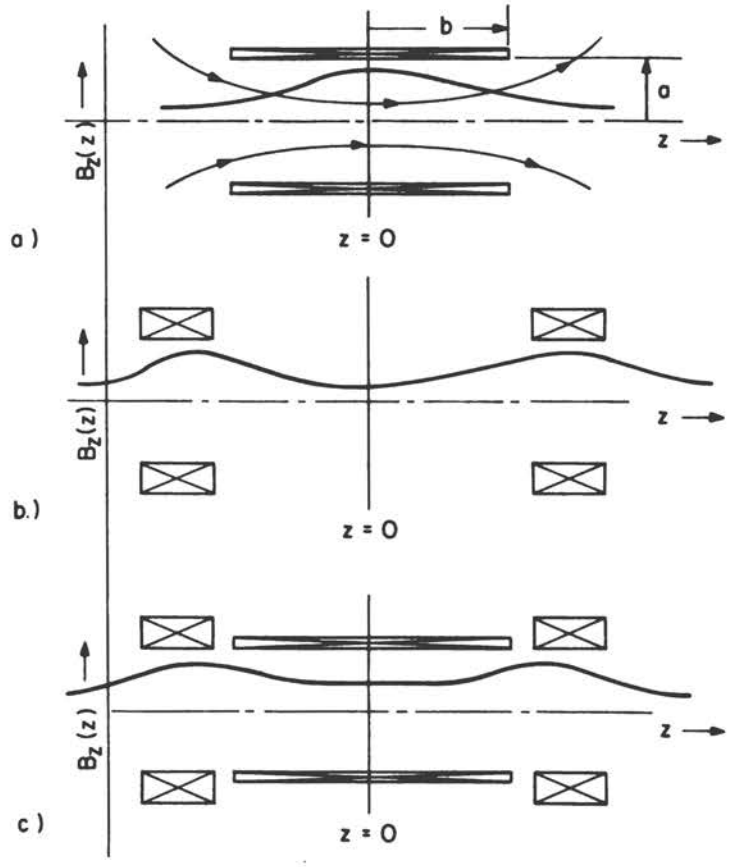

FIGURE 1 Fields in various coil configurations: a, finite solenoid; b, compensating coils; c, compensated solenoid.

compensated-coil system in which the first three even derivatives vanish at the center of the magnet--

$$\frac{\partial^2 B_z(o)}{\partial z^2} = \frac{\partial^4 B_z(o)}{\partial z^4} = \frac{\partial^6 B_z(o)}{\partial z^6} = 0. \qquad (2)$$

Moreover, because the system is symmetric in z, all odd derivatives also are zero there.

Figure 2 shows a cross section of the NML/III head-scanning system designed on these principles. The geometry is corrected through seventh order, with additional degrees of freedom used to minimize magnet volume and wire length.

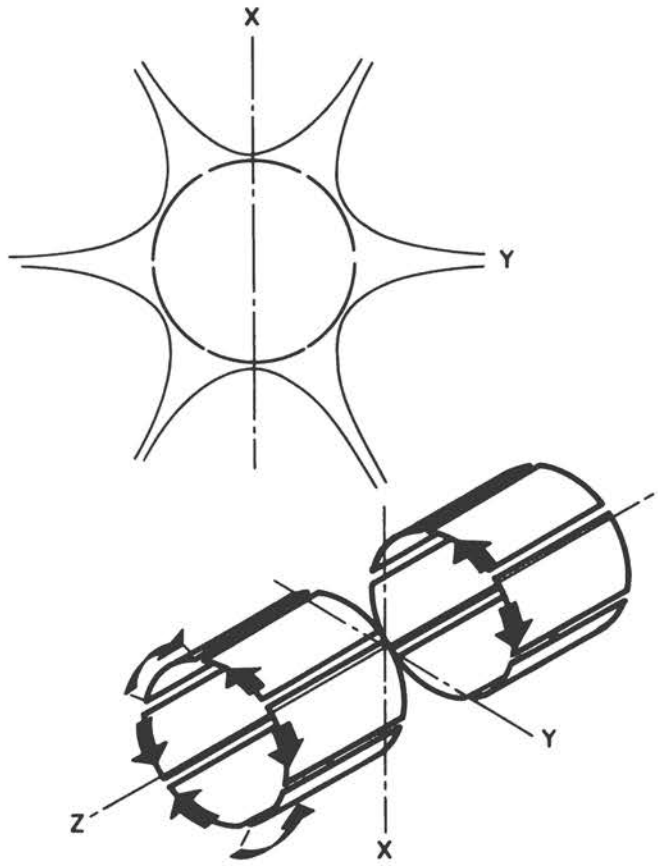

FIGURE 2 Schematic of NML/III imaging magnet coils.

SHIMMING

The compensated-coil configuration shown in Figure 2 will produce, if perfectly fabricated and free of external perturbations, a magnetic field uniform to 1 part in 10^6 over a 25-cm-diameter region. In practice, a magnet is never perfect; small winding errors or errors in the placement of the compensating coils relative to the central solenoid are inevitable. The system is particularly sensitive to errors of the latter kind; a 20-μm displacement of a compensating coil from its correct position gives rise to the 1 part in 10^6 limiting field inhomogeneity. It is hard to imagine positioning the sizable end coils with such precision. Thus, provision must be made, in the form of shim coils, to compensate for errors in magnet construction. Shim coils are also used to cancel background fields due, in most cases, to iron (beams, panels, steel reinforcing, etc.) in the building that houses the NMR systems.

The various errors that must be compensated correspond to low-order eigenfunctions of Laplace's equation,

$$\nabla^2 B_z(x,y,z) = 0, \tag{3}$$

which determines B_z. Table 3 shows the first few eigenfunctions of this equation. The fundamental, with $\ell = m = 0$, B_z constant, is, of course, the solution one seeks, but there will always be some admixture of higher-order modes due to the errors and perturbations mentioned above. Note, however, that the eigenfunctions vary as $(z/a)^\ell = (\delta)^\ell \simeq (1/5)^\ell$ at the edge of the homogeneity zone. Thus, those of small ℓ are most important; their perturbations are controlled by shim coils in imaging magnet systems.

TABLE 3

Eigenfunctions of Laplace Equation

ℓ	m	$B^\ell = F(x,y,z)$		Principal Gradient	
0	0	Constant		0	
1	0	z		z	
	1	x	:y	x	:y
2	0	$2z^2 - (x^2+y^2)$		z^2	
	1	xz	: zy	zx	:zy
	2	(x^2-y^2)	:2xy	x^2	:xy
3	0	$2z^3 - 3z(x^2+y^2)$		z^3	
	1	$x[4z^2-(x^2+y^2)]$	$:y[4z^2-(x^2-y^2)]$	z^2x	$:z^2x$
	2	$z(x^2-y^2)$	: zxy	zx^2	: zxy
	3	x^3-3xy^2	$:y^3-3x^2y$	x^3	$:y^3$

The eigenfunctions listed in Table 3 are of two types: those which depend on radial variables through the combination $x^2 + y^2 \equiv \rho^2$ and are independent of azimuthal angle about the magnet center line and those, such as $x^2 - y^2$, with an azimuthal variation. Perturbations of the former type are called axial; those of the latter are called radial. Axial perturbations are canceled by axial shim coils wound around the magnet, as shown in Figure 2. A perturbation having both axial and radial character is illustrated in Figure 3, which also shows saddle shim coils wound on the outer surfaces of the solenoid to control it.

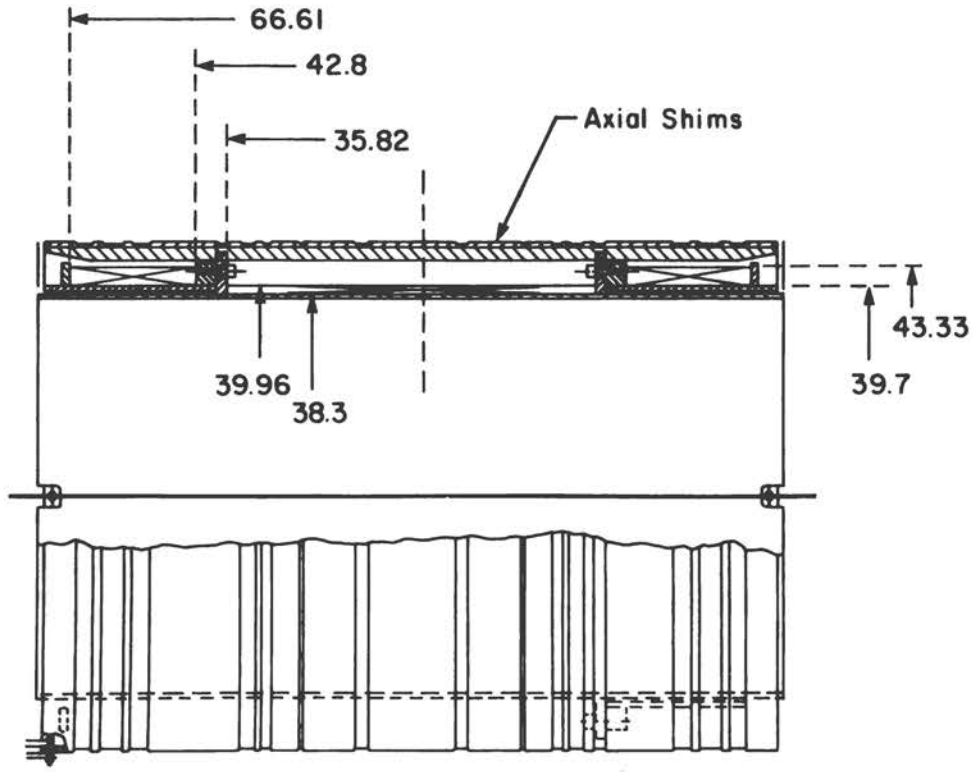

FIGURE 3 Third-order magnetic-field perturbation and corresponding shim coils.

The imaging magnets being built at NML have shim coils to control axial gradients through fourth order and radial perturbations of the form x, xz, and $x^2 - y^2$ (with their complements). For each order, both superconducting and normal shim coils are provided. There are a total of 20 shim coils.

In assembling the magnet, the compensating coils will first be positioned as accurately as possible with respect to the central solenoid. There are six degrees of freedom in this mechanical shimming process. The superconducting portions of the system will then be sealed into the dewar. Residual errors (and stray fields) are later canceled with the shim coils. The superconducting shims have a large current-carrying capacity, to permit sizable corrections via persistent currents.

QUENCH PROTECTION

NMR magnets store a good deal of energy. Thus, if a small segment of the superconducting winding should go normal--i.e.,

become resistive--much of the energy could be deposited locally and burn out the coil. That danger would be acute in a winding made of pure superconductor wire, but can be avoided if the superconductor is imbedded in a copper matrix. The NML/III magnets use wire that is 80% copper and 20% niobium-titanium. Copper provides a sizable, low-resistance parallel current path in the event of a quench, thus absorbing and dispersing heat. Calculations indicate that the temperature should not exceed 100 K in such an incident.

CONCLUSION

When they are completed, the NMR imaging systems being built by NML and III will serve as the focus for a regional facility devoted to NMR imaging research. The Massachusetts Institute of Technology is refurbishing an excellent building, across the street from NML, for this purpose. The facility will include magnet cells, shops, spectrometer and computer areas, a chemistry laboratory, animal facilities, offices, and a patient reception area. We hope to develop collaborations with major medical research groups near Boston, such as the Massachusetts General Hospital, Brigham and Women's Hospital, Harvard Medical School, and the Whittaker College at MIT. Interactions with other groups interested in biomedical research will be welcomed.

ACKNOWLEDGMENTS

The author has benefited from numerous discussions with L. Neuringer, H. Segal, and J. E. C. Williams.

TECHNICAL DEVELOPMENT OF DIGITAL SUBTRACTION ANGIOGRAPHY

CHARLES A. MISTRETTA
Clinical Science Center
University of Wisconsin School of Medicine

Subtraction has been used for more than a half-century in connection with conventional angiography, in which film is the standard image receptor. Films exposed before direct arterial injection of iodinated contrast material are "subtracted" from those exposed during peak opacification of the arteries. Because of the large concentration of iodine delivered by direct injection, image contrast is great enough to be easily displayed on the film. However, when the contrast material is more dilute, either because of direct arterial injection of a diluted mixture or because of injection through the venous system, image contrast is generally too low for adequate film display.

It would be historically tidy to be able to say that digital subtraction angiography (DSA) grew from a carefully planned approach directed at developing less invasive angiographic techniques. However, at least as far as our laboratory is concerned, the path was less direct than that.

Our involvement in work related to DSA began in 1971, when we conceived that it might be possible to obtain an image of the pulmonary arteries by performing a time-averaged subtraction of images acquired at the systolic and diastolic phases of the heartbeat. We hoped that the arteries could be visualized without contrast material because of their pulsatile motion. For this pourpose, we developed very sensitive video subtraction techniques that used silicon target-image storage tubes.[7] Unfortunately, although the apparatus performed well (sometimes), the application was ill-conceived. The pulmonary arteries, because they are attached to the heart, translate laterally more than they pulsate. How was a recent postdoctoral refugee from high-energy physics supposed to know that?

We then began to look for ways to use our imaging apparatus, which owed its sensitivity to its ability to lock on to periodic

components of image contrast. The possibility of inducing such periodicity through alteration of the x-ray beam spectrum was suggested by the thyroid-scanning work of Jacobson and MacKay[2] in Sweden. Their work made use of the iodine k-edge discontinuity at 33 keV. Below this energy, iodine produces low image contrast. Above 33 keV, it is more effective in stopping x rays than an equivalent mass of lead.

The storage-tube apparatus was used in conjunction with a rotating filter wheel placed between the x-ray tube and the image intensifier-television detector to produce periodic x-ray contrast charges that could be visualized with the signal-averaged subtraction scheme.

This system provided encouraging results and led to a number of investigations with two- and three-spectrum techniques designed to isolate iodine while subtracting both the bone and tissue components of normal anatomy. These techniques did not become clinically important at that time, because the x-ray beam intensity after filtration was limited and because it took so much care to keep the storage-tube system tuned. The latter problem led us to build a digital video-image processor[4] that could perform subtractions at real-time video rates. When this processor was completed in early 1976, our focus was on energy subtraction techniques. The ease of intravenous temporal subtraction angiography was noticed serendipitously during an experiment designed for the imaging of iodine uptake in a dog liver. The contrast was viewed in a temporal subtraction mode as the injected contrast material passed through the heart. We recognized that energy subtraction was a difficult way to make a living and redirected our efforts toward intravenous angiography. This work and related work at the University of Arizona[1] stimulated commercial interest in the technique and resulted in the introduction of commercial systems at the 1980 meeting of the Radiological Society of North America in Dallas. Since then, we are told, over 1,000 units have been installed throughout the world.

Temporal subtraction is only one of several generalized image subtraction techniques[6] made possible by digital imaging. Whereas traditional image processing techniques had emphasized operations aimed at increasing the information present in single images, generalized subtraction imaging emphasizes image combinations designed to isolate specific subsets of potentially relevant information. Temporal subtraction and energy subtraction are two examples of first-order subtraction imaging. Although computed tomography (CT) does not use subtractive algorithms, it can be thought of, at least formally, as a first-order subtraction in the variable that describes distance along the x-ray beam in conventional radiographic geometry.

Depending on the particular clinical problem to be addressed, it might be convenient to use second-order subtraction techniques in which *a priori* knowledge about more than one physical variable is exploited to form a specialized image. A recent example is the combined energy-time imaging introduced by Brody and co-workers.[3] This uses energy subtraction to eliminate artifacts in DSA caused by misregistration. The temporal subtraction portion of the imaging process removes images of bone, which generally remains more stationary than tissue. This technique has been investigated by our group,[10] but more extensively by the Stanford group.[3]

Another example of second-order subtraction techniques that may extend the capabilities of DSA is the combination of DSA and tomography recently reported by Kruger *et al.*[5] This process is conceptually equivalent to the temporal subtraction of tomograms obtained before and after contrast-material injection. It is designed to reduce the problem of vessel overlap, which is often confusing in single-projection imaging. It also reduces the artifacts due to misregistration of tissue outside the tomographic plane.

When our digital processor was conceived in 1973, the only multiple-image process that had been digitally implemented was CT. The image-processing algorithms that had been applied in medical x-ray imaging were limited to spatial operations on digitized film radiographs. These had had no important impact on the practice of radiology. All the first- and second-order subtraction images associated with energy, time, and depth dependences have now been implemented. The first-order depth (CT) and time (DSA) images have had by far the greatest impact; the other images have not been studied enough to determine their eventual impact. In general, however, as information selection is made more specific by the application of additional variables, the images become more highly specialized and the potential applications less numerous.

DSA has been successful in a wide variety of applications of intravenous angiography. It has been unsuccessful in visualizing coronary arteries after intravenous injection. For several reasons, this is more difficult than visualizing other vessels. The motion of these small vessels necessitates the use of shorter, more intense x-ray exposures than required for static vessels. The motion of the heart leads to artifacts associated with misregistration. Residual opacification of pulmonary vessels confuses the iodinated background of the coronary arteries. Superposition of the arteries with such large iodinated structures as the left ventricle complicates image display. Finally, the large variation in x-ray transmission between heart and lungs leads to severe worsening of signal-to-noise ratio in the poorly transmissive portions of the image, owing to mixing of x-ray and light information from the bright portions of the image and the dark regions that results from x-ray scattering and

image-intensifier veiling glare. In addition, the quantum statistical fluctuations are nonuniform in the image, and that contributes to lowering of contrast resolution in the dark regions of the image. Whereas some of these problems may be amenable to image processing, the last two lead to a fundamental degradation in the DSA data set that is unlikely to be offset by image processing.

One alternative is to use a scanned-slit detector system, such as that discussed by Dr. Hofstadter. Such systems eliminate the scatter and glare problem, but, when used with conventional medical x-ray systems, suffer from extreme x-ray tube loading and are not compatible with the dynamic aspects of cardiac imaging, which are also important in assessing cardiac disease. Nor do they address the problem of nonuniform contrast sensitivity in all portions of the image.

It would be advantageous to find a way to use the extensive installed base of high-quality image-intensifier systems so that their dynamic imaging capabilities were retained and produced a fundamentally improved image data set. One approach toward this goal is being pursued in our laboratory. The basic idea is an extension of the use of x-ray beam compensation filters like those which have been tried for equalization of transmission through the chest in connection with standard chest radiography. Instead of a compromise attenuator of fixed shape for all patients, a specialized filter is prepared for each imaging task. Previously, this was impossible, because filter formation took hours.[8] With computer printing technology, the process can be implemented in seconds.

After patient positioning, a low-dose image is digitized and processed in a small computer or dedicated processing hardware. This image is then used to print out an x-ray attenuating image of the patient on a transmissive substrate (such as paper) with a dot-matrix printer whose ribbon is loaded with a heavy metal (such as cerium) or an ink-jet printer whose ink is loaded with a similar material. The printed material is thickest where the patient is highly transmissive. In the most attenuating portion of the patient, no material is deposited on the paper. After the filter is formed, it is automatically positioned in the x-ray beam. The result is an imaging process in which various portions of the patient are selectively exposed to the amounts of radiation that ensure uniform transmission through the patient in the absence of injected contrast material. The problem of detector noise is reduced, x-ray scatter and intensifier glare from bright to dark regions is minimized, and contrast resolution is approximately uniform throughout the image. We believe that this approach will be extremely important in any attempt to visualize coronary arteries with large-area image-intensifier systems. Even in noncardiac DSA, such an approach will eliminate the time-consuming practice of

placing water bags and other attenuating materials around the patient to eliminate image-degrading bright spots.

The digital beam attenuator (DBA) approach described above may very well be used for chest radiography in the near future. Film is notoriously incapable of adequately displaying the large range of x-ray information transmitted through the chest. This range is increased when high-quality scatter-rejection methods[9] are used. One approach is to use scanned-slit-diode detector systems characterized by large dynamic range and availability of data in digital form. Although such systems may prove useful, their spatial resolution is inferior to that of film and they entail high initial equipment costs. Furthermore, they do not solve the problem of nonuniform contrast resolution, inasmuch as input exposure, rather than output exposure, is constant.

In the DBA approach, the printed filter functions as a blurred subtraction mask, owing to its placement close to the x-ray focal spot, which is large, in comparison with the filter's absorbing picture elements. When such a filter is placed in the beam, low-frequency image information can be canceled to any desired extent, leaving a transmission image that can be optimally displayed by the film in all regions of the image. This optimal use of the film-contrast transfer function and its high spatial resolution would lead to chest radiographs of exceptional quality.

Techniques in chest radiography have evolved to the use of a rather high average x-ray beam energy. A partial reason is that the range of transmitted intensities decreases at high energies. Unfortunately, so does the contrast of soft tissues, such as tumors. The DBA technique requires a new search for optimal beam energy, but this time the search will be governed by considerations of physics and perception, rather than by the inadequacies of a detector.

REFERENCES

1. Frost, M. M., H. D. Fisher, S. Nudelman, and H. Roehrig. A digital video acquisition system for extraction of subvisual information in diagnostic medical imaging. Proc. Soc. Photo. Opt. Instrum. Eng. 127:208-215, 1977.

2. Jacobson, B., R. S. MacKay. Radiological contrast enhancing methods. Adv. Biol. Med. Phys. 6:201-261, 1958.

3. Keyes, G. S., S. J. Riederer, B. F. Belanger, and W. R. Brody. Hybrid subtraction in digital fluorography. Proc. Soc. Photo. Opt. Instrum. Eng. 347:34-41, 1982.

4. Kruger, R. A., C. A. Mistretta, A. B. Crummy, J. F. Sackett, S. J. Riederer, H. L. Touk, M. M. Goodsitt, C. G. Shaw, and D. Flemming. Digital K-edge subtraction radiography. Radiology 125:243-245, 1977.

5. Kruger, R. A., J. A. Nelson, D. Ghosh-Rog, F. J. Miller, R. E. Anderson, and P. Liu. Dynamic tomographic digital subtraction angiography using temporal filtration. Radiology 147:863-867, 1983.

6. Mistretta, C. A. The use of a general description of the radiological transmission image for categorizing image enhancement procedures. Opt. Eng. 13(2):134-138, 1974.

7. Ort, M. G., C. A. Mistretta, and F. Kelcz. An improved technique for enhancing small periodic contrast changes in television fluoroscopy. Opt. Eng. 12(5):169-175, 1973.

8. Pennington, E. C., R. C. Murry,, and E. E. Christensen. High bandpass spatial filtering of the primary x-ray beam. Proc. Soc. Photo. Opt. Instrum. Eng. 233:176-182, 1980.

9. Sorenson, J. A., L. T. Niklason, and D. F. Knutti. Performance characteristics of improved antiscatter grids. Med. Phys. 7:525-528, 1980.

10. Van Lysel, M. S., J. T. Dobbins III, W. W. Peppler, B. H. Hasegawa, C. S. Lee, C. A. Mistretta, W. C. Zarnstorff, A. B. Crummy, W. Kubal, B. Bergsjordet, C. M. Strother, and J. F. Sackett. Work in progress: Hybrid temporal-energy subtraction in digital fluoroscopy. Radiology 147:869-874, June 1983.

CLINICAL APPLICATION OF DIGITAL SUBTRACTION ANGIOGRAPHY

DIETER R. ENZMANN
Department of Radiology
Stanford University School of Medicine

The introduction of the technology that made digital subtraction angiography (DSA) possible has had a major impact on the diagnostic role of angiography. Because of the use of the computer in the imaging process, film is no longer both the detector and the display medium. These two functions have now been separated, and the computer interpolated between them. This technology allows the tradeoff of spatial resolution for increased contrast resolution, and the increased ability to resolve small differences in contrast has allowed the reappearance of angiography that uses intravenous, rather than intra-arterial, injection of contrast medium. Intravenous injection results in a much lower concentration of contrast medium in arteries--a concentration not normally detectable by conventional film techniques. The DSA image, however, is inferior in sharpness and spatial resolution to a conventional intra-arterial angiogram.

Are we then going backward? In a sense, we are--if we consider only image quality. However, if we consider also the risk to the patient and the cost of the procedure, then these image-quality tradeoffs may be more acceptable. This technology increases the physician's flexibility in ordering and performing diagnostic tests. The cost and risk of an angiographic examination can now be balanced with the diagnostic need. The conventional angiogram permitted very little flexibility for considering cost and risk. Both the intravenous and intra-arterial forms of DSA present the opportunity to exchange some image quality, which may not be critical for diagnosis, for nonradiologic benefits, such as a decrease in cost or risk. In a health-care environment of cost-consciousness, that is important.

The greatest amount of flexibility was introduced by the intravenous form of DSA (IV DSA). This technique is procedurally quite different from conventional angiography; its major advantages, decreased risk and decreased cost, accrue at the expense of image information.[6] The features of IV DSA, however, mesh nicely with the increased demand for outpatient diagnostic procedures.

One problem most relevant to IV DSA arises simply because of superimposition of vessels, because all vessels are filled simultaneously. The problem of superimposition can be easily circumvented by applying one's knowledge of anatomy and using different projections. IV DSA relies on the concept of temporal subtraction, which has some inherent limitations, the most important of which is motion--either patient motion or vessel motion. Numerous image postprocessing schemes have been developed to minimize this problem, and by and large they have been successful. These techniques include "remasking," which entails choosing a different background for subtraction; "pixel shifting," which consists of moving one image in relation to another to reregister the background for more optimal subtraction; ECG gating, which "freezes" a moving structure, such as the heart and aorta; and hybrid subtraction, which removes overlying soft-tissue artifacts caused by motion. The hybrid technique combines the principles of temporal and x-ray energy subtraction.[2] In addition to compensating for motion problems, image postprocessing broadens flexibility by allowing manipulation of contrast-medium dose, x-ray dose, and frame rate. Integration of multiple images improves the signal-to-noise ratio and thus the quality of a DSA image.[4] Matched filtering, a more sophisticated mode of integration, further improves image quality and permits use of a lower x-ray dose.[8] Postprocessing integration allows the reduction of the IV contrast-medium dose in some circumstances.[7] The introduction of the computer into image processing therefore has added a great deal of flexibility in the technical aspects of image generation, and the attendant software programs have blunted the degree of sacrifice of image quality, compared with conventional angiography.

The application of IV DSA is wide and its appropriate clinical use depends on the anatomic region of interest. Detailed description of IV DSA for each particular angiographic application is not warranted here, but some characteristic examples can illustrate important advantages and limitations. Intracranial IV DSA examination is most effective for postoperative followup,[3] because the anatomic area of interest has been identified, the optimal projection for displaying the pathologic condition is known, and the diagnostic question to be answered is relatively simple: Has treatment been successful? For preoperative evaluation of intracranial vascular disease, IV DSA examination is not sufficient, partly because of spatial resolution and superimposition problems. For some diagnostic problems, such as carotid arterial stenosis or renal arterial stenosis (in connection with hypertension), IV DSA examination can be suitable both as a screening test and as a regular diagnostic test.[5] A computer model of the diagnostic workup of carotid stenosis has shown IV DSA examination to be cost-effective for a broad range of patients (H. S. Bell and D. R. Enzmann, unpublished manuscript). For the investigation of atherosclerosis in major arteries, such as the aorta and its major branches, IV DSA examination is efficient and accurate.

All DSA image data are in digital form, so quantitation of IV DSA data is possible; but it has not yet been fully explored. Certainly, aspects of cardiac function, such as ejection fraction and left ventricular wall motion, can be quantitated. Perfusion of vascular beds, such as the brain, can also be quantitated, but its relation to clinical pathology has not been defined. Nevertheless, the ability of digital technology to characterize the shape of a contrast bolus curve as it traverses a vessel or a tissue of interest does have potential quantitative value. This remains a fertile field for investigation.

The basic principles and limitations of IV DSA apply also to intra-arterial (IA) DSA. Unlike IV DSA, however, IA DSA does not constitute a new angiographic procedure, but rather is conventional angiography in which film is replaced with an image intensifier as the detecting medium. The advantages of this technique are different from those of IV DSA. Cost, contrast media, and physician time are saved at the expense of some diagnostic information. Inasmuch as the procedure is essentially generic angiography, risk is not appreciably decreased. One still trades spatial resolution for contrast resolution, but to a smaller degree. Spatial resolution can be substantially recouped if one is willing to sacrifice some field of view. The clinical application of IA DSA is essentially equivalent to that of conventional angiography spanning studies of all types of arteries. All the postprocessing methods for minimizing the effects of motion and improving the signal-to-noise ratio in IV DSA have direct application to IA DSA. Depending on the anatomic region and the diagnostic question to be answered, one can choose between conventional angiography and IA DSA. One can predict that conventional angiography will be largely replaced by IA DSA. The major limiting factor is the degree of spatial resolution necessary for diagnosis. With a limited field of view, the spatial resolution achievable with IA DSA is usually sufficient for even subtle diagnostic problems. Comparisons between IA DSA and conventional film subtraction have revealed differences, but these are often not important with respect to the diagnostic question being asked.[1]

Why is this loss of information with IV or IA DSA either not important or less important clinically? To answer this, we need to be aware of competing technologies. Our changing attitudes toward angiography are a direct result of the development of x-ray computed tomography (CT). In the future, the use of nuclear magnetic resonance (NMR) will reinforce this attitude change. These competing technologies have displaced angiography as the primary methods for making a large number of diagnoses where angiography once reigned supreme. Angiography therefore is no longer used in the same clinical, diagnostic fashion. CT and NMR are now used to localize and characterize lesions and to generate differential diagnoses. Angiography either is no longer used or is used only to

resolve limited diagnostic issues. Subtle angiographic features once considered to constitute important diagnostic criteria are now less important. Only in the diagnosis of primary vascular disease, such as atherosclerosis, has the role of angiography not changed appreciably. Diagnostic problems in this disease generally demand less spatial resolution. Overall, angiography has simply become less important. DSA technology has provided an opportunity to balance the quality of angiographic information needed (i.e., image quality) with other nonradiologic factors (such as cost, risk, and diagnostic speed) that are becoming important in the overall health-care system. New technologies, although blamed for the high cost of medical care, give the medical-care system an ability to respond to the new demands made by the more constrained economic and social environment.

REFERENCES

1. Brant-Zawadzki, M., R. Gould, D. Norman, T. H. Newton, and B. Lane. Digital subtraction cerebral angiography by intra-arterial injection: Comparison with conventional angiography. Am. J. Roentgenol. 140:347-353, 1983.

2. Brody, W. R. Hybrid subtraction for improved arteriography. Radiology 141:828-831, 1981.

3. Enzman, D. R., W. R. Brody, S. Riederer, G. Keyes, W. Collins, and N. Pelc. Intracranial intravenous digital subtraction angiography. Neuroradiology 23:241-251, 1982.

4. Enzmann, D. R., W. T. Djang, S. J. Riederer, W. F. Collins, A. Hall, G. S. Keyes, and W. R. Brody. Low-dose, high-frame-rate versus regular-dose, low-frame-rate digital subtraction angiography. Radiology 146:669-676, 1983.

5. Hillman, B. J., T. W. Ovitt, M. P. Capp, E. H. Prosnitz, R. W. Osborne, Jr., J. Goldstone, C. F. Zukoski, and J. M. Malone. The potential impact of digital video subtraction angiography on screening for renovascular hypertension. Radiology 142:577-579, 1982.

6. Kruger, R. A., C. A. Mistretta, T. L. Houk, S. J. Riederer, C. G. Shaw, M. M. Goodsitt, A. B. Crummy, W. Zwiebel, J. C. Lancaster, G. G. Rowe, and D. Flemming. Computerized fluoroscopy in real time for noninvasive visualization of the cardiovascular system. Preliminary studies. Radiology 130:49-57, 1979.

7. Riederer, S. J., D. R. Enzmann, W. R. Brody, and A. L. Hall. The application of matched filtering to contrast material dose reduction in digital subtraction angiography. Radiology 147:853-858, 1983.

8. Riederer, S. J., A. L. Hall, J. K. Maier, N. J. Pelc, and D. R. Enzmann. The technical characteristics of matched filtering in digital subtraction angiography. Med. Phys. 10:209-217, 1983.

FUNDAMENTAL ASPECTS OF POSITRON EMISSION TOMOGRAPHY

MICHEL M. TER-POGOSSIAN
Edward Mallinckrodt Institute of Radiology
Washington University School of Medicine

Positron emission tomography (PET) is a radiologic procedure that yields transverse tomographic images in which the image-forming variable is the distribution of a positron-emitting radionuclide that has been systemically administered to the subject being examined. PET can properly be placed within the broad definition of nuclear imaging, but a number of distinguishing features justify its identification in a category separate from that including the more "conventional" nuclear-medicine imaging procedures. PET is limited to the use of a small number of radionuclides that decay through the emission of positrons, and PET images transverse tomographic sections that exclude projections. The general approach in applying PET in biomedical imaging emphasizes the contribution of physiology to the examination more than many conventional nuclear-medicine imaging procedures, which have recently emphasized morphology. (There are many exceptions to the latter distinction.)

PET is based on the idea that biochemical processes essential to life can be studied--noninvasively, in vivo, and regionally--by labeling selected compounds of importance for the phenomenon under study, following the distribution of the radioactive label as a function of time and space, and unraveling the physiologic process of interest through the use of a suitable mathematical model. This idea is, of course, common to all in vivo nuclear-medicine procedures. What distinguishes PET is the selection of radioactive labels on the basis of chemical properties suitable for the tracing of life processes.

With very few exceptions, PET relies on the use of four radionuclides--carbon-11, oxygen-15, nitrogen-13, and fluorine-18. These radionuclides are sometimes identified as "physiologic" or "biochemical" radionuclides. Two important common physical characteristics of physiologic radionuclides are that they decay through the emission of positrons and that they have short

half-lives (Table 1). The emission of positrons optimizes in vivo imaging. The short half-lives mandate (with the exception of fluorine-18) preparation in the immediate vicinity of the site of use. In contemplating the use of one of these radioactive labels in biomedical research, it is necessary to ascertain whether its short half-life would preclude the labeling of the selected compound and, if so, whether the half-life of the label incorporated in the compound is long enough to allow the contemplated study. Most often

TABLE 1

"Physiologic" Radionuclides Most Often Used in PET

Nuclide	Half-life, min
Carbon-11	20
Nitrogen-13	10
Oxygen-15	2
Fluorine-18	110

the radionuclides are prepared in cyclotrons, many of which have been installed in medical centers specifically for use in connection with PET. The short half-lives of the physiologic radionuclides have severely impeded and still impede the development of PET, because of the cost and relative complexity of operating a cyclotron in a medical center and because of the difficulties raised by the required rapid labeling of complex molecules of biochemical importance. However, the short half-lives have now been recognized as particularly useful in most of the examinations carried out with PET.

USE OF PHYSIOLOGIC RADIONUCLIDES

The possible utility of radioactive labels--such as carbon-11, oxygen-15, and nitrogen-13--is probably obvious, in that the bulk of living matter consists of compounds of these elements and they are involved in most processes essential to life. The usefulness of a radioactive fluorine label in physical studies stems mostly from the fact that this element allows the labeling of metabolic analogues that are useful in the modeling of metabolic pathways; furthermore, some molecules of physiologic importance incorporate fluorine.

The use of the physiologic radionuclides in biology and medicine presents serious difficulties that have often discouraged their use: short half-lives and the need for a cyclotron. Work carried

out by many investigators, particularly imaginative chemists, mostly in the last 3 decades has yielded favorable solutions to the abovementioned problems. Through experience, the operation of cyclotrons in the medical environment has been, to a large degree, mastered. The difficulties raised by the rapid labeling of compounds of biologic usefulness with short-lived physiologic radionuclides exhibit a broad spectrum. Some compounds--such as gaseous oxygen, water, carbon monoxide, and carbon dioxide--can be labeled rapidly with little difficulty. Labeling of others--such as sugars, amino acids, and fatty acids--has been accomplished after a considerable amount of work through the application of ingenious labeling techniques. Finally, some molecules, such as neuroreceptor ligands, have been labeled with adequate specific activity only after years of extensive labor in the development of labeling procedures. Some potentially useful molecules probably cannot be labeled practically with one of the physiologic radionuclides. At the time of this writing, the number of compounds of proven or potential importance in the tracing of biochemical processes essential to the maintenance of life exceeds 100 and is growing rapidly. It is probably safe to say that the nonavailability of potentially useful compounds labeled with the physiologic radionuclides is no longer an impediment to the use of this technique.

The use of these labeled compounds can be effective only if the half-lives of the labels are not too short for the selected study. Fortunately, most of the metabolic processes essential to life are short enough to allow their study with physiologic labels. Some, of course, are too long for the application of this technology.

IMAGING OF POSITRON EMITTING RADIONUCLIDES--PET DEVICES

Positrons have too short a range in matter to allow the practical imaging of the distribution of positron-emitting radionuclides in living systems. However, the absorption of positrons in matter results eventually in the interaction of positrons with negatively charged electrons and in the annihilation of the masses of the two particles; their energies are converted into gamma-ray photons, each with an energy of 511 keV, traveling nearly colinearly in opposite directions. This electromagnetic radiation, the annihilation radiation, is used in the detection, in vivo, of positron-emitting radionuclides and eventually in the imaging of their distribution. The fact that the two annihilation photons from each interaction travel in opposite directions and nearly colinearly permits the effective collimation of that radiation. Two radiation detectors (Figure 1) are connected to an electronic circuit that registers a count only if both detectors are triggered simultaneously by the annihilation photons. It is

important to emphasize that this "electronic" collimation of the annihilation radiation is much more efficient in using the emitting photons than the collimation conventionally used in nuclear medicine to image radionuclides decaying through the emission of gamma rays. In the earlier applications of the physiologic radionuclides, the annihilation photons were collimated, relatively inefficiently, by conventional means, mostly through the use of lead or tungsten collimators. Electronic collimation led eventually to the imaging of these radionuclides by PET.

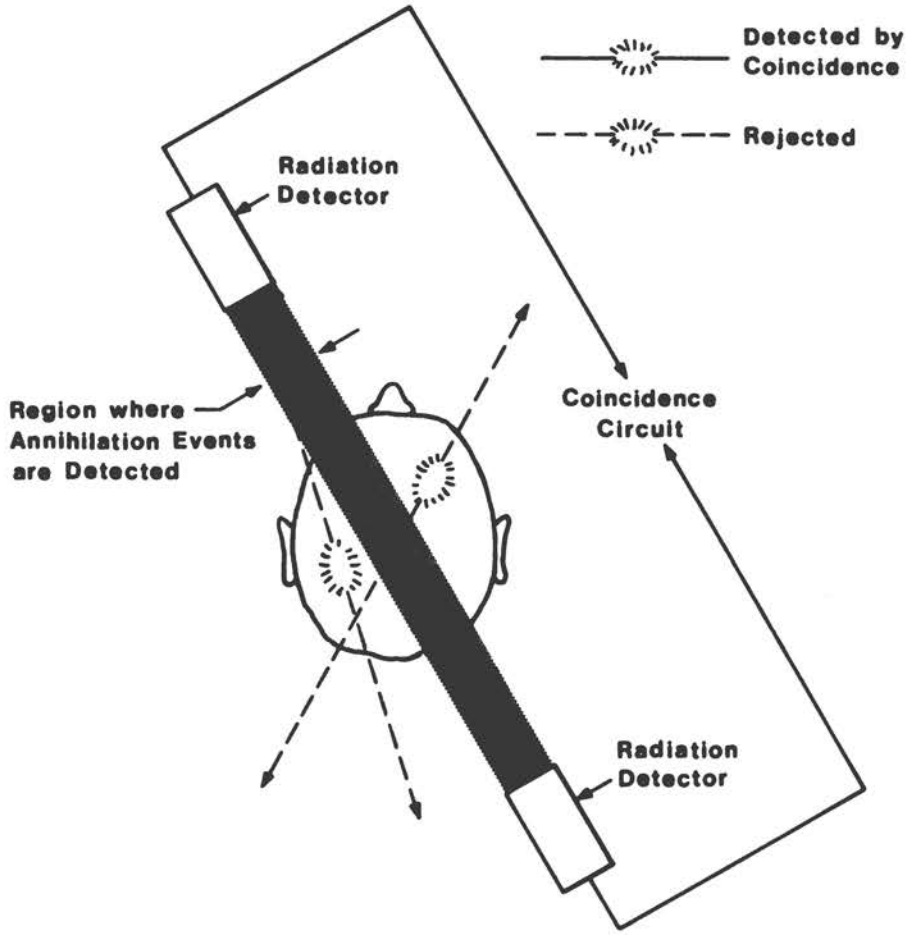

FIGURE 1 Diagram of "electronic" collimation of annihilation radiation with two detectors operated in coincidence mode. Annihilation events occurring within volume circumscribed by straight lines joining sensors of two detectors can be detected by system; annihilation events occurring outside that volume are not detected (except for some specific ases involving scattering of annihilation photons). Reprinted with permission from Ter-Pogossian.[1]

A little over 20 years ago, it was recognized that the distribution of positron-emitting radionuclides in vivo could be effectively achieved through a reconstruction process identical with the one used in transmission computed tomography through a series of radiation measurements around the object to be imaged and the reconstruction of the image from projections thus achieved. This method of reconstruction had been proposed and implemented approximately 10 years earlier for the in vivo imaging of radionuclides decaying through the emission of gamma rays. However, the method was not widely used then, and the immediate recognition of the value of PET was probably due to the combination of the highly useful chemical properties of the compounds labeled with the physiologic radionuclides and the high quality of the images obtained. The superiority of PET over the use of radionuclides emitting gamma rays stems mostly from three factors: the high efficiency of electronic collimation of the annihilation radiation by coincidence counting, the ability to correct unequivocally for the attenuation of the positrons in matter, and the high uniformity of the detection of the radiation throughout the object to be imaged, which stems directly from the physical properties of the coincidence detection of the annihilation radiation.

In the last decade, many devices have been designed, constructed, and used in PET. Radiation detectors incorporated in these devices have included scintillation detectors using various crystals, multiwire proportional counters, and solid-state detectors. Most of the PET devices used in research today include a circular array of scintillation detectors (incorporating either sodium iodide, bismuth germanate, cesium fluoride, or barium fluoride scintillating crystals) and computers similar to the ones used in transmission computed tomography. Figures 2 and 3 are a block diagram and a photograph of state-of-the-art PET devices.

Modern PET devices provide, usually simultaneously, several tomographic sections of the human body with spatial resolution of better than 1 cm, contrast resolution of a few percent, and temporal resolution as high as 10 s. It should be noted that these performance characteristics usually cannot be achieved simultaneously. Figures 4 and 5 show examples of images thus obtained. The use of annihilation-photon time-of-flight information in the reconstruction process has recently permitted a considerable improvement in the signal-to-noise ratio of examinations carried out with PET devices built for that purpose.

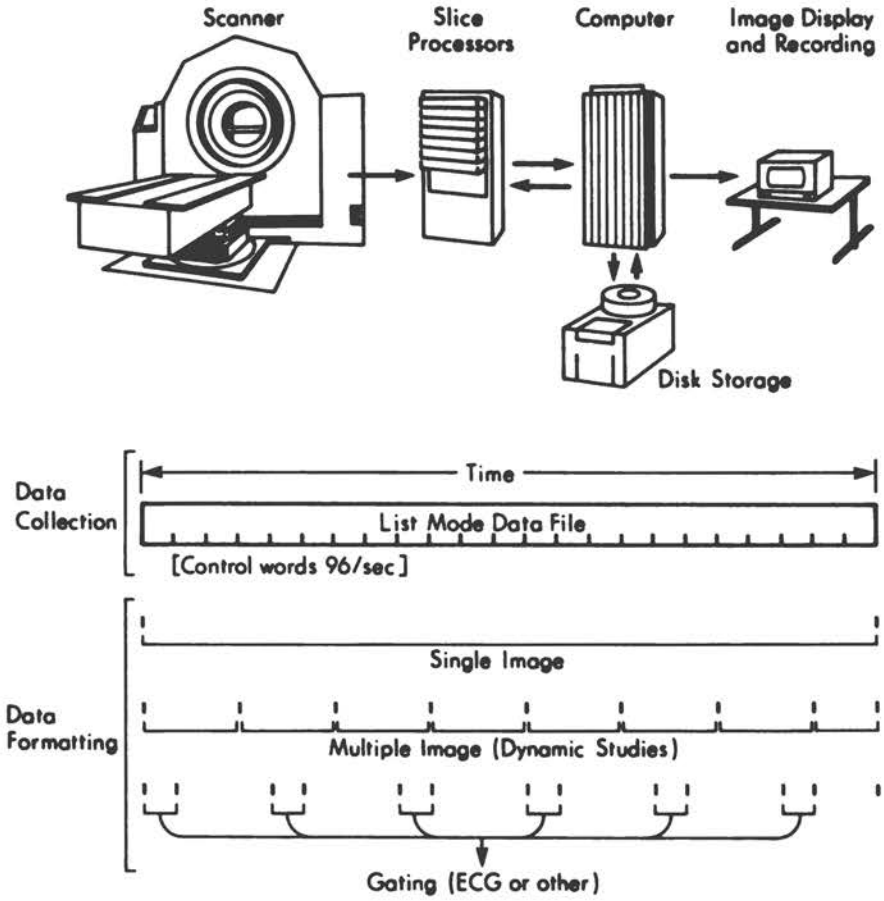

FIGURE 2 Block diagram of components of state-of-the-art PET device (Super PETT I) using photon time-of-flight information in image reconstruction.

STATUS OF PET

PET is now used in biomedical research in 40-50 centers. A PET center typically includes a cyclotron (or some other accelerator) for generating physiologic radionuclides, chemical facilities for incorporating the radioactive labels into compounds of physiologic importance, and one or more PET devices. Incorporation of the physiologic labels into compounds of interest is often automated, both to simplify that procedure and to minimize radiation exposure of the chemists and other operators--always a serious problem in the use of these labels because of the high energy of the annihilation radiation. Many physiologic characteristics inaccessible by other means have been studied with PET, including regional cerebral blood flow, oxygen and glucose metabolism, regional myocardial metabolism

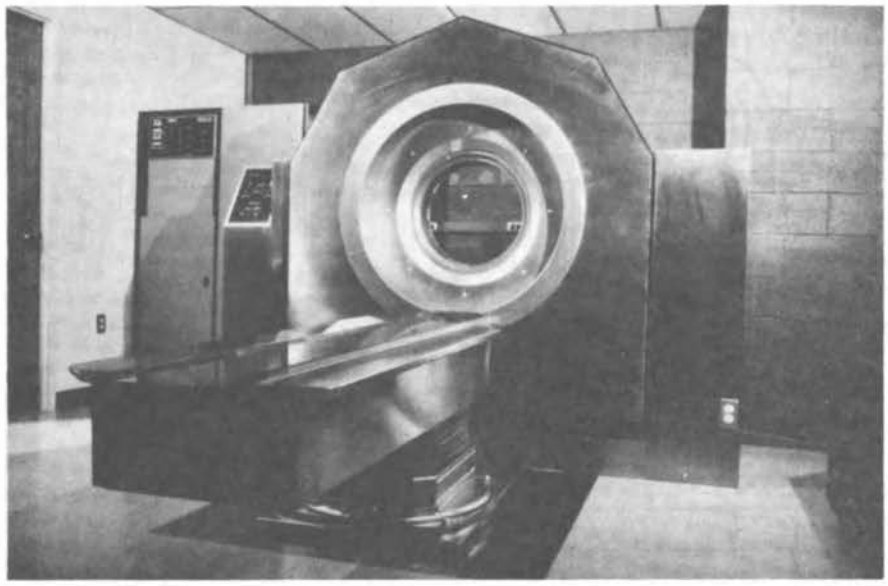

FIGURE 3 Photograph of Super PETT I.

and flow, and distribution of receptor sites. In several centers, PET is being applied, albeit in few cases, to the study of patients with epilepsy, stroke, and myocardial infarction.

Experience with PET is already ample to support a prediction that it will play a major role in biomedical research and eventually in clinical medicine.

REFERENCE

1. Ter-Pogossian, M. M. Physical aspects of emission computed tomography. In T. H. Newton and D. G. Potts, Eds. Radiology of the Skull and Brain. Vol. V. Technical Aspects of Computed Tomography. St. Louis: The C. V. Mosby Co., 1981.

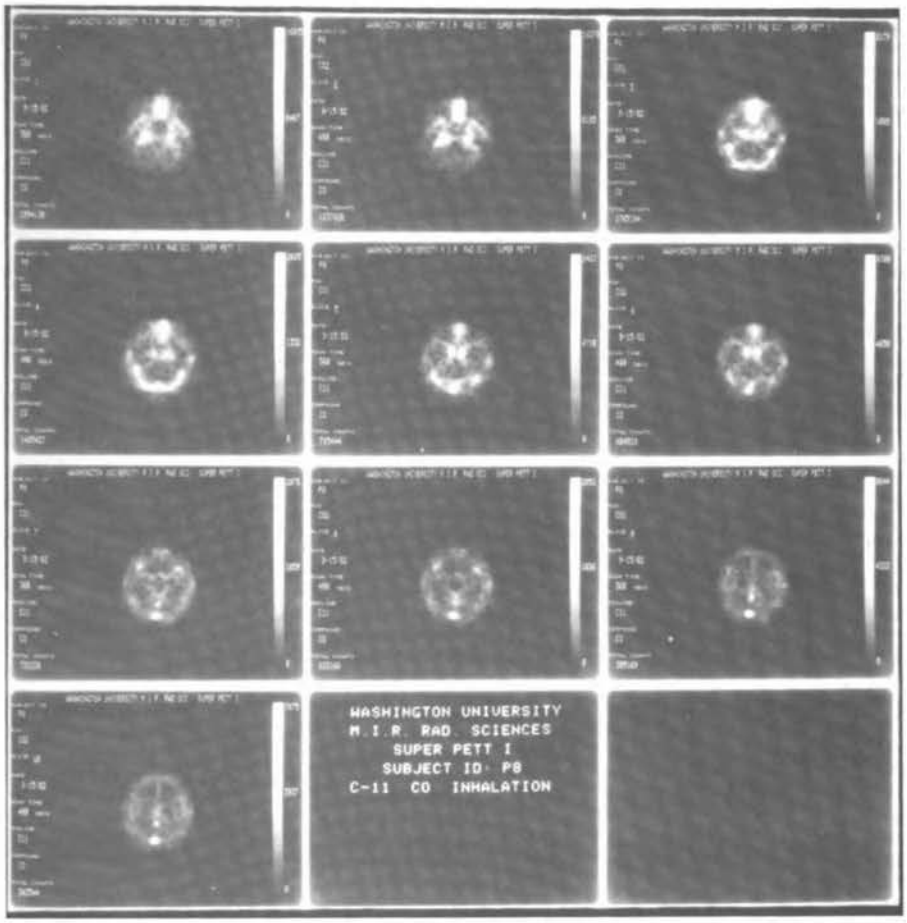

FIGURE 4 Transverse tomographic PET image of head of normal subject after administration, by inhalation, of carbon monoxide labeled with carbon-11. Images show distribution of blood in head. Images obtained with system illustrated in Figure 2.

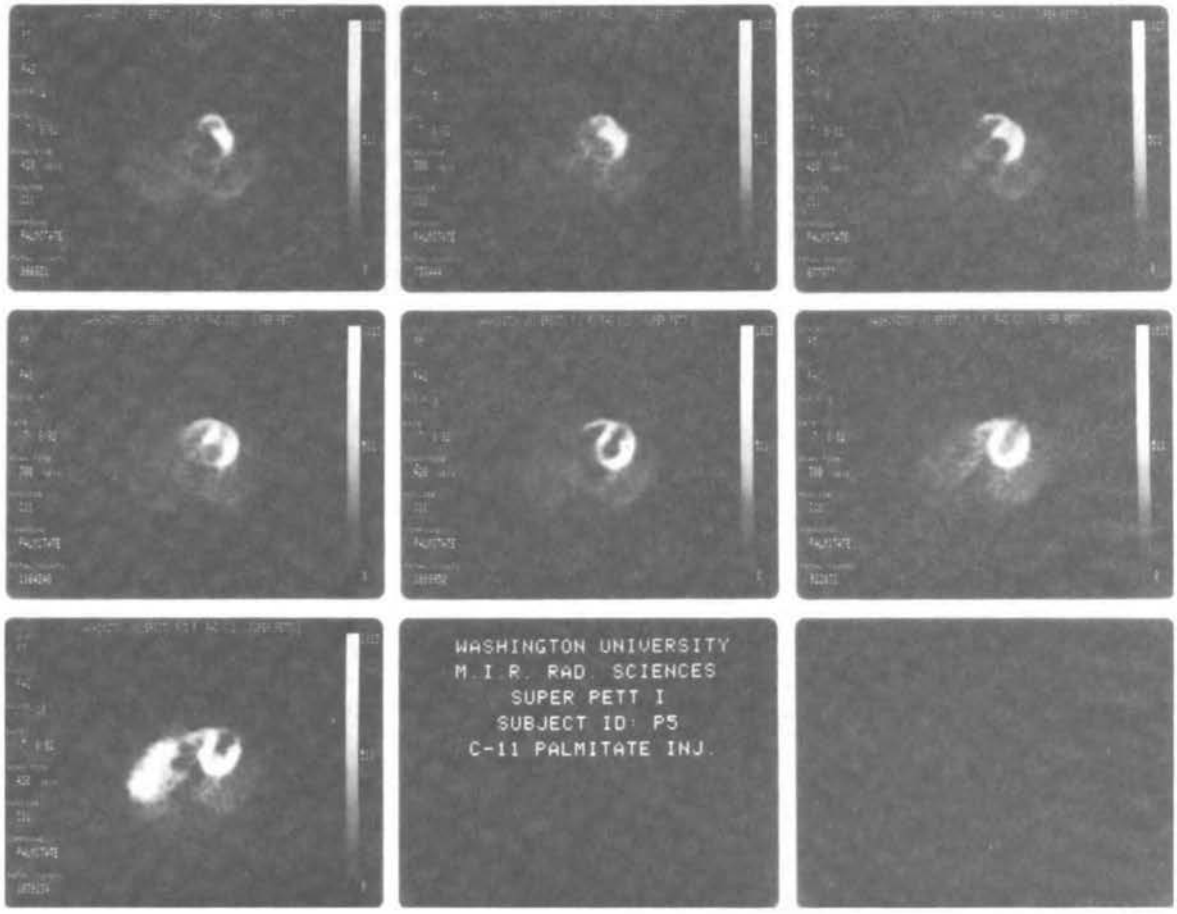

FIGURE 5 Transverse tomographic PET images of chest of patient after intravenous administration of palmitate labeled with carbon-11. Note accumulation of activity in myocardium and liver. Images obtained with device shown in Figure 3.

POSITRON EMISSION TOMOGRAPHY: PHYSIOLOGIC AND CLINICAL APPLICATIONS

PETER HERSCOVITCH*
Department of Neurology and Neurological Surgery
Mallinckrodt Institute of Radiology
and
McDonnell Center for Studies of Higher Brain Function
Washington University School of Medicine

The image obtained with positron emission tomography (PET) provides accurate regional quantitation of radiopharmaceuticals labeled with positron-emitting radionuclides. However, the ability to obtain such an image is only one element in the application of PET. One also requires the synthesis of positron-emitting radiotracers that can be used safely in humans and are suitable for the study of specific biological processes. And one requires appropriate mathematical models to describe the behavior of the radiotracers, so that biological measurements can be calculated from the tomographic data. When appropriately combined, these three components--PET imaging device, positron-emitting radiotracers, and tracer kinetic models--permit the in vivo study of physiologic and biochemical processes in a quantitative, regional manner. Although it is convenient to discuss these components separately, the successful application of PET requires an interactive process in their development and use.

POSITRON-EMITTING RADIOTRACERS

The commonly used positron-emitting radionuclides are oxygen-15 (half-life, 2 min), nitrogen-13 (10 min), carbon-11 (20 min), and fluorine-18 (110 min). Several properties of these nuclides make them uniquely suited to PET. First, oxygen-15, nitrogen-13, and carbon-11 are virtually identical chemically with their nonradioactive counterparts, which are the basic constituents of living matter, as well as of most drugs. Thus, they can be incorporated into radiotracers suitable for the study of most biological processes, as well as for studies involving the behavior of drugs. Fluorine-18, although not a nuclide of a biologically important

*Fellow, Medical Research Council of Canada.

element, can be used to label a variety of compounds of physiologic interest. Second, these radionuclides decay with short half-lives. Thus, relatively large amounts of radioactivity (e.g., 50-100 mCi of oxygen-15 and 30 mCi of carbon-11) can be administered to humans subjects to obtain PET images of good statistical quality, but with substantially reduced radiation exposure, because of the rapid decay. The typical radiation dose to the critical organ--that is, the organ receiving the greatest radiation exposure--is 1-2 rads for a single radiotracer administration. The short half-lives of some of the positron-emitting nuclides, especially oxygen-15, permit rapid repeated studies in the same subject.

A disadvantage of the short half-lives is the requirement of a cyclotron in the immediate medical environment. In addition, fast radiochemical-labeling techniques are required. These must yield radiotracers pure enough for human use and with specific activity (i.e., in millicuries per unit mass of compound) high enough for the administration of physiologically trace amounts to result in sufficient tissue radioactivity for imaging. In spite of these requirements, a wide variety of positron-emitting radiopharmaceuticals have been synthesized for potential use in PET.[2,24]

TRACER TECHNIQUES

Once an appropriate radiotracer has been synthesized and administered, its distribution in the brain can be measured with PET. The final step is the conversion of local tissue radiotracer concentration to a biological measurement. This requires the use of mathematical models that describe the biological behavior of the specific radiotracer used. Several factors must be considered in the modeling process, including the local delivery of tracer by arterial blood to the tissue, the transport of tracer across the blood-brain barrier, the metabolic fate of the tracer in the tissue and the behavior of any labeled metabolites, the presence of tracer in the vascular space, the recirculation of radiotracer or its labeled metabolites, and the potential alterations in radiotracer behavior in the presence of local disease. In addition, it must be possible to collect sufficient counts with the tomograph to permit an accurate solution of the model. This must be done in the face of limitations of the amount of radiotracer that can be administered with respect to dose considerations and of the time available for data collection, which may be limited not only by patient comfort and tracer half-life, but also by the requirement of a physiologic steady state during the scan.

Strategies have been implemented or are under development to permit a wide variety of measurements to be made with PET, including

cerebral blood volume (CBV), cerebral blood flow (CBF), cerebral metabolism of oxygen and glucose, brain protein synthesis, blood-brain barrier permeability, tissue pH, tissue lipid content, neuroreceptor pharmacology, neurotransmitter metabolism, and drug kinetics. The basic techniques most extensively applied involve the measurement of CBV, CBF, and cerebral metabolism. I will outline the approaches developed at Washington University for these measurements with ^{15}O-labeled tracers and the rapid data collection that is possible with the PETT VI tomograph.[19]

CEREBRAL BLOOD VOLUME

CBV can be measured with trace amounts of either ^{11}CO or $C^{15}O$ administered by inhalation (see Figure 1). $C^{15}O$ has the advantage of a shorter half-life. The tracer binds to hemoglobin in the red cells and remains confined to the vascular space as carboxyhemoglobin. CBV (in milliliters of blood per 100 g of tissue) is determined from the ratio of tissue radioactivity (obtained from the equilibrium CO tomographic image) to blood radioactivity.[6] One must also correct for the difference between small-vessel cerebral hematocrit and large-vessel peripheral hematocrit. CBV is of physiologic interest, because it directly reflects local cerebral vasodilation in response to changes in perfusion pressure. In addition, knowledge of CBV is often required for the correction of other PET data for the amount of radiotracer present in the vascular space of the brain.

CEREBRAL BLOOD FLOW

The measurement of CBF with PET is more complex, because PET systems cannot collect data fast enough to permit the use of conventional clearance-curve techniques developed for use with single probes. Our approach for measuring CBF with PET is based on the classical autoradiographic technique developed by Kety and colleagues for measuring regional CBF in laboratory animals.[8] We use ^{15}O-labeled water, administered by bolus intravenous injection, as the flow tracer. CBF (in milliliters per minute per 100 g of tissue) is calculated from the PET image, collected over 40 s after tracer administration, and from the arterial $H_2{}^{15}O$ time-activity curve, obtained by rapid blood sampling.[7,16] To collect sufficient counts in the PET image over the short scan interval, a relatively large amount of radioactivity, typically 50-80 mCi, must be injected. Thus, the scanner must be able to operate accurately at the resulting high count rates. A quantitative CBF image obtained with bolus intravenous injection of $H_2{}^{15}O$ is shown in Figure 2.

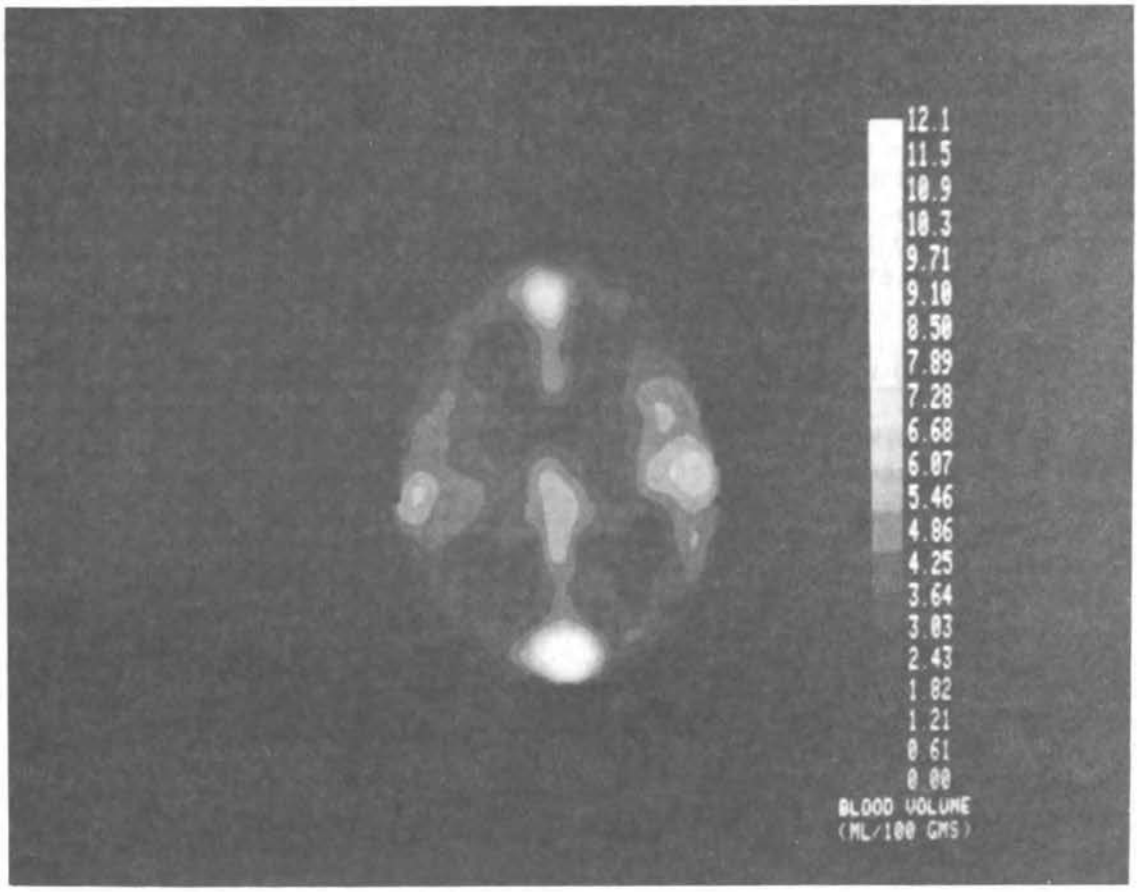

FIGURE 1 Quantitative PET image of normal human brain, obtained with ^{15}O-labeled radiotracers and PETT VI tomograph. This horizontal section and those in Figures 2-4 are at level of thalamus and are oriented with anterior up and left to reader's left. Cerebral blood volume (milliliters per 100 grams) measured with $C^{15}O$. Superior sagittal sinus is seen anteriorly and posteriorly, and differences in vascular density between gray and white matter are clearly delineated.

CEREBRAL METABOLISM

Recently a model has been developed for the measurement of cerebral oxygen metabolism that uses brief inhalation of ^{15}O-labeled oxygen.[12] This model accounts for the production and egress of water of metabolism in the brain, the activity present in the vascular space as $^{15}O_2$, and recirculating water of metabolism. After tracer inhalation, typically of 50-100 mCi, a 40-s scan is obtained, and sequential arterial blood samples are drawn. Additional data required for the calculation of the cerebral oxygen extraction fraction (OEF) and the cerebral metabolic rate for oxygen

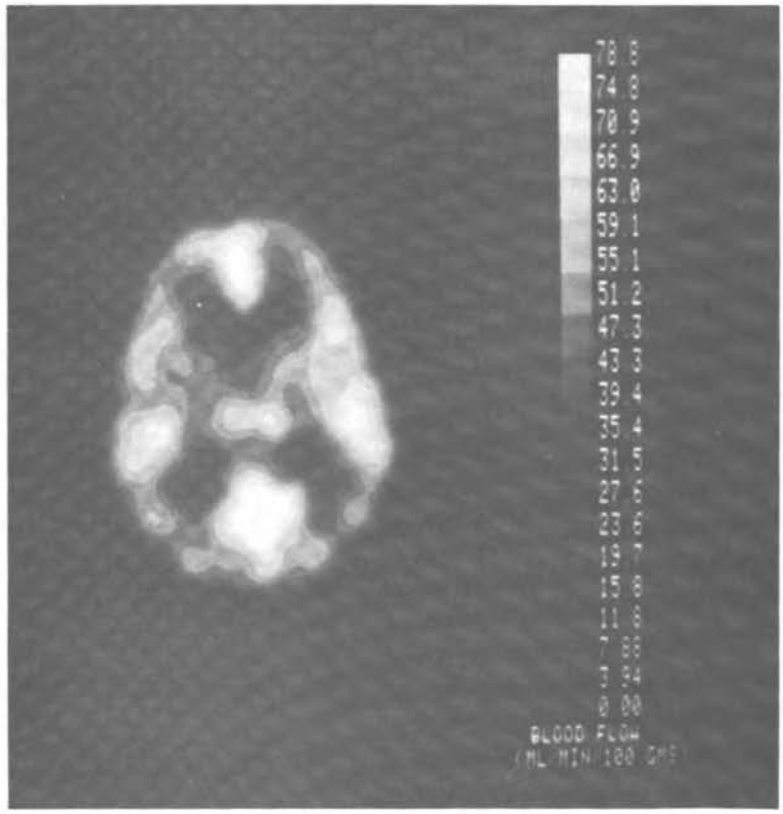

FIGURE 2 Cerebral blood flow (milliliters per 100 grams) measured with $C^{15}O$-labeled water administered by bolus intravenous injection.

($CMRO_2$, in milliliters per minute per 100 g) are the local CBF and CBV, which are obtained with separate $H_2{}^{15}O$ and $C^{15}O$ scans, respectively. $CMRO_2$ and OEF images obtained by this technique are shown in Figures 3 and 4, respectively.

An alternative, widely used method for the determination of CBF and $CMRO_2$ with ^{15}O-labeled radiotracers is the equilibrium-inhalation technique.[4] Continuous administration of radiotracer results in stable radioactivity distributions in the brain, which can be imaged over several minutes. This approach is particularly suited to PET devices that cannot operate accurately at high count rates or that cannot obtain several tomographic slices simultaneously.

Because the energy requirements of the brain are met almost exclusively by the oxidative metabolism of glucose, methods have been developed to measure the cerebral metabolic rate for glucose

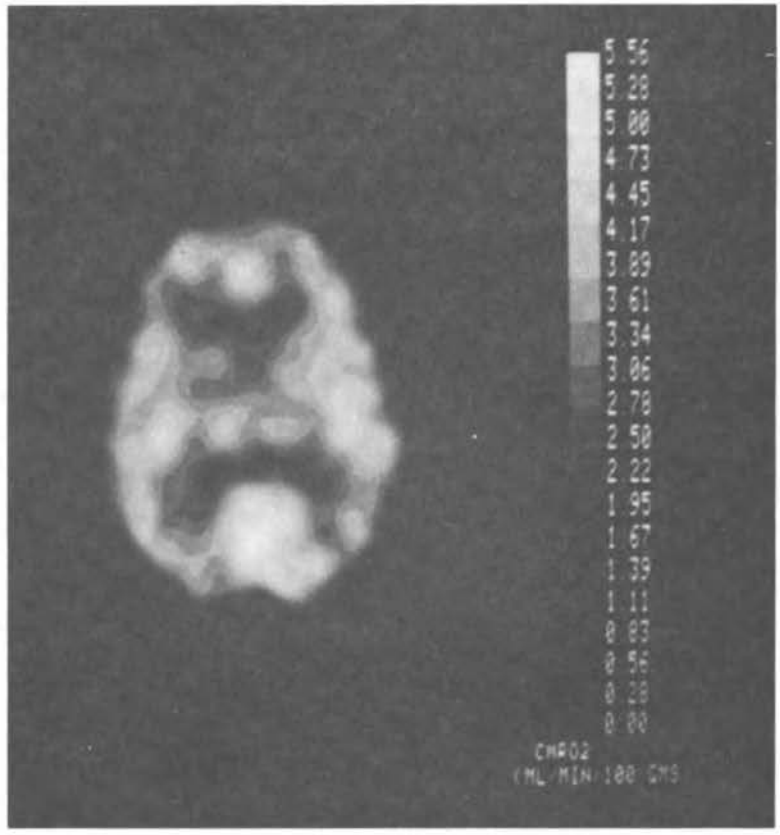

FIGURE 3 Cerebral metabolic rate for oxygen (milliliters per minute per 100 grams).

with PET. One approach applied in many centers[13,18] involves the use of the glucose analogue 2-deoxyglucose, labeled with either ^{18}F or ^{11}C. Another approach being developed for application in humans uses the labeled metabolic substrate [^{11}C]glucose.

APPLICATION OF MEASUREMENTS OF CEREBRAL BLOOD FLOW AND METABOLISM

The basic techniques for the measurement of CBF and metabolism with PET have been applied in a wide variety of physiologic and clinical problems, including functional activation studies, cerebrovascular disease, epilepsy, brain tumor, dementia, and movement disorders (for review, see Phelps et al.[14]). A few illustrative applications will be reviewed here.

Evaluation and selection of potential therapies for patients with cerebrovascular disease continue to be difficult. Cerebral revascularization by extracranial-intracranial (EC/IC) bypass surgery is used increasingly to treat patients with cerebral ischemia referable to occlusion or to surgically inaccessible

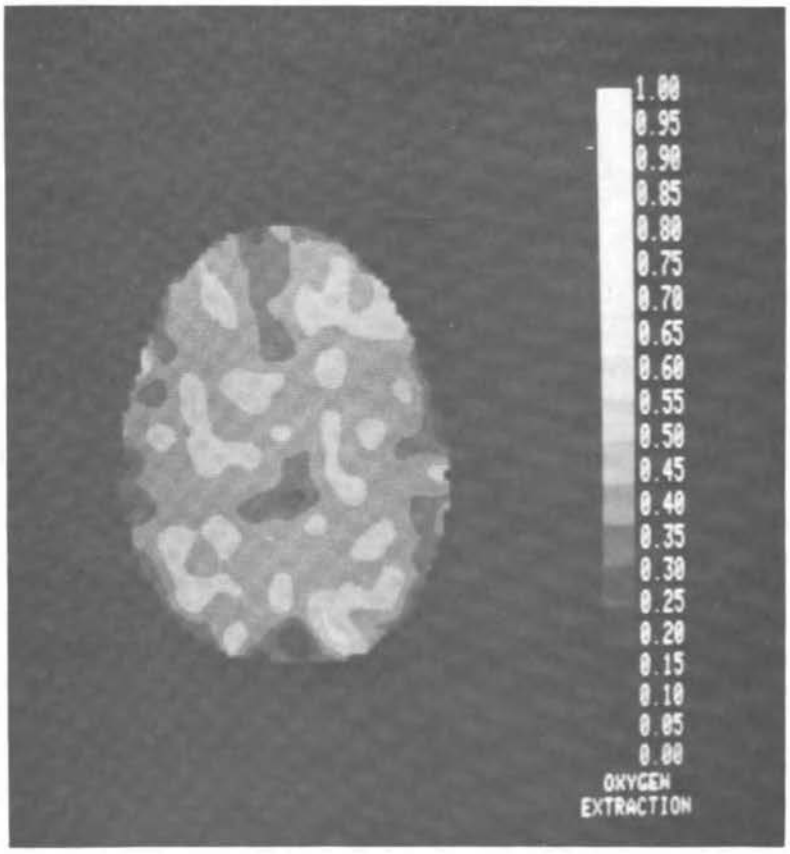

FIGURE 4. Cerebral oxygen extraction fraction (dimensionless), a measure of fraction of arterial blood oxygen that is extracted by brain. It is relatively uniform throughout brain, because areas of high oxygen metabolism have matching high blood flow, as can be seen in Figures 2 and 3.

stenosis of the carotid arterial system. The cerebral hemodynamic and metabolic effects of EC/IC bypass surgery and the potential for identifying patients most likely to benefit from such surgery are being studied.[15] Patients appear to be of several types, according to clinical, radiologic, and PET findings. One type of patient has a stable cerebral infarction distal to a vascular occlusion, with good clinical recovery. PET may show coupled decreases of CBF and $CMRO_2$ and demonstrate no change in these findings after bypass surgery. This constellation of preoperative findings suggests that blood supply is adequate to meet the needs of the damaged brain. Another group of patients presents with transient ischemic attacks only, but no asymmetries of CBF and $CMRO_2$ shown by PET. In such cases, EC/IC bypass would have no effect on already normal flow patterns. Yet another type of patient has transient ischemic attacks associated with decreased blood flow in the symptomatic hemisphere, which returns toward normal postoperatively. Preoperative PET may show other changes in these patients that indicate compensatory

mechanisms marshaled by the brain in response to a decrease in perfusion pressure. Such mechanisms include an increase in oxygen extraction to maintain oxygen metabolism and dilation of parenchymal blood vessels, which increases local CBV. Cerebral revascularization has the potential of reversing these preoperative changes in OEF and CBV.

Perinatal cerebrovascular disorders, including intraventricular hemorrhage (IVH) and hypoxic-ischemic encephalopathy, constitute a major cause of morbidity and mortality. It has been possible to define abnormalities of CBF in affected neonates with the PETT VI tomograph and $H_2{}^{15}O$ as the flow tracer. Premature infants with IVH and associated intraparenchymal hemorrhagic involvement constitute the majority of all neurologically impaired infants with IVH. To define the nature of the parenchymal injury better, we performed CBF studies in such infants within 10 d of birth.[21] Gestational ages ranged from 27 to 30 wk, and birth weights from 920 to 1,200 g. The hemisphere containing the intraparenchymal hemorrhage had a diminution of flow that was much more widespread than the anatomic extent of the localized hematoma and that involved much of the hemisphere (Figure 5). These findings indicate that the intraparenchymal hemorrhagic involvement associated with severe IVH is a component of a larger ischemic lesion and help explain the poor neurologic outcome in affected infants. Asphyxia in the full-term newborn is another common cause of perinatal brain injury. Our blood flow studies with PET in such infants (Figure 6) have often demonstrated a relative decrease in flow in the parasagittal area of the cerebral hemispheres.[22] This area is the "watershed" arterial border zone, where the three vascular territories of the brain meet and which is susceptible to damage caused by changes in perfusion. The clinical correlate of this PET abnormality consists of bilateral weakness of proximal limbs, with upper limbs more affected than lower. These studies in infants indicate the potential of PET in the investigation of perinatal cerebrovascular disorders.

Several groups are using PET to study the functional behavior of the normal human CNS. Increased functional activity of the brain increases local metabolism and blood flow to meet neuronal energy demands. Thus, regional measurements with PET can reflect not only the anatomic areas involved, but also the degree of local activation in response to specific neurobehavioral tasks. Appropriately designed PET studies therefore are potentially useful in evaluating the organization of motor activity, the central processing of sensory information, and the mechanisms involved in language and memory. Regional responses of the brain to a variety of auditory, visual, and somatosensory stimuli have been studied with ^{18}F-deoxyglucose to measure local glucose metabolism.[14] This approach has some limitations. The tracer model requires a period of approximately 45 min between radiotracer administration and

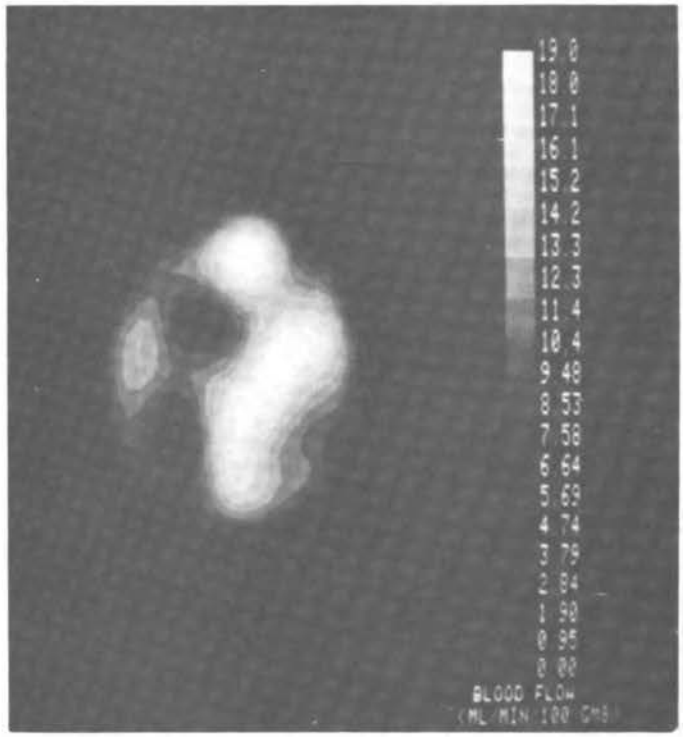

FIGURE 5 Quantitative image of regional cerebral blood flow in 5-d-old premature neonate weighing 920 g. Infant had suffered intraventricular hemorrhage with intraparenchymal hematoma localized to left frontal white matter. Note decrease in blood flow throughout affected hemisphere, compared with right side.

scanning, so it may be difficult to maintain the required physiologic steady state during the period of radiotracer uptake by the brain. And, because of the relatively long half-life of ^{18}F (110 min) and radiation dosimetry limitations, a subject can be studied only once per session and only one or two repeat studies can be performed. These factors introduce the difficulties involved in repositioning subjects for followup studies and limit the range of experimental conditions that can be studied in a given subject.

An alternative approach to functional-activation studies involves the measurement of local CBF responses with $H_2{}^{15}O$ and the modified autoradiographic technique.[16] Up to eight measurements of CBF can be performed in the same subject in a 2-h period, and that allows great flexibility in experimental design. Each flow measurement is performed in less than 1 min. Lauter *et al.*[9] have recently used this approach to study the tonotopic representation of the human auditory cortex. Higher-frequency auditory stimuli had a

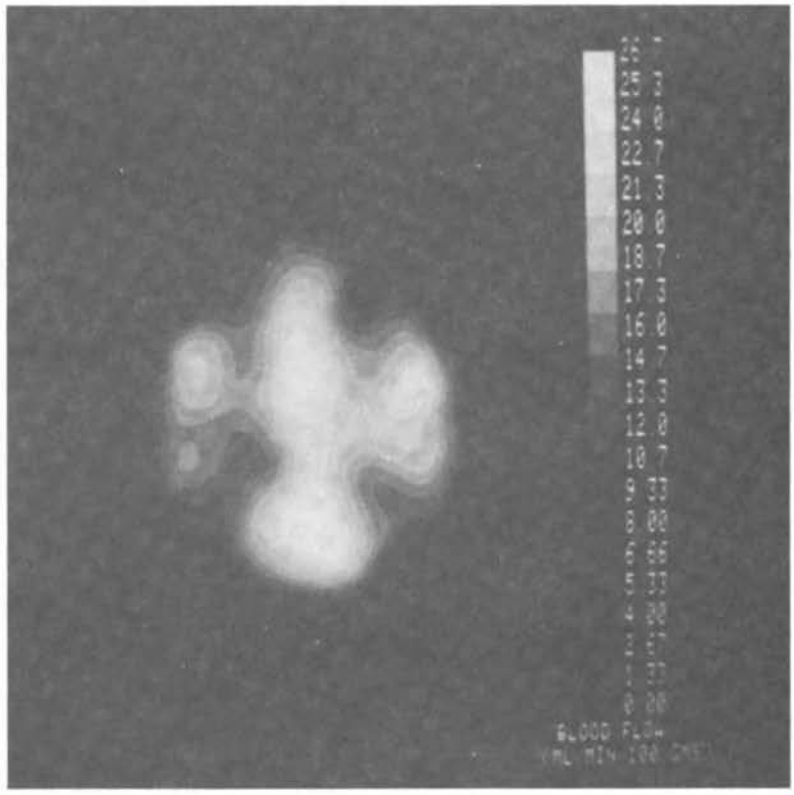

FIGURE 6 PET image of regional cerebral blood flow in full-term neonate who had experienced perinatal asphyxia. Note relative decrease in flow in parasagittal areas of both cerebral hemispheres.

more posterior and medial representation, analogous to that found in animals with neurophysiologic techniques. The response of the human visual cortex to visual flash stimulation of various repetition frequencies has also been investigated (Figure 7). A linear relationship between local CBF response in the visual cortex and stimulation rate up to 8 Hz was demonstrated.[3] Beyond this frequency, there was a decrease in local CBF response analogous to that in the amplitude of electrical cortical evoked responses at higher stimulation rates.

With PET it has been possible to demonstrate functional abnormalities in structurally intact areas of brain. Several investigators have noted areas of depressed neuronal activity, blood flow, or metabolism in structurally normal regions of brain that are distant from the site of focal cerebral damage. An example of this phenomenon, termed diaschisis, has been demonstrated for both blood flow and oxygen metabolism in the cerebellar hemisphere contralateral to frontal cerebral infarction[10] (see Figure 8).

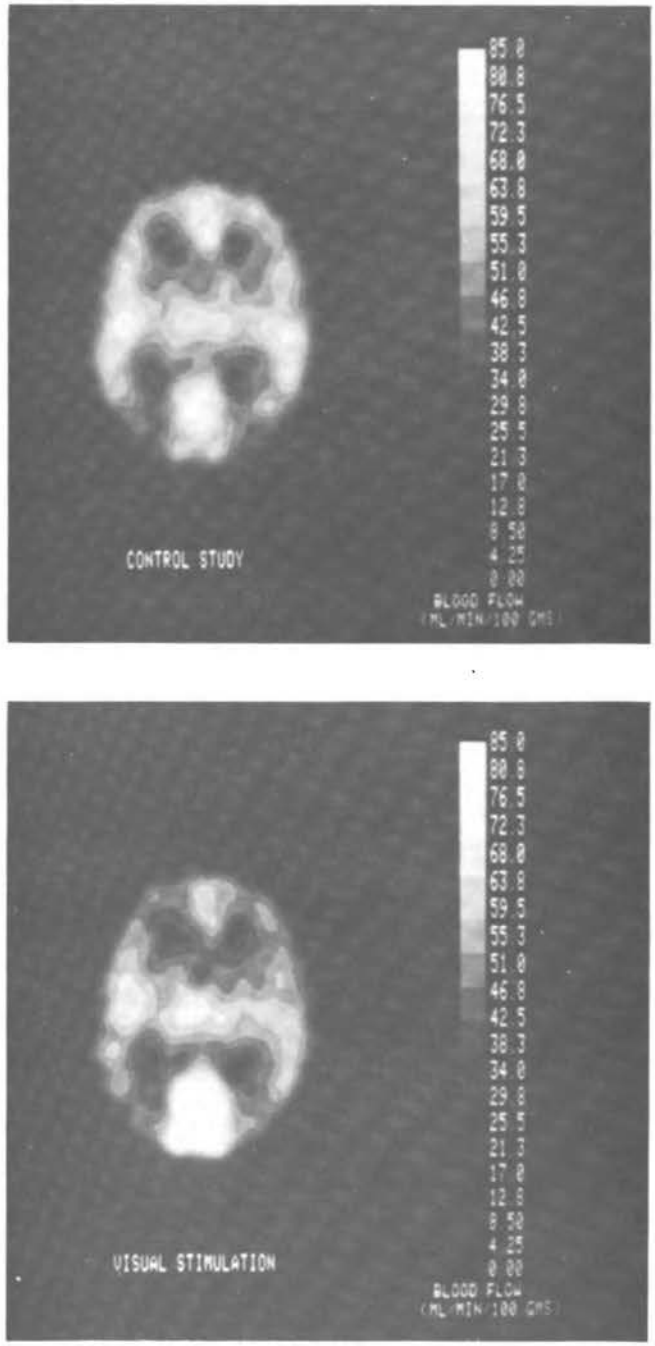

FIGURE 7 Local blood flow response to visual stimulation in normal subject. Top, control scan, with subject's eyes patched. Bottom, scan during pattern flash photic stimulation at 8 Hz, demonstrating increased flow in visual cortex. Same flow scale is used in both images.

This decrease in flow and metabolism reflects damage to neuronal inputs of the cerebellum and provides data on the source of these inputs in man. We have found focal metabolic changes in patients with amnesia.[20] For example, a patient with a stable amnesic syndrome after global hypoxic brain injury, who had normal computed tomographic and nuclear magnetic resonance head scans, had a focal decrease in $CMRO_2$ in the mesial temporal lobes. Another patient with transient global amnesia had similar PET findings involving the temporal lobes that reverted to normal when her amnesia cleared. These observations support the current theories of the importance of mesial temporal lobe structures in memory.

Abnormalities of neurotransmitter or neuroreceptor function have been implicated in several neurologic and psychiatric disorders, including Parkinson's disease, Huntington's chorea, Alzheimer's disease, depression, mania, and schizophrenia. The methods that have been used thus far to study receptor function have been indirect or logistically difficult, e.g., postmortem tissue analysis, assay of cerebrospinal fluid metabolites, and observation of clinical response to drugs. PET holds the potential for quantitating neuroreceptor function and neurotransmitter metabolism in vivo and permits serial examinations to define the natural history of specific disorders and their response to therapy. The greatest progress has been made in methods for studying the dopaminergic system. ^{18}F-labeled fluorodopa has recently been used to image the regional distribution of dopamine in man.[5] Three groups have imaged dopamine receptors in vivo; they used the receptor ligand ^{11}C-methylspiperone in man,[23] ^{11}C-spiperone in baboons,[1] and ^{18}F-spiperone in baboons[11] (see Figure 9). Furthermore, a model has been developed that uses ^{18}F-spiperone and permits, for the first time, the quantitative characterization of dopamine-binding sites.[11] The model demonstrates that the number of binding sites and the binding affinity are not separately ascertainable. Rather, their product, the "binding potential," which reflects the capacity of a given tissue for ligand-binding site interaction, can be measured. There are other unknown parameters in the model, including CBF, the permeability of the brain to the tracer, and the nonspecific binding of tracer in tissue. Although CBF can be measured independently, enough scan data in the form of sequential ^{18}F-spiperone images must be collected to solve the model for binding potential. A single image of labeled spiperone distribution is probably insufficient to quantitate neuroreceptor pharmacology. This model illustrates the complexities that may be involved in converting the PET image to useful quantitative biological measurements.

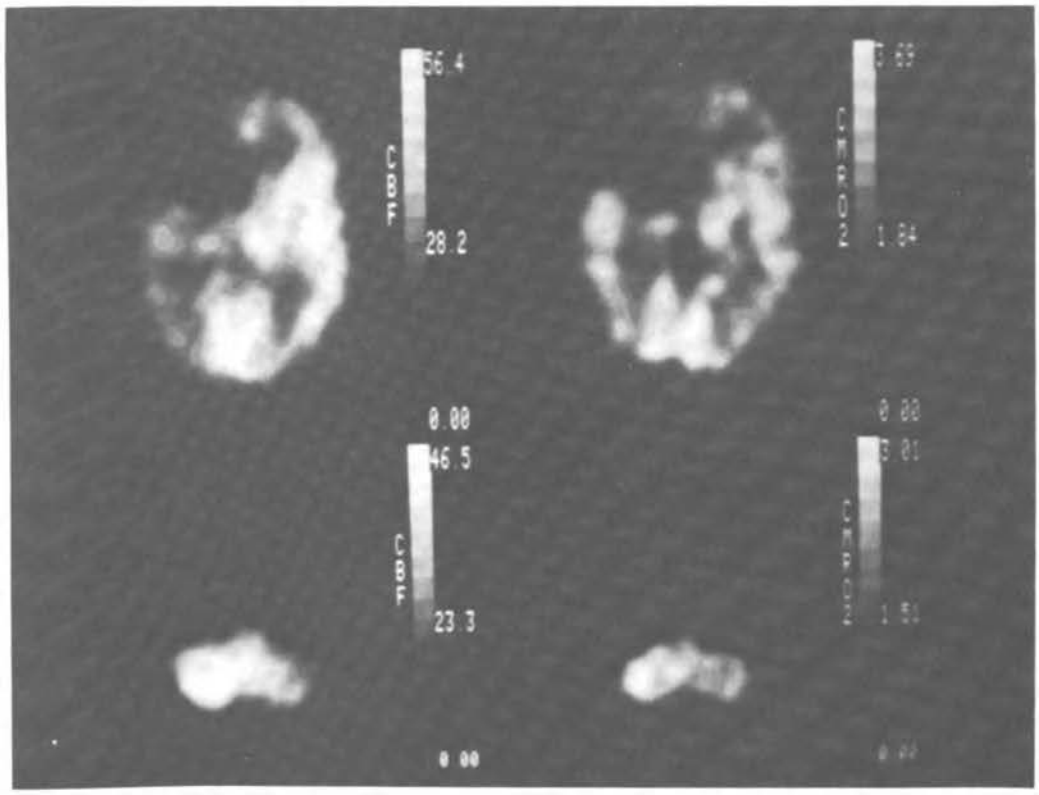

FIGURE 8 Example of crossed cerebellar diaschisis in patient with left frontal cerebral infarction. Upper scans show cerebral blood flow (left) and cerebral metabolic rate for oxygen (right). Both flow and oxygen metabolism are markedly decreased in area of infarction. In lower scans, of cerebellar blood flow (left) and cerebellar oxygen metabolism (right), both flow and metabolism are decreased in right cerebellar hemisphere, contralateral to cerebral infarction.

ACKNOWLEDGMENT

The work reported here was supported by National Institutes of Health grants NS06833 and HL 13851.

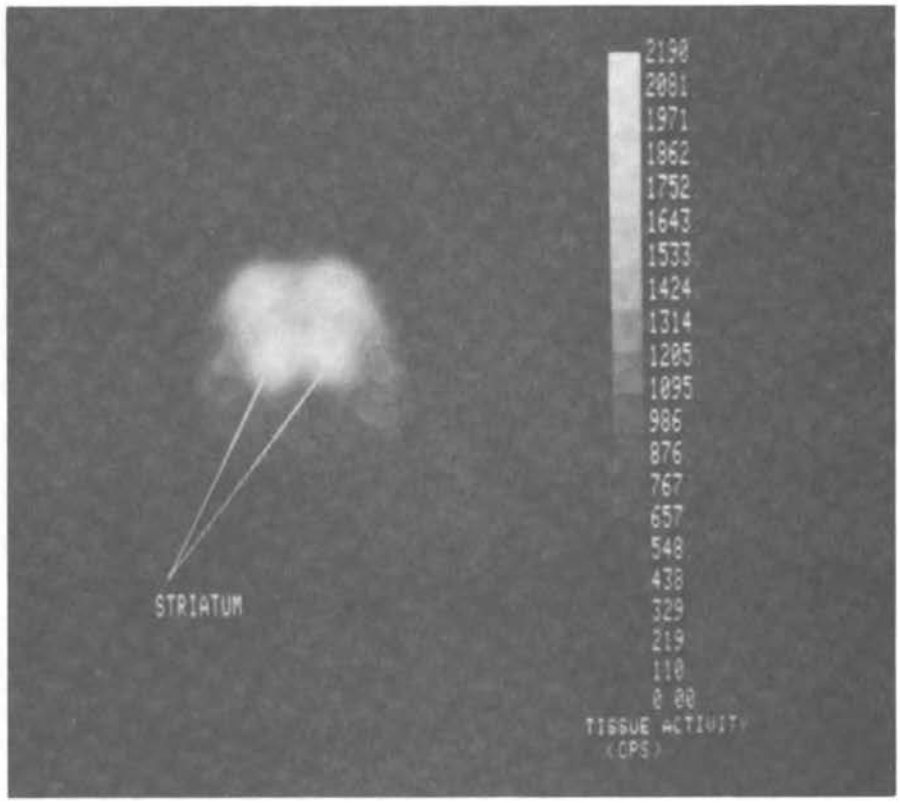

FIGURE 9 PET image of baboon brain obtained 2 h after injection of ^{18}F-spiperone. Accumulation of radiotracer is prominent in striatum. There is also tracer accumulation in retinas (anterior to striatum).

REFERENCES

1. Arnett, C. D., J. S. Fowler, A. P. Wolf, J. Logan, and R. R. MacGregor. Neuroleptic receptor labeling in vivo with [^{11}C]spiroperidol. Society for Neuroscience, Abstracts of 13th Annual Meeting, Boston, 1983:9(Part 2):1221.

2. Comar, D., M. Berridge, B. Mazière, and C. Crouzel. Radiopharmaceuticals labelled with positron-emitting radioisotopes, pp. 42-90. In P. A. Ell and B. L. Holman, Eds. Computed Emission Tomography. New York: Oxford University Press, 1982.

3. Fox, P. T., and M. E. Raichle. Temporal frequency selectivity of human striate cortex demonstrated by positron emission tomography. Society for Neuroscience, Abstracts of 13th Annual Meeting, Boston, 1983:9(Part 1):32.

4. Frackowiak, R. S., G.-L. Lenzi, T. Jones, and J. D. Heather. Quantitative measurement of regional cerebral blood flow and oxygen metabolism in man using ^{15}O and positron emission tomography: Theory, procedure, and normal values. J. Comput. Assist. Tomogr. 4:727-736, 1980.

5. Garnett, E. S., G. Firnau, and C. Nahmias. Dopamine visualized in the basal ganglia of living man. Nature 305:137-138, 1983.

6. Grubb, R. L., M. E. Raichle, C. S. Higgins, and J. O. Eichling. Measurement of regional cerebral blood volume by emission tomography. Ann. Neurol. 4:322-328, 1978.

7. Herscovitch, P., J. Markham, and M. E. Raichle. Brain blood flow measured with intravenous $H_2{}^{15}O$. I. Theory and error analysis. J. Nucl. Med. 24:782-789, 1983.

8. Kety, S. S. Measurement of local blood flow by the exchange of an inert, diffusible substance. Methods Med. Res. 8:228-236, 1960.

9. Lauter, J. L., C. Formby, P. Fox, P. Herscovitch, and M. E. Raichle. Tonotopic organization in human auditory cortex as revealed by regional changes in cerebral blood flow. J. Cereb. Blood Flow Metabol. 3(Suppl. 1):S248-S249, 1983.

10. Martin, W. R. W., and M. E. Raichle. Cerebellar blood flow and metabolism in cerebral hemisphere infarction. Ann. Neurol. 14:168-176, 1983.

11. Mintun, M. A., M. E. Raichle, M. R. Kilbourn, G. F. Wooten, and M. J. Welch. A quantitative model for the in vivo assessment of drug binding sites with positron emission tomography. Ann. Neurol. 15:217-227, 1984.

12. Mintun, M. A., M. E. Raichle, W. R. W. Martin, and P. Herscovitch. Brain oxygen utilization measured with O-15 radiotracers and positron emission tomography. J. Nucl. Med. 25:177-187, 1984.

13. Phelps, M. E., S. C. Huang, E. J. Hoffman, C. Selin, L. Sokoloff, and D. E. Kuhl. Tomographic measurement of local cerebral glucose metabolic rate in humans with (F-18) 2-fluoro-2-deoxy-D-glucose: Validation of method. Ann. Neurol. 6:371-388, 1979.

14. Phelps, M. E., J. C. Mazziotta, and S.-C. Huang. Study of cerebral function with positron computed tomography. J. Cereb. Blood Flow Metabol. 2:113-162, 1982.

15. Powers, W. J., W. R. W. Martin, P. Herscovitch, M. E. Raichle, and R. L. Grubb, Jr. Extracranial-intracranial bypass surgery: Hemodynamic and metabolic effects. Neurology. (in press)

16. Raichle, M. E., W. R. Martin, P. Herscovitch, M. A. Mintun, and J. Markham. Brain blood flow measured with intravenous $H_2{}^{15}O$. II. Implementation and validation. J. Nucl. Med. 24:790-798, 1983.

17. Raichle, M. E., M. J. Welch, R. L. Grubb, Jr., C. S. Higgins, M. M. Ter-Pogossian, and K. B. Larson. Measurement of regional substrate utilization rates by emission tomography. Science 199:986-987, 1978.

18. Reivich, M., A. Alavi, A. Wolf, J. H. Greenberg, J. Fowler, D. Christman, R. MacGregor, S. C. Jones, C. Shiue, and Y. Yonekura. Use of 2-deoxy-D[1-^{11}C]glucose for the determination of local cerebral glucose metabolism in humans: Variation within and between subjects. J. Cereb. Blood Flow Metabol. 2:307-319, 1982.

19. Ter-Pogossian, M. M., D. C. Ficke, J. T. Hood, Sr., M. Yamamoto, and N. A. Mullani. PETT VI: A positron emission tomograph utilizing cesium fluoride scintillation detectors. J. Comput. Assist. Tomogr. 6:125-133, 1982.

20. Volpe, B. T., P. Herscovitch, M. E. Raichle, W. Hirst, and G. S. Gazzaniga. Cerebral blood flow and metabolism in human amnesia. J. Cereb. Blood Flow Metabol. 3(Suppl. 1):S5-S6, 1983.

21. Volpe, J. J., P. Herscovitch, J. M. Perlman, and M. E. Raichle. Positron emission tomography in the newborn: Extensive impairment of regional cerebral blood flow with intraventricular hemorrhage and hemorrhagic intracerebral involvement. Pediatrics 72:589-601, 1983.

22. Volpe, J. J., J. M. Perlman, P. Herscovitch, K. L. Kreusser, and M. E. Raichle. Positron emission tomography in the assessment of regional cerebral blood flow in the asphyxiated newborn. Ann. Neurol. 14:355-356, 1983. (abstract)

23. Wagner, H. N., Jr., H. D. Burns, R. F. Dannals, D. F. Wong, B. Langstrom, T. Duelfer, J. J. Frost, H. T. Ravert, J. M. Links, S. B. Rosenbloom, S. E. Lukas, A. V. Kramer, and M. J. Kuhar. Imaging dopamine receptors in the human brain by positron tomography. Science 221:1264-1266, 1983.

24. Wolf, A. P. Special characteristics and potential for radiopharmaceuticals for positron emission tomography. Semin. Nucl. Med. 11:2-12, 1981.

CONTEMPORARY NONINVASIVE IMAGING METHODS: AN ANALYSIS BASED ON DETECTED SIGNALS AND PHYSIOLOGIC PROCESSES

THOMAS F. BUDINGER
Lawrence Berkeley Laboratory
Berkeley, California

The major noninvasive imaging methods of current interest and clinical application are the following:

1) Digital subtraction angiography (Figure 1).

2) X-ray transmission computed tomography (Figure 1).

3) Nuclear magnetic resonance imaging and spectroscopy (Figure 2).

4) Single-photon emission tomography (Figure 3).

5) Positron emission tomography (Figure 3).

6) Ultrasound imaging (Figure 4).

7) Heavy-particle transmission (Figure 5).

Each of these general categories includes specialized procedures, such as contrast-enhanced x-ray computed tomography and ultrasound doppler imaging. Frequently, the focus has been on the attributes of imaging procedures, rather than on the physical attributes of the detected signals and on how biological processes and tissues modulate signal amplitude, frequency spectrum, and phase. Thus, this paper has three objectives: presentation of contemporary imaging methods, identification of the physical properties measured by these methods, and summary of the major physical and medical principles underlying development and selection of instrumentation for noninvasive imaging.

DIGITAL SUBTRACTION ANGIOGRAPHY

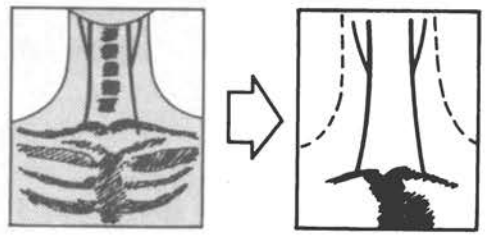

Flow channel anatomy and flow , relative motion and permeability

X-RAY COMPUTED TOMOGRAPHY (single section)

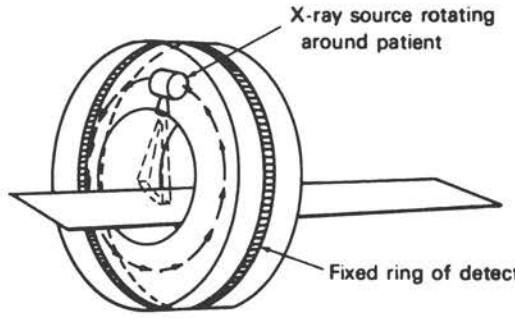

3-D Anatomy, mineral content and movement of contrast material

DYNAMIC SPATIAL RECONSTRUCTOR DSR

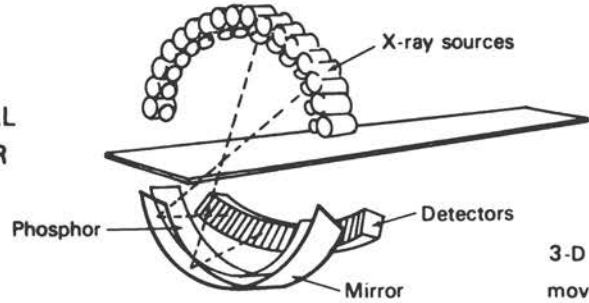

3-D Anatomy, motion, and movement of contrast material

HIGH SPEED ELECTRONIC SCANNING CVCT

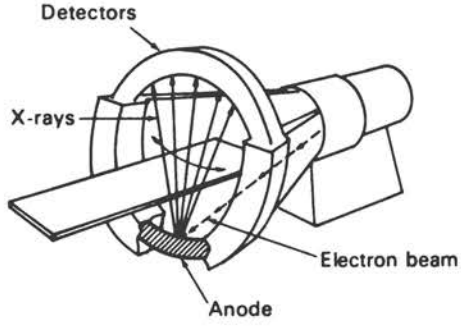

FIGURE 1 Current x-ray transmission methods include (top) digital subtraction angiography and energy-selective radiography and (below) three classes of transmission computed tomography, which can be used in projection digital radiography, as well as in computed tomographic applications.

NUCLEAR MAGNETIC RESONANCE IMAGING

(high resolution)

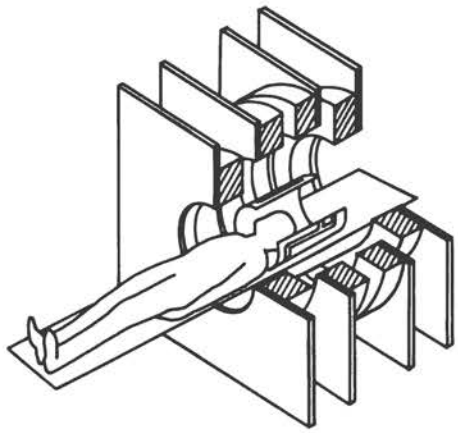

Proton density
Relative flow in vessels
Relaxation parameters T_1 and T_2

NUCLEAR MAGNETIC RESONANCE IN-VIVO SPECTROSCOPY

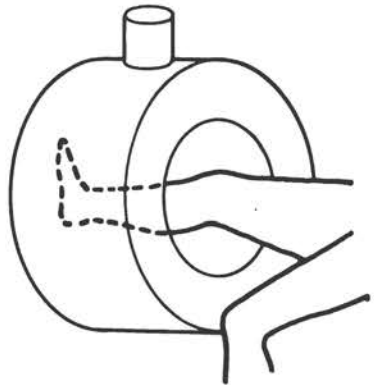

Organ concentration of nuclides, T_1 , T_2 and chemical shifts

TOPICAL NUCLEAR MAGNETIC RESONANCE SPECTROSCOPY

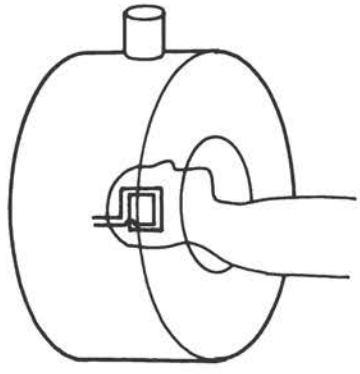

Selected regional concentration of nuclides, T_1 , T_2 and chemical shifts

FIGURE 2 In vivo nuclear magnetic resonance techniques include proton imaging and in vivo spectroscopy (nonimaging) of protons, carbon-13, phosphorus-31, and other nuclei.

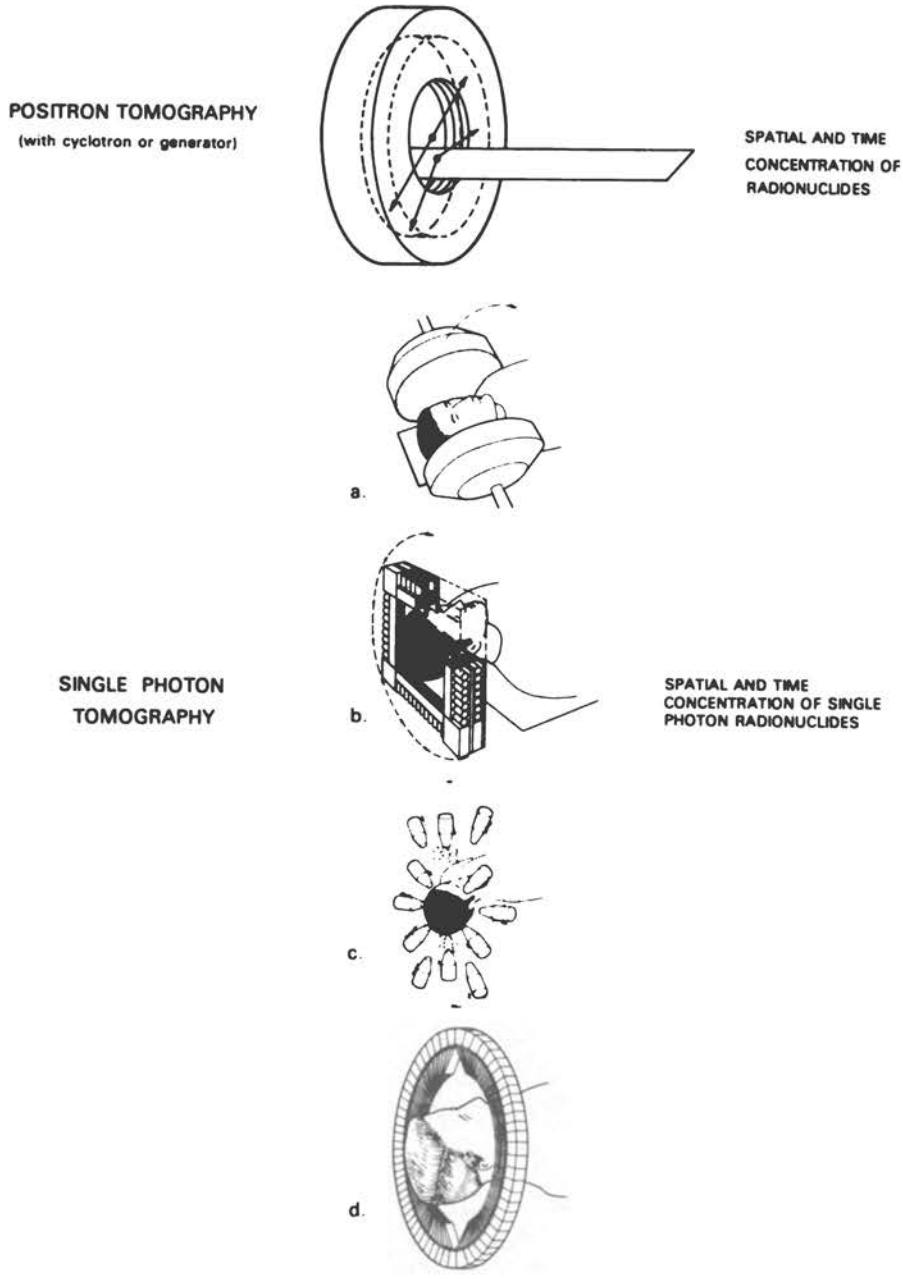

FIGURE 3 Emission tomographic methods include positron tomography and single-photon tomography with various configurations: a, rotating gamma cameras, b, four-sided multidetector system, c, multiple moving detectors, and d, circular array with movable fin collimators.

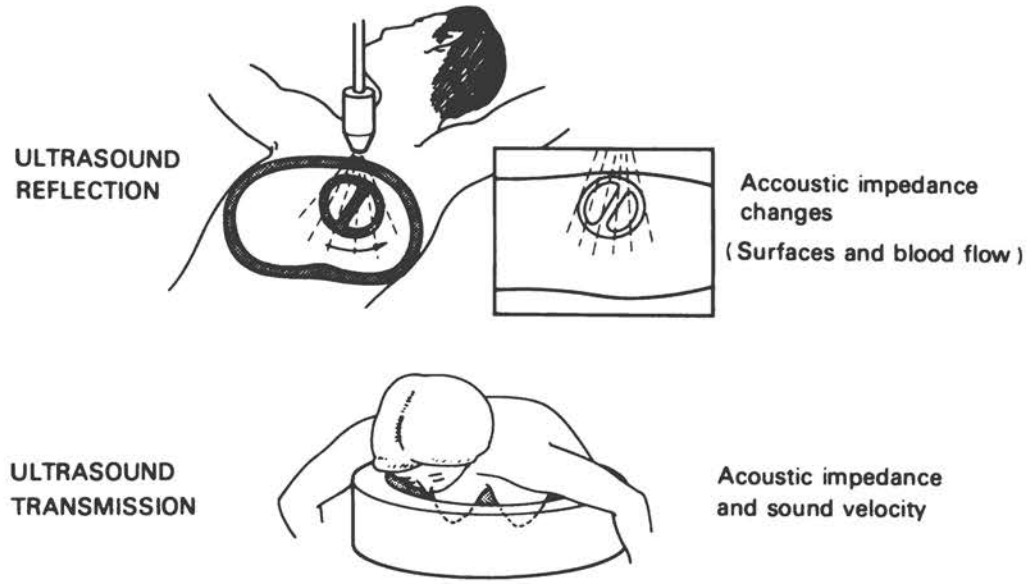

FIGURE 4 Ultrasound developments include improvements in B-scan devices, spectral analysis of signals, doppler imaging systems, and transmission computed tomography of acoustic velocity and attenuation.

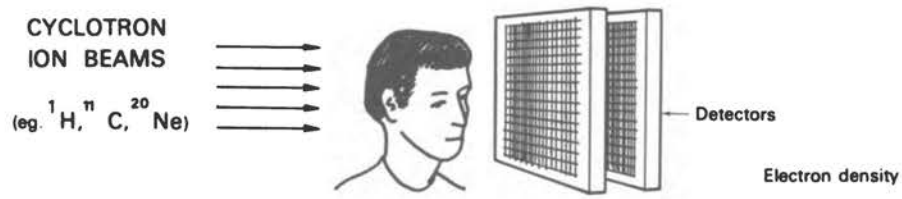

HEAVY ION IMAGING

FIGURE 5 Accelerated heavy ions are used for imaging and for exploring diffusion by injection of positron emitters and simultaneous measurement of emitted annihilation photons.

X-RAY TRANSMISSION IMAGING

Four common modes of x-ray imaging are conventional projection imaging, digital radiography, contrast-enhanced x-ray imaging and digital subtraction angiography, and tomographic imaging.

The basic physical processes involved in the modulation of x rays are photoelectric absorption and Compton scattering of x rays by tissue. The results of this modulation are changes in intensity, energy spectrum, and trajectory of the incoming photons. With rare exceptions, the energy and trajectory information is ignored or excluded, and intensity is the major signal attribute measured. The two physical phenomena that modulate the intensity and energy of photons passing through tissue, the photoelectric effect and Compton scattering, are lumped together as the attenuation coefficient.

The attenuation coefficient distribution reflects the anatomic distribution of muscle, fat, water, blood, bone, air, and other soft tissues whose photon attenuation properties are similar to those of muscle. Tumors frequently differ from normal tissues in water content or may contain foci of calcification. Thus, the attenuation coefficient is frequently different from that of contiguous soft tissues, and the x-ray techniques will detect this difference.

The attenuation coefficient depends on the atomic composition of the material through which the photons pass, as well as on the energy of the incident photons. It is important to point out these rather well-known principles of radiation interaction with tissue, because they are the basis of new methods of obtaining information on vessel distribution (by injection of contrast material) and tissue composition (by use of multiple energies).

DIGITAL RADIOGRAPHY

Ten years ago, digital radiography was limited to the point-by-point digitization of analogue x-ray images followed by various image processing methods. The shortcomings of that approach were overcome by the direct digitization of the signal from a scintillation crystal, as in the first practical modern digital radiographic system, presented by Stein[34] in 1975. Transmission profiles of the body were obtained with a single large 50-cm crystal and an x-ray beam broken up spatially and temporally by a rotating collimator. With the introduction of third- and fourth-generation computed tomographic scanners, the technical prerequisites for projection digital radiographs became available. Thus, it is possible without hardware modifications to obtain a digital radiograph with the advantages of low dose and only negligible scatter.

Various image-processing methods can be used with the digitized data corresponding to a projection image to improve visualization of structures within the body. A review of clinical problems in which this procedure has advantages over conventional radiography was offered by Hubener[17] and in a recent symposium on digital radiography.[3]

Contrast material has not been commonly used with digital radiography for whole-body surveys, because this procedure is slow. However, the combination of digital radiography with specialized equipment for subtraction angiography (Table 1) is one of the most exciting new approaches to noninvasive imaging, as discussed below.

TABLE 1

Noninvasive Imaging Methods

Method	Entities Measured	Medical Applications
Digital subtraction angiography	Contrast distribution	Flow-channel anatomy, relative motion, permeability
X-ray transmission computed tomography	Density, average atomic number	Anatomy, mineral content, movement of contrast material
Nuclear magnetic resonance (imaging or in vivo spectroscopy	Concentration of such nuclides as ^{1}H, relaxation times T_1 and T_2, frequency shifts due to chemical form	Free-water content, relative flow concentrations of some molecular species and contrast agents
Emission computed tomography (positron and single-photon)	Concentration of radionuclides	Metabolism, receptor-site concentration, flow
Ultrasonography	Acoustic-impedance mismatches, sound velocity, attenuation, frequency shifts due to motion	Anatomy, tissue structural characteristics, motion of surfaces, blood velocity
Heavy-ion imaging	Density (electron)	Anatomy

DIGITAL SUBTRACTION ANGIOGRAPHY

Digital subtraction angiography (DSA) is a method of delineating blood vessels by subtracting the tissue background image from the image of tissue plus intravascular contrast material.[3,8,26] The result is a high-contrast image of the vessels (Figure 1). The background is determined from a digitized image taken a few moments before the injection of contrast material.

The major advantage of DSA is that the subtraction technique allows extraction of a high-intensity signal from the superposed background information. In this respect, DSA achieves the objective for which computer-assisted tomography was developed: separation of the desired signals from superposed background information in projection views. It was initially explored with analogue methods, and it was not until more recent developments in image intensifiers, digital-data storage devices, and image-processing techniques that it became practical. DSA works well for one view if the object of interest gives a signal that is strong, compared with other signals that might superpose on it. This criterion is readily met for carotid, iliac, and renal arteries in most subjects, so DSA has become important in noninvasive imaging, particularly because contrast material can be injected intravenously, as well as intra-arterially.

Unambiguous information about vessel architecture can be extracted, as long as there is no superposition of many signals whose strength and position might cause distortion of the information detected from the region of interest. An example of the signal-extraction problem is the imaging of the coronary vascular tree by extraction of the strong blood-pool signal from that of the coronary arteries--a difficult but highly sought-after goal of DSA of the coronary arteries. In addition to its application to peripheral arteries, DSA can be used in clinical studies of the arterial and venous circulation of the brain and the pulmonary vasculature.

The development of contrast agents that diffuse into tissue with a high partition coefficient between tissue and blood could give DSA the ability to measure relative perfusion. The amount of contrast agent required necessitates a focus on chemical toxicity, and the promise for this approach in the near future is not great.

But intravascular flow (i.e., transit time) can be measured with the rapid sampling of digital fluoroscopic systems and fast x-ray computed tomography.[2,29]

The use of monoenergetic sources for angiography has been limited because of the low intensity available from radionuclide and

x-ray fluorescence sources. An exception is the intense synchrotron radiation produced by the electron storage rings at the Stanford linear accelerator. High intensity and good spatial coherence allow this source to be monochromatized by Braff diffraction and made available as tunable energy beams.[39] This approach is restricted to a single facility, but the potential is great for studying brain vasculature and perhaps the coronary vessels after an intravenous injection of contrast material.

X-RAY COMPUTED TOMOGRAPHY

Robb has recently reviewed the history and development of x-ray computed tomography (CT).[30] Various generations of CT machines are depicted in Figure 1. The basic biologic characteristic measured is the linear attenuation coefficient for x-ray photons of 70-140 keV. The spatial distribution of these coefficients changes with small changes in the specific atomic density of carbon, phosphorus, and calcium relative to that of hydrogen and oxygen; that relation allows x-ray CT to image the distribution of fat, muscle, white brain matter, gray brain matter, fluids, lung, and other tissues.

Permeability changes are also measurable by x-ray CT. For example, disruption of the blood-brain barrier is demonstrated by the accumulation of contrast material in brain x-ray CT. Conversely, when flow to some portion of the organ is abnormally low, the "contrast-enhanced" attenuation-coefficient distribution will reveal the areas of relatively low perfusion.

X-ray CT that uses multienergy photon sources for tissue-element characterization[22,25,31] can improve detection of tissue composition, but high-resolution, multienergy systems are not generally available. A limitation of the technique is the low intensity of nonenergetic sources, with the exception of the Stanford synchrotron radiation.[39] Energy-selective digital radiography involves the use of a modified CT scanner to provide scanned projection radiographs at two energies, so that a subtraction image may be formed with various weightings to permit separate displays of tissue-like or bone-like substances.[25,31]

Rapid scanners--such as the Mayo Clinic dynamic spatial reconstructor (DSR)[29] and the University of California, San Francisco cardiovascular computed tomograph (CVCT) system[2]--can acquire complete three-dimensional data in less than 100 ms with a full-width half-maximum (FWHM) resolution of 1-2 mm. These devices can also combine the signal-to-noise ratio improvements afforded by subtraction of background-tissue attenuation coefficients from sequential images after injection of contrast material--three-dimensional DSA.

NUCLEAR MAGNETIC RESONANCE

Various modes of noninvasive nuclear magnetic resonance (NMR) are shown in Figure 1. NMR measures the following physical characteristics:

- Concentrations of such nuclei as hydrogen, carbon, sodium, fluorine, phosphorus, and other elements with appropriate nuclear characteristics.

- T_1 relaxation time.

- T_2 relaxation time.

- Chemical shift--a small change in resonant frequency associated with the electronically induced magnetic-field perturbation due to the chemical bonds near the nuclei of interest.

The theory of NMR was discussed by Farrar and Becker,[13] and recent comprehensive discussions of NMR applications are found in Kaufman et al.,[18] Witcofski et al.,[38] Brownell et al.,[4] Mansfield and Morris,[23] Partain et al.,[27] and Margulis et al.[24] Most elements have at least one reasonably abundant isotope whose nucleus is magnetic. In an external magnetic field, such a nucleus (which can be thought of as a small magnet) can assume a low-energy state when aligned with the field or a higher-energy state when aligned against the field. A weak but rapidly alternating magnetic field of appropriate frequency applied by a coil near the subject or specimen stimulates changes in the orientation of the nucleus relative to the direction of the strong static magnetic field. This results in absorption of energy, which is emitted when the nucleus returns to the equilibrium state. The absorption and emission of energy take place at the resonance frequency, ν, given by the formula $\gamma H/2\pi$, where γ is the gyromagnetic ratio characteristic of the nuclear species and H is the static magnetic field. The nuclei of different elements, and even of different isotopes of the same element, have widely differing frequencies. For a field of 0.1 tesla (1,000 gauss), the resonance frequency of hydrogen is 4.2 MHz and that of phosphorus is 1.7 MHz.

Electrons in the molecule containing the nucleus cause small differences in the resonance frequencies. NMR spectroscopy identifies these frequencies and thus gives information on molecular identity and structure.

The time variation of the NMR signal gives two other dimensions of biologic importance: the spin-lattice relaxation time, T_1, and the spin-spin relaxation time, T_2. These depend on the motions of

the nuclei, the regional temperature, tissue viscosity, and the magnetic effects of nearby nuclei. The relaxation times of hydrogen nuclei in tissue give information on local tissue conditions and are usually prolonged when tissues are diseased.

Phosphorus chemical-state analysis has emerged as an important medical application of NMR. NMR spectroscopy can be used in vivo to measure intracellular pH and the relative concentrations of phosphocreatine, ATP, and inorganic phosphate in intact animals and humans for the investigation of oxidative phosphorylation in large tissue volumes.

Spatial information can be obtained by imposing a slight gradient on the static magnetic field. Because the resonance frequency of the signal from the nuclei is proportional to the field, it is possible to derive the position of the nuclei by imposing gradients in different directions. Three-dimensional reconstruction can be performed with algorithms similar to those for x-ray CT, but the methods used most commonly involve two- and three-dimensional Fourier transformation of signals wherein the spatial information is encoded as a frequency shift and phase change.

NMR techniques for acquring information do not have equal sensitivity for all elements; that is, NMR cannot image with the same high spatial resolution the state of phosphorus or carbon bonds or the tissue concentration of ^{23}Na or ^{31}P as well as it can measure the concentration of protons or proton T_1 relaxation. This is because of the inherent difference in sensitivity of NMR for different elements and the very low concentrations of the elements of interest relative to the concentration of protons in tissue (Table 2). For example, the concentration of hydrogen in tissue is approximately 90 mmol/g; however, ^{23}Na concentration in blood and extracellular fluid is 140 μmol/g, and ATP phosphorus concentration in brain is only a few micromoles per gram.

EMISSION TOMOGRAPHY

The unique attribute of emission imaging is the ability to measure organ function and related biochemical processes, such as iodine metabolism of the thyroid, glucose metabolism of the brain and heart, and cation trapping by the myocardium and kidney.[28,32] The quantity actually measured is the regional photon flux from the administered radiopharmaceuticals. Ter-Pogossian *et al.*,[35] Budinger,[5] and Hoffman[16] have recently discussed instrument alternatives (Figure 3). New developments are taking place in positron time-of-flight instrumentation and specialized single-photon tomography instruments.

TABLE 2

NMR Detection Sensitivity

Element	Relative Sensitivity at 0.1 T	Tissue Concentration, mmol/g	Detection Sensitivity
^{1}H	1.0	90[a]	1
^{19}F	0.83	2.6[b]	2.7×10^{-2}
^{23}Na	0.09	0.14[c]	1.4×10^{-4}
^{31}P	0.07	0.002[d]	1.6×10^{6}

[a] Hydrogen from 80% water in tissues.
[b] Blood concentration after injection of 500 cm^3 of fluorocarbon.
[c] Blood and extracellular fluid.
[d] Concentration of each P of ATP.

X-ray transmission tomography and emission tomography differ physically and biologically. In emission tomography, the information sought is the location of the source and the intensity of the gamma radiation emitted by the isotope; in x-ray transmission tomography, the spatial distribution of the tissue densities or attenuation coefficients is sought. A consequence of this difference is the need in emission tomography to compensate for the effect of attenuation. This compensation is achieved by incorporation of the attenuation coefficients in the image-reconstruction methods.[6] Emission tomography measures regional function (Table 1), whereas x-ray CT describes regional structure or anatomy.

Single-photon tomography preceded x-ray CT and provided the first demonstration of quantitative physiologic studies.[20] Single-photon tomography has recently been shown to be a practical clinical tool for the measurement of cerebral blood volume and regional cerebral blood flow.[1,15,19,21]

An advantage of positron emission tomography (PET) over single-photon tomography is its much greater efficiency or sensitivity for quantitating radiopharmaceuticals, because the single-photon technique leads to the loss of many available photons

through physical collimation. The ability to label compounds with positron-emitting isotopes of carbon, nitrogen, oxygen, and fluorine is a major basis for great expectations from PET. The potentials and limitations for use of PET for the quantitation of specific receptor sites has been reviewed recently.[11] To produce radiopharmaceuticals containing these radionuclides, it is necessary to use a cyclotron or, for some positron emitters, a portable generator. Developments in PET might be accelerated if it were more widely recognized that some useful positron emitters (Table 3) can be obtained without a cyclotron. In contrast, single-photon emitters, such as ^{99m}Tc and ^{123}I, can be obtained from noncyclotron or remote sources, and they are easier to use in chemical syntheses because of their longer half-lives.

TABLE 3

Positron Emitters from Generators

Isotope	Half-Life	Positrons	Gammas	Parent
^{52m}Mn	21 min	1.63 MeV (92%)	1.43 MeV (100%)	8.2-h ^{52}Fe
^{62}Cu	9.8 min	3 MeV (99%)	1.17 MeV (0.5%)	9.3 h ^{62}Zn
^{68}Ga	68 min	1.9 MeV (89%)	1.08 MeV (3%)	275-d ^{68}Ge
^{82}Rb	75 sec	3.2 MeV (83%)	0.78 MeV (9%)	25-d ^{82}Sr
^{122}I	3.5 min	3 MeV (100%)	0.56 MeV (10%)	20-h ^{122}Xe
^{128}Cs	3.8 min	2.9 MeV (49%)	0.44 MeV (27%)	2.4-d ^{128}Ba

Emission tomography's major limitations are poor resolution for anatomic description and poor statistics (Poisson) relative to x-ray CT and DSA, which yield about 1,000 times more data. Emission tomography is more sensitive than x-ray CT or NMR for measuring permeability changes, tissue perfusion, and the metabolism of many substrates.

ULTRASONOGRAPHY

Ultrasound measures the anatomic position and motion of surfaces. The two basic physical characteristics measured by ultrasound are tissue acoustic-impedance differences and sound-frequency shift due to motion. In addition, with CT for multiple angle transmission, one can use ultrasound to describe the spatial distribution of attenuation coefficients and ultrasound velocity (Figure 4). Three-dimensional

information is readily obtained with ultrasound, because the information is reflected from known depths.

The physical attributes of ultrasound give it a high potential for evaluation of the motion of heart valves and the ventricle walls; but, when attenuation and acoustic-impedance mismatches are great, as at air-tissue or bone-tissue surfaces encountered in imaging of the brain and thorax, ultrasound methods are not optimal. One of the practical applications of this low-cost technology is the measurement of heart ejection fraction and ventricular dimensions. The sensitivity of ultrasound to tissue characteristics makes it an ideal tool for detection of abdominal disease (such as gallbladder stones), fetal status, and cerebral structural anomalies in infants (through transfontanel ultrasonography). New developments in transmission ultrasound CT have potential in specialized applications to breast imaging[14] and perhaps to arterial tissue characterization. NMR can compete with some of these applications of ultrasound. In particular, NMR has a role in the examination of neonates and characterization of the tissue constituents of atherosclerotic plaques.

One of the strongest practical applications of ultrasound is in vessel flow measurement. Ultrasound techniques for flow measurement are CW Doppler and range-gated Doppler imaging methods.[33] These have their greatest application in the evaluation of carotid arterial disease. Previous limitations of this technique were related to low signal-to-noise characteristics of early instruments; the existence of an atheromatous plaque caused a prohibitive signal loss. Pulse Doppler techniques could not detect some instances of high velocity, e.g., in the range of 600 cm/s. Recent transducer and display developments have largely overcome this problem. DSA competes with this application of ultrasound.

ACCELERATED HEAVY-PARTICLE IMAGING

Heavy-ion imaging[10,36] involves the measurement of electron density with cyclotron-produced charged particles (Figure 5). Resolution is approximately 2 mm (FWHM) for objects the size of the head or larger. Multiple scattering is an important problem in particle imaging and is the reason for the limitation of the use of neutron radiography to thin objects.[7] The absorbed dose in accelerated ion imaging is lower than that in x-ray CT, but, because the contrast information from differences in density is less than the contrast information from differences in attenuation coefficients, this modality appears to be appropriate for heavy-ion radiotherapy planning. Another application of heavy ions is for injection of positron emitters.[9] The ions can be injected at precise locations to assist in treatment planning and to study the physiology of diffusion and flow.

INSTRUMENTATION DESIGN CRITERIA FOR SPECIFIC MEDICAL OBJECTIVES

The decision as to which instrument to use or what improvements to make in an existing instrument can be approached by considering this question: What pathophysiologic process is likely to be most basic to the disease process under investigation? Another way to approach the decision is to ask whether the instrument we select can measure the physical and chemical changes that are most closely correlated with the disease process of interest. For example, if it is suspected that amino acid transport into the brain is the key defect leading to some disorder, then it is far more appropriate to design an instrument to measure amino acid transport kinetics than to design a method for testing the I.Q. of the subject under various environments and dietary conditions. A second example is the problem of differential diagnosis of pulmonary infarction from chronic obstructive pulmonary disease. The diagnosis could be improved by a method that measures blood flow in three dimensions; with this focus on blood flow, the investigator might learn that NMR flow imaging and dynamic x-ray CT are two attractive yet essentially unexplored methods of evaluating pulmonary disease.

Once given the medical question and a selection of imaging techniques that can answer the question, it is helpful to have some guidelines for the selection of one of the competing instruments. Table 4 lists 12 factors to consider in characterizing diagnostic imaging instruments. Most are self-explanatory, but some deserve clarification and emphasis.

TABLE 4

Factors in Characterization of Diagnostic Imaging Instruments

Sensitivity and uniformity of sensitivity
Noise or signal-to-noise ratio at given resolution and imaging time
Dynamic range
Speed (electronic and practical imaging)
Spatial resolution (planar and depth)
Data-handling capabilities
Organ-selection flexibility (part-body vs. whole-body imaging)
Ease of operation
Patient risks
Accuracy of diagnosis (false-positive vs. false-negative)
Long-range effectiveness of use in medical care
Cost

Sensitivity is a measure of how well an instrument can detect the entity being measured. Some factors that improve sensitivity are increased solid angle and increased detector efficiency. A unit of

sensitivity can be the number of usable photons per dose to the patient or, in the case of NMR imaging, the signal strength per unit of concentration of the nuclei of interest. If the uniformity of sensitivity changes over the imaging field, this needs to be characterized as well. Noise is the false signal that can enter the system. This noise can be a superimposed signal, which is removed by CT, or statistical fluctuations in the signal or receiver, which are removed by increasing the data acquisition or lowering the detector noise.

Uniformity of resolution and sensitivity are of paramount importance in NMR imaging and NMR in vivo spectroscopy, as well as in positron tomography and ultrasonography. We often neglect to give estimates of the uniformity of resolution and of sensitivity. For example, variation in spatial resolution is particularly important in the characterization of ultrasound imaging equipment.

One of the most helpful tools for evaluation of instrument performance is the contrast-detail diagram. Theoretically, for an ideal system with only Poisson noise, one expects the product of contrast and resolution to be a constant. This conclusion arises from the Rose equation:

$$c^2d^2 = K^2/N_T,$$

where c, the contrast, is defined as the difference between target signal and background signal divided by background signal; d is the resolution of the object to be detected; K is the significance of the difference (Rose factor); and N_T is the total events in the image. For CT, this can be modified to:

$$c^2d^3 = A^{3/2}K^2/N_T,$$

where A is the area of the image.

A contrast-detail diagram for various competing techniques will not follow the models plotted in Figure 6 if the noise or contrast extraction mechanism differs from technique to technique. The curves are normalized around C = 0.1 and d = 1 mm. A contrast-detail diagram for a particular instrument can be misleading, because it does not give the true system resolution, which is classically defined as the shortest distance at which two sources can be detected as separate entities. Single objects much smaller than the resolution of the system usually can be detected, and a contrast-detail chart alone is not adequate for specification of contrast resolution.

The contemporary viewpoint is that for x-ray or emission CT, resolution necessitates an eightfold increase in signal or patient

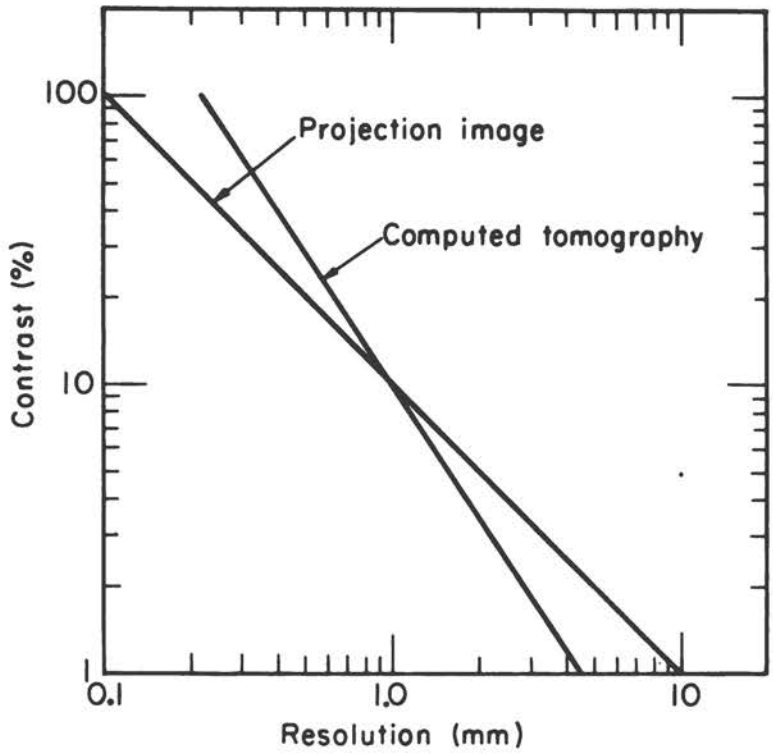

FIGURE 6 Contrast-detail behavior of projection imaging system vs. computed tomography system. Lateral shift of curves depends on point of normalization, which was arbitrarily selected here and depends on dose.

dose for a twofold improvement in linear resolution--that is, halving the linear resolution (making it twice as good) requires an eightfold dose increase. That is valid if the objective is to have the same precision per high-resolution pixel as for the low-resolution pixel. However, this relation should not hinder progress toward improvement in resolution--for two reasons. First, a measurement by a system whose resolution is approximately the same as the object to be measured will be in error by approximately a factor of 2 if the resolution is defined as the full width at half the maximum of the impulse response. The root-mean-square uncertainty of the computed quantity for a high-resolution element will be greater than that of the coarser-resolution pixel from a low-resolution system. However, the accuracy will be closer to the actual value for a given amount of data in the high-resolution system than in the low-resolution system, because the signal being detected by the low-resolution system is spread into the areas of the image adjacent to the signal itself as a result of the blurring inherent in the low-resolution

system (Figure 7). Thus, independently of statistics, one can argue strongly for improving the resolution of data acquisition.

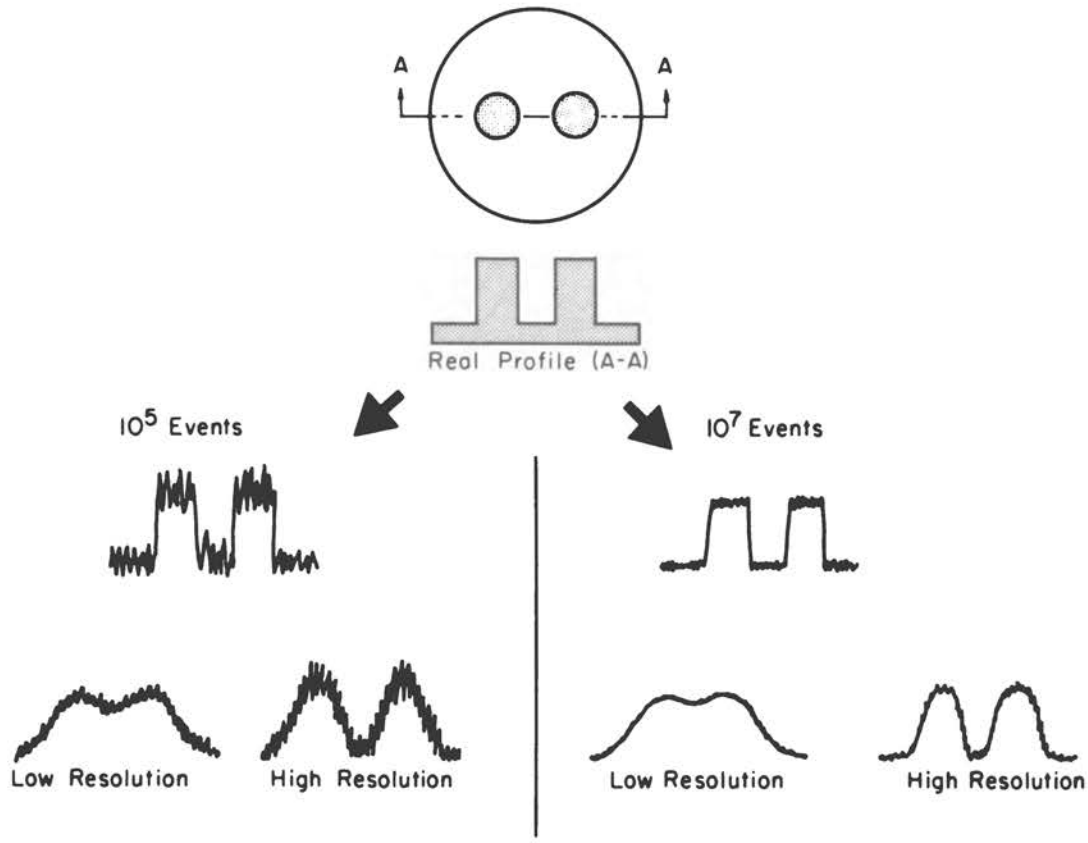

FIGURE 7 Resolution is important for quantitative imaging independently of statistics.

A second important reason for improving the sampling resolution of data acquisition is the desirability of avoiding problems associated with aliasing. Aliasing is the artifact-producing phenomenon that occurs when the data sampling is coarse relative to the fineness of details in the object being imaged. In many contemporary noninvasive imaging methods, sampling is not angularly uniform. That is true for fan-beam systems in which the angular sampling is not complete around 360°, limited-angle angular range sampling, fixed-ring positron detector systems, and B-mode acoustic imaging systems.

Technical improvements in noninvasive medical imaging can be cataloged and evaluated in two broad categories. The first is that of research medicine and physiology. Here one seeks an instrument that will answer basic questions, and instrument development is often motivated purely by a desire to improve sensitivity or accuracy in some measurement. This motivation is not easily supported by research and development funding. However, improved sensitivity and resolution have permitted great discoveries--for example, the compound microscope, the electron microscope, high-resolution x-ray CT, and NMR imaging. Unfortunately, the line between pure research and practical, clinical, diagnostic medicine is commonly left very fuzzy by those who, perhaps unknowingly, exploit a development more than the available facts warrant. The second broad category is that of routine clinical diagnosis. In contrast with research instruments, clinical instruments must undergo tests of diagnostic accuracy, and their evaluation includes elements of medical efficacy, risk, and cost.[12,37]

ACKNOWLEDGMENTS

This work was supported by the Director, Office of Energy Research, Office of Basic Energy Sciences, Biology and Medicine Division, U.S. Department of Energy, under Contract DE-AC03-76SF00098 and by the National Heart, Lung, and Blood Institute, National Institutes of Health, under Grant PO1 HL25840-02.

REFERENCES

1. Bonte, F. J., and E. M. Stokely. Single-photon tomographic study of regional cerebral blood flow after stroke: Concise communication. J. Nucl. Med. 22:1049-1053, 1981.

2. Boyd, D. P., J. L. Couch, S. A. Napel, D. L. Parker, K. R. Peschmann, R. E. Rand, and B. Herrmannsfeldt. High-speed, multi-slice, x-ray computed tomography, pp. 139-150. In International Workshop on Physics and Engineering in Medical Imaging, Asilomar, California, March 15-18, 1982. New York: IEEE, 1982.

3. Brody, W. R., Ed. Conference on Digital Radiography. Proc. Soc. Photo. Opt. Instrum. Eng., Vol. 314, 1981.

4. Brownell, G. L., T. F. Budinger, P. C. Lauterbur, and P. L. McGeer. Positron tomography and nuclear magnetic resonance imaging. Science 215:619-626, 1982.

5. Budinger, T. F. Revival of clinical nuclear medicine brain imaging. J. Nucl. Med. 22:1094-1097, 1981.

6. Budinger, T. F., G. T. Gullberg, and R. H. Huesman. Emission computed tomography, pp. 147-246. In G. T. Herman, Ed. Image Reconstruction from Projections: Implementation and Applications (Topics in Applied Physics, Vol. 32). New York: Springer-Verlag, 1979.

7. Budinger, T. F., R. J. Howerton, and E. F. Plechaty. Neutron radiography and dosimetry in human beings: Theoretical studies. Phys. Med. Biol. 16:439-450, 1971.

8. Capp, M. P. Radiological imaging--2000 A. D. Radiology 138:541-550, 1981.

9. Chatterjee, A., E. L. Alpen, C. A. Tobias, J. Llacer, and J. Alonso. High energy beams of radioactive nuclei and their biomedical applications. Int. J. Radiat. Oncol. Biol. Phys. 7:503-508, 1981.

10. Crowe, K. M., T. F. Budinger, J. L. Cahoon, V. P. Elischer, R. H. Huesman, and L. L. Kanstein. Axial scanning with 900 MeV alpha particles. IEEE Trans Nucl. Sci. NS-22:1752-1754, 1975.

11. Eckelman, W. C., Ed. Receptor-Binding Radiotracers. 2 vols. Boca Raton, Fla.: CRC Press, Inc., 1982.

12. Evens, R. G. The economics of computed tomography: Comparison with other health care costs. Radiology 136:509-510, 1980.

13. Farrar, T. C., and E. D. Becker. Pulse and Fourier Transform NMR: Introduction to Theory and Methods. New York: Academic Press, 1971. 118 pp.

14. Greenleaf, J. F., and R. C. Bahn. Clinical imaging with transmissive ultrasonic computerized tomography. IEEE Trans. Biomed. Eng. 28:177-185, 1981.

15. Hill, T. C., B. L. Holman, R. Lovett, D. H. O'Leary, D. Front, P. Magistretti, R. E. Zimmerman, S. Moore, M. E. Clouse, J. L. Wu, T. H. Lin, and R. M. Baldwin. Initial experience with SPECT (single-photon computerized tomography) of the brain using N-isopropyl I-123 p-iodoamphetamine: Concise communication. J. Nucl. Med. 23:191-195, 1982.

16. Hoffman, E. J. Instrumentation for quantitative tomographic determination of concentrations of positron-emitting receptor-binding radiotracers, pp. 141-173. In W. C. Eckelman, Ed. Receptor Binding Radiotracers. Vol. II. Boca Raton, Fla.: CRC Press, 1982.

17. Hubener, K.-H. Digital radiography using a computed tomography instrument. Front. in Eur. Radiol. 1:125-170, 1982.

18. Kaufman, L., L. E. Crooks, and A. R. Margulis, Eds. Nuclear Magnetic Resonance Imaging in Medicine. New York: Igaku-Shoin, 1981. 242 pp.

19. Kuhl, D. E., J. R. Barrio, S. C. Huang, C. Selin, R. F. Ackermann, J. L. Lear, J. L. Wu, T. H. Lin, and M. E. Phelps. Quantifying local cerebral blood flow by N-isopropyl-p-[^{123}I]-iodoamphetamine (IMP) tomography. J. Nucl. Med. 23:196-203, 1982.

20. Kuhl, D. E., R. Q. Edwards, A. R. Ricci, R. J. Yacob, T. J. Mich, and A. Alavi. The MARK IV system for radionuclide computed tomography of the brain. Radiology 121:405-413, 1976.

21. Lassen, N. A., C. Henriksen, and O. Paulson. Regional cerebral blood flow in stroke by 133-xenon inhalation and emission tomography. Stroke 12:284-288, 1981.

22. Macovski, A., R. E. Alvarez, and L. A. Lehmann. Iodine imaging using three energy spectra. Proc. Soc. Photo. Opt. Instrum. Eng. 314:140-142, 1981.

23. Mansfield, P., and P. G. Morris. NMR Imaging in Biomedicine. Advances in Magnetic Resonance, Suppl. 2. New York: Academic Press, 1982. 354 pp.

24. Margulis, A. R., C. B. Higgins, L. Kaufman, and L. E. Crooks, Eds. Clinical Magnetic Resonance Imaging. San Francisco: Radiology Research and Education Foundation, 1983. 328 pp.

25. Marshall, W. H., Jr., R. Alvarez, A. Macovski, J. Healy, and L. M. Zatz. Dual kilovoltage at computed tomography: A prereconstruction method for estimation of effective atomic number and electron density. Neuroradiology 16:605-606, 1978.

26. Mistretta, C. A., A. B. Crummy, and C. M. Strother. Digital angiography: A perspective. Radiology 139:273-276, 1981.

27. Partain, C. L., A. E. James, Jr., F. D. Rollo, and R. R. Price, Eds. Nuclear Magnetic Resonance (NMR) Imaging. Philadelphia: W. B. Saunders Company, 1983. 552 pp.

28. Phelps, M. E., D. E. Kuhl, and J. C. Mazziotta. Metabolic mapping of the brain's response to visual stimulation: Studies in humans. Science 211:1445-1448, 1981.

29. Ritman, E. L., J. H. Kinsey, R. A. Robb, B. K. Gilbert, L. D. Harris, and E. H. Wood. Three-dimensional imaging of heart, lungs, and circulation. Science 210:273-280, 1980.

30. Robb, R. A. X-ray computed tomography: An engineering synthesis of multiscientific principles. Crit. Rev. Biomed. Eng. 7:265-333, 1982.

31. Rutt, B., and A. Fenster. Split-filter computed tomography: A simple technique for dual energy scanning. J. Comput. Assist. Tomogr. 4:501-509, 1980.

32. Schelbert, H. R., E. Henze, and M. E. Phelps. Emission tomography of the heart. Semin. Nucl. Med. 10:355-373, 1980.

33. Spencer, M. P., and J. M. Reid. Cerebrovascular Evaluation with Doppler Ultrasound. The Hague: Martinus Nujhoff, 1981. 245 pp.

34. Stein, J. A. X-ray imaging with a scanning beam. Radiology 117:713-716, 1975.

35. Ter-Pogossian, M. M., N. A. Mullani, D. C. Ficke, J. Markham, and D. L. Snyder. Photon time-of-flight-assisted positron emission tomography. J. Comput. Assist. Tomogr. 5:227-239, 1981.

36. Tobias, C. A., E. V. Benton, and M. P. Capp. Heavy ion radiography, pp. 71-102. In J. H. Lawrence and T. F. Budinger, Eds. Recent Advances in Nuclear Medicine. Vol. 5. New York: Grune and Stratton, 1978.

37. Wagner, R. F., D. G. Brown, and M. S. Pastel. Application of information theory to the assessment of computed tomography. Med. Phys. 6:83-94, 1979.

38. Witcofski, R. L., N. Karstaedt, and C. L. Partain, Eds. Nuclear Magnetic Resonance Imaging: Proceedings of an International Symposium on Nuclear Magnetic Resonance Imaging, Bowman Gray School of Medicine of Wake Forest Univ., Winston-Salem, N.C., 1981. Winston-Salem, N.C.: Bowman Gray School of Medicine of Wake Forest University, 1982. 201 pp.

39. Zeman, H.D., E. B. Hughes, L. E. Campbell, R. Hofstadter, R. L. Kirk, T. J. Krolicki, J. Rolfe, J. P. Stone, S. Wilson, E. Rubenstein, A. C. Thompson, and J. T. Walton. Implementation of digital subtraction angiography with a synchrotron x-ray beam. IEEE Trans. Nucl. Sci. NS-29:442-446, 1982.

THE ROLE OF IMAGING IN HEALTH CARE—A LOOK AT THE FUTURE

P. L. McGEER
Kinsmen Laboratory of Neurological Research
University of British Columbia

INTRODUCTION

The newer biological imaging techniques have proved themselves to be valuable research tools. Many centers in North America and Europe are now developing capabilities in one or more of these modern modalities. Because nuclear magnetic resonance (NMR) and positron emission tomography (PET) are now being emphasized, discussion will focus on them. Their place in diagnostic medicine is still to be determined. Much will depend on the cost-benefit ratio associated with their use, although at this stage only the cost can be reasonably estimated. It must be remembered that NMR and PET are complementary and not competitive. NMR provides largely anatomic information. Important chemical information may ultimately be derived, but it will be limited. PET produces only regional chemical information. The resolution is not adequate for precise anatomy, so it must be used in conjunction with computer-assisted tomography (CAT) or NMR scanning.

ESTIMATED COSTS OF NMR AND PET SCANS

One can already anticipate that an NMR scan will be substantially, but not prohibitively, more expensive than its diagnostic rival, the CAT scan. The requirement for magnets of high and uniform field strength will inevitably make NMR instruments more costly than CAT scanners by a factor of 2 or more. Most NMR instruments today cost some $1-2 million when installed. The length of time to complete an NMR scan will be longer, although the amount of information that can be extracted will be higher. According to our experience at the University of British Columbia Health Sciences Center, the personnel requirements will be comparable. If efficient procedures can be developed for handling large numbers of patients, the cost of an NMR examination might be brought into $100-200

range--about twice that of a CAT scan, although the current cost is much higher.

The instrumentation and personnel required for PET are considerably more sophisticated and expensive. First, a cyclotron either totally or partially dedicated to PET use must be available. The cost of an installed cyclotron is in the millions of dollars and depends on size. The cost of a tomographic machine will approach that of a CAT scanner. Far more people are required to carry out PET investigations than NMR scans, because radiopharmaceuticals for imaging must be synthesized de novo close to the time of use. The time for scanning is considerably longer with PET than with NMR or CAT, so the number of patients that can be accommodated might be only one-tenth as high. It can be anticipated that the cost of a PET scan will be at least 10 times as high as that of an NMR scan--probably around $1,000-2,000. Actual costs today are considerably higher.

PROJECTED BENEFITS OF SCANNING INFORMATION

With the costs now and in the future known to be high, it is appropriate to consider the benefits of the information that may be obtained. It is clear from current commercial vigor that many firms in the hospital equipment field already consider proton NMR tomography to be superior to CAT scanning for routine imaging, especially of the brain. Resolution is now comparable, and the contrast produced by differing proton relaxation times in various tissues is greater than that produced by density differences in CAT scanning.

By varying the NMR pulse through such sequences as inversion recovery, spin echo, and spin saturation, one can improve particular tissue contrasts. Even greater possibilities for improving contrast might be developed through digital subtraction NMR with many of the reconstruction techniques of digital subtraction angiography as described by Mistretta (elsewhere in this volume). Contrast material would not need to be injected, however, because the differing relaxation times of the protons themselves in some molecular states would provide the contrast. A variation of this method has been used to produce blood-flow data,[17,24] as also described by Mansfield (elsewhere in this volume); contrast is provided by the low signal from blood as it moves through a particular slice being rapidly and repetitively sequenced. However, no matter how excellent the contrast produced by present or future techniques, the information from proton NMR tomography contains no chemical coding and is therefore qualitatively similar to that from CAT scanning.

A number of possibilities for obtaining substantial chemical information from NMR are being vigorously pursued. Nevertheless, the limitations need to be clearly understood for one to appreciate why NMR is not competitive with PET in chemical imaging. At any given time, only a tiny fraction of the nuclei capable of responding to a resonance pulse are excited. The equilibrium ratio is expressed by the following equation:

$$N(up)/N(down) = e^{-(\mu H/kT)},$$

where N is the number of molecules, μ is the magnetic moment, H is the field strength, k is the Boltzmann constant, and T is the absolute temperature.

For protons in a field of 3.5 kilogauss, the net magnetization is equivalent to 1.4 protons per million aligning against the field.[3] In addition to this relatively small fraction of atoms that produce the NMR signal, there is substantial absorption of signal in tissue and other losses in detection. In practical terms, this means that low sensitivity will limit the repertoire of nuclei that can be imaged in living tissue. Some indication of this is given in Table 1, where an imaging index is calculated for a number of nuclei. This value is the machine-independent factor that governs the strength of the signal. It consists of the product of the relative strength of the isotope magnetic moment (compared with a hydrogen standard), the abundance of the isotope in nature, and its concentration in tissue. For atoms that are not normally present in tissue, the table indicates the concentration that would be needed for a signal to be detected.

The table shows that the possibilities for detection of isotopes beyond hydrogen are extremely limited. The most promising material is phosphorus, but its signal strength is reduced (relative to that of hydrogen) by a factor of more than 10,000. Volume imaging of various phosphorus compounds has been achieved in vivo,[2,10] and early tomography results have suggested that superior instruments will eventually make phosphorus tomography in humans a reality.[12] Other possibilities for the foreseeable future will require an imaging index at least one-tenth that of ^{31}P. That would include ^{23}Na and ^{13}C.[13,16] Deuterium and ^{19}F compounds could be administered in a high enough concentration to be detected. To avoid toxicity, ^{19}F would need to be used in a nonionized form. This has been done with ^{19}F gases for lung imaging as described by Rinck *et al.*[23] and Lauterbur (at this conference). Detection of ^{7}Li ions would require nearly toxic concentrations. Nitrogen gives too broad a signal to be detected, despite its apparently satisfactory concentration in tissue.

Although the repertoire shown in Table 1 is thin, it contains material for important physiologic exploitation. That such exploitation is being actively pursued is indicated by the presentation of over 200 papers at the second annual meeting of the Society of Magnetic Resonance in Medicine in San Francisco during 1983. Several papers dealt with what may be described as four-dimensional NMR--the three spatial dimensions of tomography plus the chemical shift associated with a particular molecular form of the isotope being imaged. Hydrogen and ^{31}P are the promising candidates for such spectroscopy. Magnets with intensity at least 10 times greater than those currently in use for human proton NMR tomography will be necessary, thus restricting applications to the realm of research for some years to come. However, early indications are that extremely useful biochemical information may be obtainable from four-dimensional NMR. For example, the ability to image spatially such essential molecules as creatine phosphate and ATP may be invaluable in assessing a variety of diseases. The only application so far has been in a rare and peculiar disorder known as McArdle's disease,[22] but applications can easily be visualized for many common conditions, such as stroke, myocardial infarction, and other ischemic and metabolic disorders.

In summary, it can be stated that proton NMR has already reached the status whereby it can be introduced into routine diagnostic medicine and produce returns superior to those of existing techniques with respect to cost-benefit ratio. Other applications of NMR are still speculative, but it can be anticipated that four-dimensional NMR imaging will enter diagnostic service in a few years and provide even more sophisticated methods for the practitioner's armamentarium.

PET will remain a research tool for some time to come. Nonetheless, it is important to appreciate that the data that will accumulate are entirely outside the domain of any other technique. The reasons for this are shown in Table 2, which also indicates why a correlative technique, such as CAT or NMR scanning, must be used in conjunction with PET. The resolution of PET will always be poor, owing to the distance traveled through tissue by emitted positrons before electron-positron annihilation. However, its sensitivity is far higher than that of NMR. This potentially high sensitivity has not yet been fully exploited, but it will permit in vivo imaging of compounds at extremely low concentrations. In brain, compounds of particular physiologic interest occur at three different concentrations, in increments of about 1,000. As illustrated in Table 3, the greatest abundance is associated with energy metabolism. All cells have a comparable spectrum of energy intermediates, because all cells use the same metabolic cycles to burn oxygen and glucose. These intermediates occur at 10^{-6}-10^{-5} mol/g of tissue. The next category is represented by some neurotransmitter compounds--

TABLE 1

NMR Imaging Index

Isotope	Sensitivity	Abundance	Concentration, atoms/g of tissue x 10^{20}	Imaging Index
^{1}H	1	100	460	46,000
^{31}P	0.066	100	0.60	3.96
^{23}Na	0.09	100	0.42	3.78
^{14}N	0.001	100	6.00	0.60
^{13}C	0.016	1	24.0	0.38
$^{35}Cl + ^{37}Cl$	0.004	100	0.30	0.12
^{2}H	0.01	100	4.00[a]	
^{19}F	0.83	100	0.05[a]	
^{7}Li	0.29	100	0.14[a]	

[a] Not normally present in tissue; concentration required to achieve an imaging index of 4.

the specialty chemical messengers that belong only to particular classes of neurons. Their concentration is high for the neurons that use them, but they are absent from neurons of other specialties. A storage mechanism for transmitters exists in which most of the material is held. Only a small fraction is released on neuronal stimulation. The concentration of the amine neurotransmitters, such as acetylcholine or dopamine, is 10^{-9}-10^{-8} mol/g of tissue. The final category is represented by the neurotransmitter receptor sites on postsynaptic neurons. The receptors respond only to the small fraction of transmitter released in any given stimulation, so their concentration is in the range of 10^{-13}-10^{-11} mol/g of tissue.

TABLE 2

Sensitivity and Resolution of NMR and PET

Technique	Resolution, mm^3		Approximate Sensitivity Limits, units/g of tissue x 10^{20}
	Present	Estimated Achievable	
NMR	40	1	4
PET	500	64	10^{-12}

TABLE 3

Concentrations of Some Brain Materials and Specific Activities Required of Imaging Ligands

	Tissue Concentration, mol/g	Specific Activity, mCi/mmol
Energy intermediates	10^{-6}-10^{-5}	10^{-1}-1
Amine neurotransmitters	10^{-9}-10^{-8}	10^{2}-10^{3}
Receptors	10^{-13}-10^{-11}	10^{5}-10^{7}

It is practical for PET to image at all three concentration ranges because of its extraordinary sensitivity, which is due to the high energy of photons generated by the positron-electron annihilation and the short half-lives of the isotopes used. For any parenterally administered, positron-containing radiopharmaceutical, a substantial percentage of the total activity reaching the tissue can be imaged. Because creation of a PET image requires detection of emitted photons corresponding to concentrations of about 0.1-1 μCi/g of tissue, the required specific activity of radiopharmaceuticals must be sufficient to achieve such concentrations in vivo. This requires an increase in specific activity of approximately 10^3 for each category of metabolite in Table 3. The table shows that for intermediary metabolites specific activities of millicuries per millimole are necessary. For neurotransmitters the specific activities increase to the curies-per-millimole range, and for receptors to the curies-per-micromole range.

So far, most of the applications of PET scanning have used energy intermediates, particularly molecular oxygen[8,21] and fluorodeoxyglucose (FDG).[8] The objective has been to look at vascular blood flow,[1] tissue perfusion,[18] and regional metabolic rate.[8] This information has proved extremely valuable in revealing lesions caused either by vascular insufficiency or by metabolic or degenerative disorders. Valuable and unexpected information has appeared in such conditions as Huntington's disease,[15] Alzheimer's disease,[9] and epilepsy,[7] as well as tumor and stroke. In all these, important lesions can be detected after death, so the in vivo imaging gives merely an advance indication of anticipated pathologic findings.

The most revealing information from PET, however, stems from studies correlating regional FDG metabolism with cortical activation caused by sensory stimulation designed to activate the visual, auditory, or other functional area of the cortex.[19] The ability to elicit such information offers great promise not only for understanding more about brain activity, but also for probing regions of brain affected by mental and other illnesses that leave no pathologic trace after death. No other technique holds out promise for such in vivo correlations of brain activity with serious disorders, such as mental illness, whose causes are unknown.

Such probing of the brain will undoubtedly require examining the status of neurotransmitter compounds and their receptors. The effectiveness of psychopharmacologic agents that work on these receptors is the clue to this investigational approach. Recently, the first images of a neurotransmitter analogue have been obtained by Garnett *et al.* through the use of 6-fluorodopa as a catecholamine imaging precursor.[11] Advances have also been made in the imaging of receptors, with the first attempts to use benzodiazepine[5] and dopamine receptors,[25] also discussed by Herscovitch in this volume.

The difficulties inherent in developing syntheses for new radiopharmaceuticals imply relatively slow progress in exploiting the potential of PET. Nonetheless, because the information will be qualitatively unique, its value should not be discounted because of the high cost, slow progress, and uncertain ultimate contribution to routine diagnostic medicine.

The synthesis of compounds capable of achieving the high chemical sensitivity implied in Table 3 is a considerable test of organic synthetic ingenuity. Complex molecules must be synthesized, purified, and prepared for administration in a short period after the generation of the radioisotope in a cyclotron.

TRENDS IN OVERALL HEALTH COSTS

The newer imaging techniques are relatively expensive to use, and their widespread application will therefore inevitably produce some competition for health-service resources. This competition is bound to provoke discussion between scientists familiar with the potential of these techniques and health administrators, who are always faced with spending pressures that exceed available resources. It may be instructive to examine trends in health expenditures in Canada, and particularly in British Columbia, since 1969, when Medicare was introduced. In the universal Medicare scheme, all doctors' fees are paid directly. Doctors bill the medical plan, according to a negotiated fee schedule, and patients are not even informed of the services for which the doctor bills. This plan was introduced about a decade after the universal hospitalization program, which covers patients for all in-hospital costs, including drugs, surgery, diagnostic tests, and equipment of all kinds, such as cardiac pacemakers. A minimal daily room fee is charged, but the fee is almost always less than the cost of meals. Both hospital and medical programs are 50% funded by the federal government of Canada, but they are administered by the provinces, because under the Canadian constitution health is a provincial responsibility. Administrative practices from province to province are nonetheless highly similar.

Various cost trends are illustrated in Figure 1. For comparisons of size, the population of the United States is roughly 10 times that of Canada and 100 times that of British Columbia. For the 14-year period commencing in 1968 through 1982, the gross national product of Canada increased by a factor of 4.9, from $72.6 billion to $357 billion. Hospital and medical costs substantially exceeded this rate of growth, both for the nation and for British Columbia; that indicates an important shift of national resources into the health field. Canadian federal contributions to hospital insurance increased by a factor of 9.1, from $642 million to $5.83 billion. Federal Medicare contributions increased to a comparable extent, although the provinces did not all enter the scheme initially, and exact comparisons are not possible. The increase for provinces that did enter in the 1969 base year was by a factor of 8.9. From 1974, when all provinces participated, the hospital and Medicare percentage increases were almost identical.

Contributions for research from the federal government through the Medical Research Council of Canada failed to keep pace with the growth in gross national product, increasing by a factor of only 4.2, from $27 million to $114 million. This was somewhat greater than the factor of 3.4 experienced by the U.S. National Institutes of Health ($1.17 to $4.00 billion), but the per capita medical research effort in Canada is still less than one-fourth that in the

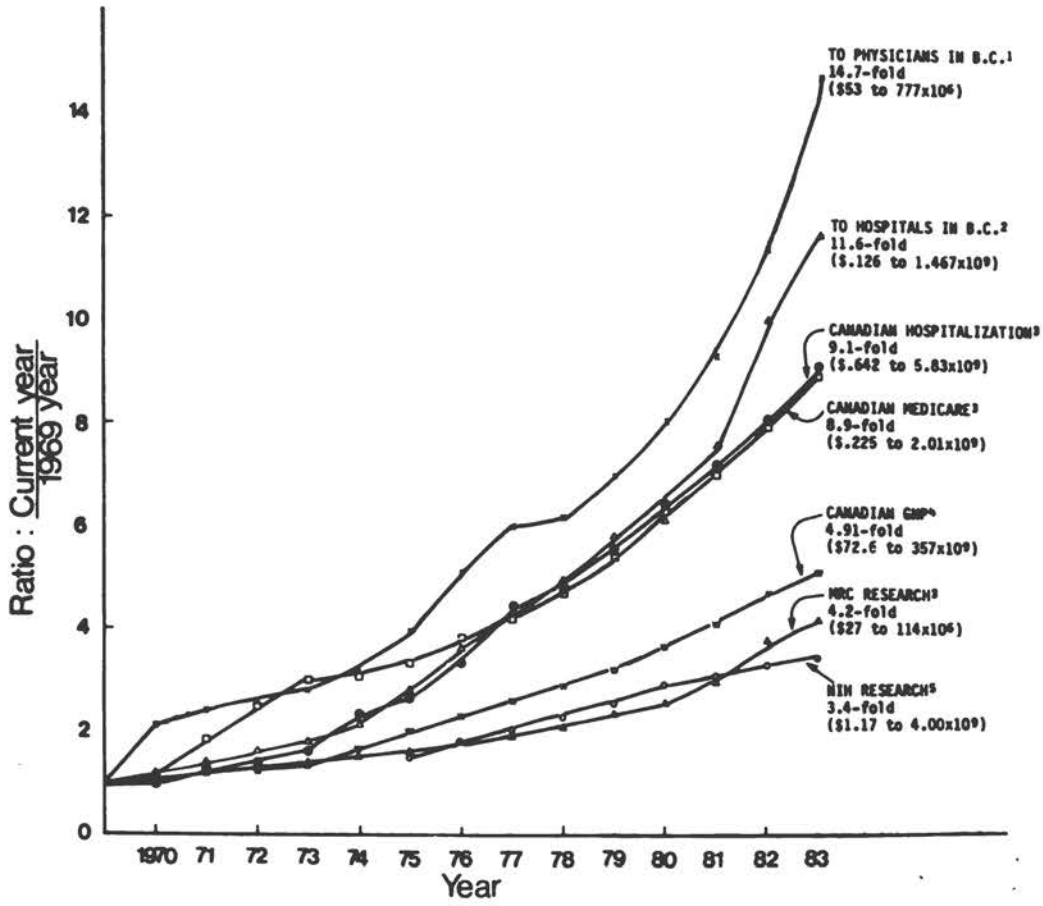

FIGURE 1 Growth trends in some health costs: ratio of expenditures to those in 1969 base year. Statistical sources: 1, Province of British Columbia, Ministry of Health, Medical Services Commission Financial Statements; 2, public accounts, Province of British Columbia; 3, Federal-Provincial Programs and Activities: A Descriptive Inventory, Federal-Provincial Relations Publications, 1968-1982, and The National Finances, published by Canadian Tax Foundation; 4, Statistics Canada, Catalog 13213, 1983; 5, Congressional Quarterly, Congressional Quarterly Inc., Washington, D.C.

United States if the lower value of the Canadian dollar ($0.81 U.S.) is taken into account.

The experience in British Columbia represents an exaggeration of the national trends. Total payments to physicians, including both federal and provincial contributions, over the 14-year period increased by a factor of 14.7 from $53 million to $777 million. Total payments to hospitals, excluding institutions for the mentally

infirm, increased by a factor of 11.6, from $126 million to $1.467 billion. These provincial figures, unlike those for Canada as a whole, are total cost figures, in that they include both federal and provincial contributions.

It is possible only to speculate on the reasons why the introduction of Medicare in Canada should have resulted in such a prolonged shift of financial resources into the health field from other sectors and why British Columbia should have experienced such an exaggerated trend. Why medical research efforts should have dwindled in intensity on both sides of the border is easier to understand. Medical research grants from governments have been kept relatively low. The trend might be explained by saying that too much was being spent on research and not enough on service in former times, and that the shift therefore represents a normalization of public priorities.

The interpretation offered here is rather different. It is that the public places a high value on its health, but is induced into relative overexpenditure on service and underexpenditure on discovery by the nature of the health programs themselves. If this interpretation is correct, then appropriate corrective action in Canada is urgently required and anticipatory action in the United States is desirable to avoid repetition of Canadian mistakes.

The Canadian hospital and Medicare schemes, although government funded, are essentially open-ended schemes that are driven by the demands of both patients and health professionals. In contrast, research allocations are determined by budgets, usually as a result of bureaucratic decision. Bureaucrats cannot control patients' visits to doctors or admissions into hospitals. Neither can they entirely control fees for doctors or salaries for health workers; these are typically set by negotiation. The control is much tighter in the case of research grants. The result is that service payments have surged beyond, and research grants have fallen behind, the expansion of the GNP. This reflects the relatively low priority of medical research in government policy circles, on the one hand, and inability to control service payments, on the other.

This hypothesis is consistent with the more extreme trends in British Columbia, compared with the rest of Canada. With respect to geography and climate, British Columbia is a preferred location and has experienced a higher than average population growth. This population growth, however, does not begin to account for the increase in health service costs. British Columbia has been a destination area for physicians who have found it relatively easy to establish profitable practices in the climate created by Medicare, and the number of doctors has increased far faster than the population as a whole. In addition, health professionals and

health-worker unions have been particularly aggressive in negotiations with government. Their aggressiveness has been rewarded, usually in the form of arbitration awards by third parties. Fees and wages are high. The system was billed in 1982, for example, by one physician for $684,119 and by several others for over $500,000.[20]

The implications of the data shown in Figure 1 are the following:

- The Canadian Medicare and hospital schemes have drawn substantial funds into the health-care field from other spending priorities. The percentage of the gross national product devoted to health care has increased substantially since these programs were established.

- These health-insurance schemes are strongly supported by the public. Because they are driven by the demands of patients and physicians, it is difficult to institute effective cost controls if the schemes are open-ended.

- Research has not participated in this sharp increase in commitment of public funds to health. Indeed, medical research appears to have diminished (in absolute terms) from its position of 15 years ago.

- Private contributions to medical research are disproportionate, because people suffering from incurable diseases recognize the inadequacies of the health-care system for their own situation. Thus, we see the formation of such associations as the Parkinson's Disease Association, the Huntington's Disease Association, and the Alzheimer's Disease Association.

- The increase in availability of funds has been directed largely at improved salaries and working conditions for physicians and other health-care workers. Medical scientists have not participated to the same degree in this improvement, and their failure to do so may make it difficult to recruit quality personnel to sustain the scientific enterprise at a desirable magnitude or even at the magnitude of many years ago.

It is probably impossible to determine a degree of medical service at which an optimal cost-benefit ratio may be achieved. It cannot be assumed, however, that unlimited service opportunities will always bring a better result, even if that result is marginal and its cost high. One of the best examples of open-ended service opportunities that bring a negative result was reported by Dyck *et al.*[6] The Saskatchewan Department of Health drew attention to the fact that hysterectomies in women over the age of 15 had increased by 72.1% between 1964 and 1971, although the number of such women

had increased by only 7.6%. This led to an announcement by the College of Physicians and Surgeons of Saskatchewan that the reasons for the increase would be investigated. The increase had not been geographically uniform throughout the province, but had been concentrated in particular major cities. The investigation precipitated a dramatic decrease in the hysterectomy rate to a point below that of 1964, with particularly sharp decreases in the cities responsible for the rise. The rate of operations proved unnecessary by the removal of normal tissue also decreased, from 23.7% at the time of the review to 7.8% after the review. Examples of more widespread practices might include the unnecessary prescribing of a variety of drugs with harmful side effects and, as has recently been suggested, the too aggressive pursuit of cardiac bypass surgery.[14]

The United States does not have comprehensive government schemes, as Canada does, but Blue Cross and comparable insurance plans cover a substantial proportion of the population and operate in much the same fashion. Indeed, the Canadian government schemes constituted a takeover and enlargement of various private plans styled along the lines of Blue Cross. Therefore, careful analysis is likely to show that trends in the United States have been similar to those in Canada.

SUMMARY OF THE ROLE OF BIOLOGICAL IMAGING

The preceding sections have emphasized previously presented[4] arguments for vigorous promotion of biological imaging in medical service and research. It has an important role to play, and its development has justified the optimism of those bold enough to promote its use in early times, when the cost of instrumentation was even higher than it is now and when the outcome of trial experiments was much less certain. Its place today must be evaluated in an era of increasing costs of medical service and relatively diminishing research commitments. Perhaps the potential of imaging techniques can illustrate ways in which complicated and expensive research can be more than worth while and indicate that increasing the availability of funds for medical service does not necessarily bring rewards in improved health.

Hospital and Medicare schemes in Canada and their public and private counterparts in the United States are based on the concept of insurance. The citizen contributes through premium prepayment or taxes when healthy and claims benefits when struck by injury or disease. But the insurer cannot redeem the claim if the citizen contracts a disease whose cause is unknown and for which effective treatment is nonexistent. Every contribution to health insurance should therefore include a substantial contribution to research as the only possible method for insuring against the vast number of

diseases in the category of currently untreatable. This principle should have been recognized when these "insurance" schemes were set up. The pace of discovery may actually be reduced by this conceptual fault, because resources applied through these schemes have taken away from other spending programs, including research--at least in Canada. The appropriate way to restore the balance would be to set aside, from each "premium" paid by the citizen through contributions to medical schemes or to taxes, a proportion that is reserved for medical advance. A suitable figure for such commitment might be 5%. If that were the case, medical research would experience a quantum leap in funding, which would make it possible to exploit aggressively the promise of such techniques as biological imaging. No one could doubt that such a leap would soon advance the health of citizens beyond what is achievable with more modest research commitments.

REFERENCES

1. Ackerman, R. H., R. Subramanyam, J. A. Correia, N. M. Alpert, and J. M. Taveras. Positron imaging of cerebral blood flow during continuous inhalation of $C^{15}O_2$. Stroke 11:45-49, 1980.

2. Bore, P. J., L. Chan, D. G. Gadian, G. K. Radda, B. D. Ross, P. Styles, and D. J. Taylor. Noninvasive pHi measurements of human tissue using ^{31}P-NMR. Kroc Found. Ser. 15:527-535, 1981.

3. Bradley, W., and H. Tosteson. Basic physics of NMR, pp. 11-29. In L. Kaufman, L. E. Crooks, and A. R. Margulis, Eds. Nuclear Magnetic Resonance Imaging in Medicine. New York: Igaku-Shoin, 1981.

4. Brownell, G. L., T. F. Budinger, P. C. Lauterbur, and P. L. McGeer. Positron tomography and nuclear magnetic resonance imaging. Science 215:619-626, 1982.

5. Comar, D., M. Maziere, J. M. Godot, G. Berger, F. Soussaline, C. Menini, G. Arfel, and R. Naquet. Visualisation of ^{11}C-flunitrazepam displacement in the brain of the live baboon. Nature 280:329-331, 1979.

6. Dyck, F. J., F. A. Murphy, J. K. Murphy, D. A. Road, M. S. Boyd, E. Osborne, D. de Vlieger, B. Korchinski, C. Ripley, A. T. Bromley, and P. B. Innes. Effect of surveillance on the number of hysterectomies in the province of Saskatchewan. N. Eng. J. Med. 296:1326-1328, 1977.

7. Engel, J., Jr., D. E. Kuhl, and M. E. Phelps. Patterns of human local cerebral glucose metabolism during epileptic seizures. Science 218:64-66, 1982.

8. Frackowiak, R. S., G. L. Lenzi, T. Jones, and J. D. Heather. Quantitative measurement of regional cerebral blood flow and oxygen metabolism in man using ^{15}O and positron emission tomography: Theory, procedure, and normal values. J. Comput. Assist. Tomogr. 4:727-736, 1980.

9. Friedland, R. P., T. F. Budinger, E. Ganz, Y. Yano, C. A. Mathis, B. Koss, B. A. Ober, R. H. Huesman, and S. E. Derenzo. Regional cerebral metabolic alterations in dementia of the Alzheimer type: Positron emission tomography with [^{18}F]fluorodeoxyglucose. J. Comput. Assist. Tomogr. 7:590-598, 1983.

10. Gadian, D. G., and G. K. Radda. NMR studies of tissue metabolism. Annu. Rev. Biochem. 50:69-83, 1981.

11. Garnett, E. S., G. Firnau, and C. Nahmias. Dopamine visualized in the basal ganglia of living man. Nature 305:137-138, 1983.

12. Haselgrove, J. C., V. H. Subramanian, J. S. Leigh, Jr., L. Gyulai, and B. Chance. In vivo one-dimensional imaging of phosphorus metabolites by phosphorus-31 nuclear magnetic resonance. Science 220:1170-1173, 1983.

13. Hilal, S. K., A. A. Maudsley, H. E. Simon, W. H. Perman, J. Bonn, M. E. Mawad, A. J. Silver, S. R. Ganti, P. Sane, and I. C. Chien. In vivo NMR imaging of tissue sodium in the intact cat before and after acute crebral stroke. Am. J. Neuroradiol. 4:245-249, 1983.

14. Kolata, G. Some bypass surgery unnecessary. Science 222:605, 1983.

15. Kuhl, D. E., M. E. Phelps, C. H. Markham, E. J. Metter, W. H. Riege, and J. Winter. Cerebral metabolism and atrophy in Huntington's disease determined by ^{18}FDG and computed tomographic scan. Ann. Neurol. 12:425-434, 1982.

16. Neurohr, K. J., E. J. Barrett, and R. G. Shulman. In vivo carbon-13 nuclear magnetic resonance studies of heart metabolism. Proc. Natl. Acad. Sci. USA 80:1603-1607, 1983.

17. Ordidge, R. J., P. Mansfield, M. Doyle, and R. E. Coupland. Real-time movie images by NMR. Br. J. Radiol. 55:729-733, 1982.

18. Phelps, M. E., E. J. Hoffman, and C. Raybaud. Factors which affect cerebral uptake and retention of $^{13}NH_3$. Stroke 8:694-702, 1977.

19. Phelps, M. E., J. C. Mazziotta, and S. C. Huang. Study of cerebral function with positron computed tomography. J. Cereb. Blood Flow Metab. 2:113-162, 1982.

20. Province of British Columbia, Ministry of Health, Medical Services Commission. Financial Statements. 1983.

21. Raichle, M. E. Quantitative in vivo autoradiography with positron emission tomography. Brain Res. 180:47-68, 1979.

22. Ross, B. D., G. K. Radda, D. G. Gadian, G. Rocker, M. Esiri, and J. Falconer-Smith. Examination of a case of suspected McArdle's syndrome by ^{31}P nuclear magnetic resonance. N. Eng. J. Med. 304:1338-1342, 1981.

23. Rinck, P. A., S. B. Petersen, E. Heidelberger. V. Acuff, J. Reinders, M. L. Bernardo, L. K. Hedges, and P. C. Lauterbur. NMR ventilation imaging of the lungs using perfluorinated gases, pp. 302-303. In Scientific Program, Society of Magnetic Resonance in Medicine, 2nd Annual Meeting, San Francisco, August 16-19, 1983. Berkeley, Calif.: Soc. Magn. Reson. Med., 1983.

24. Singer, J. R., and L. E. Crooks. Nuclear magnetic resonance blood flow measurements in the human brain. Science 221:654-656, 1983.

25. Wagner, H. N., Jr., H. D. Burns, R. F. Dannals, D. F. Wong, B. Langstrom, T. Duelfer, J. J. Frost, H. T. Ravert, J. M. Links, S. B. Rosenbloom, S. E. Lukas, A. V. Kramer, and M. J. Kuhar. Imaging dopamine receptors in the human brain by positron tomography. Science 221:1264-1266, 1983.

SPEAKERS

PAUL A. BOTTOMLEY, Physicist, Corporate Research and Development Center, General Electric Company, Schenectady, N.Y.

THOMAS J. BRADY, Director NMR Imaging, Massachusetts General Hospital, Boston, Mass.

EDWARD N. BRANDT, JR., Assistant Secretary for Health, Department of Health and Human Services, Washington, D.C.

THOMAS F. BUDINGER,* H. Miller Professor of Medical Research and Director of Medical Services, Lawrence Berkeley Laboratory, Berkeley, Cal.

LAWRENCE E. CROOKS, Associate Professor of Engineering and Assistant Director of Radiologic Imaging Laboratory, University of California, San Francisco, Cal.

RUTH M. DAVIS, President, The Pymatuning Group, Washington, D.C.

DIETER ENZMANN, Associate Professor of Neuroradiology, Department of Radiology, Stanford University, Stanford, Cal.

PETER HERSCOVITCH, Assistant Professor of Neurology, Division of Radiation Science, Washington University School of Medicine, St. Louis, Mo.

ROBERT HOFSTADTER, Max H. Stein Professor of Physics, Department of Physics, Stanford University, Stanford, Cal.

G. NEIL HOLLAND, Director, NMR Development, Picker International, Highland Heights, Ohio

PAUL C. LAUTERBUR,* Professor of Chemistry, State University of New York, Stony Brook, N.Y.

PETER MANSFIELD, Professor of Physics, Department of Physics, University of Nottingham, Nottingham, United Kingdom

ALEXANDER R. MARGULIS, Professor and Chairman, Department of Radiology, University of California, San Francisco, Cal.

---

* Dr. Budinger and Dr. Lauterbur (who was unable to submit a manuscript of his presentation for publication) prepared a summary of the conference that has been published in Science (226:288-298, 1984).

PATRICK L. McGEER, Minister of Science, Universities and Communications, Victoria, B.C., Canada

CHARLES A. MISTRETTA, Professor of Radiology and Medical Physics, Clinical Science Center, University of Wisconsin School of Medicine, Madison, Wis.

JUDITH M. S. PREWITT,* Stocker Visiting Professor of Electrical and Computer Engineering, Ohio University, Athens, Ohio, and Office of the Director, Division of Computer Research and Technology, National Institutes of Health, Bethesda, Md.

SIR REX RICHARDS, Warden, Merton College, and Professor of Physical Chemistry, Oxford University, Oxford, England

MICHEL M. TER-POGOSSIAN, Professor of Radiology, Division of Radiation Science, Washington University School of Medicine, St. Louis, Mo.

DONALD B. TWIEG, Assistant Professor, Department of Radiology, University of Texas Health Science Center at Dallas, Tex.

PETER WOLFF, Director, Francis Bitter National Magnet Laboratory, Massachusetts Institute of Technology, Cambridge, Mass.

* Dr. Prewitt was unable to submit a manuscript of her presentation for publication.

SPONSORS OF THE CONFERENCE

PHILIP H. ABELSON, Editor, Science Magazine, Washington, D.C.
WILLIAM O. BAKER, Retired Chairman of the Board, Bell Telephone Laboratories, Morristown, N.J.
CHARLES C. EDWARDS, President, Scripps Clinic and Research Foundation, La Jolla, Cal.
CECIL H. GREEN, A Founder and Honorary Director, Texas Instruments, Dallas, Tex.
DONALD KENNEDY, President, Stanford University, Stanford, Cal.
ALVIN G. LAZEN, Executive Director, Commission on Life Sciences, National Research Council, Washington, D.C.
WILLIAM C. LEVIN, President, University of Texas Medical Branch at Galveston, Tex.
PATRICK L. McGEER, Minister of Science, Universities and Communications, Victoria, B.C., Canada
COURTLAND D. PERKINS, Past President, National Academy of Engineering, Washington, D.C.
FRANK PRESS, President, National Academy of Sciences, Washington, D.C.
SIR REX RICHARDS, Warden, Merton College, and Professor of Physical Chemistry, Oxford University, Oxford, England
FREDERICK C. ROBBINS, President, Institute of Medicine, Washington, D.C.
WALTER A. ROSENBLITH, Institute Professor and Provost Emeritus, Massachusetts Institute of Technology, Cambridge, Mass.
DAVID S. SAXON, Chairman of The Corporation, Massachusetts Institute of Technology, Cambridge, Mass.
FREDERICK SEITZ, President Emeritus, Rockefeller University, New York, N.Y.
JOHN L. SMITH, Solana Beach, Cal.
CHARLES C. SPRAGUE, President, University of Texas Health Science Center at Dallas, Tex.
ANDREW D. SUTTLE, JR., Professor of Nuclear Biophysics, The Marine Biomedical Institute, University of Texas Medical Branch at Galveston, Tex.
ROBERT M. WHITE, President, National Academy of Engineering, Washington, D.C.